

**Studies on the
Vertical Structure of Horizontal Wind
Variability in the Surface Boundary
Layer over Sriharikota**

**Thesis submitted to the
Cochin University of Science and Technology
in partial fulfilment of the requirement for the Degree of**

**DOCTOR OF PHILOSOPHY
in
ATMOSPHERIC SCIENCES**

**By
SAMBHU NAMBOODIRI. K.V.**

**Department of Atmospheric Sciences
Cochin University of Science and Technology
Cochin – 682 016**

December 2000

CERTIFICATE

This is to certify that the thesis entitled 'Studies on the Vertical Structure of Horizontal Wind Variability in the Surface Boundary Layer over Sriharikota' is a bona fide record of the research work done by Mr. Sambhu Namboodiri.K.V, M.Sc., in the Department of Atmospheric Sciences, Cochin University of Science and Technology. He carried out the study reported in this thesis, independently under our supervision. We also certify that the subject matter of the thesis has not formed the basis for the award of any Degree or Diploma of any University or Institution.

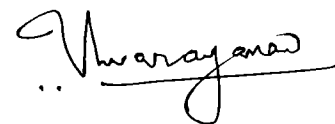
Certified that Mr. Sambhu Namboodiri.K.V has passed the Ph.D. qualifying examination conducted by the Cochin University of Science and Technology in September, 1999.

Cochin – 682 016
December 22, 2000



Prof. (Dr.) K. MOHANKUMAR
Head

**Department of Atmospheric Sciences
Cochin University of Science & Technology
Cochin, India-682 016**



Dr. V. NARAYANAN
Head (Retd.)

**Meteorology Facility
Vikram Sarabhai Space Centre
Indian Space Research Organisation
Trivandrum, India-695 022**

Preface

The characteristics of Surface Boundary Layer (SBL) wind regime in the tropics is significantly different from those at mid-latitude areas. Major reasons pertained to this difference are due to much greater insolation, vertical mixing of momentum, insignificant Coriolis force and dominating synoptic-scale trade winds in the tropics. Investigations on the properties of SBL winds over the tropical coastal station, Sriharikota (13.7°N, 80.2°E), which is the major rocket launching centre (SHAR Centre) of Indian Space Research Organisation (ISRO), are of particular interest as a source of aerodynamic loads imposed on aerospace vehicles during launch operations. Exploration of wind energy studies, air pollution impact assessments, structural design works, meso-scale meteorological modelling studies and in aviation meteorology winds of this region are also of most concern. A unique round the clock wind speed and direction measuring facility from seven levels in the 100 m layer of SBL at a data collection scan rate of every second since May 1993 provides an excellent opportunity for such studies. Many studies of the temporal and vertical spatial variations are conducted to investigate the vertical structure of horizontal wind field and presented in this thesis.

The doctoral thesis consists of ten chapters. In chapter 1, an elaborate introduction on the SBL wind in the tropics, the influence of different types of circulations in the tropical coastal wind environment, wind measurement techniques, the random nature of SBL wind flow and potential applications of SBL wind modelling are discussed.

Literature review which comprises studies, analyses and suggestions from various investigators regarding SBL wind measurements, archival, velocity profiling, turbulence, stability behaviour, probabilistic characteristics and wind variability in association with meso-scale weather phenomena are presented in

chapter 2. In chapter 3, the measurement strategy of SBL winds over Sriharikota, which include specifications on observational platform, sensors, data archival and the voluminous data used for various extensive studies are discussed.

Chapter 4 is about the salient features of SBL winds over Sriharikota covering a wide spectrum of observations in wind variability. Basic statistical properties such as Mean Scalar Wind Speed (MSWSP), Mean Resultant Wind Direction (MRWD), Mean Resultant Wind Speed (MRWSP), Steadiness Factor (SF) and Mean Peak Wind Speed (MPWSP) are thoroughly examined and the behaviours of diurnal variation pattern are investigated. Probabilistic features of mean wind speeds in different wind directions, monthly wind climatology on MSWSP, MRWSP, horizontal wind (u, v) components, intra level correlation (ρ_{uv}) of u and v are generated and the characteristics are studied. Wind speed march on a particular day, nature of winds in association with severe weather conditions, such as thunderstorms and low pressure systems are critically examined. Brief account on the exceedance probability of peak wind speed with different limits, temporal structure of certain derived wind variables in SBL, like ρ_{uv} , Coefficient of Variation (CV), standard deviations of wind directions (σ_{θ}) and Gust Factor (GF) are viewed as of great significance in SBL wind characteristics.

Chapter 5 comprises the study on the dominance of meso-synoptic scale forcing by a ratio (α) of diurnal ($\bar{I}b$) to interdiurnal (Ia) wind variabilities in the lowest 100 m of the atmosphere and to detect the features of mean wind hodographs in relation to α .

Chapter 6 gives the structure of surface roughness parameter (Z_0) and power law exponent (α) derived based on neutral logarithmic wind profile assumption. Diurnal variations of Z_0 and α for various months, their variations

with different wind azimuths, the correlation of Z_0 and α , and a comparison of α values in a normal day and cyclonic storm crossing day are studied and presented.

Chapter 7 accounts for the vertical structure of total shear and scalar shear in different months. A comparison of these shear values are also included. Through special mathematical treatment, the stability of atmosphere based on standard deviations in wind directions (σ_θ) is categorized. Diurnal variations of σ_θ are compared with wind speed variations, wind profiles during Least Stable Time (LST) and Highly Stable Time (HST) and presented in chapter 8. In addition, the frequency distribution of σ_θ for various months are brought out.

Investigations on SBL winds concentrates towards the optimum wind probability distribution models and its properties for extreme wind distribution through Weibull model and wind components distribution through Bivariate Normal Distribution are presented in chapter 9. These models are tested with mainstay statistical distributions and climatological wind features.

The concluding session of the research work carried out in the present thesis is presented in chapter 10. References appeared in chapters are listed at the end of the thesis in alphabetical order.

CONTENTS

	Page No.
CERTIFICATE	i
DECLARATION	ii
ACKNOWLEDGEMENTS	iii
PREFACE	iv
Chapter 1: Introduction	
1.1 The Wind Regime in the Tropics	2
1.2 General Wind Characteristics	3
1.3 Scales of Atmospheric Motion	4
1.4 Layered Structure of Atmosphere in terms of Wind	8
1.5 The Surface Boundary Layer (SBL) or Surface Layer or Tower Layer	10
1.6 The Wind Profile in SBL	11
1.6.1 The Logarithmic Wind Profile in Neutral Case	
1.6.2 A Reference to Eddy Viscosity in SBL	
1.6.3 The Diabatic (Nonadiabatic) Wind Profile	
1.7 Shape of Wind Profile in SBL	19
1.8 The Influence of Primary, Secondary and Tertiary Circulations in the Tropical Coastal Wind Environment	22
1.8.1 The Role of Primary Circulations	
1.8.2 The Role of Secondary Circulations	
1.8.3 The Role of Tertiary Circulations	
1.9 Wind Observational Techniques and Platforms in SBL	32
1.10 Wind and Flow	39
1.11 Potential Applications of Surface Boundary Layer Wind Modelling	41
1.12 Relevance to SBL Wind Modelling Studies in SHAR Centre, ISRO, India	45

Chapter 2: Literature Review

2.1	Wind Measurement and Archival in Automatic Surface Wind Observations	50
2.2	Wind Observations in Tower Platforms and Cup Anemometry	51
2.3	Properties on SBL Wind Velocity Profiles	53
2.3.1	Wind Velocity Profiles	
2.3.2	Roughness Length (Z_0) and Frictional Velocity (U_*)	
2.3.3	Power Law Wind Profile in Engineering Applications	
2.3.4	Wind Shear	
2.4	Atmospheric Turbulence, Gusts and Spectral Behaviour	57
2.4.1	Wind Speed Fluctuations: Atmospheric Turbulence and Gustiness	
2.4.2	Wind Velocity Spectra	
2.5	Wind Direction Fluctuations: Stability of Atmosphere	59
2.6	Probabilistic Properties of Wind Behaviour	60
2.7	Wind Variability Associated with Meso-scale systems	62

Chapter 3: Measurement Techniques of Surface

Boundary Layer Winds over Sriharikota

3.1	Introduction	66
3.2	Physiography and Terrain Features of Sriharikota	66
3.3	Observational Platform and Data Acquisition	67
3.3.1	Tower Facility	
3.3.2	Data Reduction Procedure	
3.3.3	Tower Instrumentation	
3.3.3.1	Cup Anemometer	
3.3.3.2	Wind Vane	
3.4	Data used for Studies on the Structure of SBL Winds	73

Chapter 4: Salient Features of Surface Boundary Layer Winds

4.1	Introduction	76
4.2	Methodology	76
4.3	Results and Discussion on Basic Wind Statistical Properties	77
4.3.1	Mean Scalar Wind Speed (MSWSP) (Mean Quasi-Steady State Wind Speed)	
4.3.2	Mean Resultant Wind Direction (MRWD)	
4.3.3	Wind Steadiness Factor	
4.3.4	Mean Peak Wind	
4.3.5	Probability of Mean Wind Speeds in Different Wind Directions	
4.3.6	Monthly Wind Climatology	
4.4	Wind Speed March on a Particular Day	95
4.5	Nature of SBL Winds in Association with Severe Weather	98
4.5.1	Thunderstorm Winds	
4.5.2	Thunderstorm Weather Assessment on Peak Wind Speed	
4.5.3	Winds in SBL during a Severe Cyclonic Storm	
4.5.4	Number of Occurrence of Wind Speed Events during the Progress of a Cyclonic Storm	
4.5.5	Spectral Characteristics of SBL Winds in the Influence of Low Pressure System	
4.6	Exceedance Probability of Peak Wind Speed with Different Limits	108
4.7	Temporal Structure of Derived Wind Variables in the SBL	110
4.7.1	Coefficient of Variation in relation to Mean Scalar Wind Speed	
4.7.2	The Diurnal Pattern of (u,v) Components and Intra-level Correlation Coefficients between u and v components (ρ_{uv})	
4.7.3	Diurnal Variation of σ_θ in Different Months	
4.7.4	Comparison between MSWSP and MRWSP	
4.7.5	Gust Factor Variations	

Chapter 5: Wind Variability and Elliptical

Approximation of Wind Hodographs in the SBL

5.1	Introduction	123
5.2	Observations and Data	123
5.3	Wind Variability Ratio(α)-Mathematical Formulations	124
5.4	Results and Discussion	125
5.4.1	Monthly Distribution of Wind Variability Ratio (α)	
5.4.2	Mean Wind Hodograph	

Chapter 6: Structure of Surface Roughness Parameter and Power Law Exponent

6.1	Introduction	135
6.2	Data	135
6.3	Methodology in the Derivation of Z_0 and α	135
6.4	Results and Discussion	136
6.4.1	Monthly Structure of Z_0 and α	
6.4.2	Variations of Z_0 and α with Wind Direction	
6.4.3	Relationship between Z_0 and α	
6.5	Comparison of α values in a Normal Day and in a Cyclone Day	140
6.6	A Reference to U_* values	143

Chapter 7: Vertical Wind Shear in the Lowest Layers of the Atmosphere

7.1	Introduction	146
7.2	Wind Shear	146
7.3	Methodology adopted for Shear Computations	147
7.4	Data and Presentations	147
7.5	Results and Discussion	148
7.5.1	Characteristics of Average Total Shear	
7.5.2	Characteristics of Average Scalar Shear	

7.5.3 Comparison between Average Total Shear and
Average Scalar Shear

**Chapter 8: Properties of Atmospheric Stability in the 100
meter Tower Layer**

8.1	Introduction	160
8.2	Data	162
8.3	Theoretical Considerations for the Derivation of Standard Deviation of Wind Directions (σ_{θ})	162
8.4	Results and Discussion	164
8.4.1	Features on the Monthly Diurnal Stability Variations	
8.4.2	Diurnal Variations of Wind Speeds in relation to Stability Variations	
8.4.3	Frequency Distributions of σ_{θ}	

**Chapter 9: Optimum Wind Probability Distribution
Models and its Properties**

9.1	Extreme Winds Distribution	
9.1.1	Introduction	172
9.1.2	The Weibull Model	172
9.1.3	Data and Methodology	174
9.1.4	Results and Discussion	174
9.1.4.1	Monthly Features on Weibull Curves	
9.1.4.2	Characteristics on the Cumulation of pdfs	
9.1.4.3	Comparison of Weibull and Gaussian Distribution	
9.2	Wind Component Distribution	
9.2.1	Introduction	179
9.2.2	UND and Its Limitations in Wind Vector Distribution	183
9.2.3	Bivariate Normal Distribution Model	184
9.2.4	Methodology for the Generation of BND Ellipses	184

9.2.5 Features of 90% BND Ellipses in SBL over Sriharikota	186
9.2.5.1 Data	
9.2.5.2 Results on the Properties of Ellipses	
9.2.6 Comparison of BND and UND	188
9.2.7 Advantages of BND over Conventional Wind Rose (CWR)	188
Chapter 10: Summary and Conclusions	191
References	198

Chapter 1
Introduction

1.1 The Wind Regime in the Tropics

The wind regime in the tropics is significantly different from those at mid-latitude areas. Major reasons pertained to this difference are much greater incoming solar radiation, vertical mixing of momentum, insignificant Coriolis force and dominating synoptic scale trade-winds in the tropics. Irregular chaotic atmospheric flows can be a limiting factor in the tropics where vertical air motion and consequent momentum mixing is stronger than at mid-latitudes.

The most dominating and persisting wind regimes in the tropics which influence the weather of tropics are trade winds, monsoons and thermally driven local winds such as land and sea breezes. The trade winds are among the most systematic wind systems on the planet. They emerge from the oceanic subtropical high pressures and approach the equator crossing from the southern and northern hemispheres creating the near equatorial convergence zone (called as Inter Tropical Convergence Zone, ITCZ). In the strongest central domain, they blow more than 80% of the time for an entire season with a mean wind speeds of 7-8 ms^{-1} . The northern ocean trades migrate over the yearly cycle, whereas the southern ocean trades are relatively stationary.

Monsoons are wind systems which undergo an annual variation. Prevailing wind (most frequently observed) directions vary by at least 120 degrees. Ramage (1971) carried out elaborate works on wind criteria associated with monsoon wind systems primarily. The monsoon characterise the Indian Ocean, western Pacific Ocean and equatorial Africa. Monsoon systems vary in intensity. The Indian summer monsoon is characterised by strong south westerlies blowing over the Arabian Sea, the corresponding winter monsoon flow is weak. In the deep tropics, such as the "maritime continent" of Indonesia and Philippines, prevailing winds are generally weak and the dominant winds are those generated by local diurnal heating cycles. Typically, a brisk sea breeze blow during day-time hours near the coast but the evening land breeze is weak.

1.2 General Wind Characteristics

If climatological data are available, the following wind characteristics should be assessed to know the wind pattern over an area for any potential engineering applications.

- (a) mean scalar wind speed*
- (b) standard deviation of wind (both speed and direction)*
- (c) mean resultant wind speed*
- (d) steadiness factor of wind*
- (e) directional wind roses*
- (f) annual wind variation*
- (g) diurnal wind variation and*
- (h) synoptic wind climatology*

Each of these elements is essential to project the reliability of the wind statistics for operational uses. The mean is the simplest parameter, and further analysis can be carried out with respect to its value. A large standard deviation is a concern as it may indicate frequent storms of damaging potential or disturbed weather. The resultant is a standard derived product presented in many monthly data summaries. Coupled with mean it yields the steadiness factor which is a robust estimate of reliability. Steadiness and resultant are sensitive to directional variability other than standard deviation of wind direction. In applications using the knowledge of topographic enhancements, directional variability is deleterious. The wind rose summary is especially useful in clarifying directionality. Annual variation is significant in monsoon climates and subtropical regions near oceanic high-pressure centres. Diurnal variation is important in matching power production applications such as peak power. Synoptic wind climatology clarifies the weather systems that may alter the standard general wind regime.

1.3 Scales of Atmospheric Motion

Motions in the atmosphere are characterised by a wide range, both temporally and spatially. The space scales of these features are determined by their typical size or wavelength and the time scales by their typical life span or period. Figure.1.1 (Smagorinsky, 1974) shows different atmospheric phenomena associated with motion within a grid of their probable space and time limits. The hierarchy of motion in the atmosphere ranges from the length scale equal to the circumference of the Earth to that equal to the drizzle drop. The systems and their scales of motion are: the jet streams (10^4 km), the Hurricanes (10^3 km), the cloud clusters (10^2 km), the thunderstorms (10 km), the cumulus clouds (1 km), the smoke puffs (100 m), etc. There are up and down transfers of energy from one scale to another. Man's immediate environment is characterised by micrometeorological scale motions extending from 100 m to 1 mm, several manifestations of which are visible to eye, like diffusion of smoke, plume from chimney or puff of incense.

In reality, none of these phenomena is discrete but part of a continuum, therefore it is not surprising that attempts to divide atmospheric phenomena into distinct classes have resulted in disagreement concerning the scale limits. Most classification scheme uses the characteristic horizontal distance scale as the sole criterion. A reasonable consensus of these schemes gives the following scales and their limit, represented at the top of Figure.1.1

Micro-scale	10^2 to 10^3 m
Local-scale	10^2 to 5×10^4 m
Meso-scale	10^4 to 2×10^5 m
Macro-scale	10^5 to 10^8 m

The shaded area in Figure 1.1 represents the characteristic domain of boundary layer features, and the weather phenomenon concentrating within this area have major contributions in the modifications of the boundary layer winds.

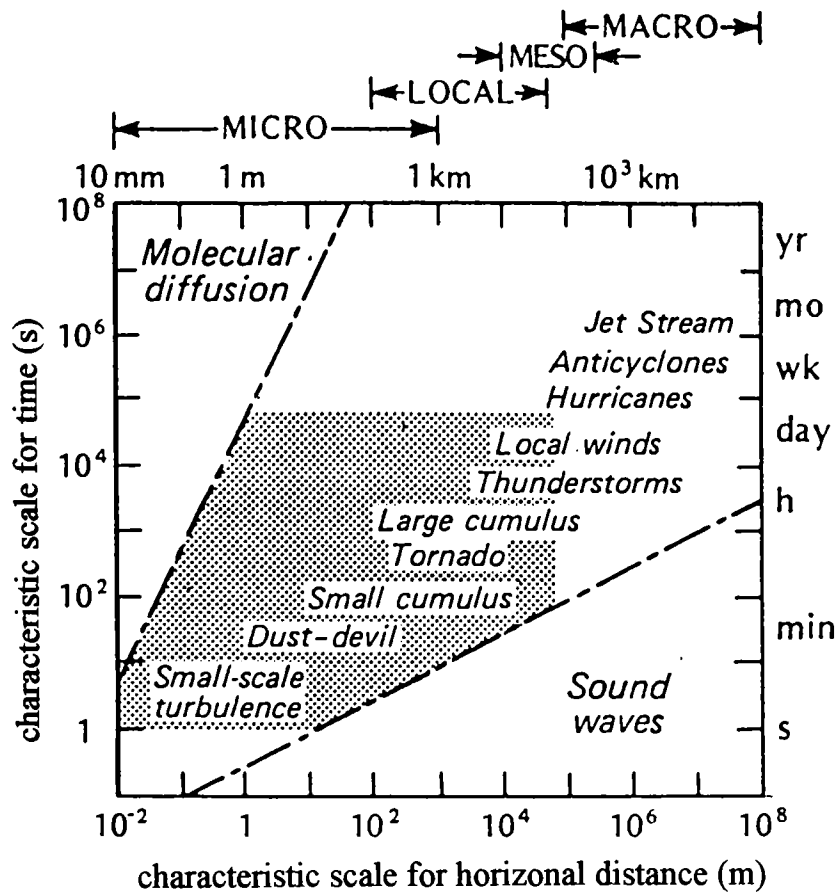


Figure 1.1 Temporal and spatial scales of atmospheric motion for different atmospheric phenomena.

Over time periods of about one day, the influence of the earth surface on the planetary atmosphere is restricted to a much shallower zone known as Planetary or Atmospheric Boundary layer (PBL or ABL). This is particularly characterised by well developed mixing (turbulence) generated by frictional drag as the atmosphere moves across the rough and rigid surface of the Earth. The PBL receives much of its heat and all of its water through this process of turbulence. The height of the PBL is not constant with time, it depends upon the strength of the surface generated mixing. When the Earth's surface is heated during the day-time by the Sun, there is an upward transfer of heat into the cooler atmosphere. This vigorous thermal mixing (convection) enables the PBL depth to extend to about 1 to 2 km. Conversely by night, when the Earth surface cools more rapidly than the atmosphere, there is a downward transfer of heat. This tends to suppress mixing and the PBL depth may shrink to less than 100 m. Thus in the simple case we envisage a layer of influence which waxes and wanes in rhythmic fashion. This vital picture can be considerably disrupted by large scale weather systems whose wind and cloud patterns are not tied to surface features or to the daily heating cycle by the Sun. With strong winds mixing is so effective that small-scale surface differences are obtained. Thus, except for the dynamic interaction between the airflow and the terrain, the PBL characteristics are dominated by tropospheric controls.

Figure 1.2 represents the vertical structure of the atmosphere modified by Tennekes (1974) in order to incorporate PBL and its layers. Within the PBL there are two other layers controlled by surface features. In immediate contact with the surface is the laminar boundary layer or sub surface layer whose depth is at most a few millimetres. This is a layer of non-turbulent air which adheres to all surfaces thus establishing an efficient buffer from the turbulent surface layer or Surface Boundary Layer (SBL) above. The SBL in Figure 1.2 is characterised by intense small scale turbulence generated by the terrain roughness and convection, by day

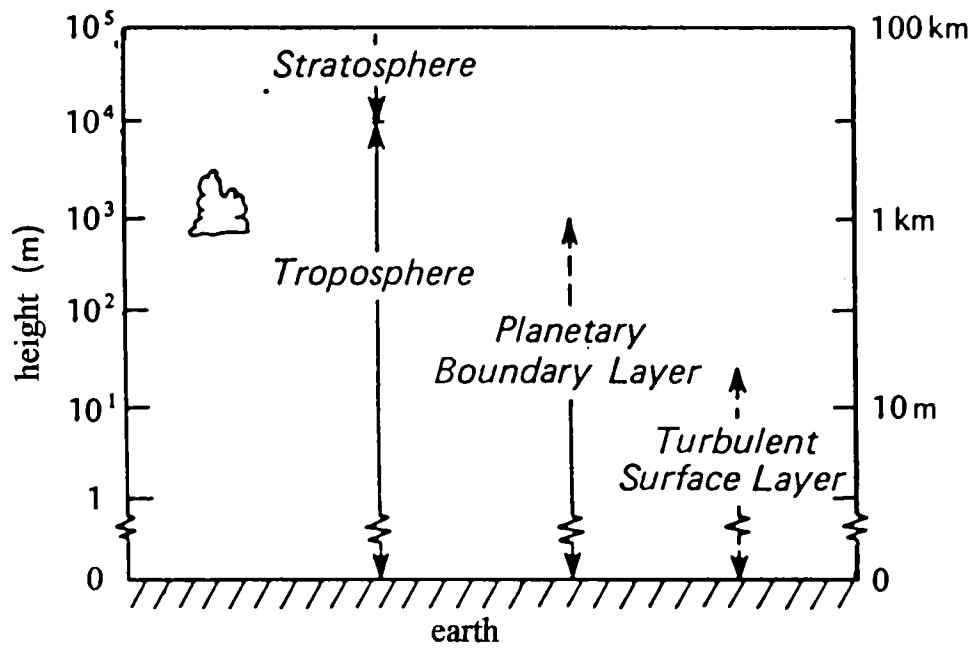


Figure 1.2 The vertical structure of atmosphere showing PBL

it may extend to height of 50 m but at night when the PBL shrinks it may be at most only a few metres in depth.

1.4 Layered Structure of Atmosphere in terms of Wind

A general outlook about the lowest layers of the atmosphere derived based on wind characteristics is shown in Figure 1.3. Immediately adjacent to the Earth surface, Surface Boundary Layer (SBL) is formed. Within this layer a very thin laminar sub layer is formed (if the Earth's terrain is smooth, otherwise SBL begins from the surface itself). Within this layer vertical eddy motions are not existing, the vertical gradient of wind $\partial V/\partial z$ attains high value and the shearing stress is due to molecular viscosity alone. The thickness of the laminar sub layer is usually within few millimeters (Figure 1.4). Above the laminar sublayer, the Prandtl layer is formed. The layer comprising laminar sub layer and Prandtl layer is called Surface Boundary Layer (SBL) or Tower Layer or Surface layer (SL), where most engineering problems are involved by Surface Layer features. The SBL is also called by Tower Layer, as the micrometeorological measurements in this layer generally use through towers equipped with meteorological instruments. Generally if tower layer is specified, the height of SBL can be treated as in between 30 and 150 m, characteristically this is the layer in which the turning of the wind with height is relatively small, and we will assume that the wind velocity, V can be treated as a scalar (Panofsky, 1973). Generally laminar sub layer does not exist, so the SBL is Prandtl layer itself.

The layer above SBL is called Ekman Spiral Layer or simply Spiral Layer. The layer comprising Prandtl layer and spiral layer is called Turbulent Boundary Layer. The top of the spiral layer is called gradient wind level. The total layer from surface to gradient wind level is called Planetary Boundary layer or Friction layer.

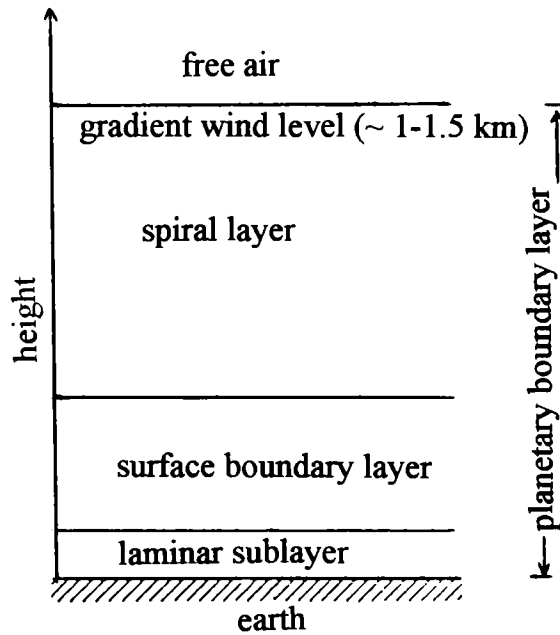


Figure 1.3 Lowest layers of atmosphere derived based on wind characteristics.

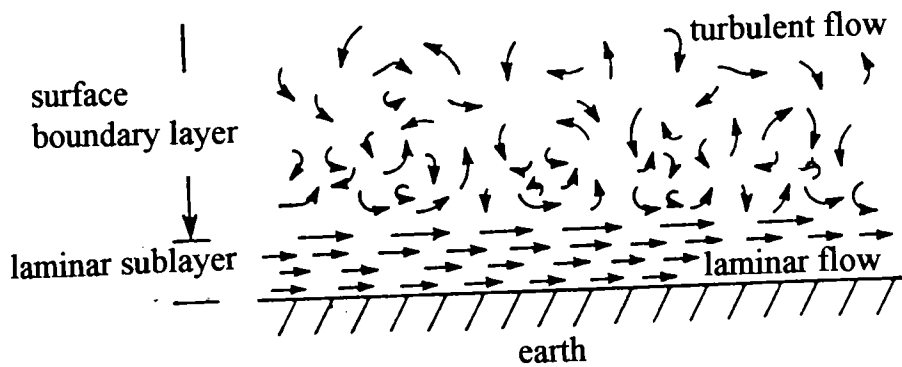


Figure 1.4 Laminar sublayer and surface boundary layer air motions.

In the Prandtl layer, the eddy stresses (due to turbulence) is an order of magnitude larger than the horizontal pressure gradient force. In the spiral layer, the eddy stress has approximately the same order of magnitude as the pressure gradient force and Coriolis force. Above the turbulent layer, free stream is found. Friction negligibly small above the PBL. The boundary of PBL and free air is the gradient level at approximately 1 to 1.5 km above the ground.

1.5 The Surface Boundary Layer (SBL) or Surface layer or Tower Layer

Under conditions of horizontal homogeneity and quasi-steady state (e.g., time changes are so small as to be dynamically negligible), the following approximations are usually applied to the SBL (Wyngaard, 1973; Mc Been, 1979; Panofsky and Dutton, 1984)

- (a) The rotation of the Earth, that is Coriolis effect is probably insignificant in the SBL.*
- (b) The SBL occupies the lowest 10% of PBL.*
- (c) Experiments have shown that the vertical variations in stress and heat flux in the SBL is within 10% and therefore called as the "Constant Flux Layer".*
- (d) In the SBL the wind direction does not change appreciably with height. Thus the mean wind is described by \bar{u} only.*
- (e) The variation of mean variables with height (z) is controlled primarily by three parameters; viz., the surface stress, the vertical heat flux at the surface and the terrain roughness.*
- (f) Transport of atmospheric properties by turbulent diffusion (eddies) is much more important than transport by molecular diffusion.*

1.6 The Wind Profile in the SBL

1.6.1 The Logarithmic Wind Profile in Neutral Case

According to Prandtl's mixing length principle due to turbulence, if an eddy of fluid originates at the level $z+\Delta z$ with mean speed $u_{z+\Delta z}$ and moves to z where the mean wind speed is u_z , then the perturbation produced at the neutral level is

$$u' = u_{z+\Delta z} - u_z \text{ where } \Delta z \text{ is small. Then}$$

$$u' = -l' \partial u / \partial z; \text{ where } l' \text{ is the mixing length} \quad (1.1)$$

Therefore, eddy stress in the X-direction,

$$\tau_{zx} = -\rho u' w' = \rho w' l' \partial u / \partial z \quad (1.2)$$

where ρ the density, w' the perturbation in the vertical component of wind. According to mass continuity, there exists a balance between horizontal and vertical eddy speeds. ie., $|u'| = |w'|$, when a fluid eddy is transported from one level to another level, on an average an equivalent mass from the new level should move horizontally with the same speed to make room for the eddy.

Thus

$w' = l' \left| \partial u / \partial z \right|$, here $\left| \partial u / \partial z \right|$ is used because w' and l' should have same sign. Therefore

$$\begin{aligned} \tau_{zx} &= \rho w' l' \partial u / \partial z = \rho l' l' (\partial u / \partial z) (\partial u / \partial z) \\ &= \rho l'^2 \left| \partial u / \partial z \right| (\partial u / \partial z) \end{aligned} \quad (1.3)$$

But $\tau_{zx} = \mu_{ex} \partial u / \partial z$; where μ_{ex} is the dynamic coefficient of viscosity.

ie., $\mu_{ex} = \rho l'^2 \left| \partial u / \partial z \right|$. Here we can define the Root Mean Square (RMS) mixing length $l_x = \sqrt{l'^2}$. Then $\tau_{zx} = \rho l_x^2 \left| \partial u / \partial z \right| (\partial u / \partial z)$ and $\mu_{ex} = \rho l_x^2 \left| \partial u / \partial z \right|$. Applying the above results in the surface layer from the above $\tau_{zx} = \rho l_x^2 (\partial u / \partial z)^2$ ie.,

$$(\partial u / \partial z)^2 = (\tau_{zx} / \rho) l_x^{-2}; \text{ ie., } \partial u / \partial z = (\sqrt{\tau_{zx} / \rho}) \cdot 1 / l_x \quad (1.4)$$

It may be noted that horizontal turbulent stress is primarily due to vertical variations of mean horizontal wind and vertical mixing by turbulence. Thus τ_{xy} , τ_{yx} eddy stress terms can be neglected. This is because of the vertical shear of mean wind is much greater than its horizontal stress. Since ρ and τ_{zx} are constant in a thin layer, the only quantity in the right hand side of equation (1.4) which can vary with height is l_x . The quantity $\sqrt{\tau_{zx}/\rho} = u_*$ is called frictional velocity, which is one parameter of the wind flow. We can integrate equation (1.4) until we specify how l_x varies with height. Right at the surface, mixing does not take place because of the solid boundary interface. As the point is away from the Earth's surface, the turbulence is less than inhibited by the solid boundary. Thus we can conclude that eddies are larger at higher altitudes within the SBL. In other words, the mixing length is zero at the Earth's surface and it increases linearly with altitude. ie., $l_x \propto z$ or $l_x = kz$; where k is the von Karman constant having values from 0.38 to 0.4. Then the equation (1.4) becomes as $\partial u/\partial z = (\sqrt{\tau_{zx}/\rho}) \cdot 1/l_x = 1/kz (\sqrt{\tau_{zx}/\rho}) = u_*/kz$. That is $k \partial u/u_* = dz/z$. Integrating this equation we will arrive to

$$ku/u_* = \ln(z) + C \quad (1.5)$$

where C is the constant of integration. In a very smooth surface, u becomes zero only at the Earth's surface but when the surface is rough the wind vanishes before the surface. Let us apply this condition $u = 0$ at $z = z_0$, where z_0 is called roughness parameter. Substituting this in the equation (1.5) $\ln z_0 + C = 0$, thereby $C = -\ln z_0$. Therefore equation (1.5) becomes as $uk/u_* = \ln z - \ln z_0$. So that

$$u = u_*/k \ln z/z_0 \quad (1.6)$$

Equation (1.6) is called logarithmic wind profile law for neutral atmospheric assumptions. Equation (1.6) can be again written as

$$\ln z = \ln z_0 + k/u_* u \quad (1.7)$$

This equation (1.7) can better be represented as the Figure 1.5. The equation (1.7) has a least-square linear regression form such that

$$Y = a_0 + a_1 X \quad (1.8)$$

where,

$$Y = \ln z \text{ and } a_0 = \ln z_0 \text{ or } z_0 = e^{a_0} \quad (1.9)$$

$$a_1 = k/u_* \text{ or } u_* = k/a_1 \quad (1.10)$$

and $X = u$. The logarithmic wind law is applicable from surface roughness (z_0), where the mean wind is presumed to be vanish at the top of the SBL. The roughness parameter z_0 has the unit of height and physically from this height wind exists and hence mixing takes place only above this level. The roughness parameter z_0 is proportional to the mean height of roughness elements. The relation of z_0 to various terrain types is shown in Figure 1.6 (ESDU, 1974). The simple logarithmic wind profile is found to be reasonable for most of the underlying surface in neutral condition. In neutral condition, mechanical turbulence predominates over thermal turbulence and it is neither augmented by thermally induced turbulence (unstable case) nor suppressed by thermal stratification (stable case).

For the case of very rough surface, such as that of dense vegetation, it is found that the vertical wind profile may be represented in the form

$$u = u_*/k \ln (z-d/z_0) ; \quad z \geq d + z_0 \quad (1.11)$$

where d is called the datum level displacement or displacement length or zero plane displacement. For a wide range of crops and trees the value of d is approximately given by

$$d = 2/3 h \quad (1.12)$$

Typical values of d is in Table 1.1, where h is the average height of crops or trees in the area. The zero plane displacement (d) can be visualised as representing

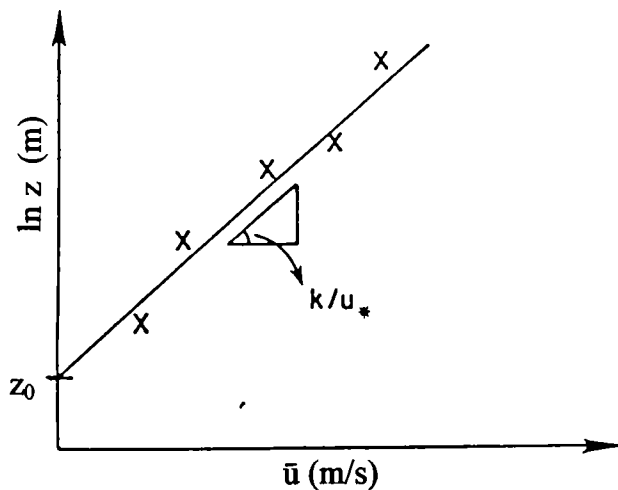


Figure 1.5 Logarithmic wind profile law, showing z_0 derivation and slope (k/u_*)

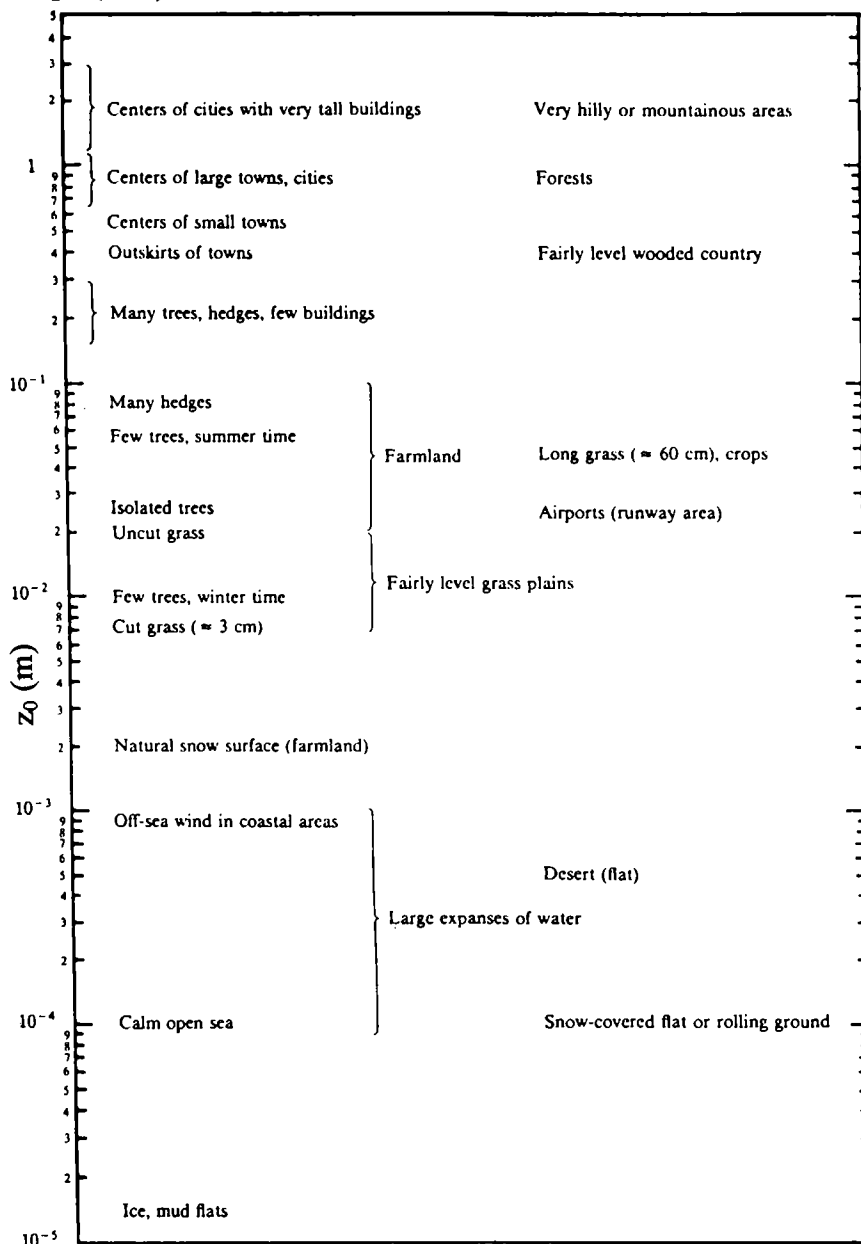


Figure 1.6 Relation of surface roughness parameter (z_0) to different terrain types

the apparent level of the bulk drag exerted by the vegetation on the air (or the level of the apparent momentum sink). According to equation (1.11) $u \rightarrow 0$ as $z \rightarrow d+z_0$. Broadly speaking, if equation (1.11) is applied to the region above fairly uniform but dense vegetation, $d+z_0$ corresponds to a level near the top of the vegetation. A profile of equation (1.11) has increasingly concave upward curvature as one approaches the datum level, $d+z_0$ from above. This is shown schematically in Figure 1.7, where the determination of z_0 is also indicated. At relatively great altitudes in the SBL, the plotted points are usually well fitted by a straight line. Extrapolating this straight line to its intercept with the $\ln z$ axis yields z_0 .

1.6.2 A Reference to the Eddy Viscosity in SBL

The eddy stress in X direction is given by $\tau_{zx} = \mu_{ex} du/dz$. Let the eddy stress for the SBL be τ_0 . Therefore,

$$\tau_0/\rho = (\mu_{ex}/\rho) (du/dz) - K_m (du/dz) \quad (1.13)$$

where K_m is the eddy viscosity (or kinematic coefficient of eddy viscosity for momentum). From equation (1.13)

$$K_m = (\tau_0/\rho)/(du/dz) \quad (1.14)$$

But $\sqrt{\tau_0/\rho} = u_*$. Therefore $\tau_0/\rho = u_*^2$ ie., $K_m = u_*^2/(du/dz)$. But $du/dz = u_*/l_x$. Therefore,

$$K_m = u_*^2/(u/l_x) = l_x u_* \quad (1.15)$$

But $l_x = kz$, so that,

$$K_m = k u_* z \quad (1.16)$$

Hence, the eddy viscosity increases linearly with distance from the surface. Since k is about 0.38 and u_* is normally of the order of 10 to 20 cms^{-1} for winds over smooth ground, at a height of 100 cm above the surface, K_m will be in the order of

Table 1.1 Typical values of Zero Plane Displacement (d) in metre

Surface	Remarks	d (m)
Water	Still-Open Sea	
Ice	Smooth	
Snow		
Sand, Desert		
Soils		
Grass	0.02 - 0.1 m	≤ 0.07
	0.25 - 1.0 m	≤ 0.66
Agricultural Crops		≤ 3.0
Orchards		≤ 4.0
Forest	Deciduous	≤ 20.0
	Coniferous	≤ 30.0

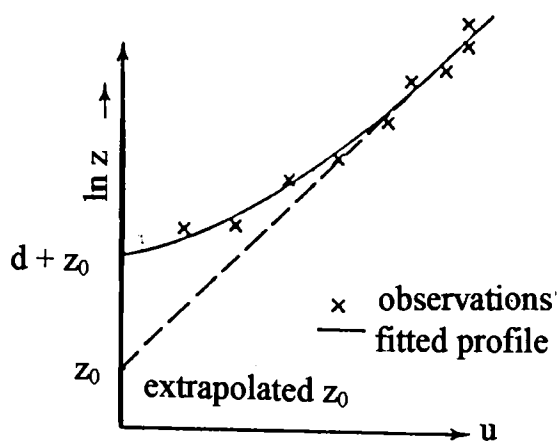


Figure 1.7 Logarithmic wind profile over a very rough surface

$10^3 \text{ cm}^2\text{s}^{-1}$. This is in agreement with estimates made by observations and the result can be stated that the mixing length is of the same order of magnitude as the height of the reference plane above the surface.

1.6.3 The Diabatic (Non adiabatic) Wind Profile

In a diabatic atmosphere, the thermodynamic change of the state of system is one in which there is transfer of heat across the boundaries of the system (Huschke, 1959). A general formula for the diabatic wind profile can be derived (Panofsky and Dutton, 1984). The non-dimensional wind shear can be defined as

$$kz/u_* (\partial u/\partial z) = \phi(z/L) \quad (1.17)$$

which represents the mean wind profile in the SBL or $\partial u/\partial z = (u_*/k) (1/z) \phi(z/L)$, if one adds and subtracts 1 on the right hand side of this equation and integrates from the ground where $z = z_0$ and $u = u_0$ to an arbitrary height z , one gets

$$u = u_*/k[\ln(z/z_0) - \psi(z/L)] \quad (1.18)$$

In equation above, ϕ and ψ are universal functions of height z , relative to the similarity scale L (Monin-Obukov length). The Monin-Obukov length L depends on both the shear stress (u_*) and the heat flux $H = \rho C_p w' T'$. This relation is given by

$$L = u_*^3 T' / kg w' T' \quad (1.19)$$

The equation (1.18) can be written as

$$u = u_*/k[\ln z/z_0 - \psi(Ri)] \quad (1.20)$$

where Ri is the Richardson Number and which is non-dimensional ratio of thermal stability to wind shear.

$$Ri = (g/\theta) (\partial\theta/\partial z)/(\partial u/\partial z)^2 \quad (1.21)$$

Since the denominator is always positive, the sign of Ri depends on the term $\partial\theta/\partial z$ in the numerator. In other words, under stable conditions (where θ increases with

height so that $\partial\theta/\partial z$ is positive) Ri is positive. On the other hand, under unstable conditions where θ decreases with height such that $\partial\theta/\partial z$ is negative, then Ri is negative. Under adiabatic conditions $\partial\theta/\partial z = 0$ and $Ri = 0$. In unstable air,

$$Ri = z/L \quad (1.22)$$

which generally prevails during day times and in stable air, which mainly during night hours,

$$z/L = Ri/(1 - 5Ri) \quad (1.23)$$

Returning to equation (1.17), most atmospheric data are well represented (Busch, 1973; Panofsky and Dutton, 1984) by the following empirical formulations.

For unstable ($z/L < 0$) conditions,

$$\phi(z/L) = (1 - 16z/L)^{-1/4} \quad (1.24)$$

For neutral ($z/L > 0$) conditions,

$$\phi(z/L) = 1 \quad (1.25)$$

and for stable conditions,

$$\phi(z/L) = 1 + 5z/L \quad (1.26)$$

Now turning to equation (1.18)

$$\psi(z/L) = \int_{z_0/L}^{z/L} [1 - \phi(\zeta)] d\zeta/\zeta \quad (1.27)$$

where $\zeta = z/L$. In practice, z/L is usually quite small, so that

$$\psi(z/L) = \int_0^{z/L} [1 - \phi(\zeta)] d\zeta/\zeta \quad (1.28)$$

Under unstable conditions, Paulson (1970) gives that

$$\psi = \ln \left[\frac{(1+x^2/2)(1+x/2)^2}{(1-x^2/2)(1-x/2)^2} \right] - 2 \tan^{-1} x + \pi / 2 \quad (1.29)$$

where,

$$x = (1 - 16z/L)^{1/4}$$

and under stable conditions

$$\psi = -5z/L \quad (1.30)$$

1.7 Shapes of Wind Profiles in SBL

The wind field in the SBL is largely controlled by frictional drag imposed on the flow by the underlying rigid surface. The drag retards motion close to the ground and gives rise to sharp decrease of mean horizontal wind speed (u) as the surface is approached. In the absence of strong thermal effects, the depth of this frictional influence depends on the roughness of the surface. Davenport (1965) presents wind speed profiles for different types of terrain roughness (Figure 1.8) during strong winds. The depth of this layer increases with increasing roughness. Therefore, the vertical gradient of mean wind speed ($\Delta u/\Delta z$) is greatest over smooth terrain, and least over rough surfaces. In light winds, the depth z_g in Figure 1.8 depends upon the amount of thermal convection generated at the surface. With strong surface heating z_g is greater than in Figure 1.8 and with surface cooling it is less.

The surface layer of frictional influence generates a surface shearing force and transmits it downwards as a flux of momentum in the form of eddies. The main momentum possessed by different levels is proportional to the profile of wind speed which increases with height. In the Figure 1.9, consider the level z_3 . Due to the effects of forced convection generated by the surface roughness and the mutual sharing between air layers moving at different speeds, turbulent eddies are continually moving up and down through z_3 . An eddy arriving at z_3 having

originated at z_4 above will impart a net increase in velocity (and hence momentum). So there in z_3 , this downdrafts experiences an increase in wind speed, or a "gust". Conversely, an updraft from z_2 would be sensed as a "lull" in horizontal wind speed. Due to the increase of wind with height, the net effect of both updrafts and downdrafts is always to sustain a net flux of momentum downwards. In neutral atmospheric conditions, where buoyancy is unimportant, such conditions are found with cloudy skies and strong winds. Cloud reduces radiative heating and cooling of the surface. Strong winds promote mixing and do not permit strong temperature stratification to develop. In the lowest layers forced convection due to frictionally generated eddies may be conceived as being circular and to increase in diameter with height (Figure 1.9). In reality they are three-dimensional and comprise a wide variety of sizes.

In unstable conditions, the vertical movement of eddies (and therefore the momentum flux) is increased. Near the surface, mechanical effects continue to dominate but at greater heights thermal effects become increasingly more important. This results in a progressive vertical stretching of eddies and a reduction of wind speed gradient as in Figure 1.10. Conversely strong stability arrests vertical movement, progressively compresses the eddies and steepens the wind gradient (Figure 1.11). Below lowest layers of SBL, the effects of forced convection dominates even in non-neutral conditions as long as there is a reasonable airflow. Above this height, the relative role of free convection grows and the possibility of stability effects on momentum transfer increases. These effects are manifested as curvature in the wind profiles from Figures 1.8 to 1.11. If the wind profile in Figures 1.9 to 1.11 are plotted in logarithm of height ($\ln z$) as Y-axis and mean wind speed (u) as X-axis, arrive to the Figure 1.12. The Figure 1.12 shows that a neutral profile makes straight line, unstable profile gives concavity upward and a stable profile concavity downward. In real atmospheric conditions, the SBL climatological profiles for different months march as in

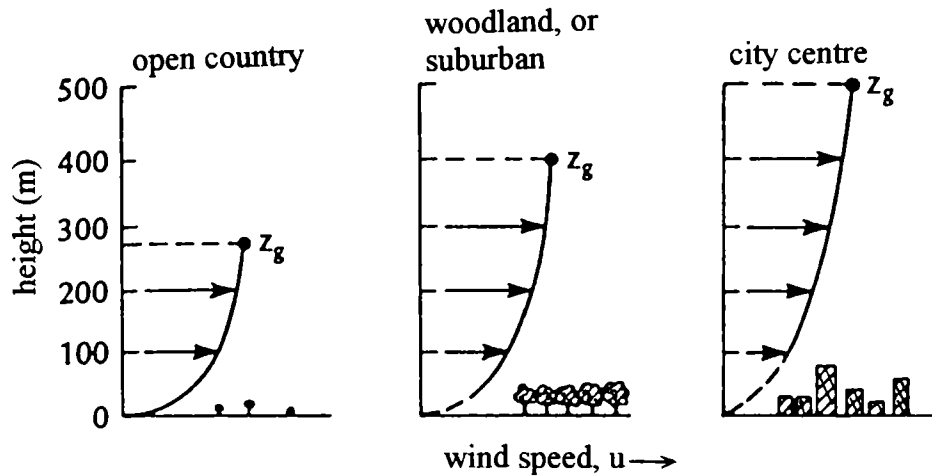


Figure 1.8 Wind speed profiles for different types of terrain roughness during strong winds.

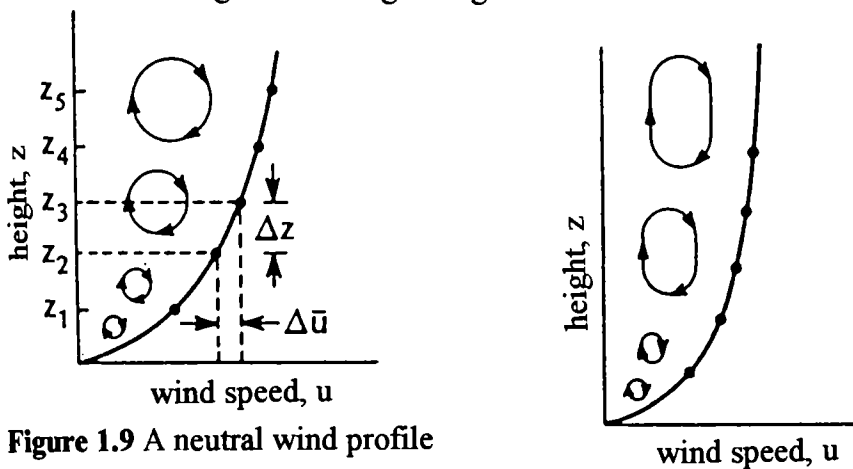


Figure 1.9 A neutral wind profile

Figure 1.10 An unstable wind profile shows reduction in wind speed gradient

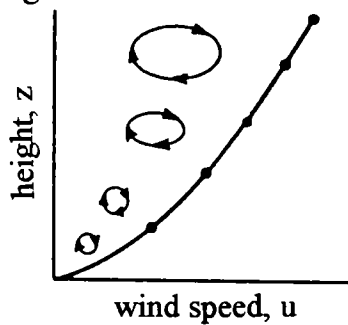


Figure 1.11 A stable wind profile shows steepening in wind speed gradient

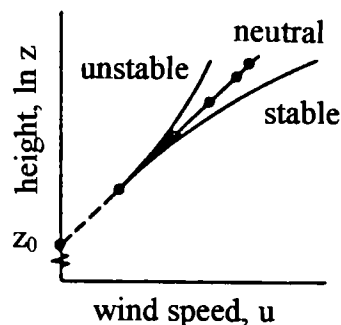


Figure 1.12 Figure 1.9 to 1.11 are plotted natural logarithm of height as Y axis

Figure 1.13 for the tropical coastal site Sriharikota, India. The Figure 1.13 gives an inference on long-term climatological profiles where unstable nature of steep slope in profile vanishes.

1.8 The Influence of Primary, Secondary and Tertiary Circulations in the Tropical Coastal Wind Environment

1.8.1 The Role of Primary Circulations

The lowest atmospheric layer wind environment in the tropical coastal stations is much influenced by circulations of meso-scale to planetary scale. In the primary circulations, interaction of general circulation features such as equatorial trough, ITCZ, equatorial westerlies and trades or tropical easterlies on the tropical wind flow are to be specified. The position, orientation, activity of these circulation features are totally depend on their seasonal variability. In equatorial latitudes, there is a weak usually broad trough of low pressure is the equatorial trough. In July, it is found in low latitudes of the northern hemisphere and in January it is displaced southward lying mainly in the southern hemisphere low latitudes. Within the equatorial trough is the ITCZ, along which north-east and south-east trade winds meet. In some latitudes, it is well defined, but in others it is weak or absent. During southwest monsoon season in India, the ITCZ activity is detected in the monsoon trough. As the trade winds cross the equator they are subjected to a change in the direction due to Coriolis forces, causes the north east trades of northern hemisphere to turn into north westerly flow in the southern hemisphere. Similarly, the south-east trades become south westerly after they penetrate into the northern hemisphere. These shallow equatorial westerlies are slightly concentrated in the summer hemisphere, they are poorly developed in the transition season. Beyond doldrums, (the belt of low pressure with calm or light variable winds near the equator) on either sides are two zones of steady wind mainly easterlies (north-east in northern hemisphere and south-east in southern

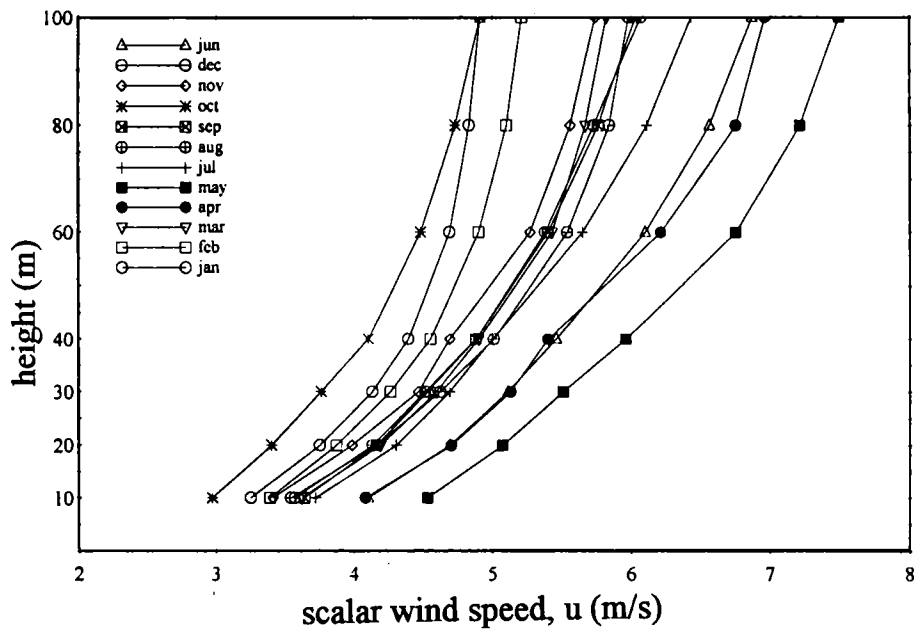


Figure 1.13 Long-term SBL climatological profiles march through different months at Sriharikota, India.

hemisphere). The flow may be weaker near equator and the boundaries. An average picture of surface wind flow and pressure pattern for representative months, January and July (Gedzelman, 1980) are depicted in Figure 1.14 and 1.15 respectively.

In the assessments of primary circulation features, the effects of day-to-day short term circulations are filtered out by averaging and smoothing over time and space. Finally the seasonal flow domination provides the climatological behaviour of the station's wind environment in both speed as well as in direction together with their steadiness.

1.8.2 The Role of Secondary Circulations

Secondary circulations constitute the links in the general circulation pattern for the exchange of air between the meridional and zonal wind currents. Secondary circulations and their behaviour are responsible for day-to-day changes in weather. They can be classified into thermal secondary circulations and dynamic secondary circulations, in which monsoons and tropical cyclones are of thermal origin and air masses are of dynamical origin.

The Asian monsoon can be compared to a giant sea breeze, with dramatic seasonal wind shift. During the northern hemisphere winter, the entire Asian landmass is cold. The ITCZ lies over the Indian Ocean south of the equator, whereas most of the southern Asia including Indian subcontinent lies under the sinking branch of the Hadley cell and therefore experience dry north east winds. These winds hold sway for several months as the continent gradually begins to warm up. After a transition period, the southwest monsoon sets in. The ITCZ moves northward, crossing India so that by July entire India experiences south west winds. This is attributed to Coriolis force on the trade winds from the southern hemisphere after crossing the equator.

Tropical cyclones and its stages such as low pressure system, depression, deep depression and cyclone can cause total disruption of seasonal wind flow

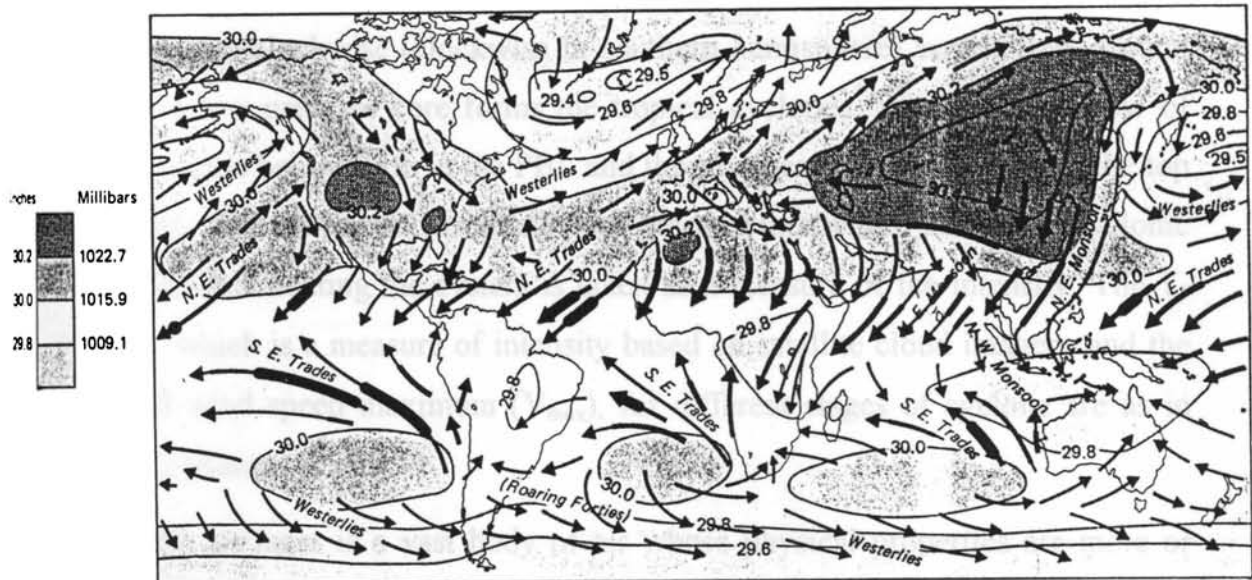


Figure 1.14 Average surface winds over the world in January. More constant wind direction depicted by thick arrows. Pressure behavior also presented.

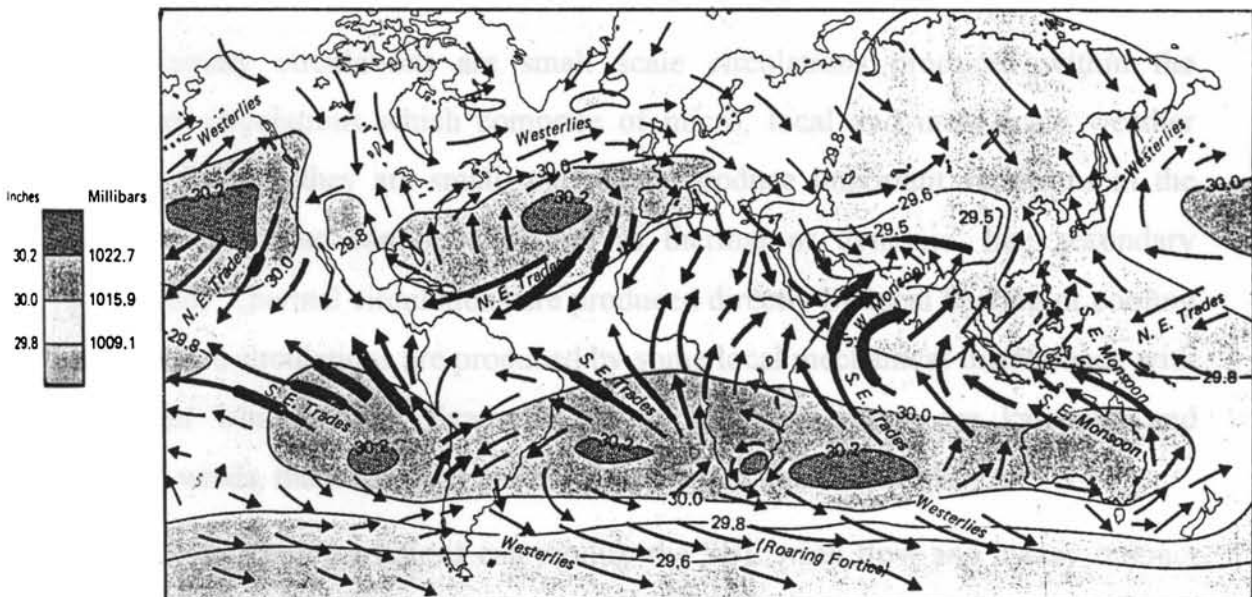


Figure 1.15 Average surface winds over the world in July. More constant wind direction depicted by thick arrows. Pressure behavior also presented.

pattern for days together. Trough movements towards coastal areas will also change the entire seasonal wind regime. In the northern hemisphere, the violently circulating anticlockwise (clockwise in southern hemisphere) vortex flow around an intense low pressure core forms the tropical cyclones. Most of the inflow of cyclone occurs below 1 km in the PBL and the strongest winds are found at the top of the SBL. The maximum sustained wind speed in the field of the closed cyclonic circulation demarcating the system is taken as a measure of the intensity. The T-Number, which is a measure of intensity based on satellite cloud imagery and the sustained wind speed maximum (V_{max}), for different stages of cyclone are as in Table 1.2 (Rama, 1998).

The air mass is a vast body of air whose physical properties are more or less uniform in the horizontal. They are not having direct influence on the wind field over the station, eventhough the weather phenomena, such as overcast cloudy skies with very low clouds and thunderstorm formations associate with air masses can impart sudden squally variations in the wind environment. Tropical maritime (Tm) and Equatorial maritime (Em) are the major air masses, which influence the tropical coastal weather.

1.8.3 The Role of Tertiary Circulations

Tertiary circulations are small scale circulations produced within the secondary circulations which comprise of micro, local and meso-scale weather features. Though they are small, they often produce important variations in the weather. They also can be classified as thermal or dynamic, like secondary circulations. Thermal circulations are produced directly by local heating or cooling and dynamic circulations are produced by some local mechanical interference with the larger wind system. Examples of thermal circulations are katabatic and anabatic winds, thermals, land and sea breezes and thunderstorms.

Topographic variations can modify the SBL wind flow and it may interact with diurnal heating cycle and can generate localised circulations. In many real

Table 1.2 Relation between T-Number, Vmax for various Stages of Tropical Cyclone

T- Number	Vmax (kmph)	Stages
1-1.5	45	Well marked low pressure
2.0	55	Depression
2.5	65	Cyclone
3.0	85	Cyclone
3.5	100	Severe Cyclone
4.0	120	Very Severe Cyclone
4.5	145	Very Severe Cyclone
5.0	165	Very Severe Cyclone
5.5	190	Very severe Cyclone
6.0	215	Very Severe Cyclone
6.5	235	Super Cyclone
7.0	260	Super Cyclone
7.5	285	Super Cyclone
8.0	315	Super Cyclone

cases, however, the existing meso-scale or synoptic-scale winds can modify, or even remove the weak geographic circulations. Local cooling at night results the gravitational downslope drainage of the locally cooled air to the bottom of deep valleys where very low temperatures are attained. This cooler and heavier air flow which slides downslope to the bottom of the valley makes gravity wind or katabatic wind (Figure 1.16). The reverse light denser air flow, after sunrise forms due to heating up of mountain slope results in valley wind or anabatic wind and it attains its maximum strength during afternoon (Figure 1.17). The uplift generally contributes convective anabatic clouds along the valley ridges. There can be anti-mountain winds and anti-valley winds as counter flow in both cases.

Winds modified due to non-uniform topographical features are having its own uniqueness, which depends on the landscape of the area. If the wind flow pattern is laminar over the upstream portion of the obstacle, may have turbulent flow just behind the obstacle produced by lee eddies. This phenomenon can be visualised in the real atmosphere of winds around an isolated hill (Figure 1.18(a)). Another two types of flow are shown in Figure 1.18(b) and Figure 1.18(c), where modifications of existing air flow affected by the perpendicular crossing of the flow over a valley and through a tunnel or a constriction. If stability of atmosphere is weaker and the winds are stronger, causing the natural wavelength of the air to match the size of the obstruction, like hill. By natural resonance, lee waves or mountain waves are formed and creates rotor circulations in the SBL (Figure 1.19(a)) or with very stronger winds, creates a cavity in the lee of the hill SBL, where reverse wind direction experiences (Figure 1.19(b)).

The wind flow in the SBL over an urban area can greatly modify by the heat island effect. Also large buildings can generate surface drag and wake turbulence in the natural SBL wind flow. Draxler (1986) pointed out the urban turbulence at night can create counter rotating vortices on opposite side of the city. Balling and Cerveny (1987) reported an increase in wind speed over the city at

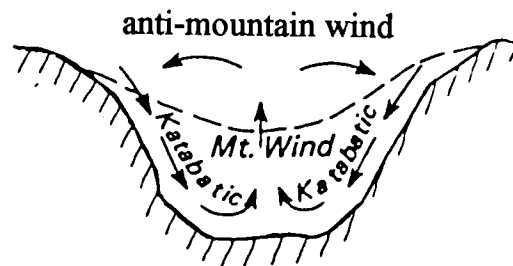


Figure 1.16 Katabatic or gravity wind system.

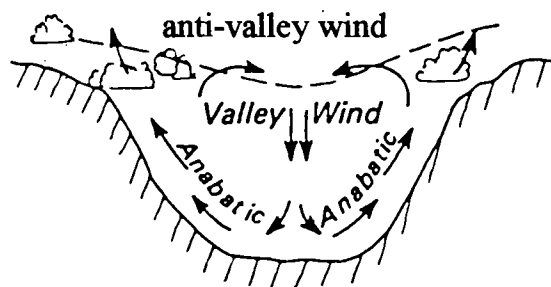


Figure 1.17 Anabatic or valley wind system

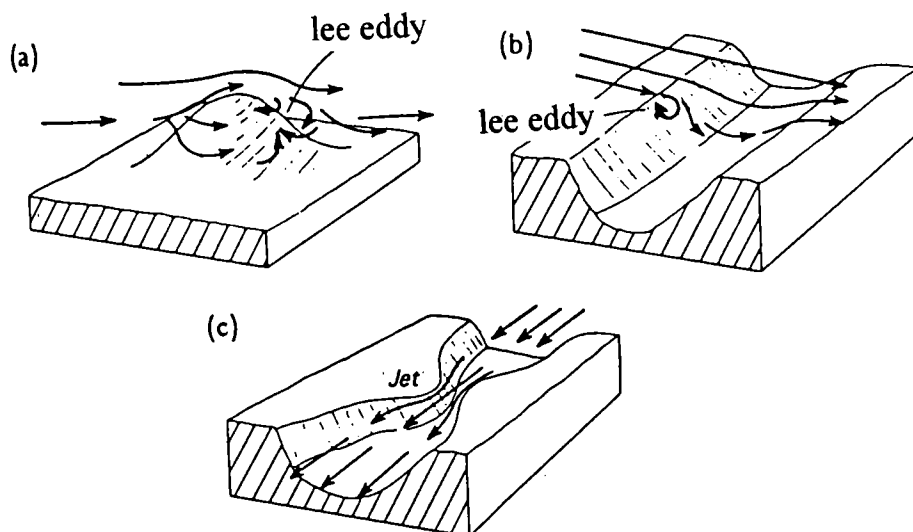


Figure 1.18 Geographical modification of SBL winds due to (a) an isolated hill (b) by perpendicular flow over a valley (c) flow through a tunnel

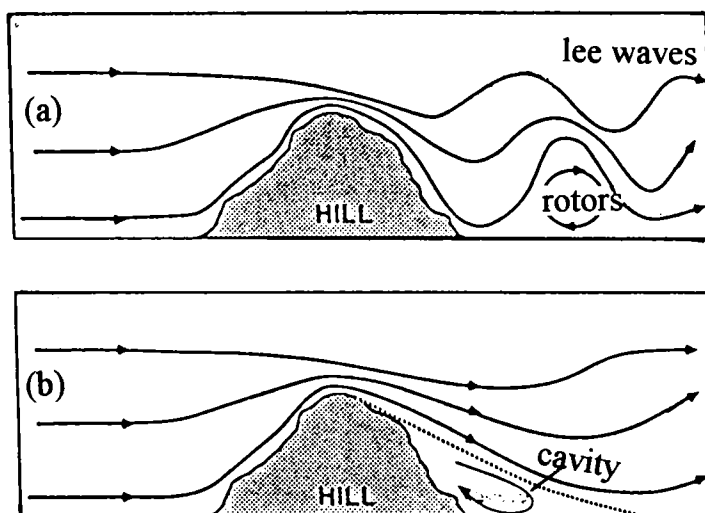


Figure 1.19 Flow over a hill when the natural wavelength of the air to the width of the hill (a) show lee waves and rotors, (b) shows cavity formation.

night. In calm wind conditions, closed wind circulations analogous to sea breeze can form over a warm city.

Thermals are tertiary circulations, in the shape of small vertical convection currents produced by local ground heating. Ideal conditions for the existence of thermals are clear sunny days with light prevailing winds over rocky or sandy surfaces devoid of vegetation. Dust devils are a type of thermals. The source region or the originating place of thermals are within lowest 2 m of SBL. Just above the source region, thermals encountered in the prevailing flow can create large turbulence in the SBL.

Sea-land breeze systems are very pronounced meso-scale phenomena of coastal areas. During day land surface gets heated up quickly than water surface. Hence the air rises from the land and pressure decreases. The temperature of the water remains cooler and the pressure becomes higher. Soon an onshore wind from sea (lake) to land or the sea breeze is established. In order to complete the circulation, there will be counter current at the upper levels of PBL. If background synoptic flow is absent, the sea breeze front can progress to land perpendicular to the coastline within less than 5 ms^{-1} and easily it can reach to 20 to 50 km inland at the end of the day. Sea breeze fronts from opposite shores if any can converge and collide during the day producing strong upward motions. Also sea breeze fronts with adequate moisture can trigger cloud lines and form thunderstorms. (Namboodiri et al., 1994). The sea breeze wind direction at low levels can be influenced with Coriolis force and baroclinicity between land and sea, can generate wind direction turning during course of day (Lyons, 1975), and pollutants emitted in the sea breeze can be recirculated back to the coastline. If the synoptic flow also in the same direction of sea breeze, it can cover more than 100 km if no obstacles are encountered. Pearson, et al., (1983) found, the speed of sea breeze front is a linear sum of the imposed background wind component perpendicular to the front, and the speed of the front in the still air. During opposite synoptic flow,

the sea breeze can arrest near the coastline or can be totally eliminated as the mean wind flows from land to sea. If synoptic flow is parallel to coastline, the sea breeze front becomes broader and diffuse.

At night the process of sea breeze is reversed. The land cools fastly while the sea remains warm. The offshore wind or land breeze blows from the land to sea at the surface level with a counter current from sea to land aloft. The wind associated with land breeze is lighter and short duration. The onset of sea breeze is abrupt, whereas land breeze is of slow onset. As insufficient studies on the propagation of land breeze over waters, the stretch of land breeze to sea is unclear. An artistic view of sea-land breeze is in Figure 1.20(a) and Figure 1.20(b)

Extreme manifestation of atmospheric instability leads to thunderstorms are meso-scale systems. They can form due to diurnal heating process, when the area of formation is favoured with a process which produce adequate supply of moisture towards its saturation and conditional instability aloft. The major vulnerability of thunderstorms to the SBL is through its high wind potential. The downdrafts from thunderstorm lead to drastic change in wind speed and direction (Fujita, 1955) called as squall. In the coastal areas of India squall can reach even more than 30 ms^{-1} associated with super thunderstorm formations. (Figure 1.21) The thunderstorms in tropical coastal areas are associated either with diurnal heating during favourable conditions or with low pressure systems.

1.9 Wind Observational Techniques and Platforms in SBL

Early wind measuring methods include non-instrumental practices. In 1805 Admiral Sir Francis Beaufort encountered the problem of finding out wind speed qualitatively, known as Beaufort scale (Table 1.3). Vegetation deformities can be a good indicator of high wind sites. Hewson et al., (1979) derived Griggs-Putnam index in order to give qualitative picture of wind intensity through various degrees of tree deformity (Figure 1.22(a)). Species of trees should be the same while

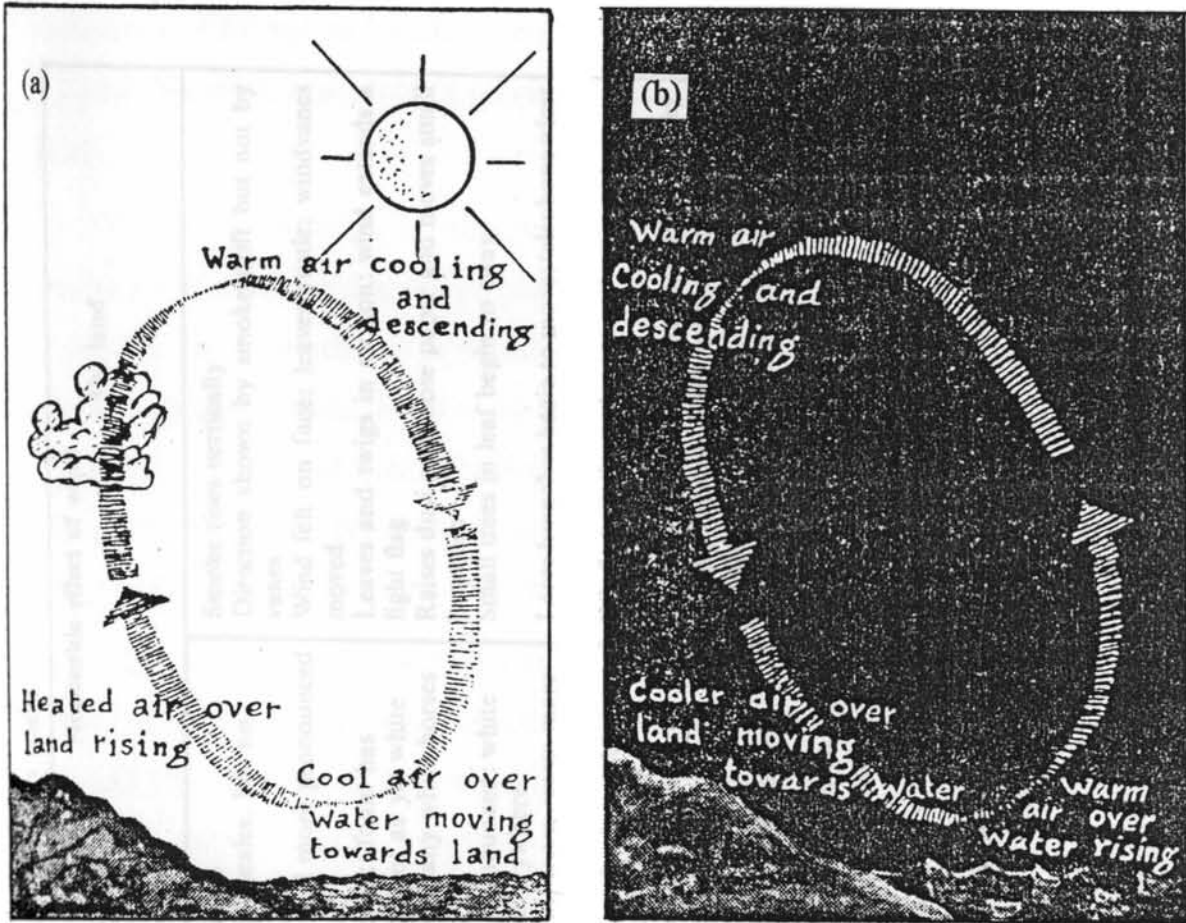


Figure 1.20 (a) Sea breeze wind system. (b) Land breeze wind system

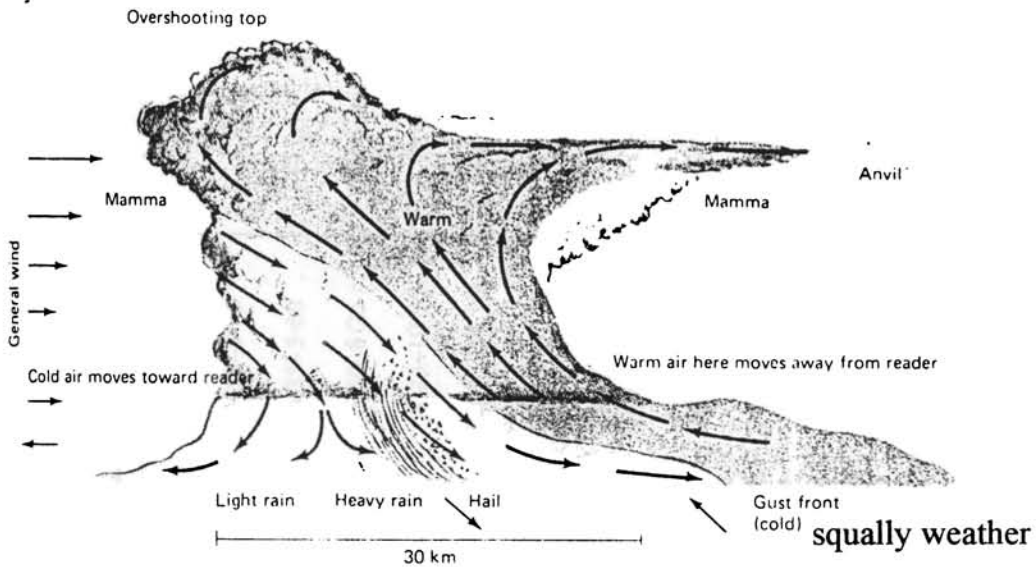


Figure 1.21 Schematic picture of supercell thunderstorm

Table 1.3 Beaufort scale

Beaufort range	Hourly average windspeed limits of ranges (m s ⁻¹)	Description of wind	Noticeable effect of wind	
			At sea	On land
0	<0.45	Calm		Smoke rises vertically
1	0.45-1.55	Light	Sea is mirror-smooth Small wavelets like scales, but no foam crests	Direction shown by smoke drift but not by vanes
2	1.55-3.35	Light	Waves are short and more pronounced	Wind felt on face: leaves rustle: windvanes moved
3	3.35-5.60	Light	Crests begin to break: foam has glassy appearance, not as yet white	Leaves and twigs in motion: wind extends a light flag
4	5.60-8.25	Moderate	Waves are longer: many white horses	Raises dust and loose paper and moves small branches
5	8.25-10.95	Fresh	Waves are more pronounced: white foam crests seen everywhere	Small trees in leaf begin to sway
6	10.95-14.10	Strong	Larger waves form: foam crests more extensive	Large branches begin to move: telephone wires whistle
7	14.10-17.20	Strong	Sea heaps up: foam begins to blow in streaks	Whole trees in motion
8	17.20-20.80	Gale	Waves increase visibly: foam is blown in dense streaks	Twigs break off: progress generally impeded
9	20.80-24.35	Gale		Slight structural damage occurs: chimney pots removed
10	24.35-28.40	Strong gale	High waves with long overhanging crests: great foam patches	Trees uprooted: considerable structural damage
11	28.40-32.40	Storm	Waves so high that ships within sight are hidden in the troughs: sea covered with streaky foam:	Damage is widespread: seldom experienced in England
12	> 32.40	Hurricane	Air filled with spray	Countryside is devastated: winds of this force are encountered only in tropical revolving storms

comparing winds of two places through this index. Deformation pattern based on asymmetry of foliage and angle of growth of the trunk is another indicator (Figure 1.22(b)). Wind sacs provide a quick look about the wind directions in industrial areas.

Different varieties of structures, from masts to tall television towers, microwave towers or micrometeorological towers dedicated to take measurements in the SBL are as platforms to mount instruments to measure winds according to the level of applications. Both wind speed and direction are highly variable. That variability in space and time is having great significance in selecting wind sensors for specific purposes. Wind observation sensors can be categorised into two, such as slow-response wind sensors and the other is fast-response wind sensors.

Cup anemometers, propeller anemometers and wind direction vanes are in the list of slow-response wind sensors and they are well established by its virtues in simplicity, ruggedness and dependability. For mean wind speed and direction readings, they perform excellent job. A common configuration for cup anemometer - wind vane system is a three cup wind speed sensor and a direction vane installed side by side on a common mounting axis. Cup anemometers does not require any alignment to wind direction. Typical starting speeds are 0.5 ms^{-1} , and distance constants (63% recovery time converted to distance) between 2 and 5 m with an accuracy of $\pm 1\%$. Estimates of "overspeeding" error range from 5% to 10%. In propeller anemometers "overspeeding" can be eliminated, but they operate most dependably when pointing directly into the wind. Two and four-blade propellers are available, the later performs for low wind speeds ($0.5 - 35 \text{ ms}^{-1}$), and the propeller can be flat or helicoid. True cosine response have to be made when they are in a fixed configuration, otherwise correction to true cosine response are to be incorporated in order to get correct values. Accuracies and distance constants for propeller types are comparable to cup anemometers.

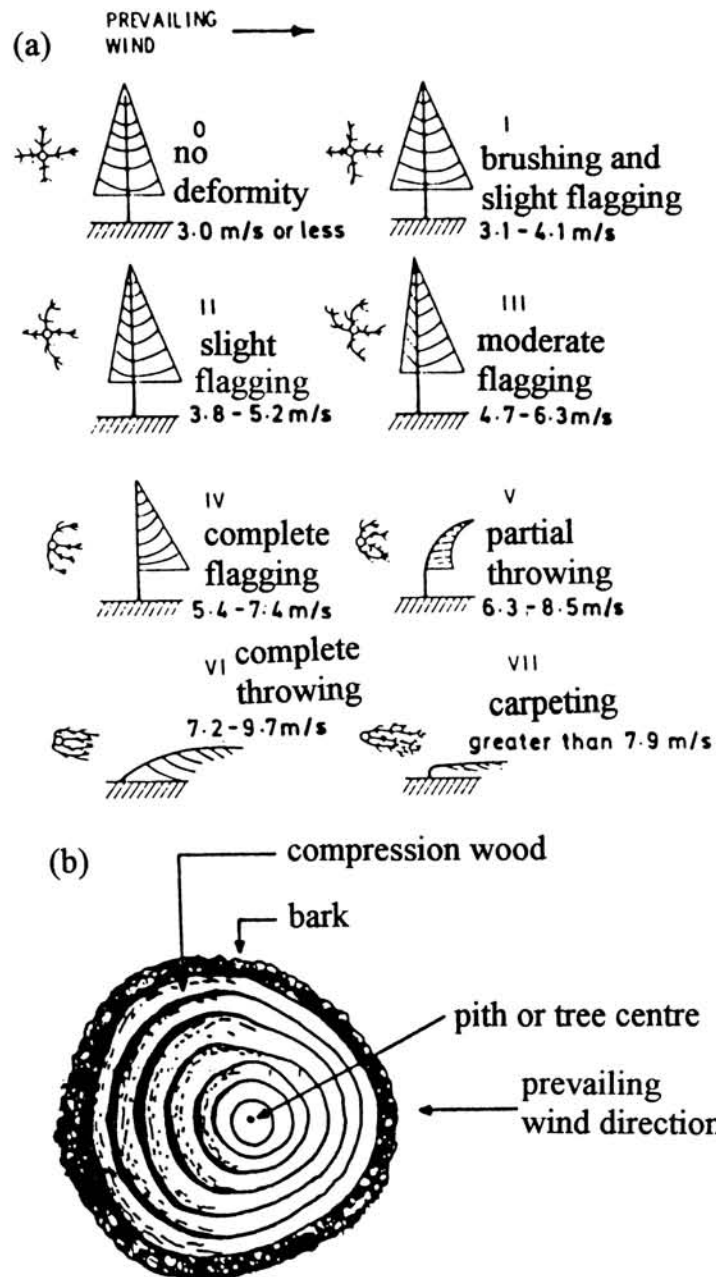


Figure 1.22 (a) Griggs-Putnam index, the wind speed scale based on the degrees of tree deformity (b) tree trunk cross-section of a tree growing in a windy location.

Fast-response wind sensors are particularly used for turbulence studies. No other sensor can match the high frequency resolution (on the order of 10 kHz) of the hot-wire anemometer in the generation of fast-response wind sensors. The susceptibility to calibration shifts in atmosphere and fragility are two major drawbacks of hot-wires. Generally, fast-response wind sensors are to be used in SBL from days to week in order to gather time series data on turbulence properties. In such cases sonic anemometers are highly preferable, as they are deprived of drawbacks like in hot-wire anemometers. Different SBL wind measuring methods and the principle of operations are tabulated in Table 1.4

Instrument platforms provides the physical and structural support for the sensor. The common platforms in SBL wind monitoring are masts, towers, and kytoons.

A mast is a pole upon which instruments can be placed at different heights. A typical mast height is 10 m to 50 m and they are inexpensive and easy to erect. Wires carry the signals down the mast to a data logger or data trailer close by.

Towers are dedicated platforms for micrometeorological observations, and they are expensive. A microwave tower performs the need for observations in some extent. Meteorological towers are large structures with built in elevators and many support guy wires. Because towers are so large and rugged to stand for any type of extreme winds over an area, it disturbs the flow close to it and downwind of it. To avoid this, these towers have large horizontal booms that project horizontally away from the tower at different heights, upon which sensors are mounted. Permanent buildings for data loggers, communication maintenance and computer facilities are to be available along with tower facilities.

Kytoon is an aerodynamically shaped helium/hydrogen filled plastic balloon that is tethered to a winch on the ground, and the shape allows it to soar upward. In typical application, a sensor package is suspended a short distance below the balloon on lines different from the tether lines. To make measurements

Table 1.4 Wind Measuring Sensors/Scales and Principle of Operations

Sensors/Scales	Method/Principle
Cup Anemometer	Drag against cups causes rotation on axis perpendicular to wind.
Propeller Anemometer	Turns blades on axis parallel with wind
Hot Wire Anemometer	Electrical current needed to maintain temperature of wire against cooling of wind
Sonic Anemometer	Speed of sound
Pitot Tube	Dynamic pressure increase associated with deceleration of wind into orifice.
Drag Sphere	Drag force experienced by sphere, measured by strain gauges.
Pivot Arm	Hanging rod or plate that is blown against gravity or spring.
Gust Vane	Measures v' and w' via lateral forces on vane.
Pibal	Pilot Balloon tracked by theodolite
Venturi	Pressure drop related to Bernoulli effect
Rotometer	Fluid moving vertically in conical tube lifts a ball in tube.
Wind Vane	Points in horizontal compass direction wind comes from.
Bivane	Pivots up/down as well as left-right to give elevation angle and compass direction.
Beaufort Scale	Noticeable effect of wind on sea/land.
Griggs-Putnam index	Vegetation deformities
Fujita Scale	Damage assessments.

at different heights, the winch is used to draw in or feed out more line until the desired height is reached. The balloon is kept at each height of interest for 5 to 30 minutes to gather a statistically stable sample, before altering its altitude. While ascending and descending of kytoon, it can make observations. Data transmission can either through cable attached with the tether or tele transmission. Kytoons are available even upto 2 km, and they are excellent in temporary field experiments, but they are limited to light winds.

1.10 Wind and Flow

The winds in the SBL are characterised by very complicated three-dimensional flow patterns with random variations in space and time. The random wind can be divided into mean wind, turbulence and waves. Mean wind is responsible for very rapid horizontal transport or advection. They can be derived into its components based on its magnitude and direction, which gives horizontal components (u,v) of wind. The wind direction is measured in degrees clockwise from true north and is the direction from which the wind is blowing. The wind magnitude (the modulus of the vector) is the scalar quantity and is referred to as wind speed or scalar wind. A statistical description that accounts for the wind as a vector quantity appropriate and requires a coordinate system. In Figure 1.23, the polar and Cartesian forms for the meteorological coordinate systems are defined.

V = Wind speed, scalar wind, or magnitude of the wind vector in ms^{-1}

θ = Wind direction, θ is measured in degrees clockwise from true north and is the direction from which the wind is blowing.

u = Zonal wind component, positive west to east and negative east to west in ms^{-1} .

v = Meridional wind component, positive south to north and negative north to south in ms^{-1} .

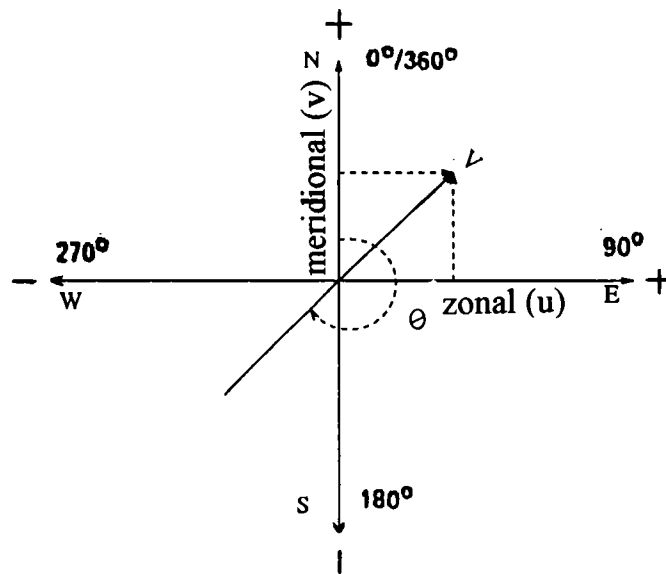


Figure 1.23 Meteorological coordinate system for wind representation.

The components θ and V define the polar form, and the u - v components define the Cartesian forms.

$$u = -V \sin \theta, \quad 0 \leq \theta \leq 360^\circ \quad (1.31)$$

$$v = -V \cos \theta$$

Figure 1.24(a) gives scalar wind speed (V) and Figure 1.24(b) gives zonal and meridional components (u, v) as a random process for three levels (20, 60, 100 m) in the tower layer. In this real situation the turbulence or perturbations (V') are superimposed on a mean wind (\bar{V}), such as

$$V = \bar{V} + V' \quad (1.32)$$

The term mean denotes an average over a time interval. Different statistical properties are to be studied in order to model the process of randomness in wind variable (Figure 1.25)

1.11 Potential Applications of Surface Boundary Layer Wind Modelling

The characteristics of wind in the SBL are of major significance as a source of aerodynamic loads imposed on aerospace vehicle during launch operations. Also in the exploration of wind energy studies, air pollution impact assessments, structural design works, weather forecast modelling, runway constructions and aviation meteorology, winds of this region are of major concern. Temporal and spatial variation studies conducted to investigate the vertical structure of horizontal wind field through statistical and mathematical micro-meteorological models as well as studies to know the wind flow during extreme weather conditions poses a quite lot of applications.

In Aerospace and Range meteorology, critical monitoring and prediction of winds in the SBL are so sensitive in static testing of rocket motors, safe propellant loading operations, transport of motors and satellite for integration to launch pad, in order to set sounding rockets on the launcher to minimise the effect of winds on

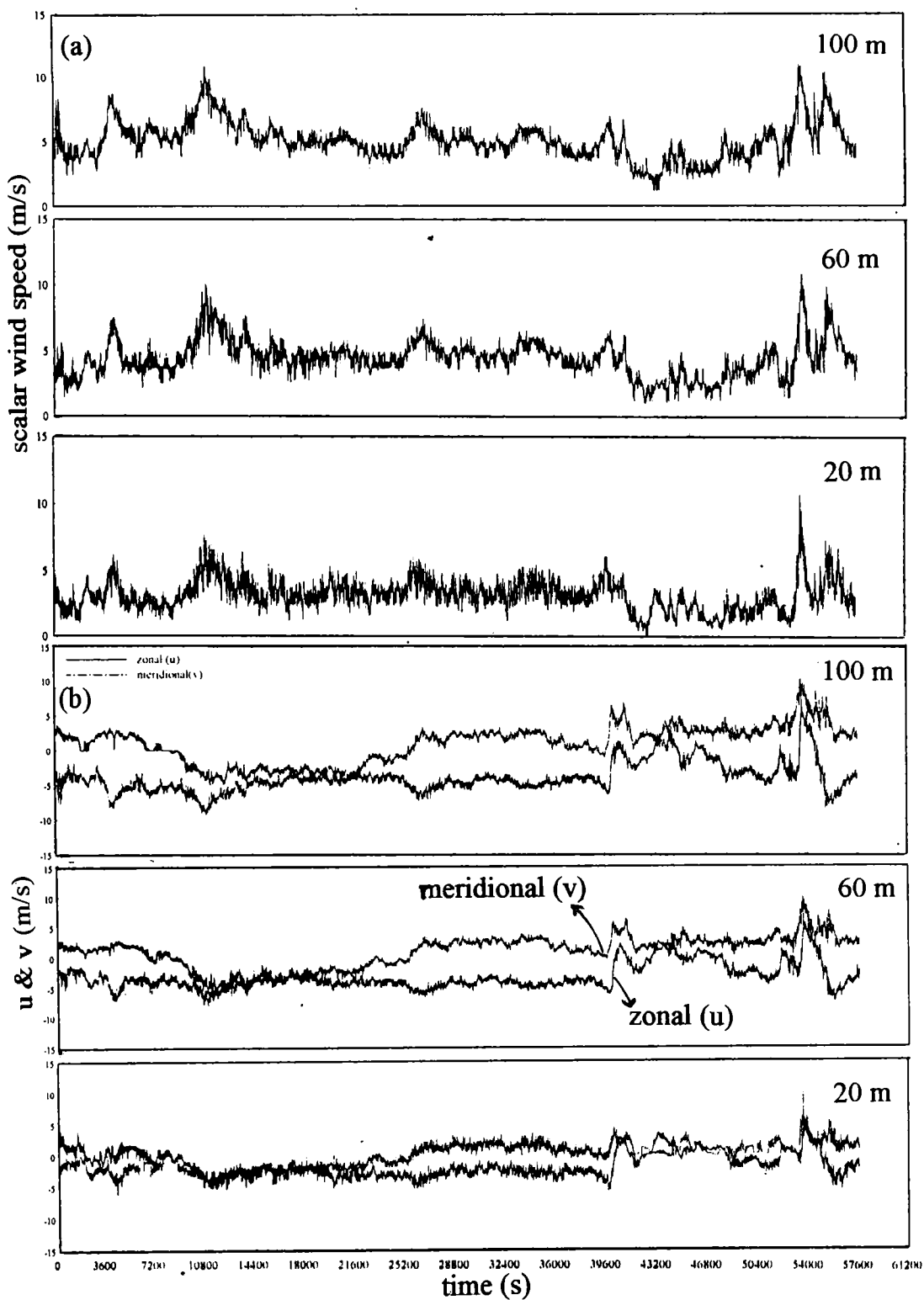


Figure 1.24 Time series random process of wind variations at different SBL levels at Sriharikota, India. (a) scalar speed variation (b) wind component (u,v) variation.

05th October 1999::from 1615 IST

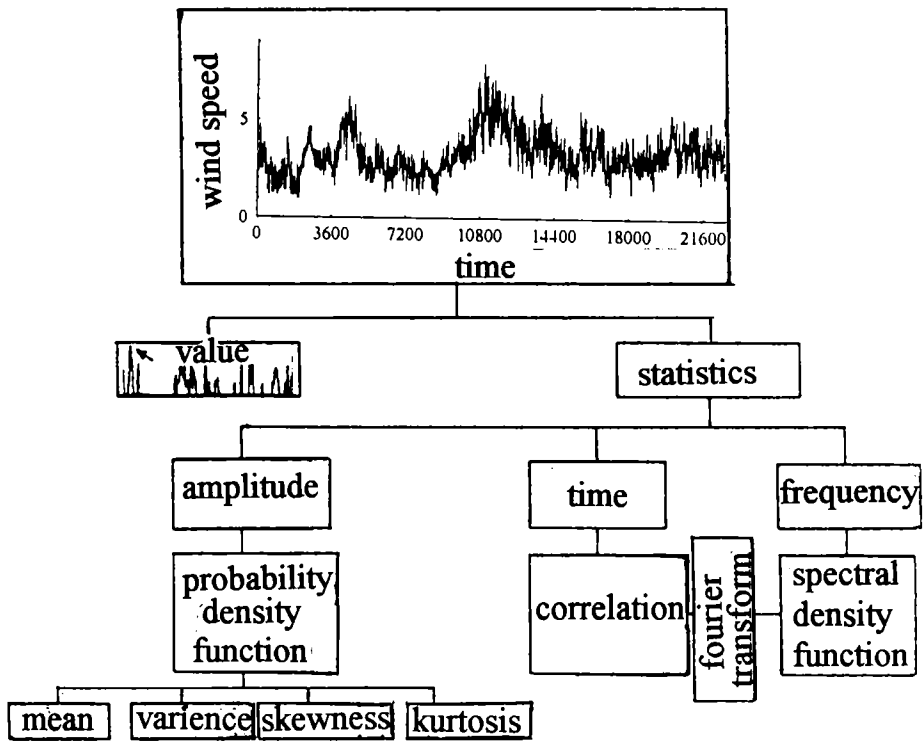


Figure 1.25 Statistical description of wind as a random process.

the nominal trajectory and to ensure positive clearance of launch vehicle from pedestal ring during lift-off.

Of the several alternative energy sources, wind is the most suitable and cost-effective for electric power production. The micro-siting for the generation of climatological wind maps and wind power, critical wind energy extraction assessments need lot of SBL wind flow pattern modelling studies. The importance of wind energy is enormous, as just 1% of Earth's winds could theoretically meet the entire world's needs. Not only is wind power plentiful, but it is popular with the public because of its environmental benefits, such as no contribution to pollution, acid rain, global warming or ozone destruction.

Regulatory agencies need appropriate meteorological data as an important inputs to air pollution modelling exercise, in which wind in SBL is of prime notice. On-site measurements of wind speed and direction assess the transport path of the plume. Also atmospheric stability derivation and its diurnal variations is required for fixing pollutants disposal timings.

In structural operations, construction efficiency may decline when wind speeds more than 7 ms^{-1} by standards. Wind stresses on partially completed structure may cause damage at speeds well below the design wind speed for the completed structure. Managing for crane operations, loose material handling are difficult in high wind speeds. Winds combined with other weather elements cause corrosion and rusting. In tropical areas studies on design wind speeds at different height levels in SBL is required for either low-rise or high-rise buildings, as tropical areas are known by the occurrence of thunderstorms and cyclones.

Micro and meso-scale meteorological modelling parameterization process, surface layer scaling parameter inputs are required for prognostic modelling. Knowing structure of turbulence and spectral estimates paves some proof to theoretical considerations. Derivation of surface roughness parameter gives topographical and wind flow directionality fixations in such models.

In runway constructions or in any transportation demands, require steady-state wind inputs, through proper statistical models. From conventional wind rose to theoretical wind distributions provide its suitable applications in the wind persistency.

In aviation meteorology, low level wind shear is hazardous to landing and departing operations to aeroplanes. Effect of head wind and tail wind on aircraft, can lead projection down or up from the landing glide slope flight path. Also there can projection down or up from nominal climb-out path during take off with enormous variations in head and tail winds. The increasing right to left cross winds in the aerodrome, project flight path to left, and decreasing right to left cross wind can project path to the right. So GO or NO GO decisions for aircrafts to be planned based on the behaviour of SBL winds.

1.12 Relevance of SBL Wind Modelling Studies in SHAR Centre, ISRO, India

As the investigations are made in the space port of India, SHAR Centre of Indian Space Research Organisation, the utilisation of such a specialised study is of significant consequences in the ongoing crucial Range and Aerospace applications. The SBL wind concerned activities in the Range are briefed here.

Critical monitoring and prediction of wind flow in the lowest layers of atmosphere are so essential in static testing of rocket motors, safe propellant filling operations and in the transportation of various vehicle components. Diurnal climatology of various wind parameters, exceedance probability, extreme wind informations are suitably in application for planning various launch missions. The advent of high altitude performance of unguided sounding rockets has made the consideration of factors causing trajectory deviations or dispersion a necessity. One of the major contributors to the dispersion of an unguided vehicle is wind, and real time SBL wind monitoring is essential in order to fix the rocket in launch pad for lift off with minimum deviation from a planned trajectory. The process of

finding out the angles (elevation and azimuth) the rocket is to be fired for getting maximum performance is called wind weighting.

It is well established that wind loads are a primary design input for various class of guided rockets. SBL wind considerations have established some ground handling requirements. Winds and turbulence associated with extreme weather events like thunderstorm outflows, low pressure systems are critical factors in operational considerations. It is impossible to design a satellite launch vehicle so that it can perform its mission with sufficient structural margin to insure integrity under all conceivable unions of wind velocity, wind shear and turbulence or gustiness. Hence, a major consideration in the decision to launch is the ambient wind.

For planning a launch in particular time window, the pre-launch and during launch window environment effects are to be specified from various wind derived parameters. There are three primary sources of wind loads in the pre-launch and launch regimes-steady state drag loads resulting from mean scalar wind speed in the entire height of rocket, unsteady drag loads resulting from wind direction fluctuations which in turn arising from wind gusts and turbulence. Wind gust steady inputs can be derived from gust factor and turbulence steady components by coefficient of variation. Steadiness in wind can both expressed by steadiness factor and standard deviations in wind directions. The third wind loads affecting the rocket is lateral unsteady loads associated with vortex shedding. SBL wind concern is so critical just at the time of lift off (lift off dynamics) so as to get enough clearance between the vehicle and the umbilical tower support. The launch vehicle designer needs to know the effects of the wind environment on control, stability, structural loads and ground handling requirements, namely (1) on the basis of past experience (2) by means of tests with mathematical as well as statistical wind models.

Wind effect on aerospace launch facilities can have significant consequences for the design of those facilities. Strong winds from cyclones and thunderstorms can affect launch facilities. Because of the unique nature of launch facilities and the often thin margin of safety requirements, wind loads can seldom be adequately specified from building codes or standards. Wind effects for aerospace facilities include wind loads for structural survival in extreme wind events, and for operational phases such as vehicle erections and mobile service tower movement, translation of winds from a meteorological tower to launch site, prediction of gas concentrations at critical locations from rocket exhausts or from accidental gas releases, and prediction of heat transfer. For all these a detailed vertical climatological structure of winds in various conditions are to be quantitatively specified.

Wind shear near the surface (for design purpose) is a shear which acts on a space vehicle free-standing on the pad or at the time of lift off. The design wind shear is computed from the selected design percentile wind speed envelope by using peak wind speed at the top of the vehicle and quasi-steady state wind speed at the base of the vehicle with respect to the height of the base above the ground. Peak wind speed samples introduced the concept of exposure period probabilities into the design and operation of space vehicles. To perform loading and response calculations resulting from steady state random turbulent loads and von Karman vortex shedding loads, the engineer requires information about the vertical variation of mean wind speed and the structure of turbulence in the SBL. The procedure is to extrapolate the peak wind statistics upward into the atmosphere with a statistical peak wind profile model and to obtain the associated mean wind speed profile by dividing the peak wind speed with a gust factor which is a function of speed and height. At this point, the engineer can calculate the steady-state loads resulting from the mean wind profile and the response due to discrete gusts. The gust factor accounts for the loads beyond these resulting from the quasi-

steady state wind profile-in short the turbulence. In some aerospace applications, representation of the turbulence can be given in the form of a spectral model, especially spectral characteristics associated with extreme weather conditions. Once mean wind speed profile, surface roughness parameter or frictional velocity are known, the spectral properties can be normalised in representations.

In all respect, the ever changing engineering demands for rocket launch operations and in the construction of launch facilities, a wide spectrum of wind modelling studies are required.

Chapter 2
Literature Review

2.1 Wind Measurement and Archival in Automatic Surface Wind

Observations

Wind sampling strategy and archival methods are of serious concern among potential wind users requirements. The concerns mostly relate to wind observations that do not conform to international recommendations for averaging period, short averaging periods representative of small-scale motions rather than large-scale motions that have predictability. The scales of atmospheric motion and its link with wind spectra in the frequency range from 0.0007 to 900 cycles per hour was studied by Van der Hoven (1957). Smedman-Hogstrom and Hogstrom (1975), Panofsky and Dutton (1984) and Champagne-Phillippe (1989) are studied about the position of spectral gap in the wind spectrum. Champagne-Phillippe (1989) computed spectral density from 12 hr of consecutive 3 s average wind data from 10 m masts (14400 points) in a coastal station. They reported that the low frequency peak caused by synoptic and meso-scale weather systems with time scales greater than 1 hr and high frequency peak near 1 min due to micro-scale turbulence, and the spectral gap correspond to time periods of 10-100 min. Pierson (1983) suggested that the spectral gap movement is dependend on wind speed. According to Panofsky and Brier (1965) the wind measurements with averaging periods corresponding to the spectral gap are unaffected by small-scale turbulent fluctuations. There are recommendations of averaging times for surface wind observations, based on the positioning of spectral gap as 4 min averaging by Sparks and Keddie (1971), 20 min averaging by Pierson (1983) and 1 hr by Panofsky and Dutton (1984). The capability of wind measurements, averaged over time periods within the spectral gap to separate scales of motion, will depend upon the frequency of measurement, density of observing site, the compatibility of the media to storage and retrieval, and easy handling of data for different mathematical as well as statistical analyses.

Powel (1993) conducted an informal survey among representatives from several user groups, concerned about Automatic Surface Observing System (ASOS) in wind sampling strategy and archival methods. He summarised that the optimum averaging time for surface wind observations depend upon applications. In ASOS, the sampling strategy is for every second collection of speed and direction data. Five second averages of speed, direction along with peak (gust) in the five seconds are computed, from the collected every second (raw) data. Further, two min averages are derived out of 5 s means (out of 24, five second means). The last 2 min data in an hour archived at the end of an hour, represents surface hourly observation, along with the peak (gust) of that last 2 min derived by using 5 s peaks (24 peaks in 2 min).

The World Meteorological Organisation (WMO) recommends a 10 min wind average for synoptic observations from automatic weather stations and WMO suggests 2 min wind averaging periods for wind indicators in air traffic services (WMO, 1988). Numerical weather prediction suggest hourly or even 10 min frequency surface wind data may suffice (Stauffer et al., 1991). For dispersion and diffusion modelling of a particular site requires 1 hr averages and standard deviations of speed and directions, for a period of at least 1 year (EPA, 1987). In structural engineering applications, International Standard Organisation recommends a peak 2-3 s mean gust. 1 and 10 min mean winds occurring at the *time of peak* gust also having wide interest in structural analysis.

2.2 Wind Observations in Tower Platforms and Cup Anemometry

Towers offer convenient platforms for observing mean and turbulent properties of flow in the boundary layer. In air quality modelling and meso-scale observing networks small towers are in use and tall towers are necessary for assessing various boundary layer theoretical models. Towers, booms and mounts used for supporting a sensor can interfere with the wind flow (Moses and Daubek,

1961). They noticed that when the air flow on the lee side of the tower may be reduced to nearly one-half of its true value for light winds and nearly 25% for speeds of 10-14 mph. An increase in measured wind speed exceeding 30% occurred when the wind blowing toward the anemometer made an angle of 20 to 40° with respect to the sides of the tower adjacent to the anemometer. The effect on direction was relatively smaller, with greatest mean deviation of 11°. In general they found out the wind shadow effect, as when the wind blow through the tower before reaching the anemometer, there was a substantial reduction in speeds, the effect being greatest with high winds.

Accuracy of wind measurements on towers and stacks are studied by quarter-scale models in large wind tunnel by Gill et al., (1967). Their analysis showed that in the wake of lattice-type towers disturbances is moderate to severe, and in the wake of solid towers and stacks there is extreme turbulence with reversal of flow. For an open triangular tower with equal sides D , the wake is about $1-1/2D$ in width for a distance downwind of at least $6D$. Sensors mounted $2D$ out from the corner of such a tower will usually measure speeds within $\pm 10\%$ of that of the undisturbed flow for an arc of about 330° . The disturbance by very dense towers and stacks is much greater. Wind sensors mounted 3 diameters out from the face of a stack will measure wind speeds within $\pm 10\%$, and directions within $\pm 10^\circ$ of the undisturbed flow for an arc of about 180° . The study made some recommendations on mounting of wind sensors. In relatively open towers in order to achieve measurements of wind speed that are accurate within $\pm 10\%$ of the true value, the sensor should be placed not less than $1D$ out from the tower, and extending outward from the corner into the wind of primary concern. Wind sensors should preferably be located at heights of minimum tower member density, and above or below horizontal cross members. For this configuration and location, measurement of speed are true within $\pm 10\%$ for a 310° sector of arc. If the boom is extended to $2D$, the wind speed is accurate within $\pm 10\%$ for a 330°

sector of arc. For these two arcs, the measurements of wind direction are accurate within at least $\pm 10^\circ$, and probably within $\pm 5^\circ$.

The measurement of atmospheric winds using cup anemometer and wind vane are common, and the errors in cup anemometer response to wind speeds are widely discussed (Wynngaard et al., 1974; Busch and Kristensen, 1976 and Kaganov and Yaglom, 1976). Hyson (1972) investigated into cup anemometer response to fluctuating wind speeds and noted that the anemometer overruns under fluctuating wind conditions and the percentage overrun depends on the wind speed, frequency, and amplitude of fluctuations. Surrige (1982) discussed the use of orthogonal propellers for the routine measurement of wind, and compares it with the traditional cups and vane system. In this study, prevailing winds are shown to be approximately the same for the two systems. It is also shown that the integration time of wind will have a marked effect on results.

2.3 Properties on SBL Wind Velocity Profiles

2.3.1 Wind Velocity Profiles

In air pollution and wind energy studies, knowledge of the mean wind profile is important. The logarithmic wind law has been found to satisfy observations in the lower atmosphere up to 100 m or more during adiabatic (neutral) conditions (Lumley and Panofsky, 1964; Tennekes, 1982). In diabatic conditions when the surface heat flux is significantly differ from zero, stability correction should be made to the logarithmic relationship. The stability corrections are important in the correct simulation of diurnal variation of wind speed. Also the frequency distribution of wind is affected by stability variations. Monin and Yaglom (1971) applied Monin-Obukhov similarity theory for the atmospheric surface layer in order to incorporate stability corrections. Dyer (1974) and Yaglom (1977) presented a review of flux-profile relationships for the diabatic surface layer. Logarithmic wind law represents the wind profile over uniform terrain up to

heights of at least 150 m in thick boundary layers with strong winds (Carl et al., 1973). Observed wind profiles up to 150 m over reasonably homogeneous terrain under neutral conditions do not seem to deviate significantly from logarithmic (Thuillier and Lappe, 1964). Hsu (1972) analysed the wind profiles for different timings over a flat coastal environment and reported that the diurnal variations in wind speed profiles are either concave upwards during day or concave downwards during night except during transitional period between land breeze and sea breeze (Hsu 1973).

2.3.2 Roughness Length or Parameter (z_0) and Frictional Velocity (U_*)

Andre et al., (1978) provided a sample of diurnal variation of frictional velocity. Charnok's relation (1955) relates Z_0 and U_* , which found quite useful for Z_0 computations over oceans. Typical values of the roughness length are obtained from Nappo (1977), Smedman-Hogstrom and Hogstrom (1978), Hicks, et al., (1975), Kondo and Yamazawa (1986), Thompson (1978) and Garratt (1977). Directional dependence of wind direction fluctuation (σ_θ) is studied at an Indian coastal site of Madras, with significant inhomogeneity in roughness elements distribution around the location of measurement (Panchal and Chandrasekharan, 1983). They suggested incorporation of Z_0 in Pansquill stability classification (Pansquill, 1961) in a non-homogeneous terrain. Pansquill (1974) relates U_* with wind direction fluctuation (σ_θ) which in turn can relates with surface roughness under neutral conditions. Hicks (1972) suggested relations connecting drag coefficient with frictional velocity and roughness length under neutral atmosphere. Ramachandran et al., (1994) has studied the variability of Z_0 for Indian coastal station, Thumba and noted that the Z_0 values are low during southwest monsoon season than in other seasons. Variation of Z_0 and its dependency on wind directions are also specified in their findings. For the same station, Sen Gupta et al., (1994) have shown that Z_0 is maximum when on-shore flow is perpendicular to the coast. When the wind flow is perpendicular to the coastline, the wind

experiences a sudden change in roughness from smooth sea to rough land surface. When the wind is parallel to the sea coast Z_0 has an average value of 0.07 m and for on-shore flow it is 0.25 m (Prakash, 1993). Narayanan Nair et al., (1994) showed that the U_* is height dependent for nonuniform terrain and for Thumba, U_* peaks at 1300 hr IST. Panofsky and Petterson (1972) computed Z_0 for the immediate surroundings of the tower vary with wind direction.

2.3.3 Power Law Wind Profile in Engineering Applications

For engineering applications *in situ* measurements of the roughness length Z_0 are not always available. Many wind profile laws, such as simple logarithmic distribution, cannot be applied. Therefore, many engineers have resorted to the power law wind profile, which, to a large degree, is quite accurate and useful for engineering applications (Panofsky and Dutton, 1984; Arya, 1988). From the recordings of many investigators, such as Davenport (1965), Panofsky and Dutton (1984) and Justus (1985), approximate values of the exponent in the power law can be obtained for practical coastal zone applications. Hsu (1982) obtained α for flat, open coast, towns and cities under different atmospheric stability conditions. The results show for unstable conditions $\alpha = 0.18$, for neutral conditions $\alpha = 0.22$ and $\alpha = 0.50$ for stable conditions. Narayanan Nair et al., (1994) found α for night time stable condition is 0.58 ± 0.02 , morning unstable conditions is 0.13 ± 0.04 , mid day turbulent internal boundary layer conditions is 0.25 ± 0.02 , and for evening neutral conditions 0.28 ± 0.05 for Thumba. Over smooth open terrain a value of α close to $1/7$ (or 0.14) is usually found with neutral lapse rate (Blackadar, 1960).

Zhang (1981) made a statistical analysis of the power law and the logarithmic law using wind data from a 164 m tower. In their study, the wind speed distribution with height is analysed by using hourly data for a full year record at 6 levels, and a statistical error analysis shows that power law and logarithmic law are best applicable when the wind is strong. For the height range from 16 to 164 m, the power law represents the actual speed distribution better

than does the logarithmic law. Joffre (1984) stated that the power law profile has the advantage that it permits analytical solutions to be devised for the diffusion equation. This is not possible with the exact logarithmic profile and the exponent is not universal but dependent on roughness, stability and height. Many empirical investigations (eg., Frost, 1947; De Marris, 1959; Touma, 1977; Sedefian, 1980; Hsu, 1982) have been carried out in order to estimate α as a function of roughness length Z_0 and hydrostatic stability, in which most of them are over moderately rough terrain. De Marris (1959) showed α apparently decreases slowly with increasing instability but with a larger scatter under strongly unstable conditions due to some higher values of α .

2.3.4 Wind Shear

Method of shear computation is elaborately discussed by Heald and Mahrt (1981), by specifying two ways as average total shear and average speed shear. According to them the directional changes of wind might be an important factor in shear and largest shears normally occur with strong stratification which most frequently develops on clear nights. In thunderstorm outflows, Fujita and Byers (1977) reported shears of 0.12 s^{-1} extending up to 100 m. Different studies in WMO (1969) show that at most locations, the shear of the 5 or 10 min averaged wind above the surface layer is greater than 0.1 s^{-1} less than 1% of the time. Rijkoort (1969) expressed an increase of maximum shear values as the averaging time and the depth of the layer of computation decreases. Narayanan and Devassy (1972) studied seasonwise structure of shears in the 200 ft lower atmospheric layer over Thumba, India. There exists high wind shears in the afternoon in the layer 2-10 m and 40-50 m in summer and uniform shear in southwest monsoon. Hindu daily (1997) published an article about Madras airport Low Level Wind Shear (LLWS) reports during 1979 to 1988, having importance in landing and take-off from the airport, in which both horizontal as well as vertical shear (30 to 500 m

above ground) are explained, and monthwise and timewise distribution over the port are critically assessed.

2.4 Atmospheric Turbulence, Gusts and Spectral Behaviour

2.4.1 Wind Speed Fluctuations: Atmospheric Turbulence and Gustiness

Properties of turbulence are described by Lumley and Panofsky (1964). Taylor (1938) suggested that for some special cases, turbulence might be considered to be frozen as it advects past a sensor, and derived the Taylor's hypothesis.

Willis and Deardorff (1976) suggests that Taylor's hypothesis should be satisfactory when the turbulent intensity is small relative to mean wind speed, and made a condition to satisfy the requirements that the eddy has negligible change as it advects past a sensor as $\sigma_M < 0.5 M$, where σ_M the standard deviation in wind speed and M the mean wind speed. σ_M is a measure of intensity of turbulence or turbulent kinetic energy.

Turbulence and gusts of wind are closely interrelated. Sutton (1953) summarised much of the empirical data for the development of turbulence theory through gustiness examinations. Poppendiek (1951) described, the diurnal variation of turbulence is ascribed to a preponderance of mechanical turbulence in the lower layers, whereas effects of thermal turbulence (or buoyancy) dominate at higher elevations and are associated with larger diurnal variations. Observational studies of the instantaneous values of wind speed and direction show that one or other of thermal or mechanical turbulence may predominate.

2.4.2 Wind Velocity Spectra

In turbulent spectrum numerous eddies of different periods are superimposed, apparently randomly, upon the mean state of the lower atmosphere. The difficulty of separating out these eddies accounts, in the main, for the complexity of atmospheric turbulence. Van der Hoven (1957) measured the

horizontal wind power spectrum with the wide range from 0.0007 to 900 cycles per hour at about 100 m height and found that the length of the obvious period is 4 days, 12 hours, and about 1 min. respectively. Quite a remarkable number of studies aimed about atmospheric fluctuations and its spectral characteristics because of its capability to give picture into the wide range of scales over which atmospheric motions occur. (Hwang, 1970; Mori, 1980; Ishida, 1990; Oort and Taylor, 1969). Also it is now clear that kinetic energy of the atmosphere is not spread uniformly over all the wavelengths but has certain preferred scales with gaps between. (Smedman-Hogstrom and Hogstrom, 1975; Fiedler and Panofsky, 1970). The modelling of turbulent velocity spectra dealt by Kaimal et al., (1972), where surface layer velocity spectra in the neutral atmospheric limit and stable conditions are treated. The shape of the unstable spectra is treated by Kaimal et al., (1976), Panofsky (1978) and Peltier et al., (1996)

Studies on the effect of local meso circulations like sea breeze on spectral behaviour are very few for equatorial coastal stations. Prakash et al., (1992) made a spectral behaviour of SBL parameters over the equatorial coastal station, Thumba, India. They detected the characteristics of unstable wind spectrum with a +1 slope in the energy containing region and a spectral fall of $-2/3$ in the inertial sub range, whereas the stable spectrum gives a -2 slope in the buoyancy sub range as in Lumley (1964) and Weinstock (1981). With the onset of sea breeze, there is a shift in the spectral peak and an increase in longitudinal (u) spectral power is reported. The spectral gap is seen about 8×10^{-4} Hz before the onset of sea breeze and widens after onset. Recently Narayanan Nair (1999) analysed wind spectrum during the incidence of Low Level Jet (LLJ) over Thumba, and he detected a spectral enhancement in the lateral (v) component and the spectral fall in the longitudinal (u) component of the wind field at the low frequency side, and during this time it is observed that the LLJ as a thin stream of fast moving meridional flow conserving vorticity. Luo and Zhu (1995) presented the power spectrum at 8

levels for the frequency range from 0.000225 to 0.5 cycles per second. They detected obvious peaks in the period range from several seconds to more than ten minutes in the spectrum, which differ from the former results. In the study, it is found that there is evident relationship in horizontal wind power spectrum at different levels, and the relationship is more clear in low frequencies than in high frequencies.

2.5 Wind Direction Fluctuations: Stability of Atmosphere

As standard deviation of wind speed can be a representation to intensity of turbulence or turbulent kinetic energy. Wind direction fluctuations through standard deviations (σ_θ) can be looked as a measure of atmospheric stability. The investigations of atmospheric stability in the lowest part of the atmosphere is very crucial input in air pollution dispersion modelling.

Considerations for the derivation of σ_θ are through various methods. Jones and Pansquill (1959), Brock and Provine (1962) devised sigma computers convert the fluctuating input voltage from the wind direction transducer to a continuous voltage signal proportional to the standard deviation of the input. Harris and McCormick (1963) determined σ_θ from accumulated unidirectional angle and the number of reversals of directions determined from charts records. Sachdev and Rajan (1971) devised an automatic method to output unidirectional angle and number of reversals of directions from a wind vane. Markee (1963) provides a simple and convenient relationship between wind direction standard deviation and the range of wind direction fluctuations, where the range divided by 6 for a sampling periods of the order of 1 hr has taken as σ_θ . Theoretical computation procedures to derive σ_θ from the collected speed and direction data are given by Ackermann (1983), Verrall and Williams (1982) and Yamartino (1984). All these theoretical computations are resulted due to the discontinuity of wind direction scale at 360°. Ackermann algorithm assumes that individual point values are

measured as orthogonal components or have been converted from polar speeds and directions to rectangular components. The components would then have been averaged and their variances and covariances computed for a desired time period. These component statistics are then used by the algorithm to compute estimated means and standard deviations of the speed and direction for the time period of interest. Verrall and William (1982) devised the method for estimating σ_θ from the cosines and sines of direction angles. Yamartino's (1984) method includes the addition of a constant in the σ_θ derivation. Comparison of above methods are done by Turner (1986) and the eight hours of real atmospheric data applied to each methods show no significant difference between the methods.

Zhong and Takle (1992) measurements of σ_θ revealed an abrupt increase and decrease in low level turbulence associated with passage of sea breeze front over Merritt Island. Pramila Goyal and Nivedika karmakar (1982) made σ_θ computations in order to know monthwise stability frequencies over Mathura, India and they found out thermal instabilities in the lower atmosphere prior month to winter. Panchal and Chandrasekharan (1983) detected the monotonic decrease of σ_θ with stability classes from A-F for a land breeze and increase ranging from D to F.

2.6 Probabilistic Properties of Wind Behaviour

The main parameter which measures the variability or dispersion of the individual wind observations are standard deviation and coefficient of variation. They should be specified along with the main measure of central tendency, the mean of wind observations. The process of computing them as basic statistical conceptual tools are elaborately discussed for SBL studies by Stull (1994). The probabilistic nature of wind and its statistical tools for its assessments are thoroughly expressed in Lawson (1980)

Winds are three dimensional but for almost all direct application purposes, especially in engineering needs, they are considered only in their two dimensional form along horizontal surfaces. Crutcher (1962) described the estimation of frequency of winds from any given point, sector or area is only possible with the use of estimates of statistical parameters of a wind distribution. Crutcher (1957) and Scott (1956) provided the general bivariate normal elliptical distribution in order to represent sets of data. Smith et al., (1990) made wind models for aerospace vehicle ascent trajectory biasing for wind load alleviation through bivariate normal probability distribution.

As the bivariate normal distribution theory plays as the best modelling tool for horizontal components of winds, Weibull probability density function, can be as a good model for wind speed distributions. The statistical tool, the Weibull distribution by Swedish physicist Weibull (1951) is one of the major area in Extreme Value Theory (EVT). The Weibull distribution gives a precise quantitative statement of the otherwise vague notion that the more extreme the event, the less likely it is to happen (Smith, 1990). Hennessey (1977) suggested that the Weibull model for the wind power density has many computational advantages, and the wind power studies based solely on the total mean wind power density omit much valuable information about the wind power potential of a site. Justus et al., (1978) reported some of the advantages of Weibull model and described methods of estimating the two Weibull parameters (scale factor, c and shape factor, k) from simple wind statistics. The Weibull distribution is shown to give smaller root-mean-square errors than the square root normal distribution when fitting actual distributions of observed wind speed. Takle and Brown (1978) summarised procedures developed and used for coping with the problems caused by low or zero wind speeds, for computing the Weibull parameters, and for easily ascertaining the qualitative resemblance of a given wind speed distribution to the Weibull. Justus and Mikhail (1976) proposed a set of formulas which allows

Extrapolations to be made to the Weibull scale factor, c and shape factor, k . Doran and Verholec (1978) are given a note on vertical extrapolation formulas for Weibull velocity distribution parameters proposed by Justus and Mikhail (1976), and suggested its usefulness in ensemble averages, but the technique can lead to significant errors in individual cases. Stewart and Essenwanger (1978) are found that frequency distributions of wind speed near the surface are skewed to the right and the mean is usually greater than median, and proposed Weibull distribution as a good analytical approximation to the cumulative distribution and is particularly useful for the 90-99% thresholds. Essenwanger (1976) explained a three parameter Weibull model and later Auwera et al., (1980) applied this model and found out the model generally gives more reliable fit to the empirical wind speed frequency data. Bardsley (1980) suggested an alternative three parameter Weibull distribution for the description of wind speed data with low frequencies of low wind speeds. Conradsen et al., (1984) made a review of the relevant statistical methods for the estimation of Weibull parameters is given with emphasis on efficiency. In summary, they stated in estimating Weibull statistics from measured wind speed data, one should preferably use the method of maximum likelihood owing to its large sample efficiency.

2.7 Wind Variability associated with Meso-scale Systems

Diurnal patterns of wind speed are extensively studied by Matveev (1967), Oke (1978), Reil (1972), Adiga (1981). Haurwitz's (1947) treatment of the sea breeze is generally recognised as an important milestone in sea breeze theory. The mathematical results are expressions for the horizontal wind components at the surface as a function of time, with Coriolis parameter, amplitude of diurnally oscillating pressure-gradient force, and coefficient of linear friction as parameters. The results are presented as wind hodographs depicting the variation of direction and speed over the diurnal period. Defant (1950) proposed linear mathematical

model of the sea breeze circulation similar to Haurwitz theory and Pearce (1955), Estoque (1961) and Fisher (1960) are provided solutions to nonlinear models, relate the physical aspects of the problem in a way that leads to realistic results. Observations by Fisher (1960) and Staley (1957) indicate that local topography not included in the theory, is very crucial to the air motions at individual locations. Frenzei (1962) brought out resultant winds obtained from routine surface and upper air observations in an area which contains both a sea coast and a huge interior valley and to compare these observations with the results of above theories, indicates that oscillations in air interior are in phase with coastal areas with diurnal circulation most well developed below 1000 m.

From the above pioneer investigators, it has been known that the direction of sea and land breezes makes, at any given locality, a complete 360° turn over diurnal cycle, provided that the general wind flow is weak. Neumann (1977) is drawn attention to the observational fact that the rate of turning of the direction of sea and land breezes is far from uniform over the diurnal cycle. Alpert (1983) examined the anticlockwise rotation (in northern hemisphere) or clockwise rotation (in southern hemisphere) of the wind hodograph in the boundary layer, and found out usually the pressure-gradient term is the leading one and the advection term is very small.

Observational studies on the diurnal variation of boundary layer winds are made by investigators for different topographical locations. Reed (1979) analysed anemometer records from five levels on a 151 m meteorological tower over Cape Canaveral and the results show an almost elliptical clockwise diurnal oscillation of the sea breeze component of the wind. The oscillation amplitude increases with height. Hahn (1981) made a study on the diurnal behavior of boundary layer winds, in which rapid clockwise rotation of the wind vector occurred during the period of increased wind speeds. Zhong and Takle (1992) constructed hodographs of the hourly wind vectors at 16.5 m over Kennedy Space Center for three

locations, which reveal the evolution of the low-level wind vector over the diurnal cycle in the areas surrounding these towers. Veering is noticed in all locations with different rate of rotations. A rapid rotation in afternoon and midnight hours noticed in all locations with a quasi-steady state for 3 to 5 hr before sunrise. Their observations of forcing responsible for the rotation was not uniformly distributed in either time or space, which is consistent with Neumann's (1977) theory. Alpert and Eppel (1985) proposed an index for meso-scale activity. The suggested index provides between diurnal to interdiurnal wind variabilities can be used to assess meso-scale or synoptic-scale forcing dominance for a station.

There are a few studies only on thunderstorm effects on winds in SBL. Fujita, (1955) explained the drastic change in wind speed and direction in association with downdrafts from thunderstorms. Luo and Zhu (1995) in the spectrum analysis of strong winds, they found that all frequency range have almost not obvious difference, but undulation is much more and the amplitude is stronger in high frequency range in thunderstorm strong winds. Narayanan Nair et al., (1994) reported a change in meridional wind shear, amplification of vorticity, vertical wind fluctuations during night time and cyclonic circulation and thunderstorm during early morning hours followed by shallow land-sea breeze circulation over Thumba.

Chapter 3

Measurement Techniques of

Surface Boundary Layer Winds over

Sriharikota

3.1 Introduction

Winds in the Surface Boundary Layer (SBL) of the atmosphere are characterised by very complicated three-dimensional flow pattern with rapid variations in space and time. Winds having turbulent structure in this layer are crucial inputs, when the satellite launch vehicle is stationary on the launch pad and during first few seconds after lift off. The SBL winds are generally called as ground winds in aerospace meteorology. In the launching of unguided rockets wind compensations are to be taken into consideration for launcher settings in order to avoid deviation of the vehicle from the nominal trajectory. The need for quantitative data and better understanding of the statistical properties of wind characteristics for aerospace as well as engineering applications has led to the construction of a 100 m tower facility at SHAR Range, Sriharikota (13.7°N, 80.2° E) which is the major rocket launching centre of the Indian Space Research Organisation (ISRO). Figure 3.1 shows the position of Sriharikota in the Indian sub-continent. It is a barrier island with an area of 180.93 km² sandwiched between Pulicat lake and Bay of Bengal, located on the southern most part of south coastal Andhra Pradesh, India.

3.2 Physiography and Terrain Features of Sriharikota

The island is a narrow and elongated strip of land with almost straight coast extending towards northern and southern ends from the main bulge. The maximum elevation is about 10 m above MSL. A general slope is towards south-east. There are two streams, viz., Peddavagu and Chinnavagu flowing parallel to each other in the middle of the island in north-south direction. There are several mechanically excavated water pits of oval or circular from 3 to 15 m in diameter, which are filled with water during rainy season and some of them are perennial. The island is mostly covered by stabilised dune sand. Sand dunes are localised all along the beach. These occur as linear water bodies with a length varying from 100 to 200 m

and width 3 to 5 m. Figure 3.2 shows the locality map and the position of tower platform in the map. Located about 400 m from the coast of Bay of Bengal, the tower is situated in a well-exposed area, free of nearby structures that could interfere the air flow.

The vegetation map of the island is shown in Figure 3.3. The tower location area is sandy with open scrubs of height less than one-half meters high. There is a narrow shelter belt of casuarina plantations about 350 m east of the tower in line with the coast, which are about 10 m tall and about 20 m in width. Far 400 m western portions of the tower are thick, with plantations like eucalyptus, cashew, dry ever green forests, closed scrubs and their heights are of the order of 15 m.

3.3 Observational Platform and Data Acquisition

3.3.1 Tower Facility

The complete tower structure comprises, a massive triangular shaped 100 m MET tower supported by guy wires having one meter face width. The instrument arms are of 2.5 m length (2.5 times of the face width) positioned at seven levels viz., 10, 20, 30, 40, 60, 80 and 100 m (Figure 3.4). A motor driven winch system is also provided to move the instrument arms for installation or maintenance of sensors at required levels. The instrument arms are projected towards 135° azimuth i.e., towards south-east direction in order to cover the more prevailing wind directions. Horizontal cross-section of the 100 m MET tower is shown in Figure 3.5. Cup anemometers and wind vanes for monitoring wind speed and direction are installed at seven different levels as mentioned above. Wind speed and direction from these levels are scanned at one second interval round the clock. The speed and direction of wind data are first reaching to a data acquisition system, kept in a kiosk close to the tower. The data then transfer to the PC based data logger kept almost 8 km away through data modems. In this data logger, every seconds informations on speed and direction from seven levels are further

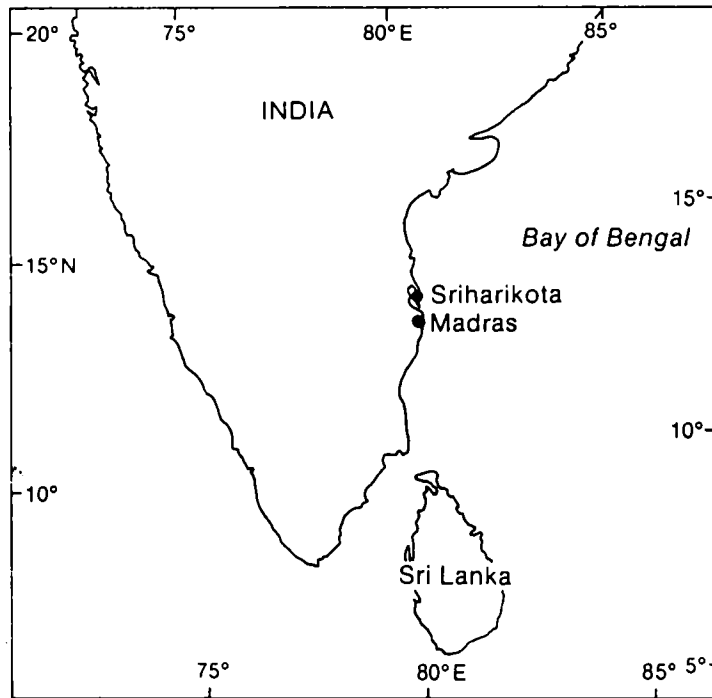


Figure 3.1 Position of SHAR Range, Sriharikota in the Indian sub-continent

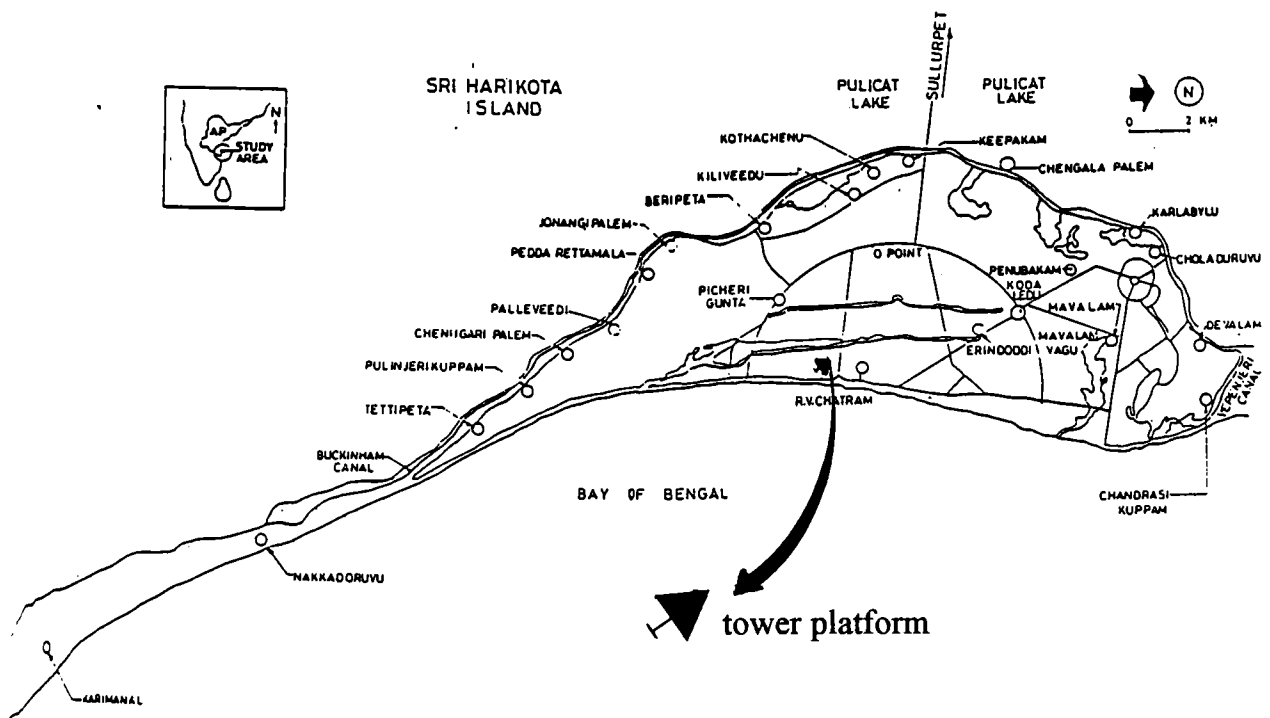


Figure 3.2 Location map and position of tower platform in the map

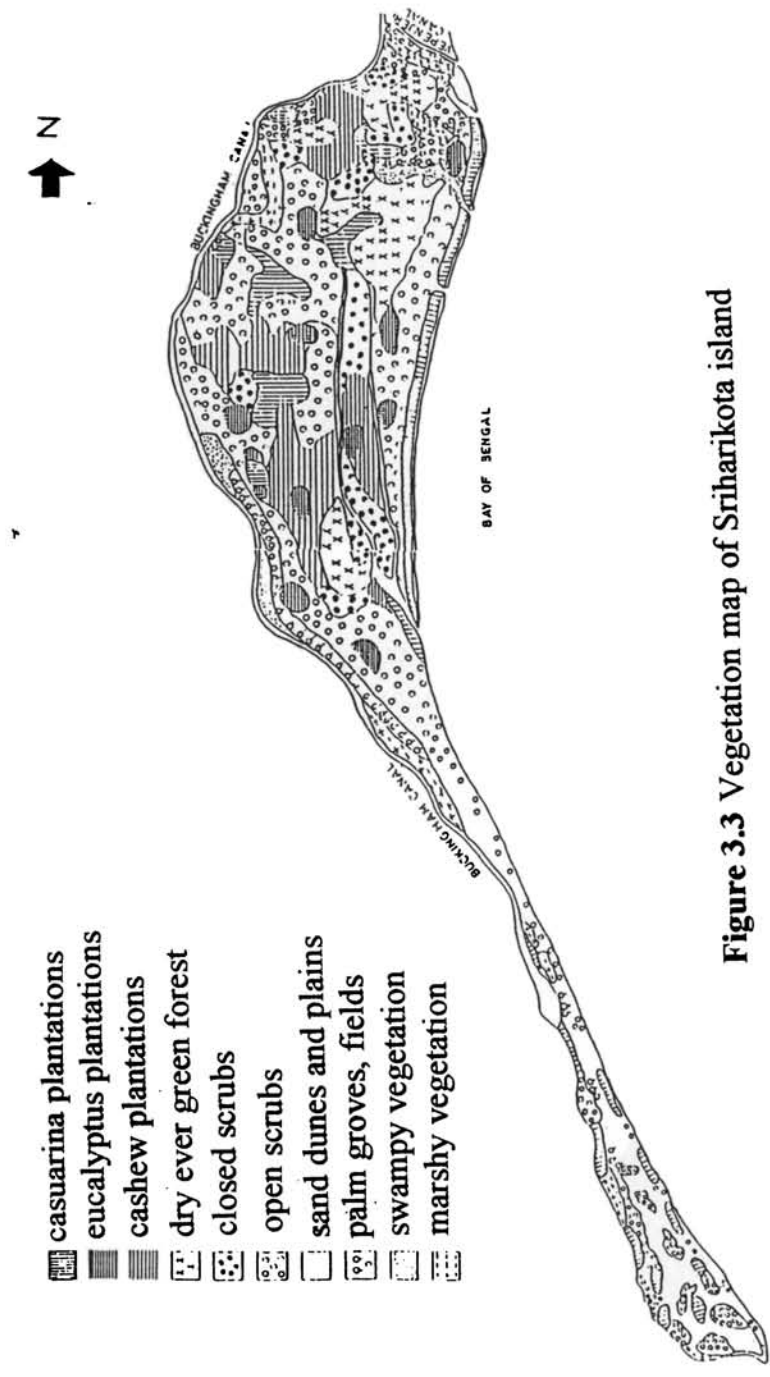


Figure 3.3 Vegetation map of Sriharikota island



Figure 3.4 100 m tower structure showing insrument arms and guy wires

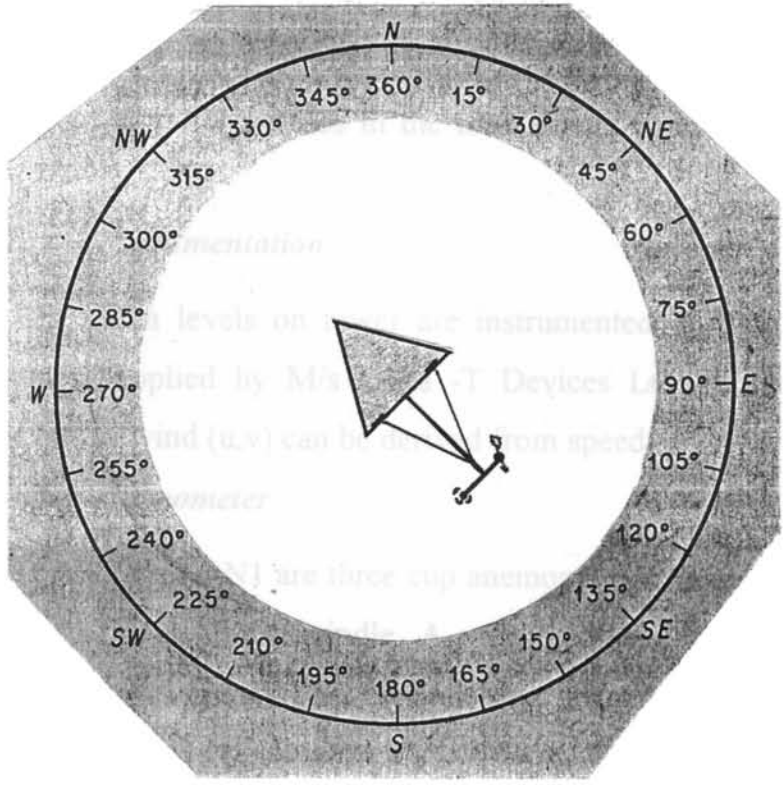


Figure 3.5 Horizontal cross section of Sriharikota 100 m tower

converted in to a general usable format by the use of a software package residing in the PC.

3.3.2 Data Reduction Procedure

The final form of data generation is as follows. At the end of full fifth minute, the average wind speed and direction based on last 120 one second samples are estimated individually for seven levels to represent as quasi-steady state wind (Geissler, 1970). Apart from this data, the peak wind occurred at each level in every five minute as well as the peak observed in the last 120 second samples (called as gust in aviation and aerospace meteorology) in the five minute are also recorded along with quasi-steady state wind speed and direction. This raw data is transferred to main frame computer, VAX/VMS 11/785 from PC based data logger system through File Transfer Protocol (FTP) software or through floppies/compact discs. In VAX, the voluminous data are archived in system hard disc as well as in optical discs after thorough validation processes. The entire tower facility set up is shown in Figure 3.6. In order to make extensive mathematical and statistical explorations, data pertaining to a month are processed and archived in different files in the main frame computer and in other storage media.

3.3.3 Tower Instrumentation

The seven levels on tower are instrumented with cup anemometers and wind vanes supplied by M/s Delta -T Devices Ltd., England. The horizontal components of wind (u,v) can be derived from speed and direction data.

3.3.3.1 Cup Anemometer

Delta-T type AN1 are three cup anemometers. Two stainless steel ball-race bearing support the rotor spindle. A magnet on the spindle causes a mercury-wetted read switch to make and break contact once per revolution of the rotor.

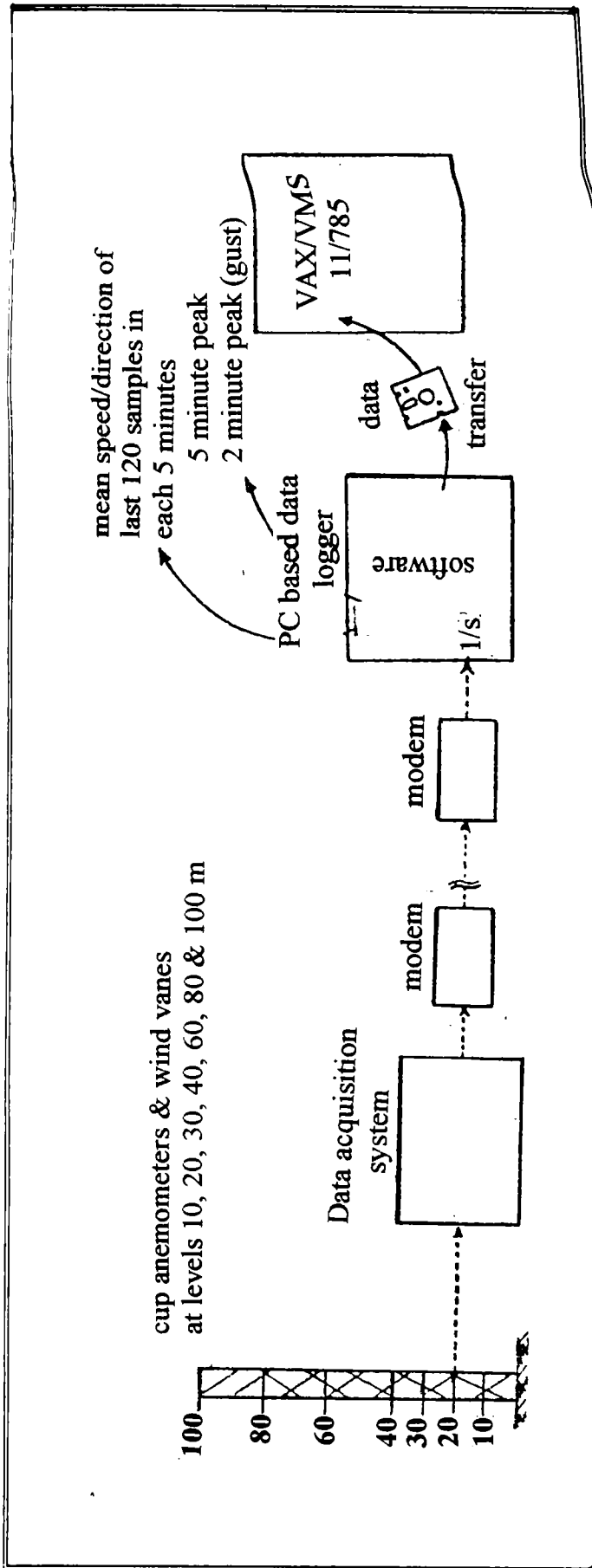


Figure 3.6 Complete 100 m tower facility

The performance specifications are

Threshold:	0.3 ms ⁻¹
Maximum wind speed:	75 ms ⁻¹
Accuracy:	1% ± 0.1 ms ⁻¹
Distance constant:	5 m
Calibration:	0.80 revolutions per meter nominal or 1 pulse per 1.25 m

3.3.3.2 Wind Vane

Delta-T type WD1 is a 358 degree micro-torque wire wound potentiometer.

The specifications are

Threshold:	0.6 ms ⁻¹
Maximum speed:	75 ms ⁻¹
Distance constant:	2.3 m
Accuracy:	± 2° for steady winds over 5ms ⁻¹
Resolution:	0.3°

3.4 Data used for Studies on the Structure of SBL Winds

Every five minute data pertaining to a specified month are stored in different files from May 1993 to August 1999 (SET I) and from May 1993 to April 1996 (SET II). In the derivation of basic statistical properties of wind over the station SET I is used. Almost all other studies encountered in the thesis work SET II is utilised. A comparison between SET I and SET II shows the statistical differences are within 0.5 ms⁻¹ in mean wind speeds and within 5° in mean resultant wind directions which confirms stabilisation of data. The monthly distribution of number of observations of 5 minute wind data for seven levels of SET II, which is used for most of the studies in this present work is presented in Table 3.1. More than 120 data points are observed for a particular fifth minute data slot in SET I and more than 80 data points in SET II in any of the month. (for example, at 0055 hr IST in March from SET I, comprises 123 data points at level

10 m for quasi-steady state wind speed, direction, five minute peak and gust). Other than the above specified data, various other meteorological parameters which are found useful to relate wind variations are also used in case studies.

Table.3.1 Number of five minute observations available from SET II

Month	Height (m)						
	100	80	60	40	30	20	10
Jan	23321	23224	22900	21424	21422	21397	21115
Feb	22541	22457	22223	20985	20983	20973	20498
Mar	23853	23760	23644	22730	22728	22719	22279
Apr	23358	23269	17568	17462	17456	17456	17302
May	26530	26407	23995	23995	23995	23995	20762
Jun	23375	23286	22649	21747	13706	13704	13666
Jul	23873	23110	22790	20762	20698	20678	20557
Aug	20984	20886	20794	19940	19932	19928	19885
Sep	13803	13713	13656	13243	13230	13230	13202
Oct	15679	15614	15318	14365	14357	14350	14314
Nov	20362	20273	20102	19132	19127	18932	18710
Dec	24653	24561	24471	23629	23629	23629	23378

Chapter 4

Salient Features of

Surface Boundary Layer Winds

4.1 Introduction

The importance of climatological details of wind in the lowest 100 m layers of atmosphere is manifold as its application in air pollutant dispersal, numerical weather modelling, wind energy, structural analysis, etc. In aerospace meteorology, winds having irregular chaotic motions in this layer is of greater significance both when the satellite launch vehicle is on pad without any shelter like Mobile Service Structure or in lift off dynamics studies. Incidence of severe weather meso-scale features like thunderstorms and synoptic-scale features of cyclonic circulations over a tropical coastal station is not uncommon. The characteristics wind flow in SBL is associated with these weather phenomena are of particular interest in planning different launch related operations in a space port. This chapter brings, a detailed quantitative analysis on the structure of SBL winds over the tropical coastal station SHAR Range, Sriharikota.

4.2 Methodology

Computations of the statistical properties of the tower derived wind are described as follows:

Mean Scalar Wind Speed (MSWSP) or Mean Quasi-Steady State Wind

$$\text{MSWSP} = \frac{\sum_{i=1}^N V_i}{N} \quad (4.1)$$

where V_i is the scalar wind speed and N is the number of observations.

Mean Resultant Wind Direction (MRWD)

$$\text{MRWD} = \tan^{-1} \left[\frac{\sum_{i=1}^N v_i / N}{\sum_{i=1}^N u_i / N} \right] \quad (4.2)$$

where u and v are zonal and meridional wind components.

Mean Resultant Wind Speed (MRWSP)

$$\text{MRWSP} = \sqrt{\sum_{i=1}^N (u_i/N)^2 + \sum_{i=1}^N (v_i/N)^2} \quad (4.3)$$

Steadiness Factor (SF) in %

$$\text{SF} (\%) = (\text{MRWSP}/\text{MSWSP}) \times 100 \quad (4.4)$$

and Mean Peak wind Speed (MPWSP)

$$\text{MPWSP} = \sum_{i=1}^N V_{\max i} / N \quad (4.5)$$

where V_{\max} is the peak scalar wind.

The above said statistical parameters on winds are derived for every five minutes at each level in order to assess the diurnal variation pattern in a particular month.

4.3 Results and Discussions on Basic Wind Statistical Properties

4.3.1 Mean Scalar Wind Speed (MSWSP) (Mean Quasi-Steady State Wind Speed)

The diurnal variation of mean scalar wind speed in different months from January to December are depicted from Figures 4.1(a)-(l). The wind speed generally increases with height in the Surface Boundary Layer throughout the year. In the SBL, there observes two prominent entities, such as a level from 10 m to 40 m and 60 m to 100 m based on the phenomenon of "wind merging". In wind merging, the wind speed start building up from surface to 40 m and a decreasing trend from 60 to 100 m so as to form a region of minimum wind speed gradient with height. The most intense merging time and the difference of wind speeds between 10 m and 100 m are shown in Table 4.1 This merging phenomenon has already reported by various investigators (Matveev, 1967; Oke, 1976; Adiga, 1981 and Reihl, 1972). Vertical exchange of momentum due to the turbulent convection caused by ground heating leads to increase of wind speed near the ground up to 40

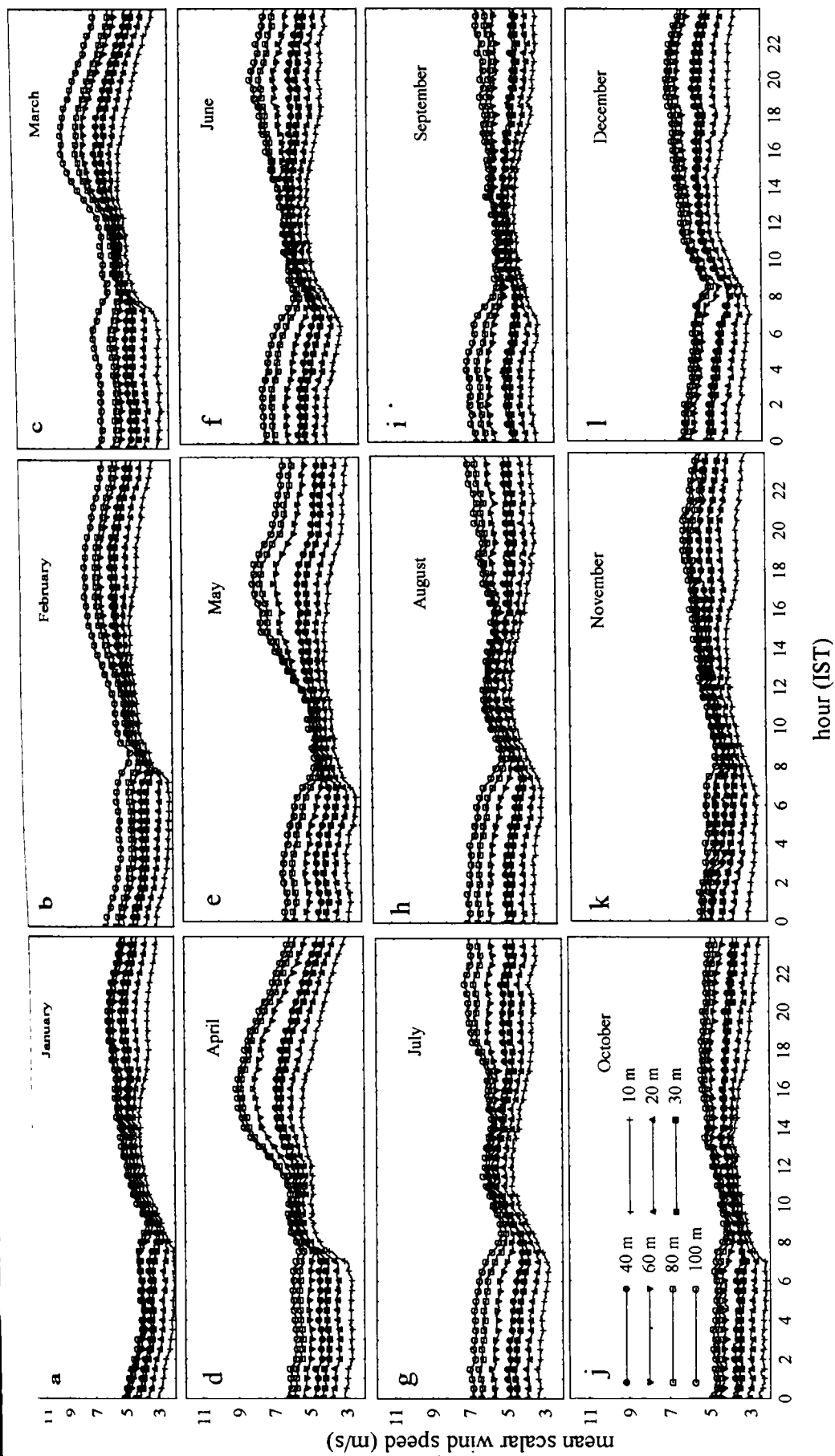


Figure 4.1.a-l Diurnal variation of mean scalar winds in different months

Table 4.1 Wind speed merging timing and difference in speeds between 10 m and 100 m level

Month	Difference in Speeds between 10 m to 100 m	Time of Intense Merging
January	1.0 m/s	0930 hr
February	1.2 m/s	0900 hr
March	1.2 m/s	1000 hr
April	1.0 m/s	1000 hr
May	1.0 m/s	0930 hr
June	1.3 m/s	0930 hr
July	1.4 m/s	0930 hr
August	1.3 m/s	0930 hr
September	1.0 m/s	1200 hr
October	0.9 m/s	1030 hr
November	1.2 m/s	1000 hr
December	1.7 m/s	0930 hr

m and decrease of speed at the upper boundary layer. During this time, the atmosphere is in unstable conditions causing high rates of momentum transfer towards the ground. This results hike in wind speed at lower SBL levels and decrease in wind speed at higher levels. Such variations are present throughout the year. Over Sriharikota the wind speed build up from lower levels (10-40 m) prior to the intense merging time begins before 1 to 1 $\frac{1}{2}$ hours whereas the wind speed starts dipping before 2 $\frac{1}{2}$ hours in layers above 60 m. Eventhough momentum transfer to ground commences early, the establishment of its effect on lower layers take almost one hour delay. The feature of least wind shear or wind speed gradient with height during the period from around 0800 hr to 1100/1300 hr IST is independent of prevailing wind speed and direction.

The time of occurrence of maximum wind speed at levels in the diurnal variation for different months are listed in Table 4.2. From November to May, the maximum wind values are occurring at around same time for all levels. In other months, the separate two layers viz., 10 m to 40 m and 60 m to 100 m maxima are occurring distinctly at two timings. April and May are strong wind months with wind speeds of the order of 9 ms⁻¹ and October is the shallow wind month.

4.3.2 Mean Resultant Wind Direction (MRWD)

Variations of MRWD in different months are shown from Figures 4.2(a)-(l) Only 20 m and 100 m level diurnal variation curves alone are shown as variations of other levels are having the same trend and lying within these two curves. This confirms direction variability between levels in SBL is minimum. As the coastline orients N-S direction, wind direction less than 180° azimuth is treated as sea breeze and greater than 180° up to 360° is treated as land breeze for the station. However, in November and December, generally MRWD is NE, and NNE tendency around 0600 hr to 0800 hr IST is due to the influence of land breeze flow with embedded NNW winds between 20 m and 100 m. The wind directions in January is almost dominated by ENE winds except the land breeze time (i.e., from

Table 4.2 Maximum wind speed in different levels and its time of occurrences

Month	Level	Time of Occurrence
January	All	2000 hr
February	All	1830 hr
March	All	1700 hr
April	All	1600 hr
May	All	1730 hr
June	10-40 m	1330 hr
	60-100 m	2000 hr
July	10-40 m	1200 hr
	60-100 m	2130 hr
August	10-40 m	1200 hr
	60-100 m	0000 hr
September	10-40 m	1330 hr
	60-100 m	0400 hr
October	10-40 m	1330 hr
	60-100 m	1730 hr
November	All	2000 hr
December	All	2000 hr

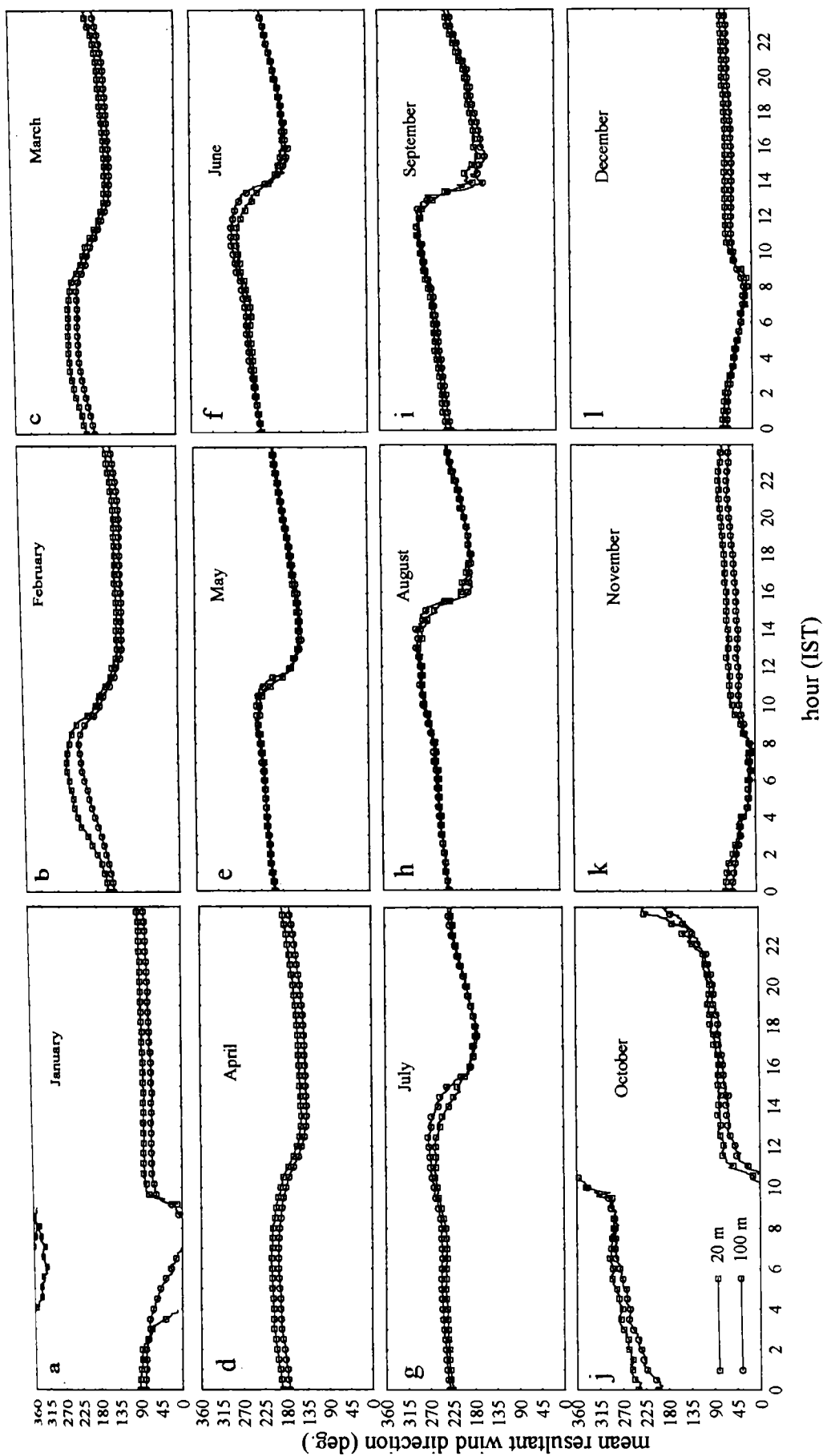


Figure 4.2a-l Diurnal variation of mean resultant wind direction in different months

0400 hr to 0900 hr IST) then it is NNW winds. The vertical time section graphs from Figure 4.2.1(a), (b), (c) for November, December and January months respectively show that the wind direction initially changes from NE to S, then SW and reaches NW and later return back to NE through S, which implies an occurrence of a veering (clockwise) and backing (anti clockwise) phenomena in direction with time in the lower SBL. During February to May of land breeze from SSW prevails between 0200 hr to 0900 hr IST, and sea breeze from SSE in the remaining part of the day. In the month of May sea breeze sets by about 1030 hr and continues till 2000 hr IST. During southwest monsoon months (June to August) south west monsoon current is the dominating feature. Delayed sea breeze onset compared to other months is a notable characteristic in these months. In September, sea breeze persists for more hours compared to south west monsoon months, and is generally from 1400 hr to 2000 hr IST. In the shallow wind speed month, October the effect of sea breeze and land breeze are shared almost equally for about 12 hr, ie., from 1000 hr to 2200 hr IST sea breeze occurs and the remaining period land breeze prevails.

The vertical time section graphs on wind direction give an insight into the change over of land breeze to sea breeze. As the sea breeze front and its effect on wind flow experiences throughout the SBL almost at the same time. An example is given for June month in Figure 4.2.2. A complete establishment of sea breeze regime in the entire SBL takes approximately one hour and is so prominent in intense sea breeze months.

4.3.3 Wind Steadiness Factor

Diurnal patterns of steadiness factor are shown in Figures 4.3(a)-(l). A high value steadiness factor implies high steady wind, both in speed as well as in direction. Since direction changes are so markable, direction steadiness is the dominating feature in wind steadiness factor extraction in this tropical coastal station. A dip followed by increase in slope in steadiness factor in all levels are

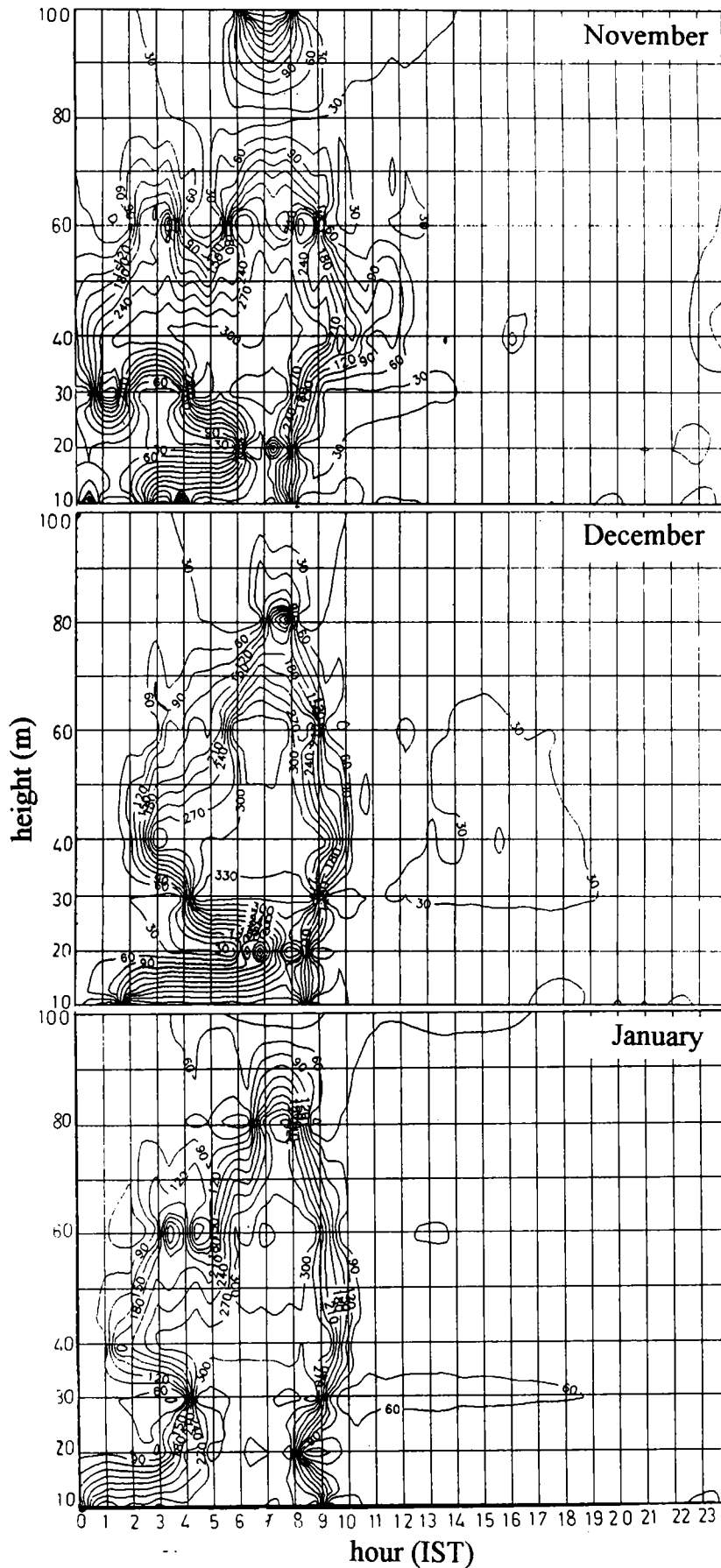


Figure 4.2.1a-c Vertical time section plots of wind direction in November, December and January showing veering and backing with time

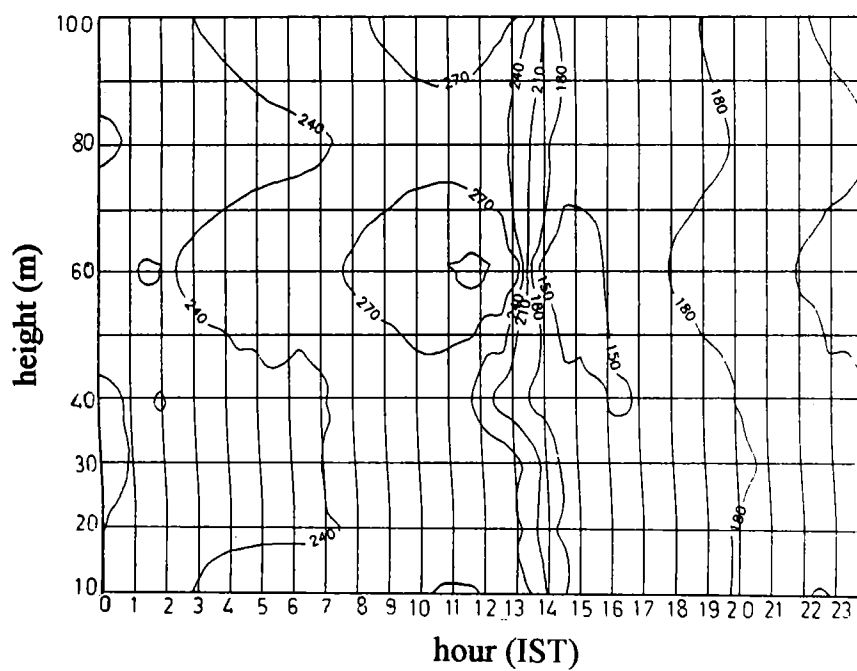


Figure 4.2.2 Vertical time section plot on wind direction in June showing change over of sea breeze/land breeze

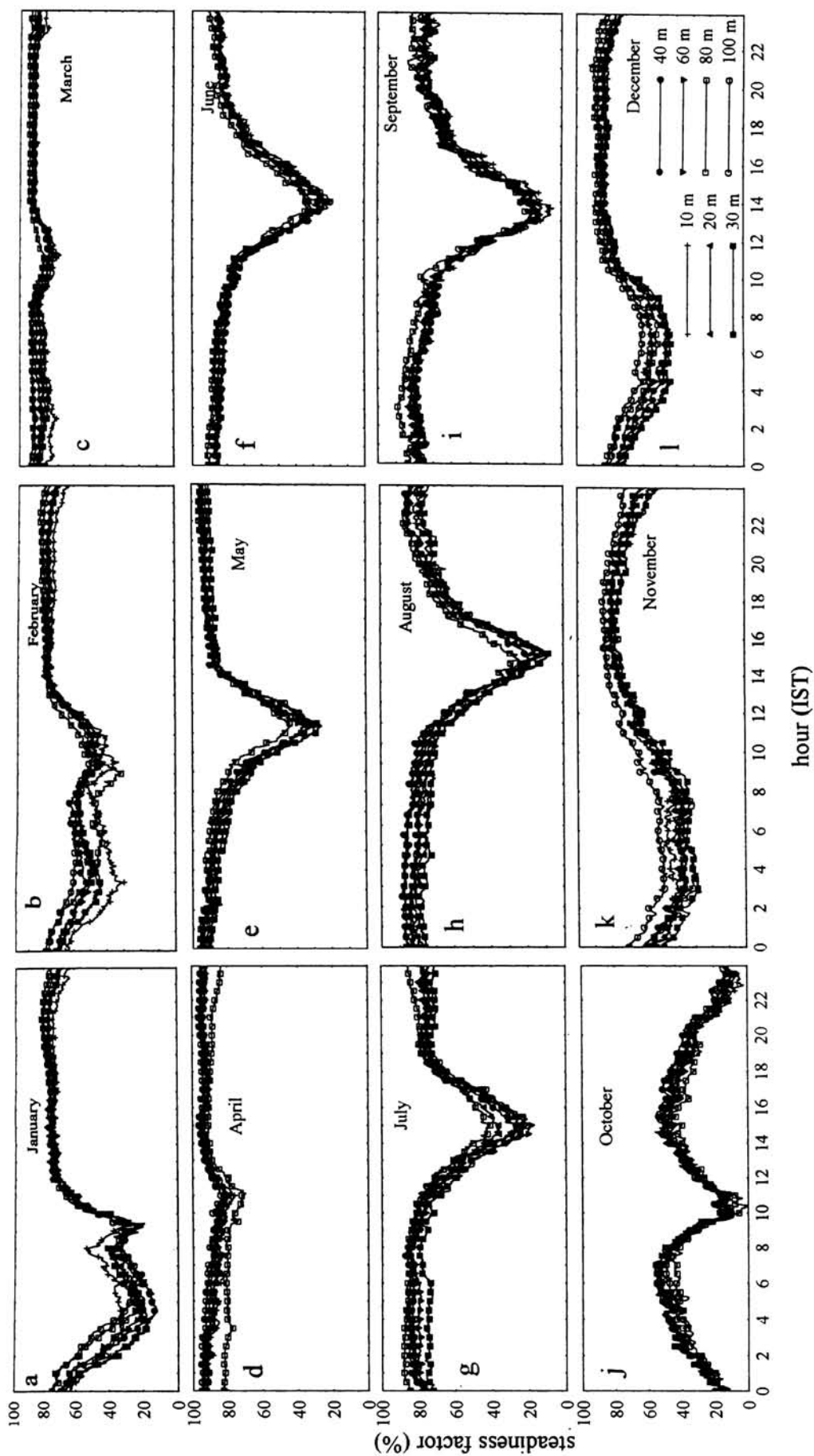


Figure 4.3a-l Diurnal variation of steadiness factor in different months

seen in association with change overs of land and sea breeze regime. The dip in steadiness factor for change over from land breeze to sea breeze are so abrupt and intense, and is equally contributed in all levels at the same time. Thus the steadiness factor forms an excellent parameter to delineate the onset timing of sea breeze over the station and is illustrated in Table 4.3. During November and December, NE winds generally prevail round the clock and there is no significant abrupt variation in steadiness factor.

4.3.4 Mean Peak Wind

Variations of mean peak wind speed in different months are shown from Figures 4.4(a)-(l). The trend in diurnal pattern seen in mean scalar speed is also reflected in mean peak wind. The maximum values in March to May show peak winds of the order of 7 to 10 ms^{-1} in the diurnal curves, whereas in other months it is less than 8 ms^{-1} . In October all values are less than 7 ms^{-1} .

4.3.5 Probability of Mean Wind Speeds in Different Wind Directions

Elaborate analysis in the voluminous data SET I is carried out in order to assess the probability of wind speeds in different wind directions (8 compass points) and for different months. In this treatment, percentage probability of mean wind speeds in different wind directions are presented for different months in Figures 4.5(a)-(l). Each plot provides informations for 10 m level to 100 m level. The wind direction on the X-axis is made in such a way that $\pm 22.5^\circ$ changes from the selected direction, (for example, N represents $0/360^\circ \pm 22.5^\circ$, NE represents $45^\circ \pm 22.5^\circ$, so on). Exceedance probability in percentage for different limits such as 0-5 ms^{-1} , 5-10 ms^{-1} , 10-15 ms^{-1} , and $>15 \text{ms}^{-1}$ are assessed along with each direction slot. In all months a general behaviour of percentage probability decrease in the lowest speed class as height increases is noticed. At the same time the probability of the very next higher class interval (with higher speeds) increases with height. Seasonal prevalence of wind direction is also reflected in these

Table 4.3 Values of steadiness factor associated with sea breeze onset

Month	Value of Steadiness Factor (%)	Time of Onset of Sea breeze
January	20	0930 hr
February	45	0930 hr
March	70	1100 hr
April	75	1100 hr
May	30	1130 hr
June	20	1400 hr
July	20	1500 hr
August	9	1530 hr
September	5	1330 hr
October	5	1030 hr
November	No Significant Variations	
December	No Significant Variations	

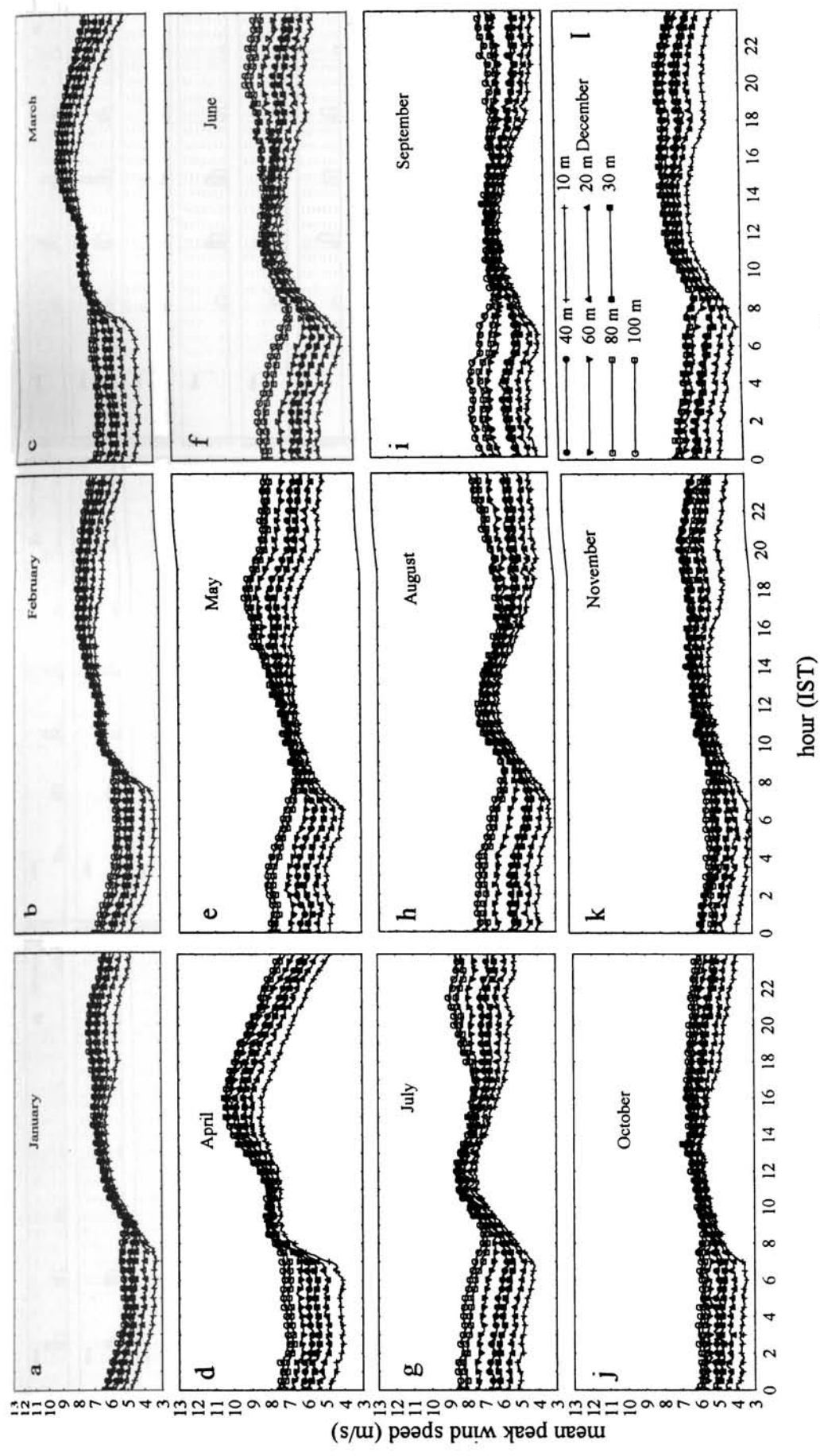


Figure 4.4a-l Diurnal variation of mean peak wind in different months

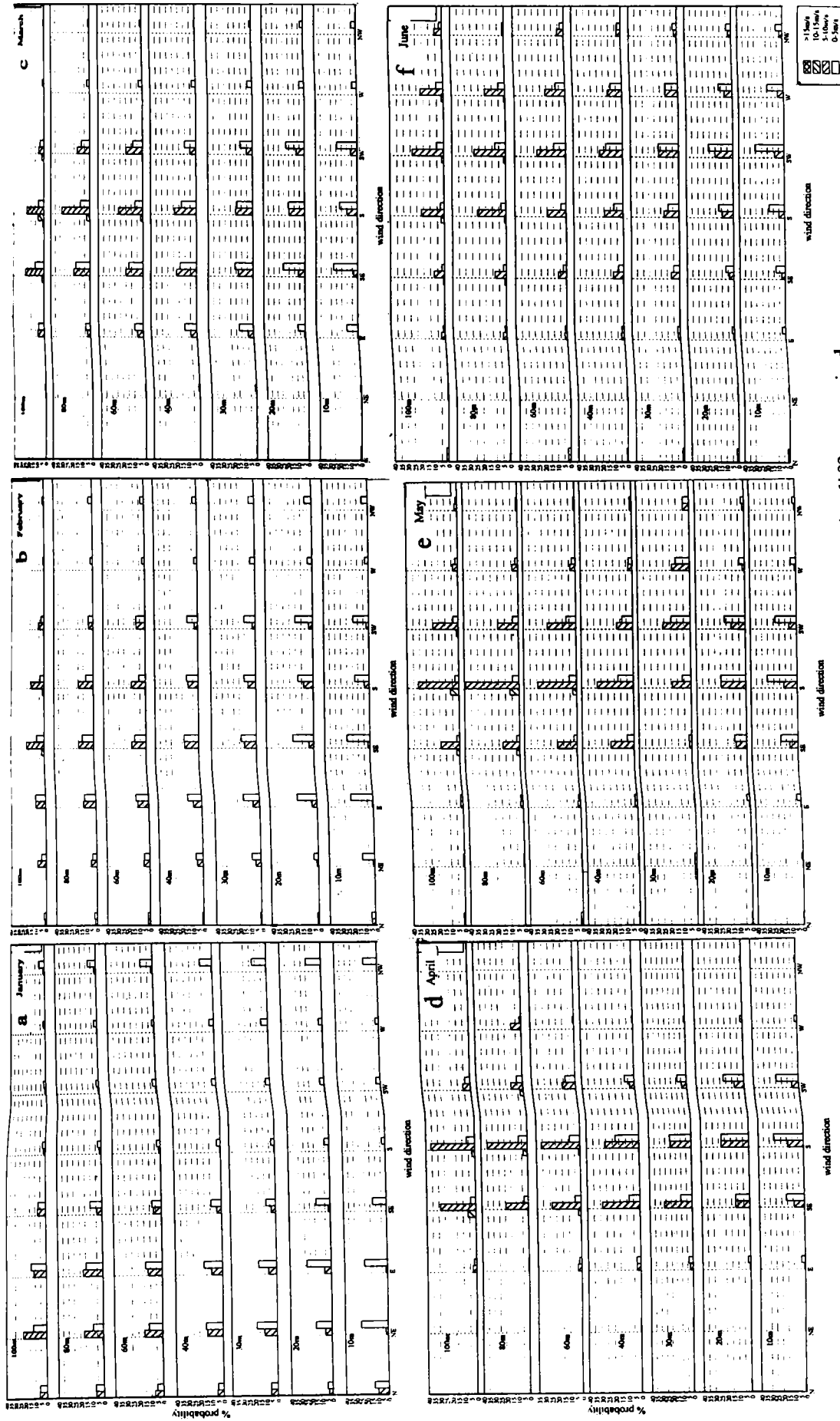


Figure 4.5a-f Percentage probability of mean wind speeds in different wind directions for different months



Figure 4.5g-1 Percentage probability of mean wind speeds in different wind directions for different months

frequency distribution. Events of probability less than 2% are treated as insignificant in presentations.

4.3.6 Monthly Wind Climatology

Monthly SBL wind climatology over the station are computed on MSWSP, MRWSP, MRWD and (u,v) components. The correlation coefficients of horizontal wind components in various months are also derived. Figures 4.6(a)-(e) depicts the pattern of above said computations for seven levels in the SBL. The vertical climatology of MSWSP is already mentioned in chapter I of the thesis (Figure 1.13). MSWSP is always greater than MRWSP and the difference is of the order of 2 ms^{-1} . The prominent maxima in the annual variation of MRWSP and MSWSP occur in May and the prominent minima occurs in October for all levels. The May maximum is attributed to strong sea breeze due to the persisted of high pressure system in Bay of Bengal and adjoining areas and the lull in October is due to transition season behaviours.

The MRWD varies from NNE in October to SSW in September and the quadrant from 270° to 360° clockwise i.e., westerlies to northerlies are free from wind flow in the climatological pattern in any month. Horizontal component (u,v) contribution is shared equally in October and all months obey seasonal regime. The correlation coefficient between u and v components (ρ_{uv}) is computed as

$$\rho_{uv} = \frac{\sum_{i=1}^N (u_i - \bar{u})(v_i - \bar{v})}{\sigma_u \sigma_v} \quad (4.6)$$

where \bar{u} , \bar{v} are mean values of zonal and meridional wind components. σ_u and σ_v are standard deviations of zonal and meridional wind components. The standard deviations are computed by

$$\sigma_u = \sqrt{\frac{1}{N-1} \left[\sum_{i=1}^N u_i^2 - \frac{(\sum_{i=1}^N u_i)^2}{N} \right]} \quad (4.7)$$

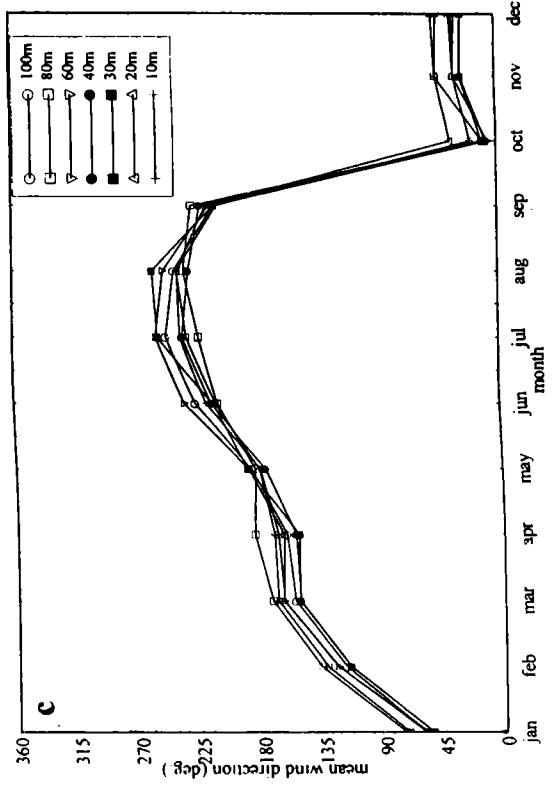
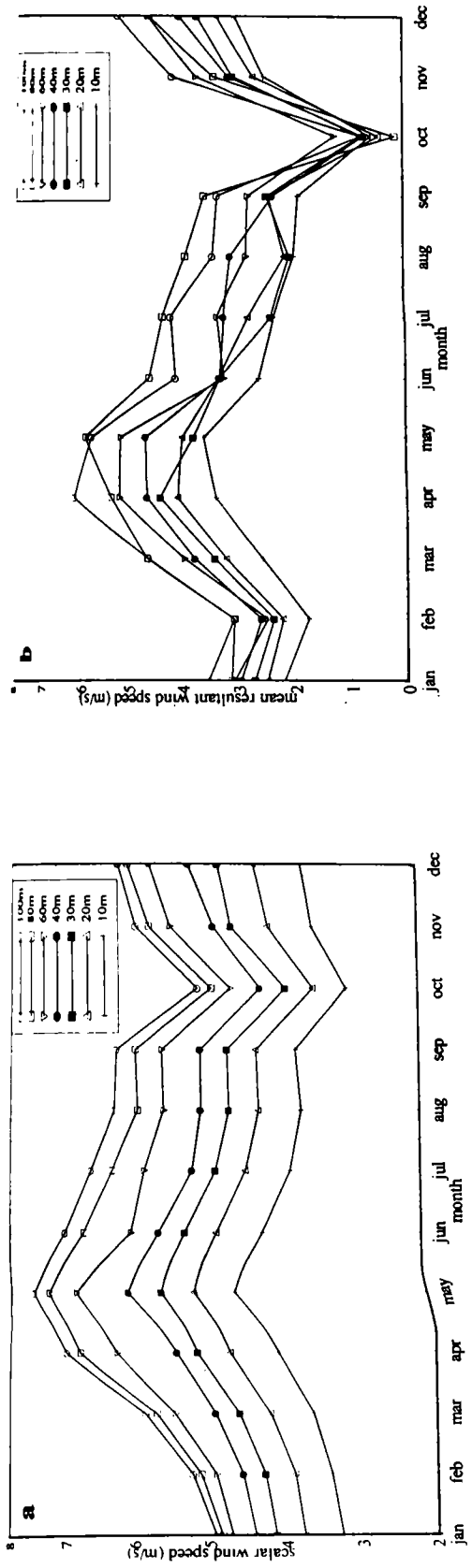


Figure 4.6a-c Monthly SBL wind climatology in (a) MSWSP (b) MRWSP (c) MRWD

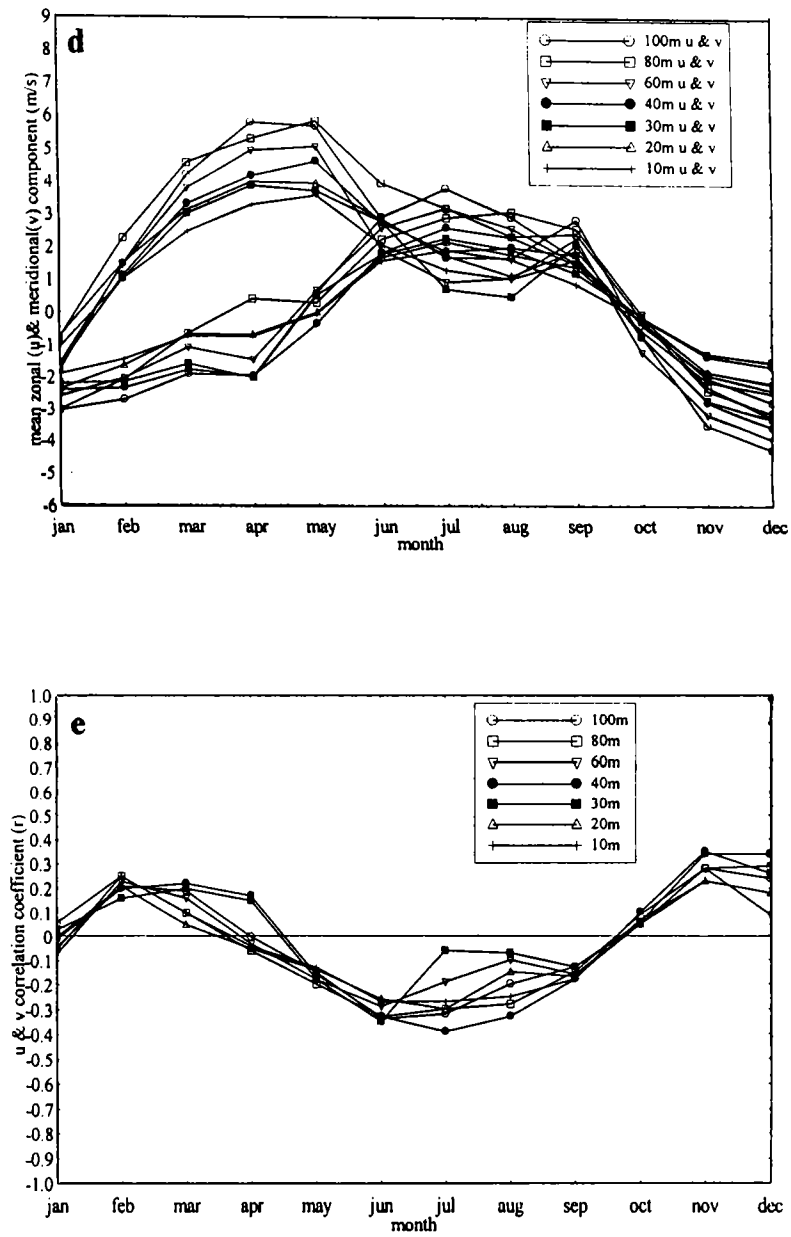


Figure 4.6d-e Monthly SBL wind climatology in
 (d) Mean (u,v) components (e) Correlation of u and v

$$\sigma_v = \sqrt{\left[\sum_{i=1}^N v_i - (\sum_{i=1}^N v_i)^2/N \right] 1/(N-1)} \quad (4.8)$$

In pre-monsoon and southwest monsoon months (May to September) there is negative correlation exists whereas in other months both u and v components give positive correlation coefficients. October month shows less relation among all other months.

4.4 Wind Speed March on a Particular Day

Figures 4.7(a) and 4.7(b) represent diurnal wind speed variations for four levels in SBL during a representative cloudy day August 12, 1997 and a representative clear day August 30, 1997. On the cloudy day, the bright sunshine duration was absolutely zero and on clear day the duration of bright sunshine was more than ten hours, detected by sunshine duration recorder charts. On cloudy day, due to highly unstable atmosphere, wind merging in all levels creates a region of least wind shear that occurs late compared to the clear day. The wind speed magnitude between level to level show high differences around 0200 hr to 0900 hr IST for the cloudy day. In order to delineate stable-unstable regime of atmosphere on the clear sky day, wind profiles are drawn for each hour on August 30, 1997, by taking logarithm of height as ordinate and wind speed as abscissa as in Figures 4.8(a) and 4.8(b). Figure 4.8(a) represent profiles from 0000 hr to 1100 hr IST and Figure 4.8(b) shows profiles from 1200 hr to 2300 hr IST. Usual concave downward curves exhibit from 1700 hr to 0900 hr IST through 0000 hr, shows presence of stable SBL layers elapses for 16 hours. Other profiles are generally concave upwards, which show unstable atmospheric conditions.

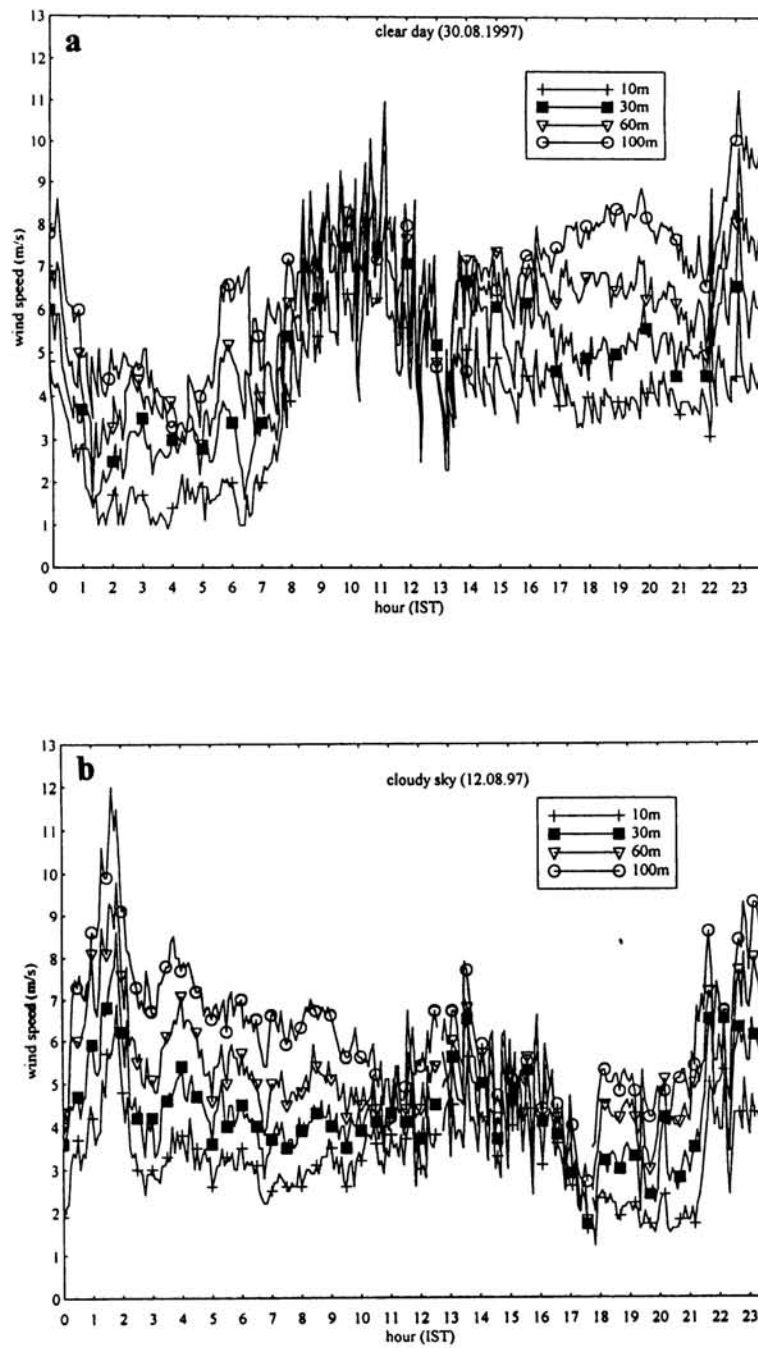


Figure 4.7a,b Diurnal variations in wind speed on a particular day

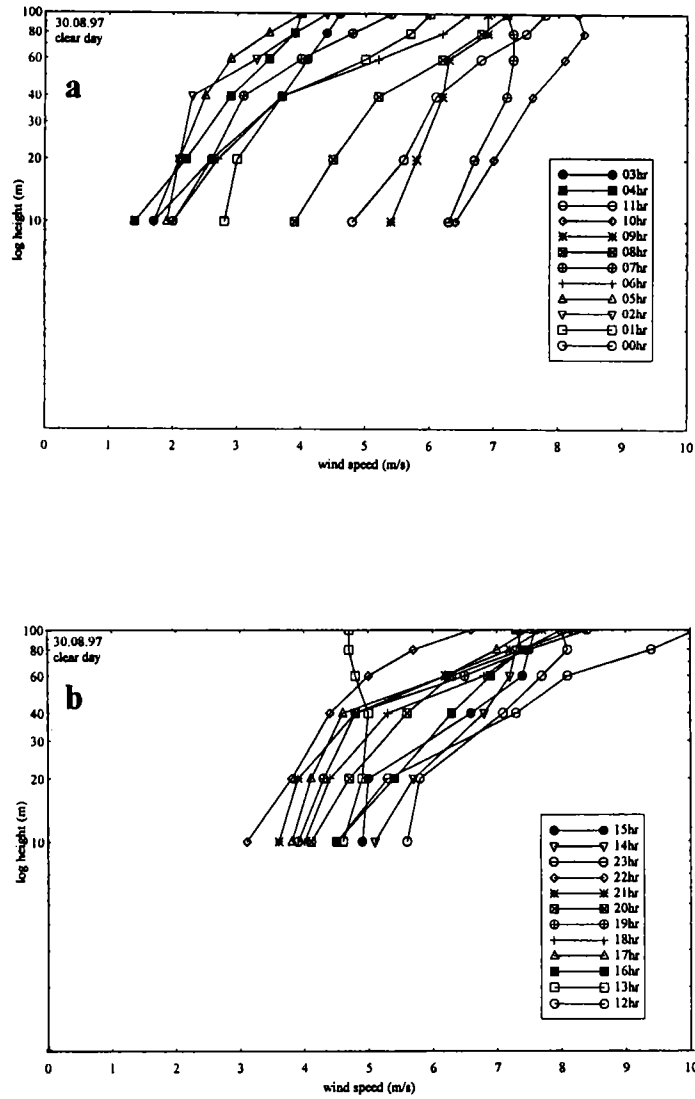


Figure 4.8a,b Logarithmic wind profiles on clear day condition

4.5 Nature of SBL Winds in Association with Severe weather

4.5.1 Thunderstorm Winds

Thunderstorms are associated with downdrafts, leads to drastic change in wind speed and direction. In Figure 4.9 a thunderstorm case wind behaviour for each successive five minute interval period, average wind speed and maximum wind speed are presented. During 2350 hr IST, the difference between average wind speed and maximum wind speed are at the order of 10 ms^{-1} at levels, which is due to the passage of thunderstorm. As direction variability associated with thunderstorms are very high, wind direction fluctuations (σ_θ) are computed for various thunderstorm cases where maximum wind speeds are $> 20 \text{ ms}^{-1}$. σ_θ computed for different tower levels and the period for the computation was 30 minute which is presented in Figure 4.10. Five cases are presented, in which May 01, 1996 was a sandstorm event, in this case σ_θ is shown more than 40° .

4.5.2 Thunderstorm Weather Assessment on Peak Wind Speed

In this study every five minute peak wind at the level of 20 m is considered. In elapsed time information about peak wind, continuous five minute packets are considered in association with the life history of a thunderstorm cell. Figure 4.11 shows probability of peak wind associated for $\geq 15 \text{ ms}^{-1}$ at 20 m level in the SBL. The percentage probability values are to be viewed, in accordance with the monthly number of observations (N). For example, in March, the percentage probability is highest of around 40% means. Out of 5 events there are two severe events with wind speeds exceed 15 ms^{-1} . This indicates though number of events in March are less than in south west monsoon, there is a good probability to reach severe storm wind speeds with $\geq 15 \text{ ms}^{-1}$. Generally 22% probability of $\geq 15 \text{ ms}^{-1}$ can be seen with southwest monsoon thunderstorms. Events with $\geq 15 \text{ ms}^{-1}$ in December to February are not reported. Least percentage probability of exceedance with $\geq 15 \text{ ms}^{-1}$ in October is noted though number of events are of the order 113.



R
551,552
SAM

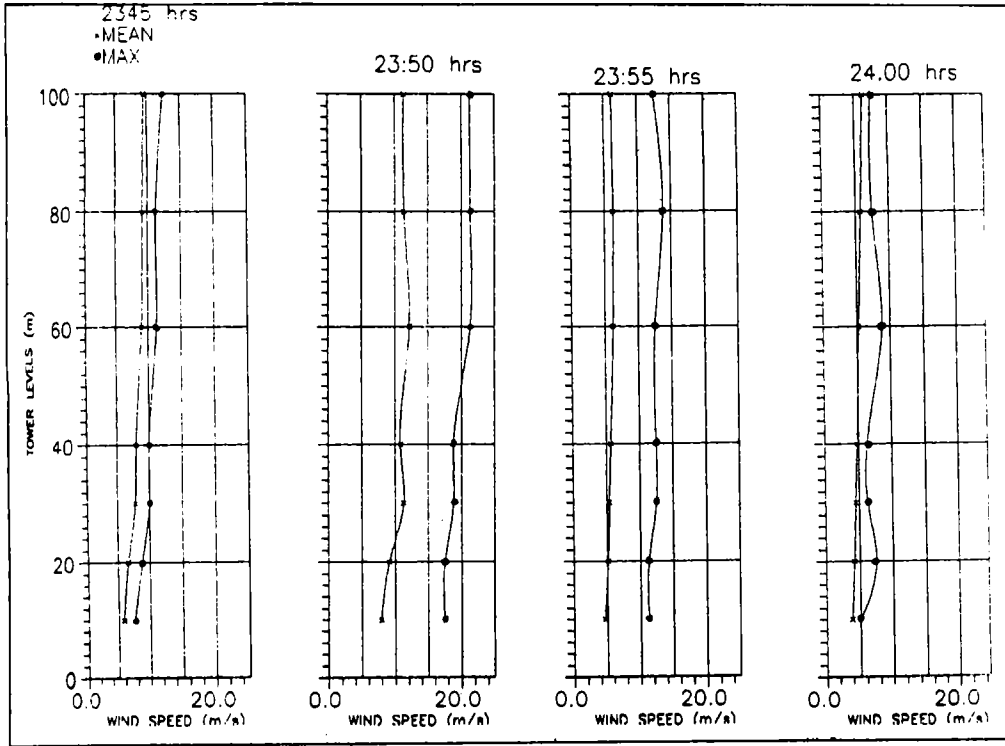


Figure 4.9 Thunderstorm winds in SBL on 08-03-1993

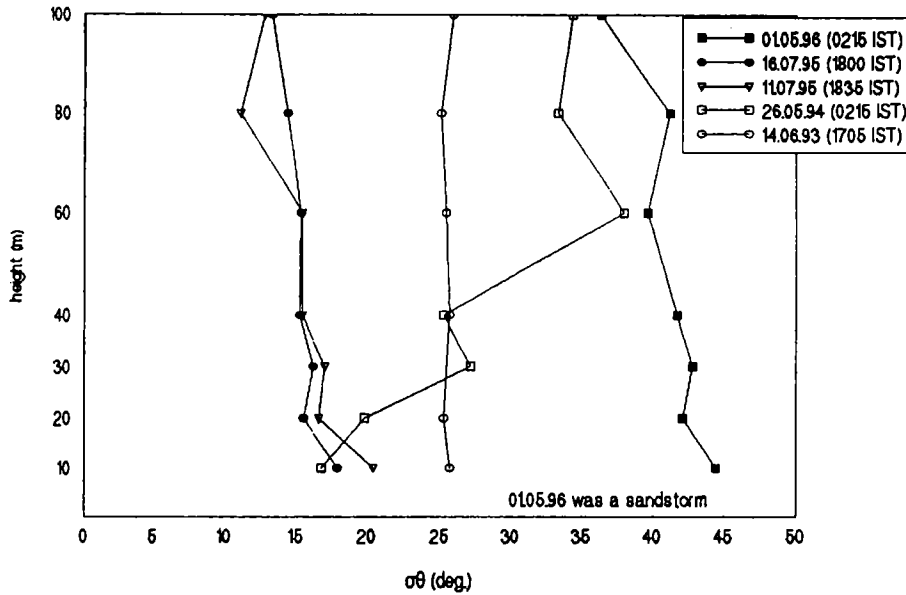


Figure 4.10 Standard deviations in wind directions (σ_{θ}) for thunderstorm winds of $\geq 20 \text{ ms}^{-1}$ at 20 m SBL level

Figure 4.12 tells us about the events of $\geq 15 \text{ ms}^{-1}$ peak wind scenario and its duration. There were 86 events in 11 years (including the data obtained at 20 m level from a MET pole). 47% of events are sustained only for 5 min duration. 30% with 10 min duration. All others are of meagre incidences. Only one case was reported for about 55 min on July 09, 1997 from 2050 to 2145 hr IST.

Generally, ground winds of $\geq 20 \text{ ms}^{-1}$ is associated with a specific synoptic/meso-scale weather phenomena near SHAR region. Table 4.4 provides thunderstorm peak wind speed history of $\geq 20 \text{ ms}^{-1}$ over SHAR at 20m level. Ten events are observed from the available thunderstorm history. Out of the events May 01, 1996 was a severe sandstorm episode in which the peak wind speed of $\geq 20 \text{ ms}^{-1}$ sustained for about 15 min was observed.

Thunderstorm peak winds segregated for $\geq 15 \text{ ms}^{-1}$ at 20m level are checked along with occurrence or non occurrence of rain during the event and is shown in Figure 4.13. For this a total number of 117 peak wind events of $\geq 15 \text{ ms}^{-1}$ are considered, out of which only ten occasions are noted without rain over the station. More than 70% of rain in association with peak winds of $\geq 15 \text{ ms}^{-1}$ are ended with rainfall intensity of less than 10 mm per hour.

4.5.3 Winds in SBL during a Severe Cyclonic Storm

After the establishment of 100 m tower facility at SHAR Range, a severe cyclone passed over the station on October 31, 1994. Based on mean wind speed and direction, peak wind speed in 5 minute duration variations with time at different levels during the peak cyclonic activity over the station are presented in Figure 4.14(a)-(c). Maximum mean wind speed was 14 ms^{-1} at 10 m level and 32 ms^{-1} at 100 m level (Figure 4.14(a)), ie., 100 m mean wind speed doubled from 10 m level mean wind speed. Corresponding peak wind speed at 10 m level was 30 ms^{-1} and 38 ms^{-1} at 100 m level. (Figure 4.14(b)). From these it may be noted that though there is significant difference in mean wind speed with height, it is not so

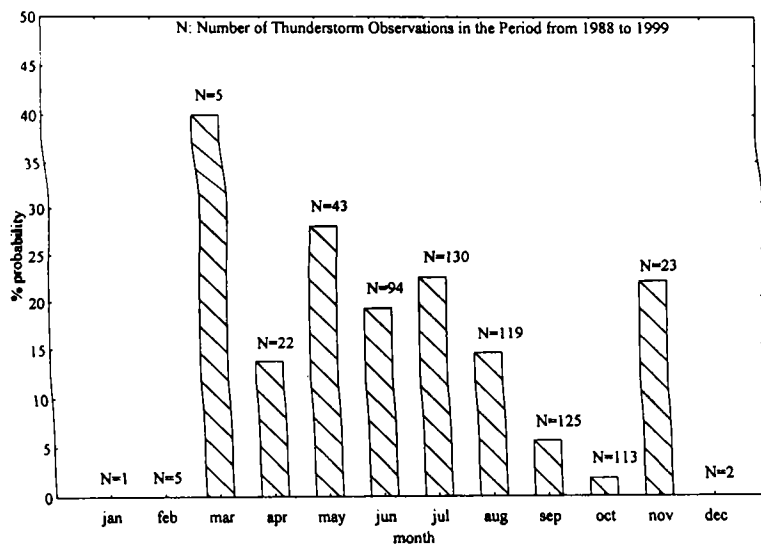


Figure 4.11 SHAR % probability of peak wind speed $\geq 15 \text{ ms}^{-1}$ associated with thunderstorms in 20 m level (excluding thunderstorms during low pressure systems)

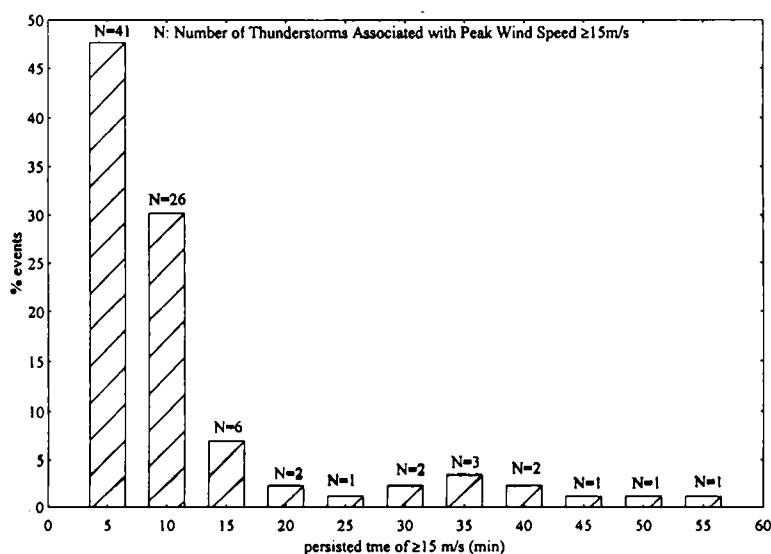


Figure 4.12 SHAR elapsed time of thunderstorm peak winds $\geq 15 \text{ ms}^{-1}$ in 20 m level out of 86 events (excluding thunderstorms during low pressure systems)

Table 4.4 Thunderstorm peak wind history of $\geq 20 \text{ ms}^{-1}$ over Sriharikota at 20 m level

No	Date	Time	Maximum Wind $\geq 20\text{m/s}$ (Vmax) m/s
1	22.05.89	0200	24.60
2	14.06.93	1705	21.30
3	10.11.93	1135	21.30
4	26.05.94	0215	20.00
5	14.07.94	1945	20.00
6	11.07.95	1835	20.00
7	16.07.95	1800	21.20
8	16.07.95	2105	21.20
9	01.05.96	0140	30.00
10	30.06.98	1705	23.80

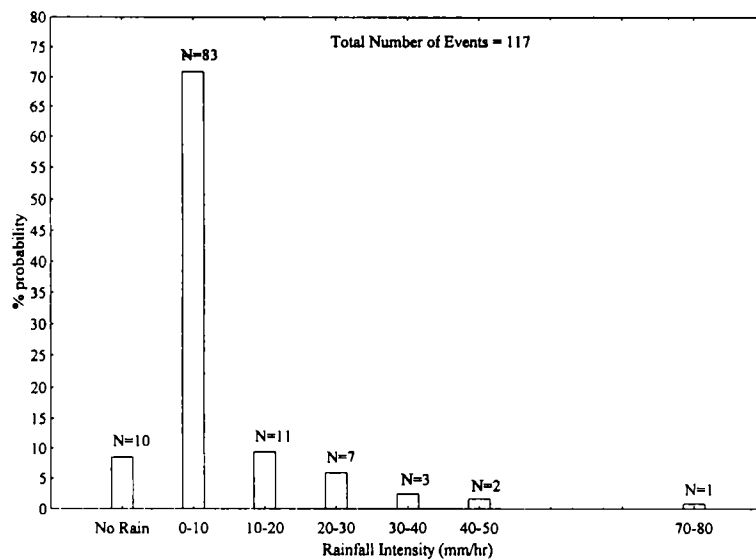


Figure 4.13 Thunderstorm peak winds of $\geq 15 \text{ ms}^{-1}$ and associated rainfall intensities (excluding thunderstorms associated with low pressure systems)

in the peak wind speed. A slight veering (clockwise with height) of wind direction is observed from lower levels to 100 m level, throughout the phase of cyclone crossing (Figure 4.14(c)).

4.5.4 Number of Occurrence of Wind Speed Events during the Progress of a Cyclonic Storm

In the developmental process of the severe cyclonic storm which crossed very near to the station on October 31, 1994 is studied in detail based on the number of occurrence of wind speed events from October 28, 1994 onwards, in order to understand the clustering of maximum occurrences of wind speed values as in Figure 4.15(a)-(d) at 100 m level. On October 28, 1994, the low pressure region in the Bay of Bengal is not affected the station through its wind potential. There was a single maximum centered between 2.5 to 5 ms^{-1} , but the clustering of occurrences distributed below 60 number of occurrences in all speed classes (Figure 4.15(a)). On October 29, 1994 the low pressure area deepened further into a depression and the clustering around an upper wind class of 6 ms^{-1} , with less than 45 number of occurrence is seen (Figure 4.15(b)). In the deep depression and cyclonic stage on October 30, 1994, there was three modal classes, or three maxima concentrated classes viz., around 7.5 ms^{-1} , 12.5 ms^{-1} and 17.5 ms^{-1} . All histograms are flattened or widened from the previous day, and the number of occurrences are less than 30 (Figure 4.15(c)). On October 31, 1994, the system of severe cyclonic storm potential crossed the coast. When the system is very near to the coast the land fall wind speed events contributed histogram formations of > 15 ms^{-1} wind events and there was no specific model class, other than a single class around 19 ms^{-1} and different independent classes of maxima (Figure 4.15(d)). Figures 4.15(a)-(d) confirms the change of wind clustering classes from single to more than two model classes in a day, as the approach of a cyclonic storm towards the station.

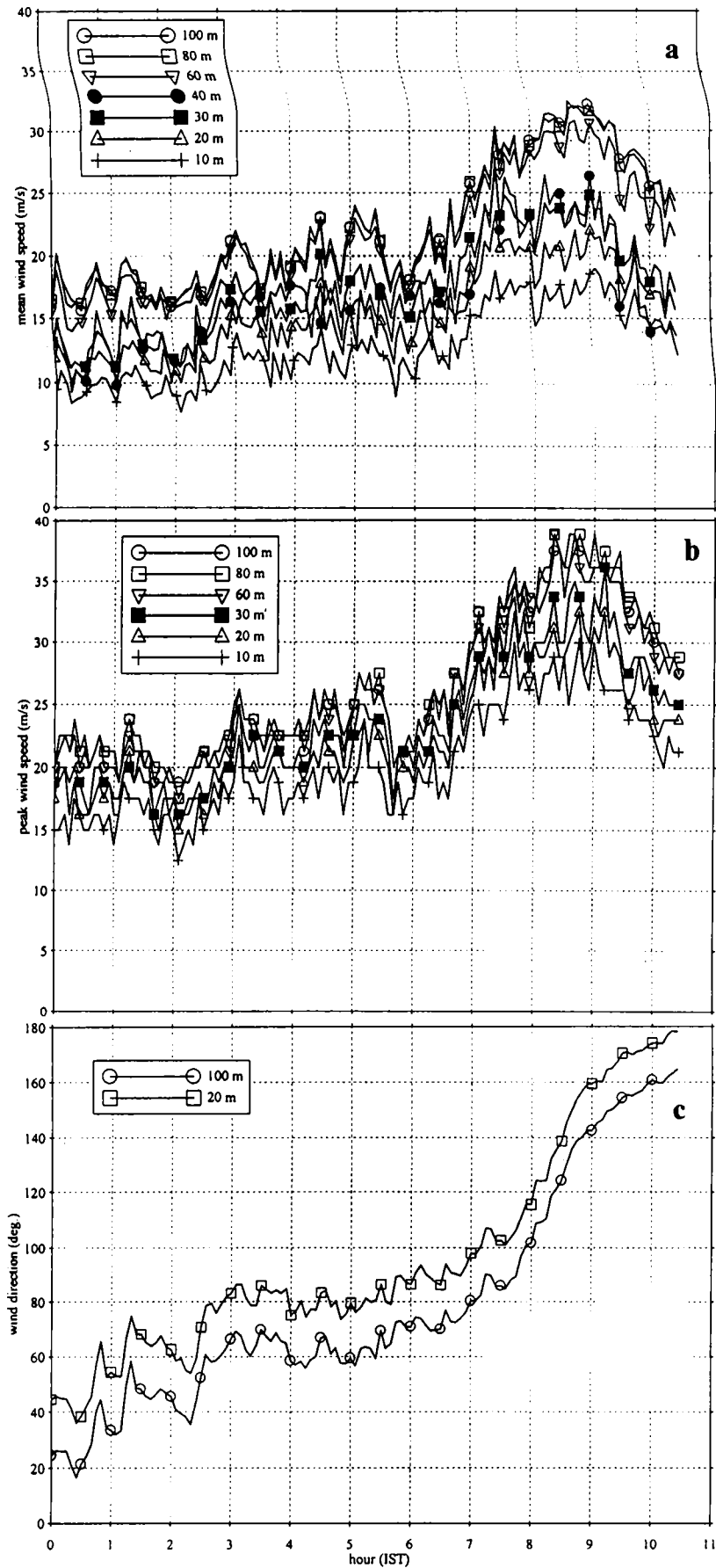


Figure 4.14a-c SBL wind during severe cyclone passage on 31.10.1994 (a) mean wind speed (b) peak wind speed and (c) wind direction

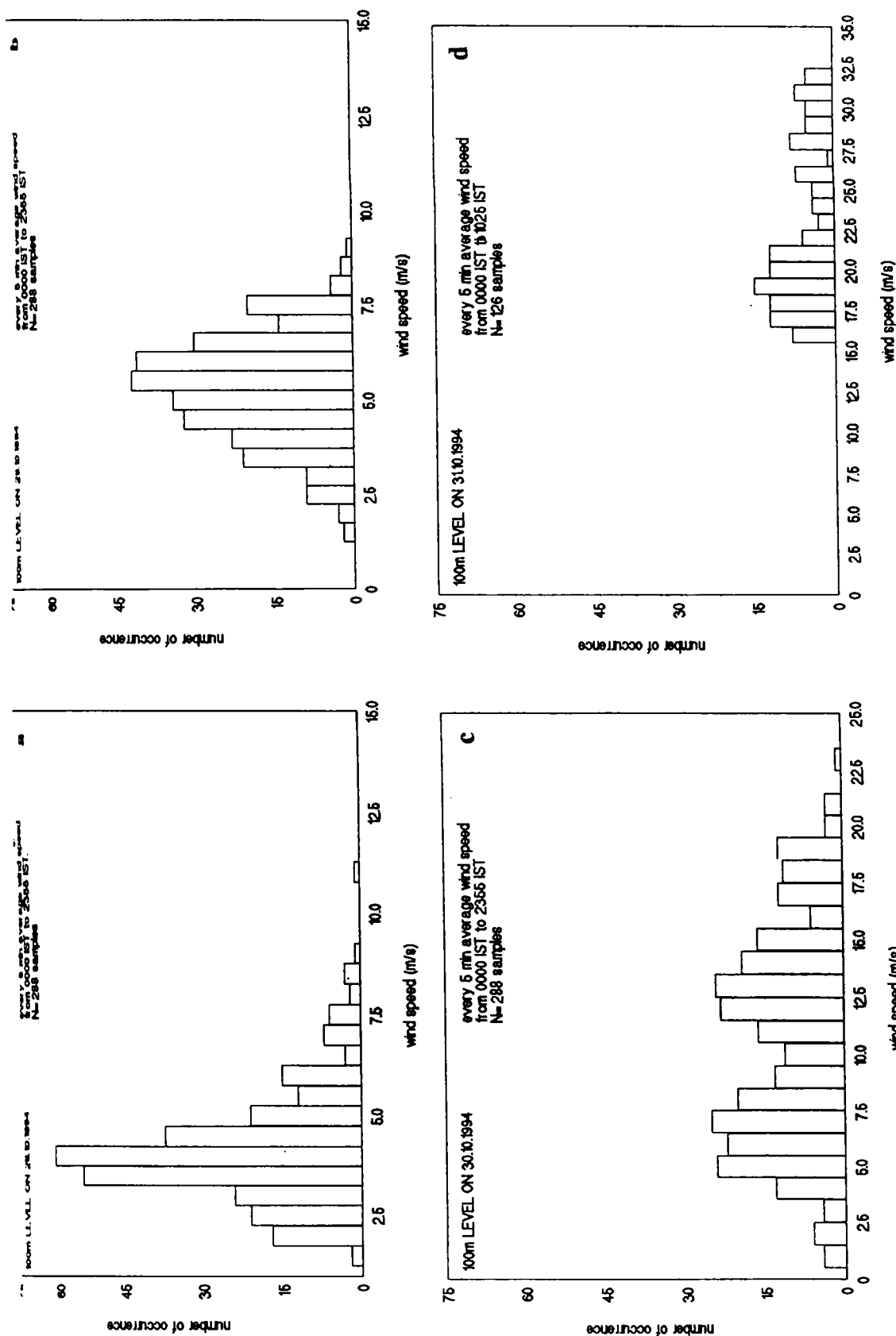


Figure 4.15a-d Number of occurrence of wind speed events at 100 m level from low pressure formation (28.10.1994) to severe cyclonic stage (31.10.1994)

4.5.5 Spectral Characteristics of SBL Winds in the Influence of Low Pressure

System

In this section, spectral properties of SBL winds in the influence of low pressure systems are examined. On October 05, 1999, INSAT cloud imagery of 0830 hr IST shows the existence of a low pressure system in the south east coast of peninsular India (Figure 4.16). Low pressure systems are associated with intermittent rainfall, thunderstorm formations etc. The time series of wind variations are already presented in Figure 1.24 from October 05, 1999, 1615 hr IST onwards. There was a wind speed hike in all levels noticed around 54000 s in association with a thunderstorm.

Standard Fast Fourier Transformation (FFT) (Cooley and Tukey, 1965) technique is applied to the 1 s data for a period of 9 hour. In this 1 second data points the thunderstorm wind also included, so as to get spectral picture of a typical low pressure system. In FFT, Hamming windowing is applied in order to minimise the distortions of the spectrum.

Clear peaks are seen in the period range from several seconds to more than ten minutes in the spectrum. The horizontal u component spectrums are critically examined for levels 20 m and 100 m (Figure 4.17(a) and 4.17(b)). Two spectral plots showed very identical periodicity and energy values confirm energy distribution in all levels in SBL are equal for low pressure systems. According to selected run, the frequency range analysed is from 3.05×10^{-5} to 1 cycle per second, corresponding to a period range from 1 to 32768 s, so as to cover micro to meso-scale meteorological spectrum. Low frequency part is considered above 1 min and high frequency spectrum below 1 min. In high frequency range there is an obvious period at 8 s and the valley sloping rightwards and attains a minima around 1.3 min. A prominent maxima around 54.6 min followed by a strong lull around 1.8 hr. This lull diminishes for a secondary dominating peak at 2.8 hr and

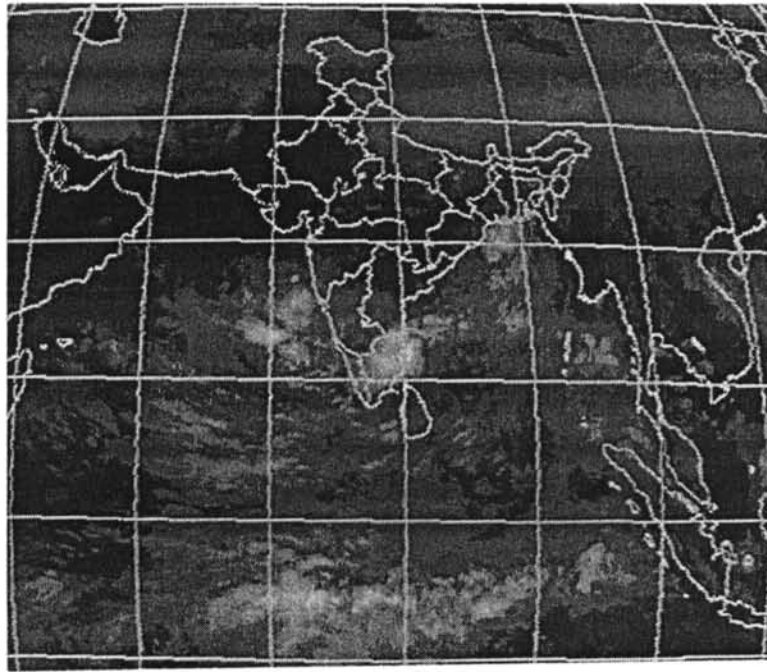


Figure 4.16 INSAT cloud imagery showing low pressure area over SHAR region on 05.10.1999

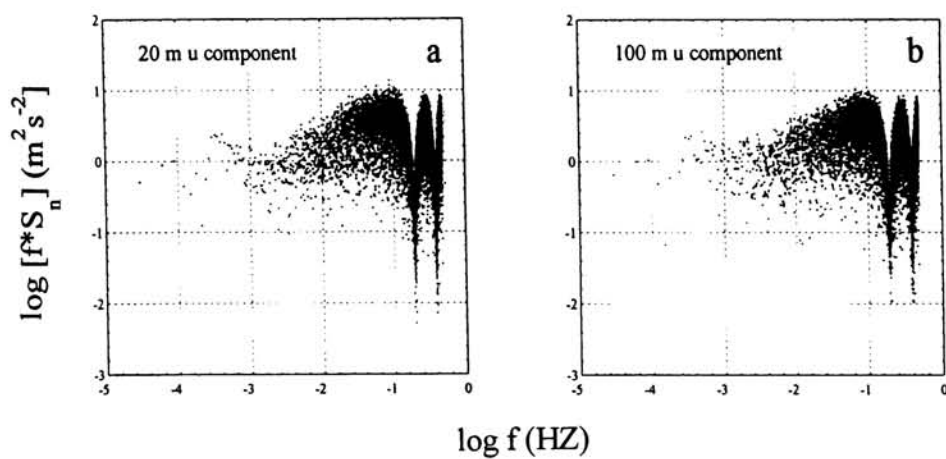


Figure 4.17a,b Horizontal u component spectrum at 20 m level and 100 m level in the SBL associated with low pressure system over SHAR region

again dropping to a lull at the period of 3.6 hr. So in low frequencies every hour there will be an incidence of high and low amplitudes alternately, which may be significance of a typical low pressure system.

4.6 Exceedance Probability of Peak Wind Speed with Different Limits

Exceedance probability of extreme wind events in the SBL over a station is having potential applications in wind load and wind energy studies. For a space station, these models are of significant importance in taking decisions in the count down phase of launch. Both meso and synoptic features viz., thunderstorms, sea breeze, passage of troughs over the station, low pressure system formations can contribute major modifications in the distribution of peak wind speed events in temporal scale.

The exceedance probability of peak wind speed over a certain limits like 5 ms^{-1} , 10 ms^{-1} , 12 ms^{-1} and 15 ms^{-1} are studied. If the exceedance probability of wind speed with mentioned limit prevail less than 20 min and if it is observed at only 2 to 3 levels or about less than 5 % the same is considered as 'InSignificant' (IS) and NIL indicates for not even a single record with that observation of crossing the limit are presented in Table 4.5. In this table, exceedance probability of different limits of wind speeds ($> 5 \text{ ms}^{-1}$, $> 10 \text{ ms}^{-1}$, $> 12.5 \text{ ms}^{-1}$ and $> 15 \text{ ms}^{-1}$) are presented for different months and for different times of the day. The day is divided into 4 parts of 6 hour each, as early hours of the day (00-06 hr), morning (06-12 hr), afternoon/evening (12-18 hr) and late evening/night (18-24 hr). The 100 m SBL is divided into three parts as the Lower Boundary Layer (LBL) from 10-30 m, the Middle Boundary Layer (MBL) 30-60 m and the Upper Boundary Layer (UBL), 60-100 m. The distribution of exceedance probability in percent is shown in the Table 4.5 according to the time and height specifications mentioned.

Frequency of exceedance probability of $> 15 \text{ ms}^{-1}$ at any time in a day is mostly IS or NIL. However, around 5% chances are there between 1200 hr and 1800 hr IST in the MBL during April and May.

The exceedance probability of 12.5 ms^{-1} is about 25 to 30% in the evening during April and May. The frequency increases from 1200 hr to 1800 hr IST and then decreases from 1800 hr to 2400 hr IST which is normally associated with building up of sea breeze and then withdrawal phase of sea breeze respectively. During June, July and August the frequency is about 5 to 10% in the evenings. Generally, exceedance probability of 12.5 ms^{-1} may be due to passage of trough or thunderstorm over the station. Hence IS events are mostly seen in the Table 4.5.

The exceedance probability of 10 ms^{-1} during afternoon and night of April and May is about 50 to 60% in MBL and UBL. The exceedance probability generally increases from afternoon to evening and decreases towards night. Mostly this exceedance probability is about 10 to 20% during afternoon and evening in the remaining months. However, it is IS or NIL during January and February in the early hours of the day.

Exceedance probability of 5 ms^{-1} during afternoon and evening is about 60 to 95% on any day of the year. This indicates the prevailing wind speed in the SBL over the station may touch 5 ms^{-1} at any time. Moderately strong winds of the order between 5 and 10 ms^{-1} exist during afternoon to evening.

4.7 Temporal Structure of Derived Wind Variables in the SBL

4.7.1 Coefficient of Variation in relation to Mean scalar Wind Speed

Estimation of Coefficient of Variation (CV) stands as a tool to measure the dispersion of any events of statistical significance from mean of the events. The CV derived as a ratio between standard deviation (σ_v) to MSWSP expressed in percentage or 100 times the coefficient of dispersion based upon standard deviation is called Coefficient of Variation (CV) as

$$CV = (\sigma_v / MSWSP) \times 100 \quad (4.9)$$

where,

$$\sigma_v = \sqrt{\frac{\sum_{i=1}^N V_i^2 - (\sum_{i=1}^N V_i)^2 / N}{N-1}} \quad (4.10)$$

and MSWSP is represented in equation (4.1). CV is the percentage variation in the mean, standard deviation being considered total variation in the mean. For comparing the variability of two series, CV are computed. The series having greater CV is said to be more variable than the other and the series having lesser CV is said to be more consistent.

Diurnal variation of CV in relation to MSWSP is presented in Figure 4.18(a)-(1). In the wind merging period described, the standard deviations of wind speed show high values in the diurnal variation. The maximum values in the diurnal pattern of CV occur during this wind merging period.

Monthly variation ranges can be summarised as in Table 4.6 keeping near representative value for all values together. It is observed that there is no significant variation in CV from May to August within a day, so that the dispersion from mean, CV is from 25 to 40%.

4.7.2 The Diurnal Pattern of (u,v) Components and Intra level Correlation

Coefficients between u and v Components (ρ_{uv})

Mean (u,v) components are derived and analysed their relation within the level (intra-level) through correlation coefficient (ρ_{uv}). Figures 4.19(a)-(1) show the mean (u,v) components and ρ_{uv} diurnally for each month. The computation of ρ_{uv} is carried out based on equation (4.6). ρ_{uv} variations categorise two major entities viz., February, March and April in the first category and June, July, August and September in the second category. Among the first category ρ_{uv} reaches 0.8 around 1100 hr IST and is the highest correlation value in an year. In

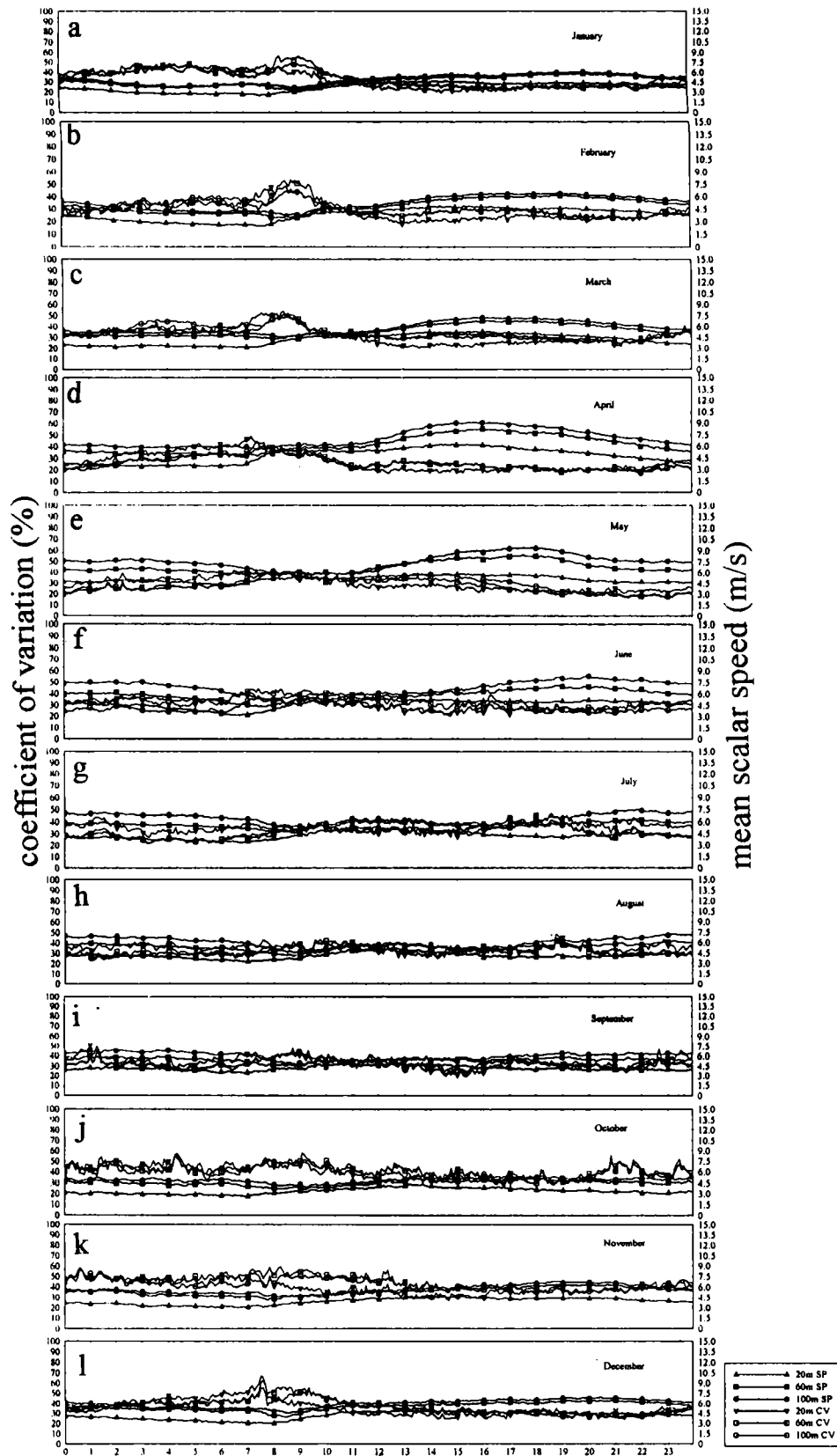


Figure 4.18a-l Diurnal variation of Coefficient of Variation in relation to MSWSP in different months

Table 4.6 Coefficient of Variation in different months

Month	Minimum CV (%)	Maximum CV (%)
January	25	40-53
February	18-25	42-52
March	25	40-50
April	20	35-45
May	20	35-40
June	25	25-40
July	25	25-35
August	25	25-35
September	25	45
October	35	45
November	35	55
December	30	40-55

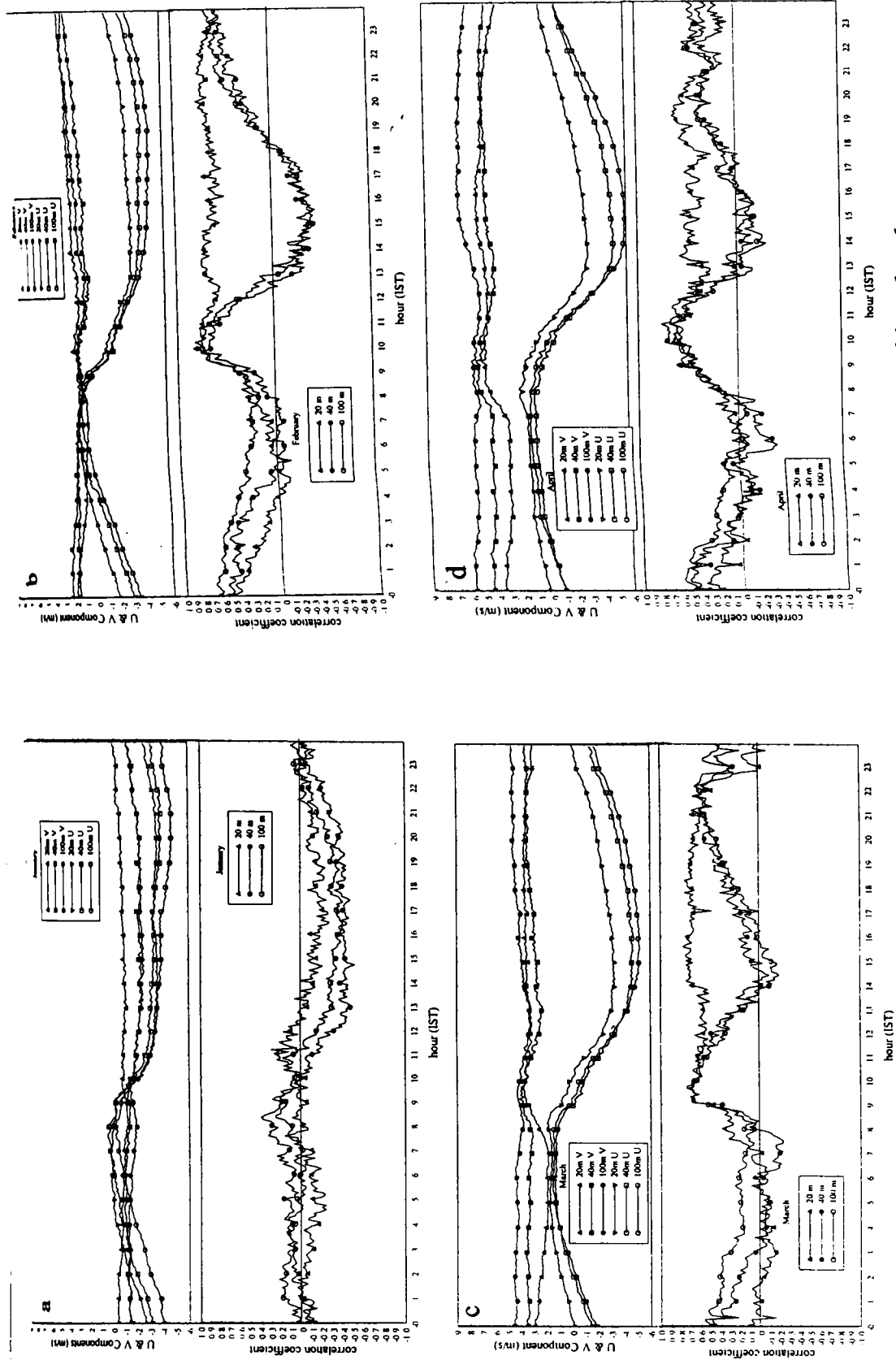


Figure 4.19a-d Diurnal variation of mean (u,v) components and intralevel correlation coefficient (ρ_{uv}) in different months

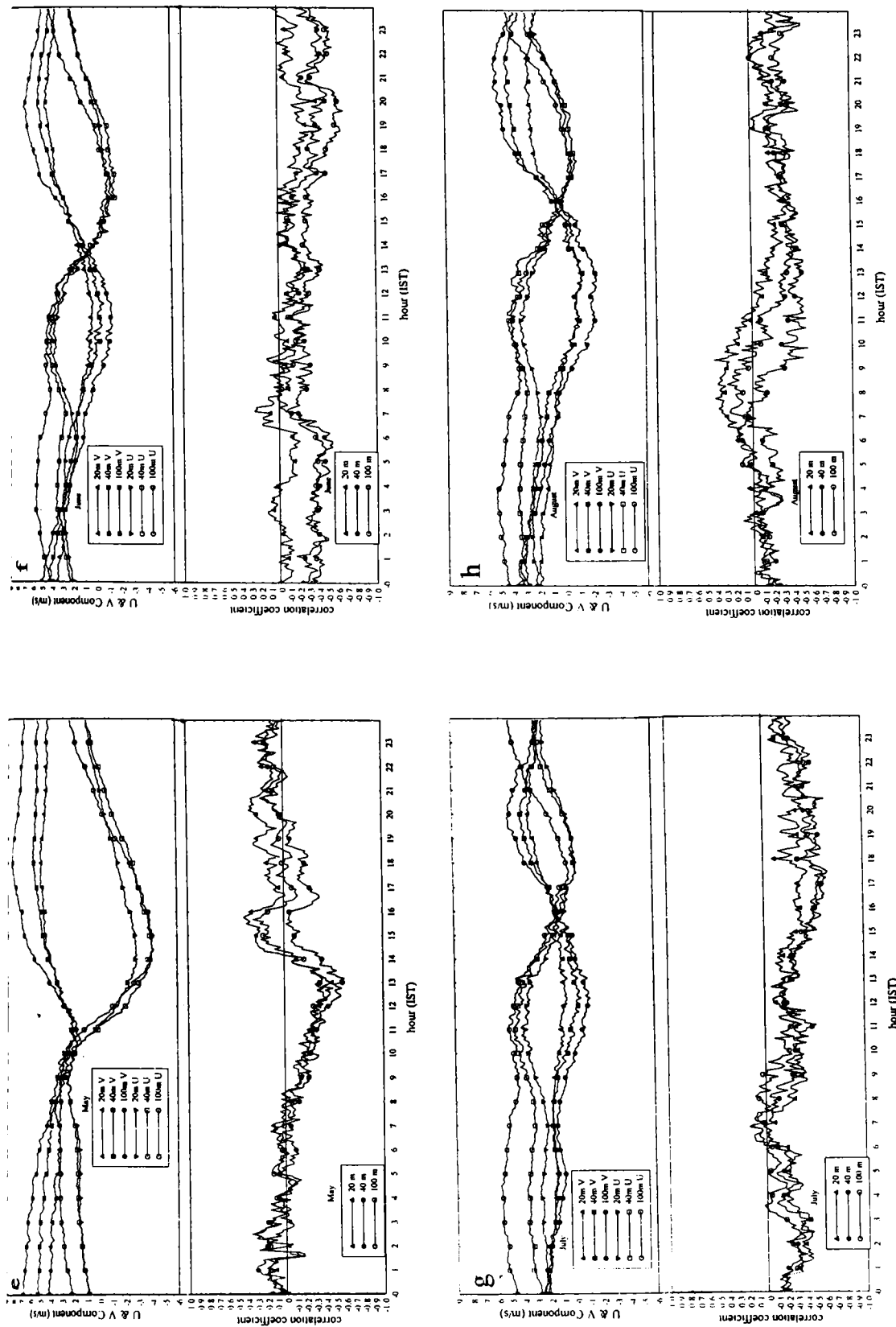


Figure 4.19e-h Diurnal variation of mean (u, v) components and intralevel correlation coefficient (ρ_{uv}) in different months

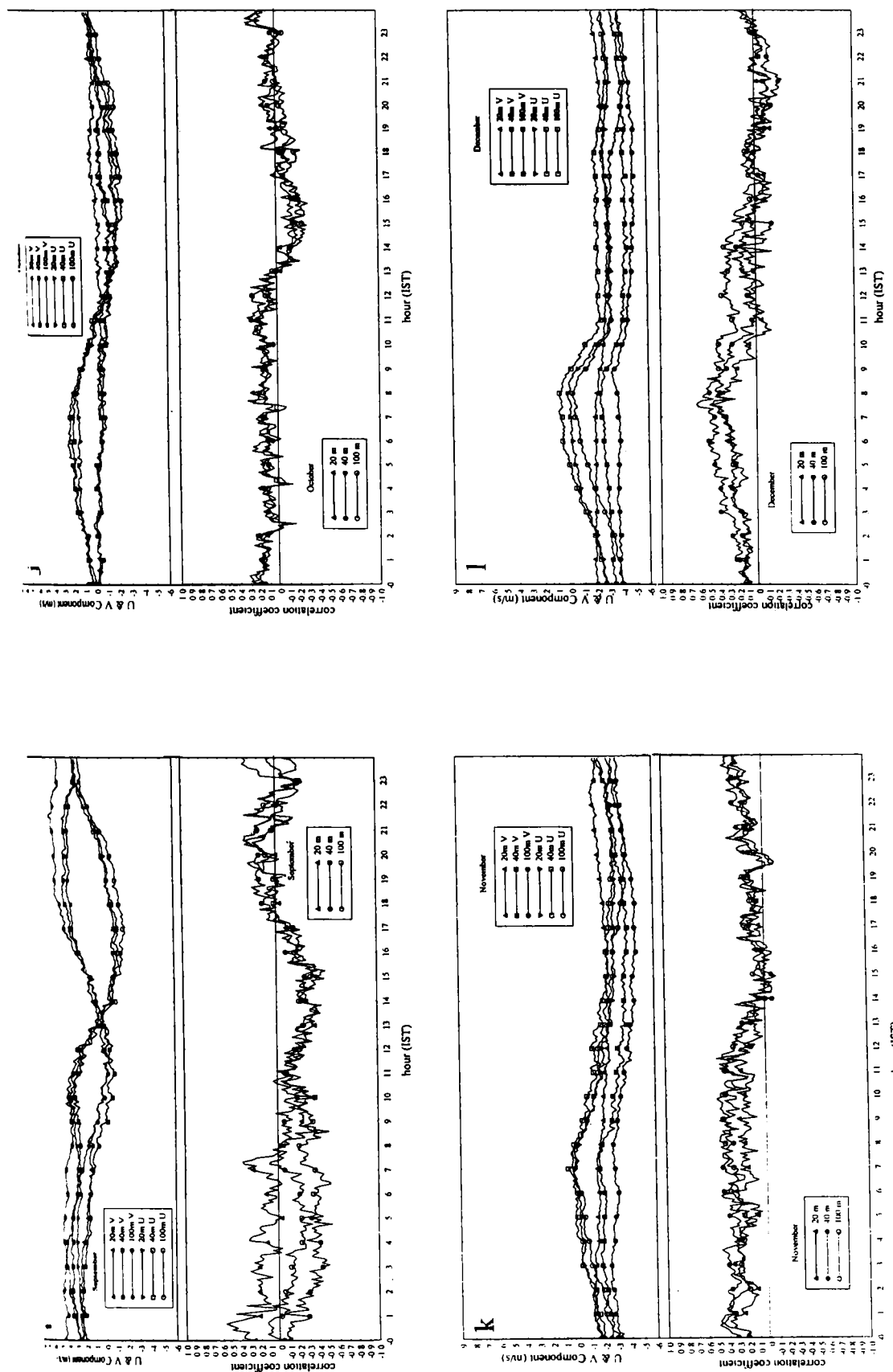


Figure 4.19 i-l Diurnal variation of mean (u, v) components and intralevel correlation coefficient (ρ_{uv}) in different months

the second category, generally negative ρ_{uv} values are dominating in the diurnal curves. Similarity in u , v component variations exist within each categories separately. Least relations among u and v are observed in October and the values are ranges 0.3 to -0.3.

4.7.3 Diurnal Variation of σ_θ in Different Months

The standard deviation of wind directions are calculated and presented as diurnal variation in each month from Figure 4.20(a)-(l). High inverse relationship is observed between the previously discussed property of wind steadiness factor and σ_θ , ie.,

$$\text{SF (\%)} \propto 1/\sigma_\theta \quad (4.10)$$

High steady winds are associated with low σ_θ and low steady winds with high σ_θ values. Throughout the year σ_θ values vary between 15° to 45° , April and May months show generally less values of σ_θ . This implies high steadiness factor and thereby direction oscillations are less. Change over times of land breeze to sea breeze are most prone to high σ_θ values, where the values generally cross 40° in intense sea breeze months from May to September. In October, σ_θ values are of the order of 40° or higher as the month is a representative month having change over of two monsoon seasons viz., southwest monsoon to northeast monsoon. As steadiness factor is taken as a measure of sea breeze onset timing, σ_θ also shows similar variations. Both steadiness factor and σ_θ variation curves are do not show any dependency or specific pattern of one level over the other.

4.7.4 Comparison between MSWSP and MRWSP

Figure 4.21(a)-(l) make comparison between MSWSP and MRWSP. MSWSP is greater than MRWSP at all level. An abrupt dip followed by an intense increase in MRWSP is seen during change over times of land breeze to sea breeze. During this time, the difference between MRWSP and MSWSP are at its highest for any level. Highest difference occurring portion in the diurnal curves are

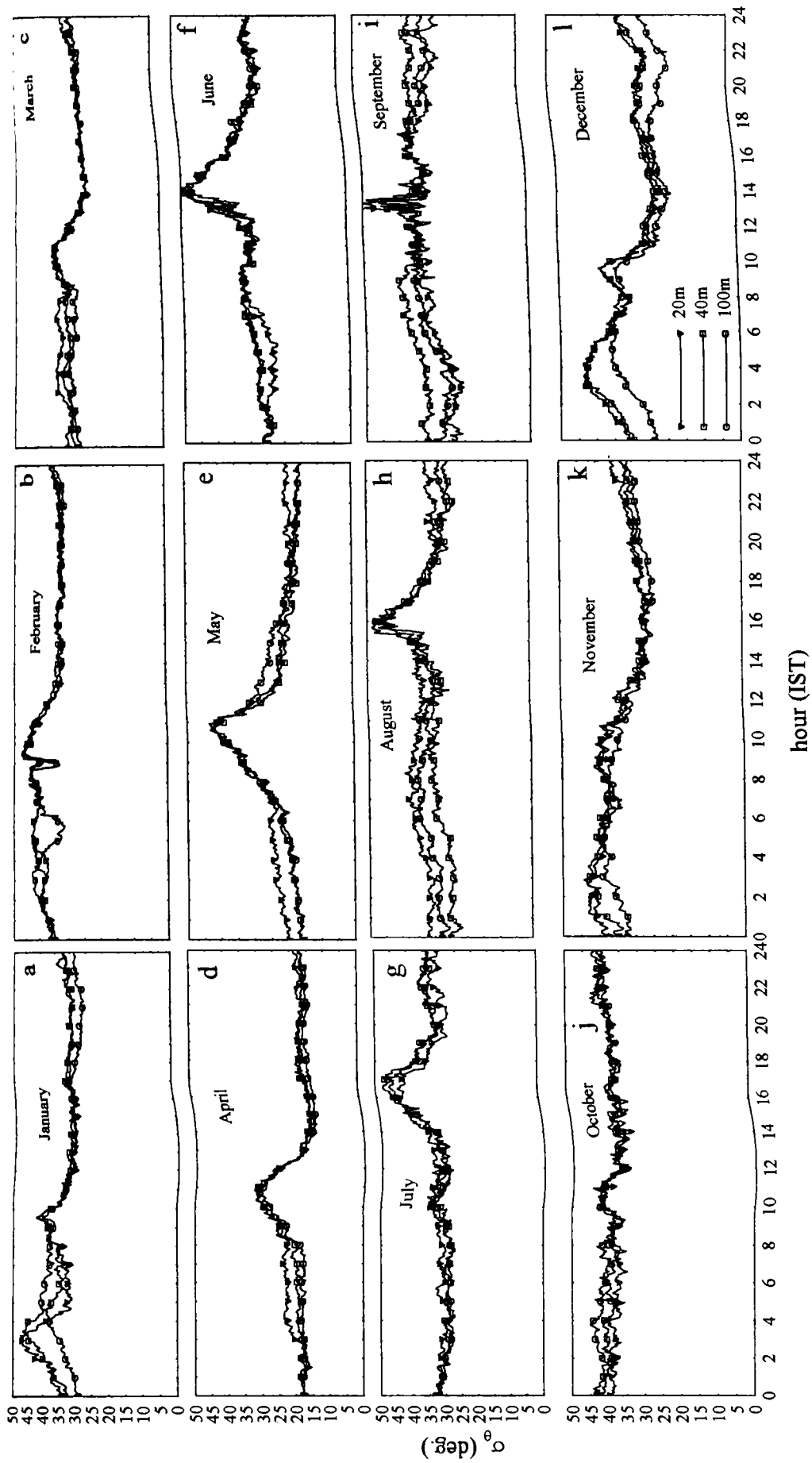


Figure 4.20a-l Diurnal variation of standard deviation of wind directions (σ_{θ}) in different months

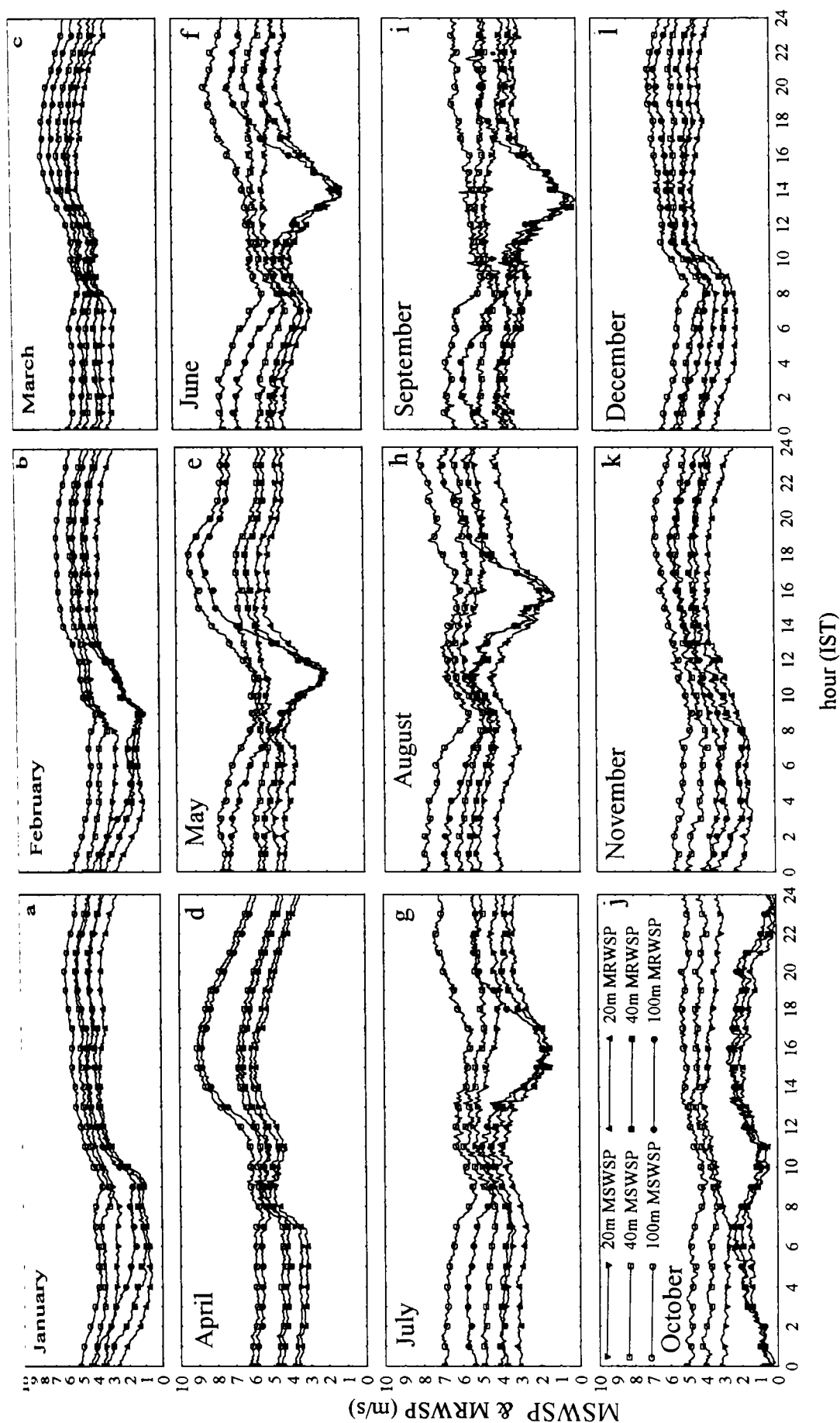


Figure 4.21a-l Comparison between MSWSP and MRWSP in different months

markedly departed in southwest monsoon months as land breeze and sea breeze flows are most differentiable. The difference between MRWSP and MSWSP are in the least during April, where σ_θ values are least comparing to other months. So fluctuations in wind direction within a day is the main factor keeping the relation between MRWSP and MSWSP.

4.7.5 Gust Factor Variations

Gust Factor (GF) can be measured as

$$GF (\%) = (V_{\max} - V_{\text{mean}}) / V_{\text{mean}} \times 100 \quad (4.11)$$

For this calculations quasi-steady state wind and two minute peak (gust) winds from SET II is used. Figure 4.22(a)-(l) show the diurnal variations in GF through various months. For these plots mean GF are computed. GF of three levels viz., 20 m, 40 m and 100 m are shown in figures. As height increases GF decreases. In the diurnal variation curves, 100 m GF curve positioned bottom most and other levels are sequentially fallen one over the other. This indicates that SBL winds are more gusty in levels near to the surface compared to upper levels. The GF difference between lowest level to highest level is in the order of 20% to 30%. During wind merging period, the winds are in highly gusty in the diurnal variations throughout the year.

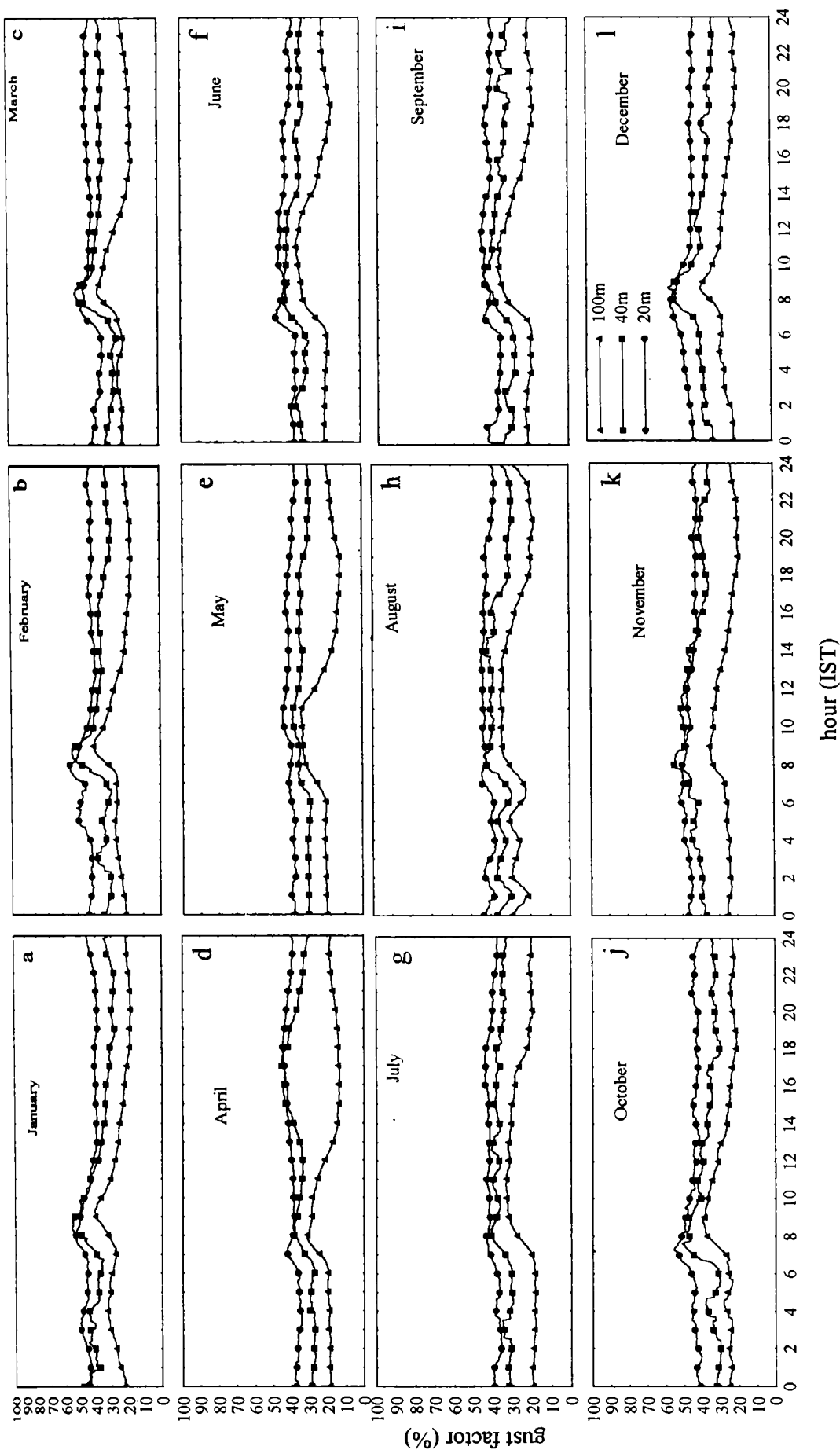


Figure 4.22a-l Diurnal variation of gust factor in different months

Chapter 5

*Wind Variability and Elliptical
Approximation of Wind
Hodographs in the SBL*

5.1 Introduction

The quantitative characteristics of meso-scale weather systems, like sea and land breezes are thoroughly studied and well established. When the synoptic-scale pressure gradient is weak this diurnal cycle of onshore winds during day (sea breeze) and offshore winds at night (land breeze) will be the dominating weather features for a coastal station. The modelling of meso-scale circulations in coastal regions due to boundary layer forcing has got significance in the field of short range weather forecasting and local weather predictions. Meso-scale contribution arising from differential heating and radiational cooling of land and its interactions with synoptic-scale weather patterns is the cause of diurnal cycle of wind variability. The present study is, therefore carried out by the help of a ratio (α) between diurnal and interdiurnal wind variabilities (Alpert and Eppel, 1985). Same technique is adopted at the outset of this study in order to classify the monthly wind variability in the SBL over Sriharikota and thereby the dominance of meso- and synoptic-scale forcings. Later part of the study is confined to mean diurnal oscillations of wind components at different height levels in SBL for each month. Extensive studies, both theoretical as well as observational were reported on diurnal oscillations of wind components (Haurwitz, 1947; Staley, 1989; Reed, 1979; Garrett and Smith, 1985 and Zhong and Takle, 1992)

5.2 Observations and Data

SET II data (May 1993 to April 1996) from the tower levels are considered as the input data for the analysis. Computation of wind variability ratio (α) is carried out on every fifth minute zonal wind components at each level for different months. The zonal flow is taken into consideration because the momentum advection for meridional component is only a very small difference between its local and total derivatives compared with zonal advection. Also, variance of x-component velocity is not so sensitive to changes in stability (Lumley and

Panofsky, 1964) and less dependence to surface roughness parameter (Z_0) (Ramachandran et al, 1994). As the coastline lies in 360-180° azimuth the zonal wind component represents the wind component normal to the station which is having significance in boundary layer studies. The wind variability ratio (α) derived with zonal wind component and the wind component derived normal to the coastline (head wind component) shows similar values for all months in all SBL levels which confirms zonal flow consideration is enough for such studies over the station. For the construction of wind hodographs, every half an hour zonal (u) and meridional wind (v) components are computed and averaged out. Three point moving average technique on the components decrease the noise level of the data used to construct wind hodographs.

5.3 Wind Variability Ratio (α)-Mathematical Formulations

The method proposed by Alpert and Eppel (1985) to study the meso-and synoptic-scale wind variability is as briefed below.

The normalised diurnal wind variability or diurnal relative gustiness

$$I_b = \left[\sum_{i=1}^n (U_{ij} - U_j)^2 \right]^{1/2} / (n U_j) \quad (5.1)$$

where U_{ij} is the zonal component of wind at i^{th} minute in the hour and day j , n the number of samples. In the present study each five minute data constitute a total of 288 samples per day and

$$U_j = \left(\sum_{i=1}^n U_{ij} \right) / n$$

is the average diurnal wind in the zonal direction for the j^{th} day. The average value of I_b over a period of N days is given by

$$\bar{I}_b = \left(\sum_{j=1}^N I_b \right) / N \quad (5.2)$$

In similar fashion it is concluded the normalized interdiurnal wind variability I_a as

$$I_a = \left[\sum_{j=1}^N (U_j - \bar{U})^2 \right]^{1/2} / (N \bar{U}) \quad (5.3)$$

where $\bar{U} = \left(\sum_{j=1}^N U_j \right) / N$

A ratio (α) between \bar{I}_b to I_a gives an index for the meso-scale activity over the station, such as

If $\alpha = \bar{I}_b / I_a > 1$, predominancy for diurnal wind variability and thereby meso-scale forcing

$\alpha = \bar{I}_b / I_a < 1$, dominancy for interdiurnal wind variability and thereby synoptic-scale forcing

Generally speaking, \bar{I}_b is the representation for micro-meso contributions to the station and I_a is the synoptic contribution. The α index will serve as a measure of the extent that the faithfulness of mean hodograph constructed by taking zonal and meridional components (u,v) with time during the course of a day to actual wind observations.

5.4 Results and Discussion

5.4.1 Monthly Distribution of Wind Variability Ratio (α)

Figure 5.1 depicts the monthly wind variability ratio (α) for different levels in the SBL. Mean wind speed generally in SBL increases with altitude as going up

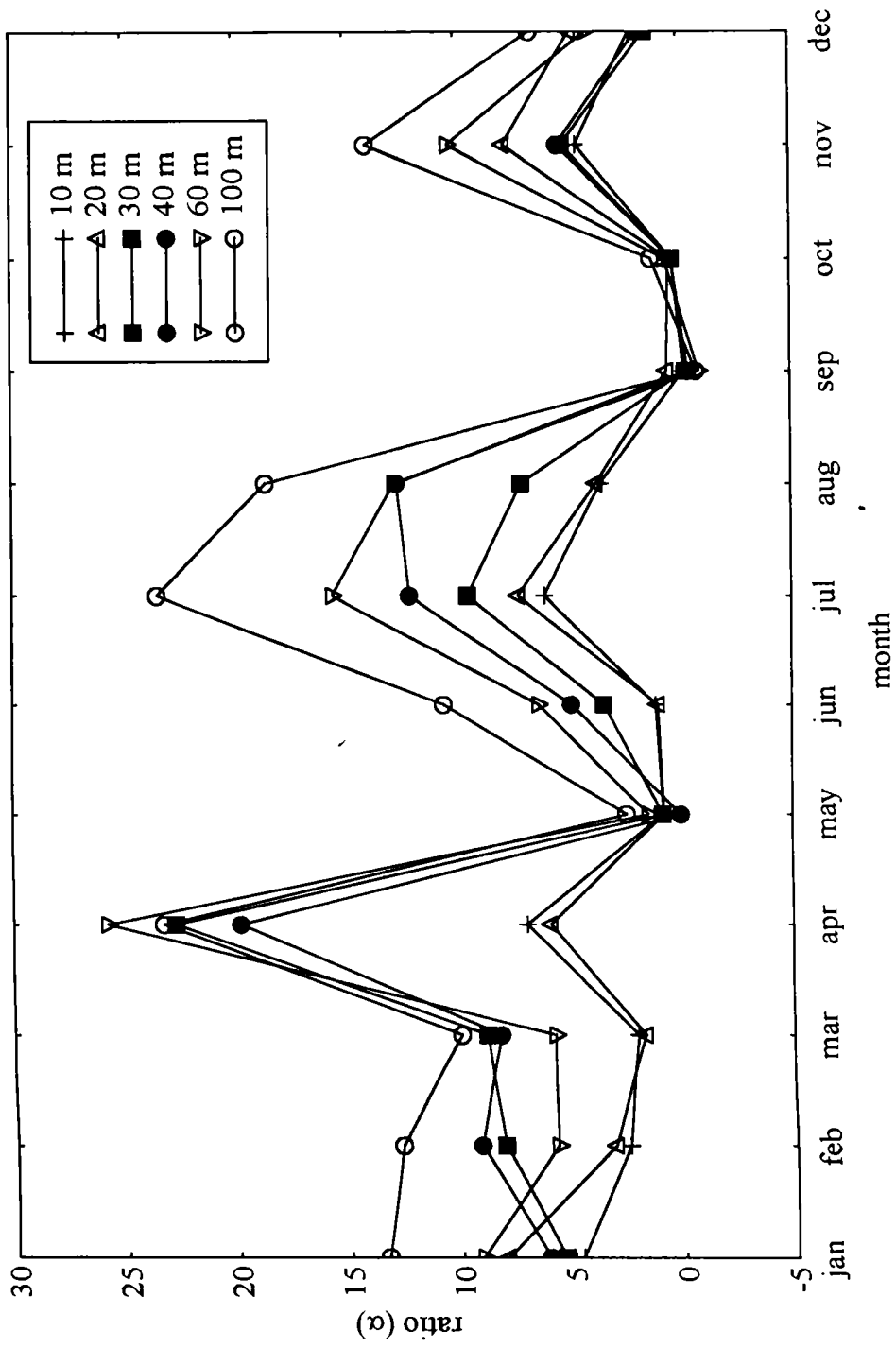


Figure 5.1 Wind variability ratio (α) in different months for different levels

from the ground level. Diurnal and interdiurnal variabilities have same sort of increase as going up and also in the wind variability ratio (α).

In winter months (December, January and February), the land-sea temperature contrast over Sriharikota is less and thereby meso-scale systems like land-sea breezes and thunderstorms are infrequent. Also the winter months are free from migrating low pressure synoptic-scale systems. Because of least effect of large scale features affecting the weather over the station, the dominancy for diurnal wind variability compared to interdiurnal variability and thereby giving moderate α of about 2 to 13.5 from 10 m to 100 m level is noted.

The equinoctial month March behaves like a change over month between winter and summer and it keeps it's behaviour as earlier winter months.

April is characterised by very strong diurnal differential heating over the SBL and it enables to create large local pressure gradient forces. Hence, it is a month of higher percentage occurrence of large diurnal wind variability making mechanism, the sea-land breezes (Sivaramakrishnan and Prakash Rao, 1989). A sudden rise in the ratio is seen at all levels and attains the maximum of the year during April. The values of α ranges from 6 to 26 for 10 m to 100 m levels. This indicates a clear picture of strong local diurnal boundary layer forcing.

In May, the pre-monsoon month, Bay of Bengal and adjoining land areas will be under the influence of transitions of high-low pressure systems. Generally lower atmospheric wind flow is so strong compared to other months and is from southeast as explained in the previous chapter. This is reported as the month of highest sea breeze occurrence over the station. The sea breeze component of wind gets interacted and boosted up from most persistent high pressure over adjacent Bay of Bengal regions. Even though strong diurnal differential heating is noticed over the region, the station experiences synoptic-scale (ie., interdiurnal) forcing

and α becomes less than 1. This confirms the dominance of interdiurnal wind variability during the month of May.

In south west monsoon months (June to September), this part of the country is under the influence of summer monsoon currents carrying more moisture. The strong diurnal heating and sea breeze enhance conditional instability aloft for sufficiently moisturised air mass and develops into thunderstorms (Namboodiri et al., 1994). Sriharikota is its own "entity" in having local weather dominated by meso-scale systems. Overall features in these months are unaffected by synoptic-scale forcing and giving another maxima region in the monthly distribution of α from June to August, in which July is the highest ratio of 6 to 23 from 10 m to 100 m. In September, passage of troughs over the station is quite common. As a result, the effect of diurnal forcing reduces thereby reduction in α values to less than 1 is noticed. This shows the predominancy of interdiurnal wind variability and synoptic-scale forcing.

In October, average position of Inter Tropical Convergence Zone (ITCZ) is concentrating over the region (Menon and Rajan, 1989) usually affecting the coastal weather situations and gives a least α value of the order as that of September. So the station experiences interdiurnal wind variability during October.

Sriharikota is prone to low pressure systems brewing over Bay of Bengal during November. The life span of such systems is about a week. Hence, diurnal boundary layer forcing playing a dominant role. November gives a tertiary maximum in α value of less intensity compared to other two maxima of the order of 4.5 to 14 from 10 m to 100 m level.

Overall observations on the monthly variations of wind variability ratio in the lowest 100 m of atmosphere over Sriharikota show an increasing trend as going upward and their distribution is having three maxima during April, July and

November, respectively. Moderate values from December to March through January. May, September and October months give minimum ratios and are less than 1.

The significance of any meso-scale modelling is lying on to what extent the station is affected by diurnal boundary layer forcing. Alpert and Eppel's (1985) proposed index (α) applied to SBL of Sriharikota giving a vivid overall dominancy of diurnal wind variability. Keeping in view of the general dominancy of diurnal wind variability in the SBL, wind hodographs are constructed on different levels and details are discussed in the next section.

5.4.2 Mean Wind Hodograph

Near elliptical approximation of diurnal wind variation of components during the course of a day detected and qualitatively studied by Loomis (1871) in the sea-land breeze studies. Much theoretical explanation of this near elliptical clockwise rotation (in northern hemisphere) and anticlockwise rotation (in southern hemisphere) given later by Haurwitz (1947), Smith (1947), Pierson (1975) and Neumann (1977). This veering (in northern hemisphere) and backing (in southern hemisphere) explained by using contributions of land-sea breeze temperature contrast, the coriolis force, friction, vertical variations in eddy diffusivity, vertical stability, the geostrophic wind and topography by various investigators as quoted earlier.

From Figure 5.2(a)-(l) show the mean wind hodographs for different levels for various months. For clarity of the phenomenon under discussion three level wind hodographs for the three levels 20 m, 60 m and 100 m are presented in these plots. The mean wind hodographs are showing circulation feature during the course of the day in association with α value more than 1. In all hodographs, initial observation starting at 0000 hr IST and closing the hodograph at 2330 hr IST in clockwise time progressing manner. A clockwise rotation showing arrow has drawn in hodographs, wherever an almost ellipticity approximation holds good

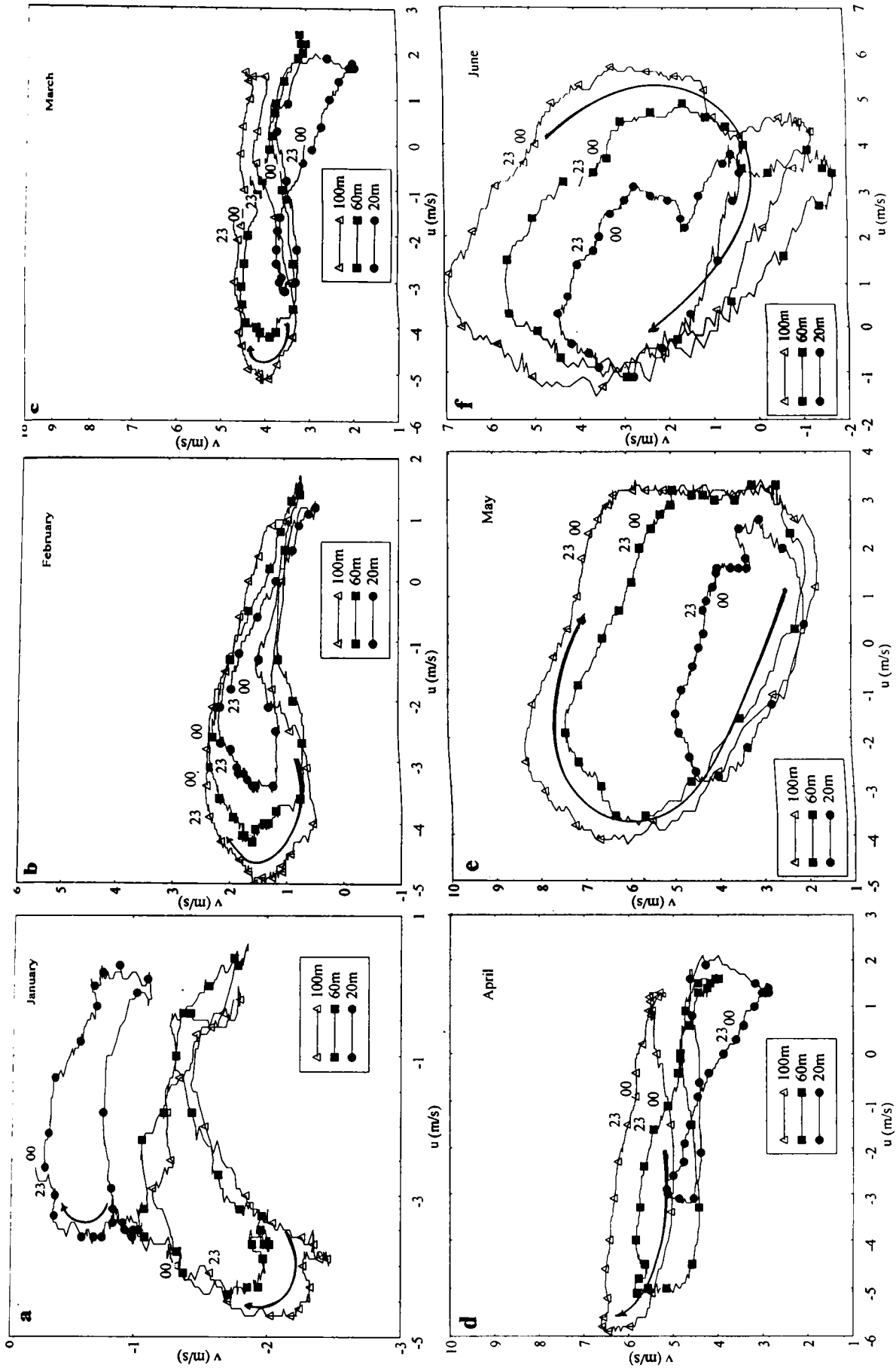


Figure 5.2.a-f Mean wind hodographs for different months

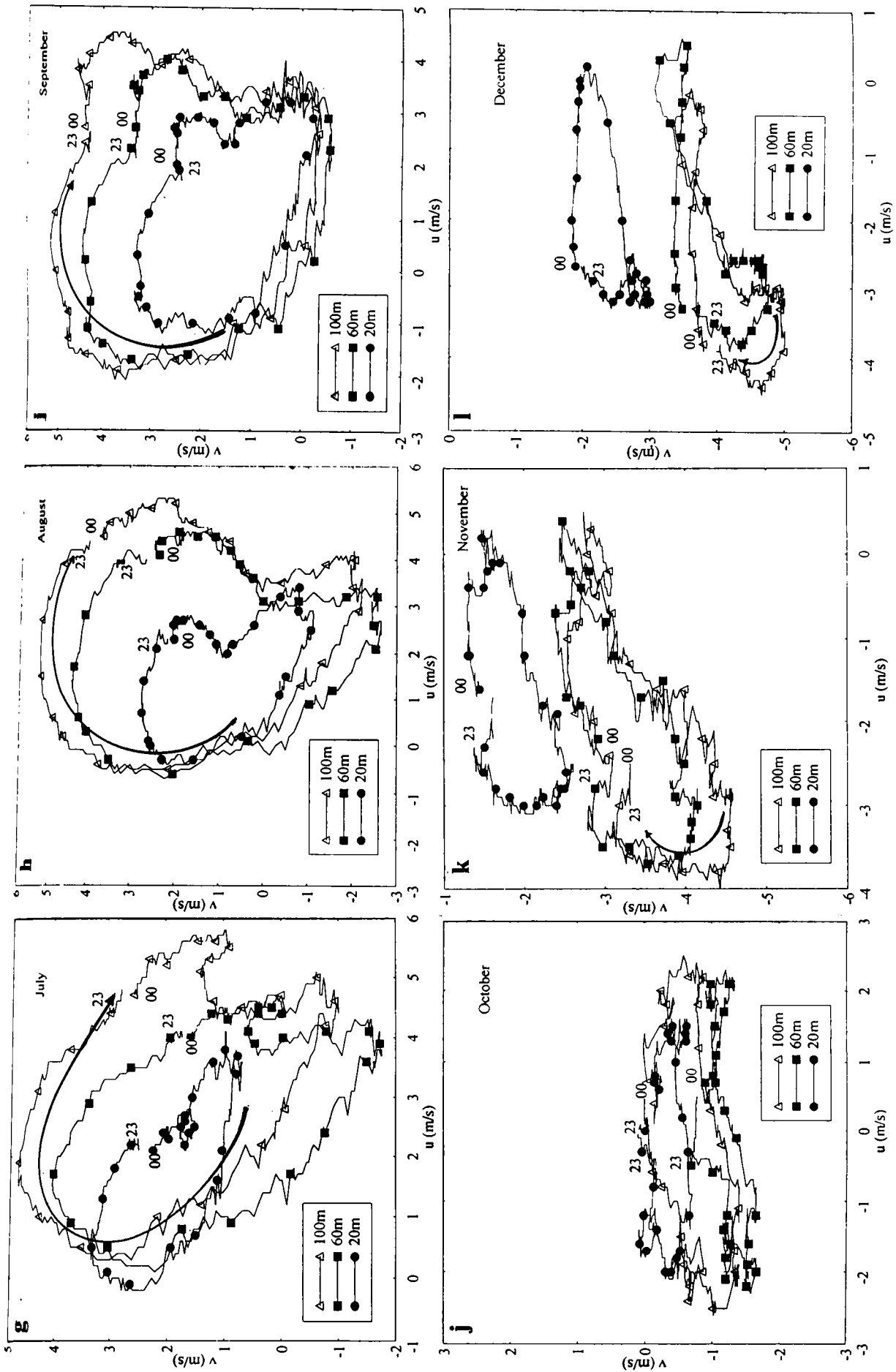


Figure 5.2 g-l Mean wind hodographs for different months

at its maximum extend. Monthly variations in wind components show strong oscillations in both u and v during strong diurnal wind variability dominating months and is from 5.3 to 8 ms^{-1} in u component and 1.2 to 8.4 ms^{-1} in the case of v component between 10 m and 100 m of SBL.

During morning hours, the hodograph is disturbed in its course when land breeze prevails over the station. Months having strong meso-scale forcing in the boundary layer (May to August), the period of disturbed nonuniform turning of the wind ellipse is from 0100 hr to 1000 hr IST. This may be attributed by the pressure gradient force which contributes significant modifications in the geostrophic wind and thereby the loss of uniform turning in actual wind. The portion of nonuniformity in the turning lies in the right hand side of the wind hodographs.

Generally the hodograph size increases with height. Among all levels 10 m hodograph shows much disturbed path which may be attributed to high surface roughness parameter of average value of the order of 0.5 m . From May to September very close approximation of ellipse forms at all levels. The size of ellipse in these months show large variations with v component amplitude and therefore the v component geostrophic wind places a major criteria on the size of the ellipses. More rapid increase or decrease in v component can be seen in the left hand side and right hand side of the hodographs, corresponding to morning and evening winds respectively. Very shallow variations in v component during afternoon and late night implies v component geostrophic wind will have sharp changes within a short span of time during morning and evening hours.

The feasibility of getting elliptical path with time for wind hodographs during the course of a day is very dominating feature in the months having meso-scale forcing on boundary layer. This plays high role to have local weather phenomenon like sea breeze and thunderstorms to the station. Generally this tropical station is having highest degree of incidence for diurnal wind variability

which is the necessary and sufficient condition for any meso-scale modelling studies.

Chapter 6

Structure of Surface Roughness

Parameter and Power Law

Exponent

6.1 Introduction

The aerodynamic roughness or surface roughness parameter (Z_0) is a basic parameter with respect to many aspects of the flow in the Surface Boundary Layer (SBL). The inclusion of terrain features in micrometeorological models requires the knowledge of the level Z_0 , where the mean wind is presumed to vanish. However, the capability of Z_0 estimation is not always available. In such cases, the calculations of exponent (α) in power law wind profile which to a larger degree is quite accurate and useful. By correlating Z_0 and α it is possible to find out the value of Z_0 for a given value of α . The variation of Z_0 with direction of wind flow is well established (Ramachandran et al., 1994). In this chapter, studies on the monthly structure of Z_0 and α , the variation of Z_0 and α with respect to wind azimuth, relationship between Z_0 and α , α variations during normal day and in a cyclone day in SBL over Sriharikota are reported.

6.2 Data

SET II data (May 1993 to April 1996) has been used for the analysis. As the vertical variations in stress and heat flux are within 10% in the SBL, changes in wind direction with height are negligible. So 20 m level wind direction is taken as a representative for the analysis.

6.3 Methodology in the Derivation of Z_0 and α

Z_0 and α are estimated by equations (6.1) and (6.2) assuming neutral atmosphere with logarithmically fitted SBL wind profiles.

$$\bar{U}_z = (U_*/k) \ln (Z/Z_0) \quad (6.1)$$

$$\bar{U}_z/\bar{U}_1 = (Z/Z_1)^\alpha \quad (6.2)$$

where \bar{U}_z is the wind speed at level Z , \bar{U}_1 is the wind speed at any level Z_1 , U_* is the frictional velocity and k is the Von Karman constant. The logarithmic fitting of

SBL profiles and derivation of Z_0 have been carried out as follows using every five minute mean wind profiles. Equation (6.1) can be represented as

$$\ln Z = \ln Z_0 + (k/U_*) \bar{U}_z$$

which has a least square linear regression form. The above equation is the form $Y = C + mx$, where $Y = \ln Z$ and $C = \ln Z_0$. It may be noted that the C is the Y -intercept from which Z_0 can be calculated. Further $m = k/U_*$ is the slope which contains information regarding frictional velocity U_* (see Figure 1.5). By the use of regression analysis for the best fitting and deriving Z_0 , and also from the logarithmic mean wind profile

$$m = [\Sigma \bar{U}_z \ln Z - (\Sigma \bar{U}_z \Sigma \ln Z) / n] / \Sigma \bar{U}_z^2 - \bar{U}_z^2/n; \text{ and}$$

$$C = \Sigma \ln Z / n - m \Sigma \bar{U}_z / n;$$

where n is the number of tower levels. Since $C = \ln Z_0$, we have $Z_0 = e^C$.

The power law by Arya (1988) shown in equation (6.2) provides a reasonable fit to the logarithmically fitted SBL profile for engineering applications (Hsu, 1988), which is the usual and simplest approach for statistically representing shear in SBL. The exponent α depends on Z_0 , stability, eddy viscosity or diffusivity of momentum and mean mixing length (Arya, 1988., Panofsky and Dutton, 1984). α values are found out for different height combinations with 20 m level as Z_1 and corresponding wind speed as \bar{U}_1 .

6.4 Results and Discussion

6.4.1 Monthly structure of Z_0 and α

α values are found out for different height combinations viz., 100 m, 80 m, 60 m, 40 m, 30 m, taking 20 m level as Z_1 (ie., α_{100-20} , α_{80-20} , α_{60-20} , α_{40-20} and α_{30-20} respectively). In Figure 6.1(a)-(l), α_{100-20} and α_{30-20} along with Z_0 are illustrated for different months. The variations in Z_0 show strong direct proportionality with α . As α value increases/decreases, Z_0 value also changes correspondingly. Z_0 and

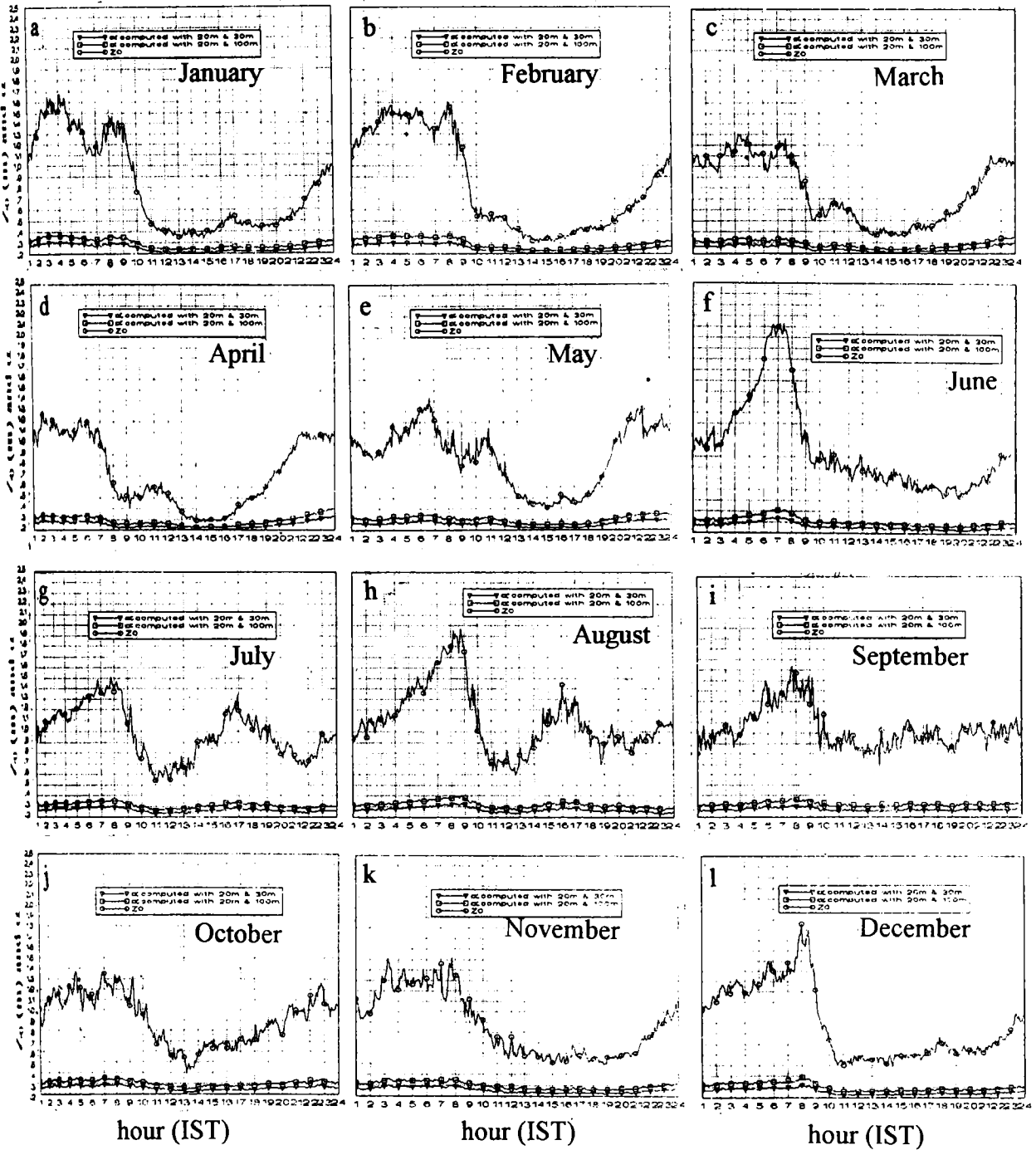


Figure 6.1a-l Diurnal variations of surface roughness parameter (Z_0) and power law exponent (α) in different months

α show higher values in the diurnal curve generally up to 0730 hr IST and late night. During these hours, Z_0 value is greater than 1 m throughout the year. Highest values of both Z_0 and α can be attributed to highly stable atmosphere during these duration of the day. The nature of the variations in Z_0 and α were discussed in literature (De Marris, 1959 and Smedman and Hogstrom et al., 1978). Highest values of Z_0 and α occur around 0800 hr IST followed by a steep downward slope in diurnal variation in all months. This is due to the atmospheric instability prevails in the SBL during these timings. The slanting slope dip in Z_0 is the order of 1 m and dip in α is of the order of 0.1 for all months. This portion of steepness in diurnal curve continues 2 to 3 hr in all the months except in October and November, where it is more than 4 hours. Z_0 is less than 0.5 m between 1030 hr to 1900 hr IST during January to May. The lowest values of Z_0 and α in diurnal curve may represent the unstable nature of the atmosphere during these hours. Eventhough the analysis has been carried out with neutral logarithmic wind profile and the α value is derived from logarithmically fitted profile, the measured α values are more than 0.142 which is higher than the neutral atmospheric α value (Lettau and Davidson, 1957). These observations are in agreement with their results, which confirm the unattainability of exact neutral atmospheric conditions in the real atmosphere, other than "near neutral". An interesting feature is the occurrence of peak value in α and Z_0 around 0800 hr IST in June and August among all the months.

6.4.2 Variation of Z_0 and α with Wind Direction

An attempt has been made to understand the variations of Z_0 and α with prevailing wind direction. The monthly variations are presented in polar diagrams as in Figure 6.2(a)-(l). Onshore winds generally indicate lesser Z_0 values of the order of 0.5 to 1.0 m, whereas offshore winds indicate values more than 1.0. As the coastline of Sriharikota oriented in 180° - 360° azimuth ie., in S-N orientation, the right portions of the S-N line in polar plots can be treated as Bay of Bengal and

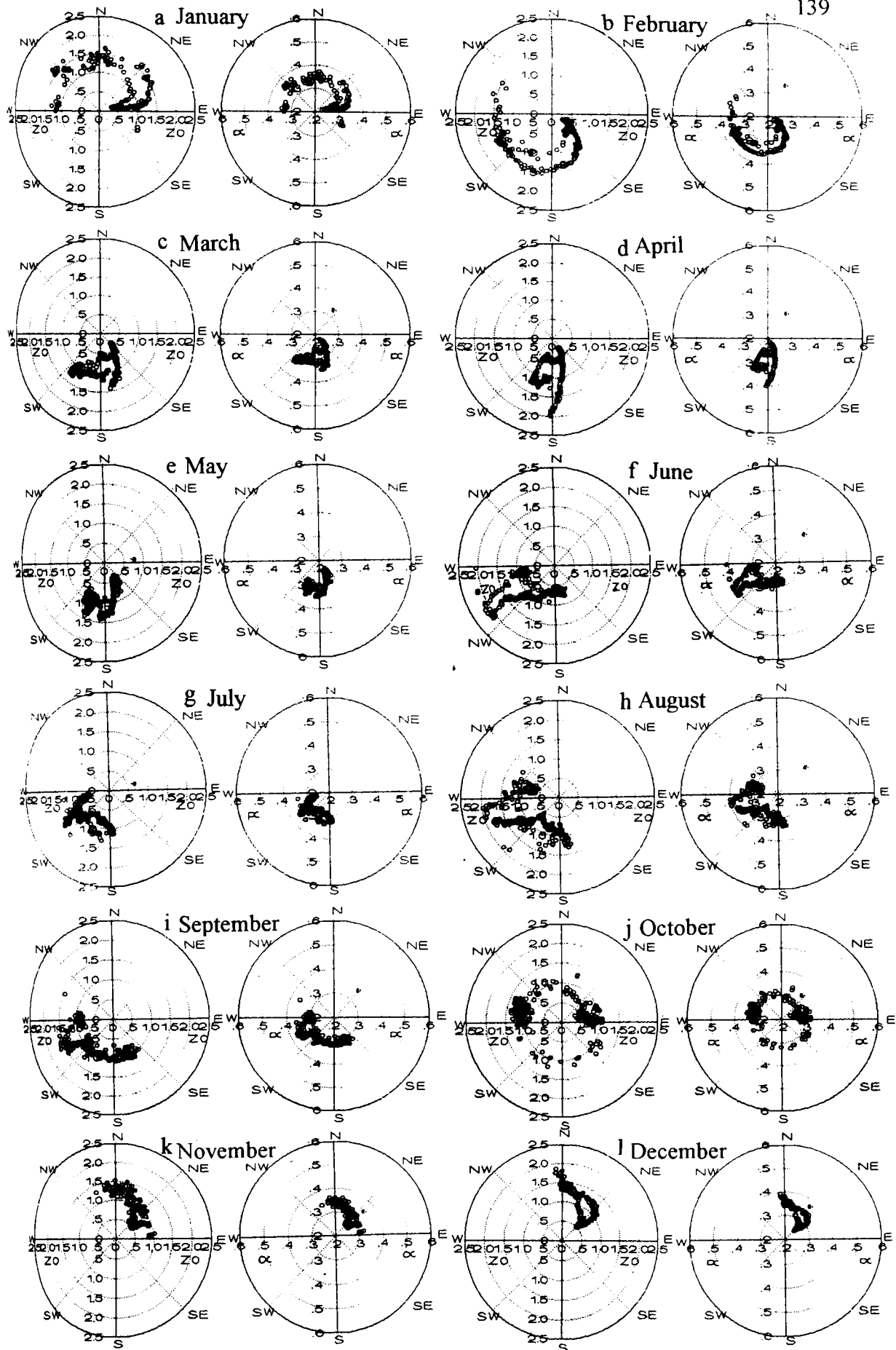


Figure 6.2 a-l Distribution of Z_0 and α with wind directions for different months

the left portions as land area. Wind makes meso-scale land and sea breeze circulations during the course of a day, in addition to the seasonal wind flow, either from the sea or from the land area. When the winds are coming from the sea, the scattering of Z_0 and α values are near to the origin of the polar plots. The sea breeze changes gradually to land breeze, either through southerlies or northerlies either caused to seasonal effect and/or meso-scale weather systems. The spread of Z_0 and α are moving away from the origin during this change over and the reverse is true for land breeze to sea breeze change.

6.4.3 Relationship between Z_0 and α

The relation between Z_0 and α is computed with regression equation

$$\alpha = b + A Z_0 \quad (6.3)$$

where,

$$b = (\bar{\alpha} - A \bar{Z}_0) \text{ and}$$

$A = \Sigma [(Z_0 - \bar{Z}_0)(\alpha - \bar{\alpha})] / [n \sigma_{Z_0}]$, where n is the number of observations, σ_{Z_0} standard deviations of Z_0 and bar line indicates mean values. Table 6.1 provides results on the regression analysis between Z_0 and α computed for different height combinations, viz., 100 m, 80 m, 60 m, 40 m and 30 m by taking 20 m level as reference level Z_1 . The relationship of these combinations with Z_0 shows increasing trend in both b and A with altitude in the SBL.

6.5 Comparison of α values in a Normal Day and in a Cyclone Day

Figure 6.3(a)-(d) represent exponent variation for a normal day (October 25, 1994) and during a severe cyclone day (October 31, 1994). The α values were computed for these days by taking reference level Z_1 as 20 m, and derived are for 30 m, 40 m, 60 m and 100 m keeping 20 m level as the reference level. The α values are inversely related with the wind speed. It is seen from the figures that α variations with time in a cyclone day is less than that of a normal day. The cyclone

Table 6.1 Relation between Z0 and α

MONTH	Z0 & α_{100_20}	Z0 & α_{80_20}	Z0 & α_{60_20}	Z0 & α_{40_20}	Z0 & α_{30_20}
JAN	$\alpha = 0.2549 + 0.0446 Z_0$	$\alpha = 0.2459 + 0.0415 Z_0$	$\alpha = 0.2350 + 0.0374 Z_0$	$\alpha = 0.2280 + 0.0352 Z_0$	$\alpha = 0.2229 + 0.03342 Z_0$
FEB	$\alpha = 0.2525 + 0.0469 Z_0$	$\alpha = 0.2441 + 0.0433 Z_0$	$\alpha = 0.2336 + 0.0389 Z_0$	$\alpha = 0.2250 + 0.0368 Z_0$	$\alpha = 0.2221 + 0.0344 Z_0$
MAR	$\alpha = 0.2621 + 0.0341 Z_0$	$\alpha = 0.2529 + 0.0320 Z_0$	$\alpha = 0.2412 + 0.2864 Z_0$	$\alpha = 0.2339 + 0.0270 Z_0$	$\alpha = 0.2284 + 0.0259 Z_0$
APR	$\alpha = 0.2539 + 0.4318 Z_0$	$\alpha = 0.2454 + 0.0399 Z_0$	$\alpha = 0.2343 + 0.0362 Z_0$	$\alpha = 0.2272 + 0.0338 Z_0$	$\alpha = 0.2221 + 0.0325 Z_0$
MAY	$\alpha = 0.2725 + 0.0313 Z_0$	$\alpha = 0.2623 + 0.0295 Z_0$	$\alpha = 0.2500 + 0.0265 Z_0$	$\alpha = 0.2419 + 0.0250 Z_0$	$\alpha = 0.2370 + 0.0233 Z_0$
JUN	$\alpha = 0.2715 + 0.0381 Z_0$	$\alpha = 0.2617 + 0.0392 Z_0$	$\alpha = 0.2617 + 0.0315 Z_0$	$\alpha = 0.2420 + 0.2900 Z_0$	$\alpha = 0.2372 + 0.0272 Z_0$
JUL	$\alpha = 0.2880 + 0.0234 Z_0$	$\alpha = 0.2770 + 0.0217 Z_0$	$\alpha = 0.2634 + 0.0196 Z_0$	$\alpha = 0.2549 + 0.01825 Z_0$	$\alpha = 0.2491 + 0.0171 Z_0$
AUG	$\alpha = 0.2869 + 0.0299 Z_0$	$\alpha = 0.2759 + 0.0279 Z_0$	$\alpha = 0.2621 + 0.0251 Z_0$	$\alpha = 0.2532 + 0.0234 Z_0$	$\alpha = 0.2474 + 0.0223 Z_0$
SEP	$\alpha = 0.2984 + 0.0174 Z_0$	$\alpha = 0.2858 + 0.0163 Z_0$	$\alpha = 0.2722 + 0.0144 Z_0$	$\alpha = 0.2628 + 0.0135 Z_0$	$\alpha = 0.2556 + 0.0185 Z_0$
OCT	$\alpha = 0.2816 + 0.0248 Z_0$	$\alpha = 0.2711 + 0.0230 Z_0$	$\alpha = 0.2582 + 0.0206 Z_0$	$\alpha = 0.2495 + 0.0194 Z_0$	$\alpha = 0.2436 + 0.0185 Z_0$
NOV	$\alpha = 0.2713 + 0.0305 Z_0$	$\alpha = 0.2617 + 0.0283 Z_0$	$\alpha = 0.2492 + 0.0256 Z_0$	$\alpha = 0.2401 + 0.0240 Z_0$	$\alpha = 0.2352 + 0.0214 Z_0$
DEC	$\alpha = 0.2693 + 0.0345 Z_0$	$\alpha = 0.2597 + 0.0316 Z_0$	$\alpha = 0.2479 + 0.0286 Z_0$	$\alpha = 0.2401 + 0.0267 Z_0$	$\alpha = 0.2342 + 0.0256 Z_0$

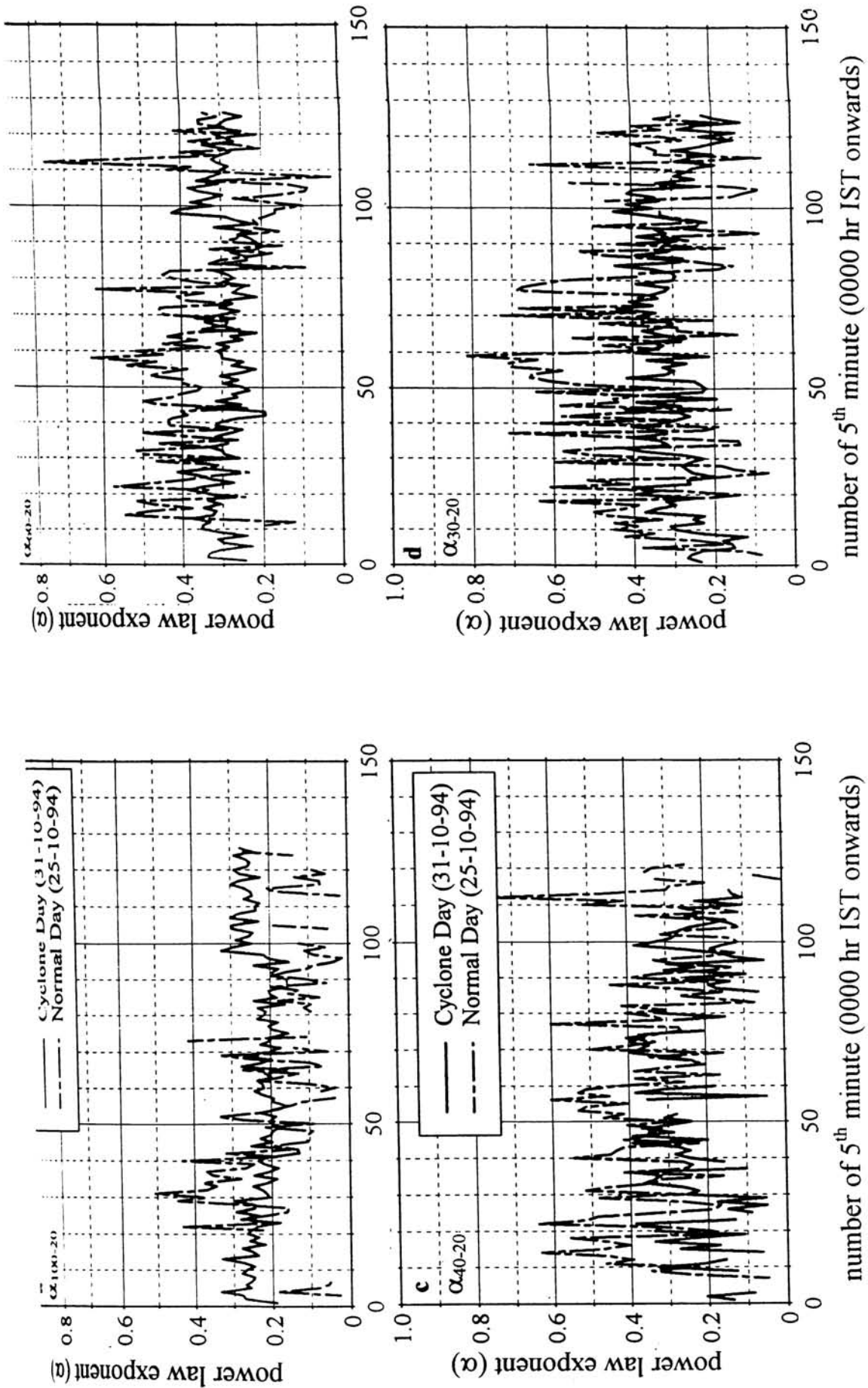


Figure 6.3 a-d Variation of exponent (α) in power law during a normal day and in a cyclone day

day α values are of the order of 0.2 to 0.3 and in a normal day the α becomes more than 0.5. As height increases with respect to the reference level 20 m, α value decreases for both the normal day and the cyclone day.

6.6 A Reference to U_* values

Diurnal variations in U_* values for various months are presented in Figure 6.4(a)-(1). The values are generally within the order of 0.4 to 0.6 ms^{-1} . Higher values are observed slightly above 0.6 ms^{-1} in April and May during 1600 hr IST. The frictional velocity gives a measure of the vertical kinematic turbulent flux of horizontal momentum in the SBL. When horizontal wind flow over roughness elements, drag slow down the wind speed near the surface compared to aloft, which creates wind shear. With greater surface roughness parameter and high horizontal wind speed, the resulting wind shear is greater which triggers mechanical turbulence. High mechanical turbulence leads to high values in frictional velocity. In April and May wind speeds are high around 1600 hr IST where Z_0 values are not so high compared to other months. Large values in U_* in these months are solely caused by horizontal wind speeds. Lowest values in U_* are observed in October and is characterised by shallow wind speeds and low Z_0 values.

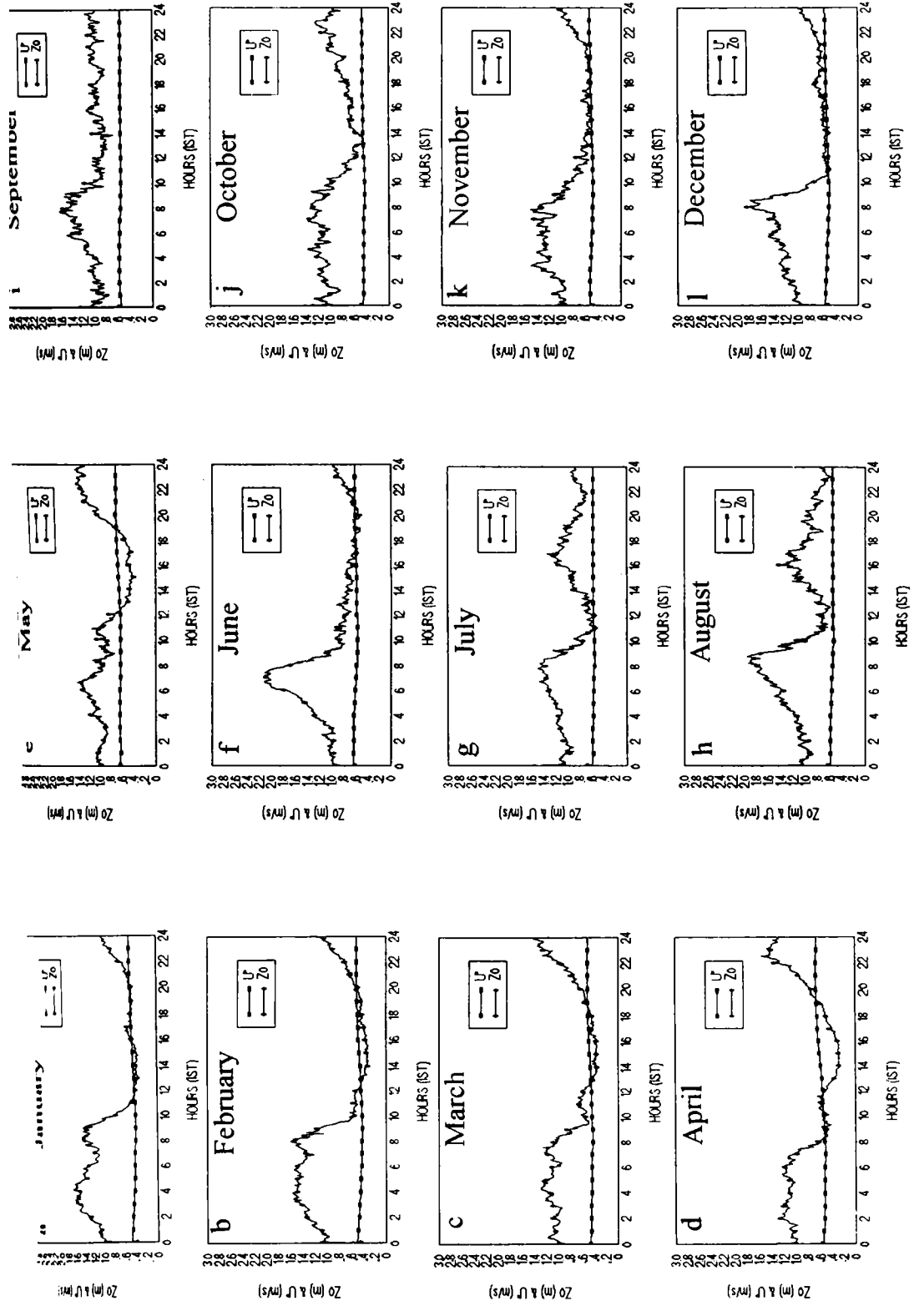


Figure 6.4a-l Diurnal variation of frictional velocity (U_*) along with Z_0 variations

Chapter 7

*Vertical Wind Shear in the Lowest
Layers of the Atmosphere*

7.1 Introduction

The study of vertical shear of horizontal winds in the lowest few meters of the atmosphere is of great significance to aircraft operations, on the estimation of wind power potential and atmospheric pollutants dispersal. In satellite launch vehicles, knowledge of wind shear is of importance as it can impart changes in bending moment either when the vehicle is stationary on the pad and few seconds after lift off. Narayanan and Devassy (1972) studied seasonwise structure of shears in the 200 ft lower atmospheric layer over Thumba. Quite a number of studies were carried out for different locations around the globe as reported in WMO (1969). Large wind shears can be attributed due to thunderstorms. Fujita and Byers (1977) computed shears of 0.12 s^{-1} extending 100 m atmospheric layer throughout due to downdrafts from thunderstorms. Variations in atmospheric stability modify much on the structure of wind shear and is studied by Heald and Mahrt (1981).

In this chapter, the monthly structure on the diurnal variations of scalar and total wind shear through vertical time section analysis and a comparison between total and scalar shears in different months over the station for different height combinations have been carried out.

7.2 Wind Shear

A wind shear is a change in wind speed or direction between two points in the atmosphere. Such types of changes can occur either due to changes in the horizontal or vertical component of wind speed. Wind shear arises mainly due to the variation in atmospheric air motions ranging from small scale eddies and gustiness to large scale flow of one air mass layer past an adjacent layer. Since uniform wind in all directions and at all levels is not possible at any time, wind shear is bound to be present always and at all levels in the atmosphere. In the present chapter wind shears in horizontal wind vectors (\mathbf{V}) and scalar wind (U) are taken into consideration.

7.3 Methodology adopted for Shear Computations

Shear of horizontal wind is defined as $\partial \mathbf{V} / \partial z$, where \mathbf{V} is the horizontal wind vector. If only wind speed (U) is known, the shear can be $\partial U / \partial z$. In the present analysis, total shears are computed by taking shear of each wind component, find out the magnitude of shear vector or wind velocity change between two levels as

$$\partial \mathbf{V} / \partial z = \sqrt{[(\partial u / \partial z)^2 + (\partial v / \partial z)^2]} \quad (7.1)$$

For computation of scalar shear

$$|\partial U / \partial z| \text{ is used.} \quad (7.2)$$

Both total shear and scalar shears computed are expressed in s^{-1} . u is zonal component and v is meridional component of wind.

7.4 Data and Presentations

Quasi-steady state wind speed and direction data from SET II (May 1993 to April 1996) is considered as input for the analysis. Total shear and scalar shears are computed for every five minute interval for the "shear levels" separated by 20 m apart i.e., with $\partial z = 20$ m. Computed shear values are represented in the mid level as at 20 m for 10 and 30 m, 30 m for 20 and 40 m, 50 m for 40 and 60 m, 70 m for 60 and 80 m and the highest shear level 90 m for 80 and 100 m by maintaining the constant interval of 20 m. Average total shear and average scalar shear are generated for a specified 5th minute time period (for all shear levels) for particular month and those every 5th minute average values pertained to a month are used in the analysis and presentations.

7.5 Results and Discussion

Figure 7.1(a)-(l) gives vertical time section plots of average total shears and Figure 7.2(a)-(l) depict average scalar shear variations. A particular shear level variation alone is assessed in both average total as well as average scalar shears in order to assess diurnal variations through different months of the year. These cross section plots are shown from 7.1.1(a)-(e) for average total shear and in Figures 7.2.1(a)-(e) for average scalar shear.

7.5.1 Characteristic of Average Total Shear

In winter months (December, January and February), variation in the total wind shear throughout the day is small compared to other months and their variations are observed in the order of 0.06 to 0.08 s^{-1} in the entire 100 m layer.

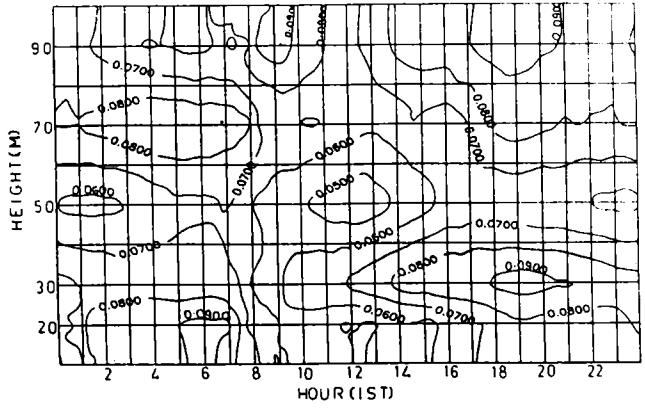
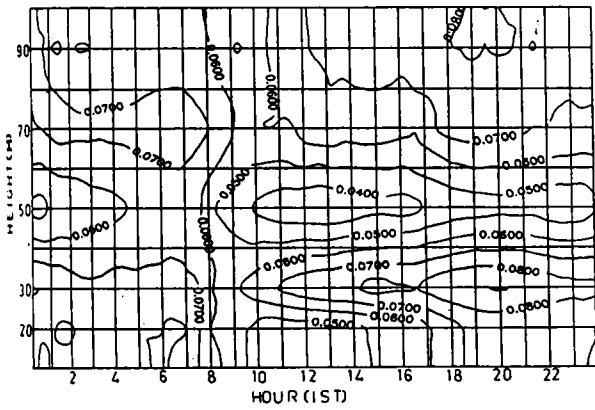
In transition months (March and April) in the 20 m shear level, the total shear variations are from 0.07 to 0.1 s^{-1} with highest values in early morning. In 30 and 50 m shear levels, they are of the order of 0.07 to 0.08 s^{-1} between 0000 hr and 0800 hr IST . In 70 m shear level, March shows a high regime of 0.1 s^{-1} and decreases to a value of the order 0.04 s^{-1} in April. The variation above 20 m from 0800 hr IST is of the order of 0.08 to 0.1 s^{-1} , in which the high values of 0.1 s^{-1} concentrates in the shear layer between 80 m and 100 m for the period of 1400 hr to 2000 hr IST .

In the pre-monsoon month, May the order of shear values are maintained almost constant throughout the day, highest shears are observed between 10 m and 30 m of the order of 0.1 s^{-1} . Whereas the next shear level onwards, they are in the order of 0.08 to 0.09 s^{-1} .

The shear behaviour in the south west monsoon months, belong to the same entity in the variation pattern. The entire day variations can be classified as two regimes of maxima and two regimes of minima. From 0000 hr to 0700 hr IST shears vary from 0.09 s^{-1} to 0.18 s^{-1} in all these months. Among these, high shear

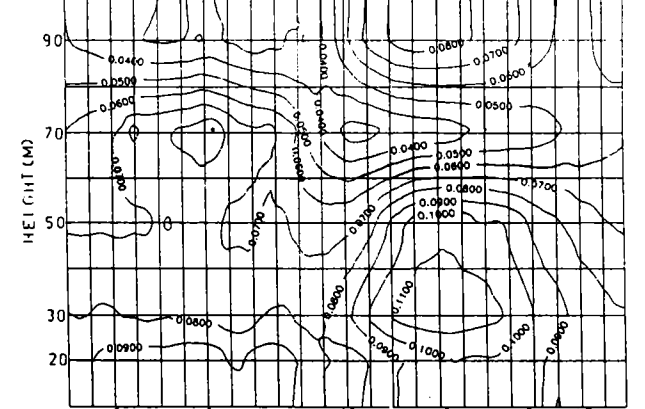
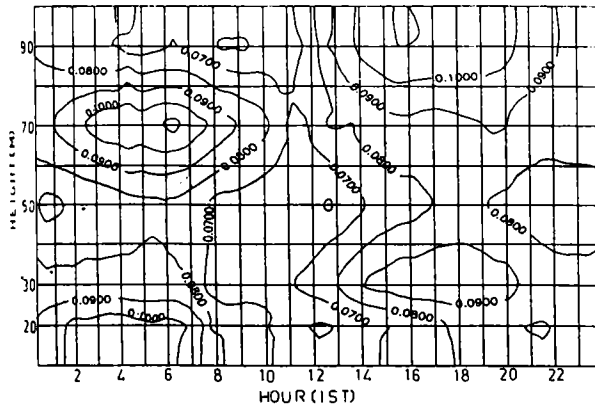
a January

b February



c March

d April



e May

f June

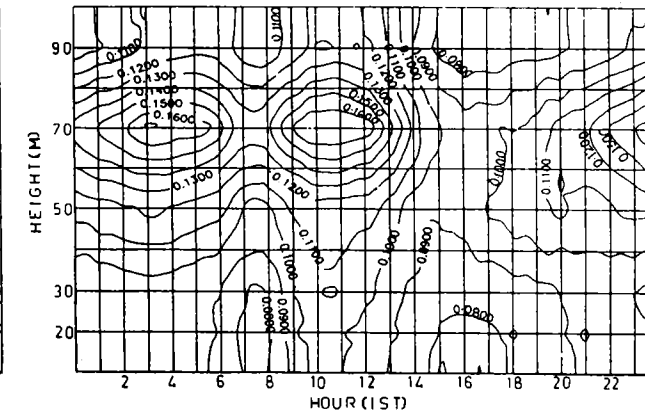
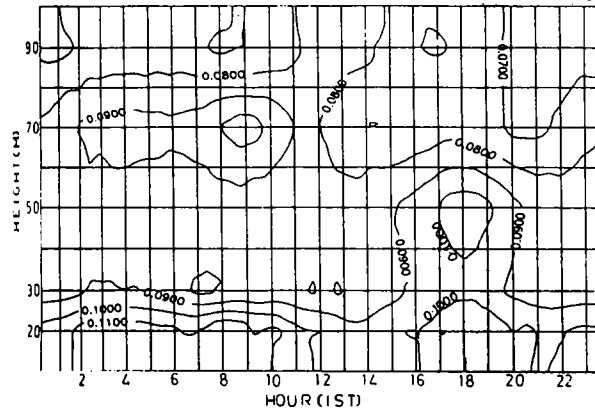


Figure 7.1 a-f Average total shear in different months

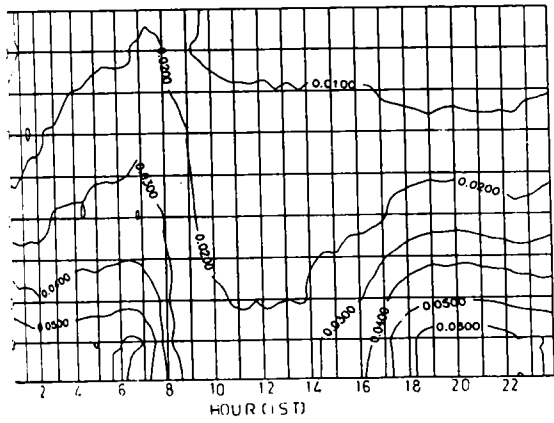
values are observed generally in July and August around 0300 hr to 0400 hr IST. After around 0700 hr IST to a period of approximately 2 hours i.e, upto 0900 hr IST, there experiences a 'COL' region, where shears are of almost constant low values. After the incidence of this COL region, wind shears slowly build up again with time and around 1200 hr to 1400 hr IST, they attain a secondary maxima of intensity around 0.13 s^{-1} upto 50 m shear levels. It is observed that the two occurrences of maxima are of almost same intensity. After the occurrence of second maxima, the shear values dip again to form a second COL region of minimum and constant values elapses from about 1400 hr to 1700 hr IST. The shear pattern builds up further as time progresses in order to form the first maxima in the diurnal cycle.

In the months of September and October, the diurnal variations are meagre. The values are within 0.08 s^{-1} to 0.12 s^{-1} in all the shear levels in September and October. November shows similar variations as that of winter months.

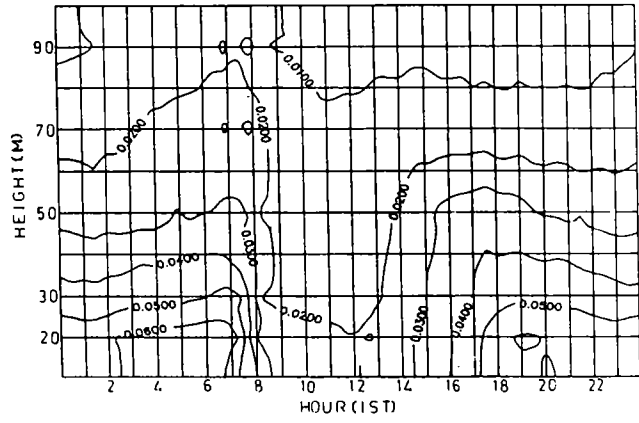
7.5.2 Characteristics of Average Scalar Shear

The variations are quite systematic and prominent in the case of average scalar shears, unlike the complex variations in average total shears. All variations are observed within the range from 0.01 s^{-1} to 0.07 s^{-1} throughout the year for all shear levels. High shears are encountered in lowest shear levels, and becoming less as going to higher levels. For all the months, early hours of the day upto 0600 hr IST shear values are high and they are of the order of 0.06 to 0.07 s^{-1} in the lowest shear level. It systematically decreases and attains around 0.02 s^{-1} in the topmost 70 m shear level and above. Throughout the year, the shear values between 0600 hr and 0900 hr IST show a constancy in structure. It remain a constant value of 0.05 to 0.04 s^{-1} from 0600 hr to 0900 IST in all the months for the lowest 20 m shear level. As height increases, the shear values decrease and attain of the order of 0.02 s^{-1} at 90 m shear level without changing the specific pattern. Between 0900 hr and 1300 hr IST shears are generally of the order 0.03 to

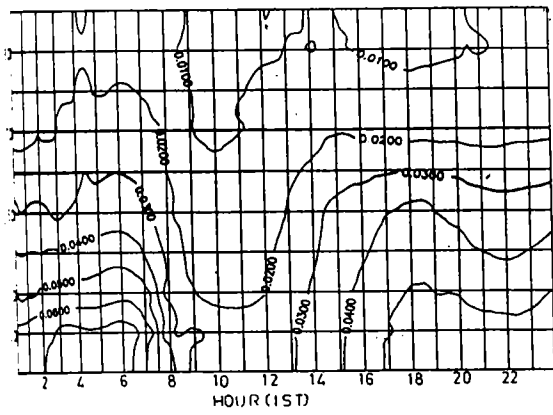
a January



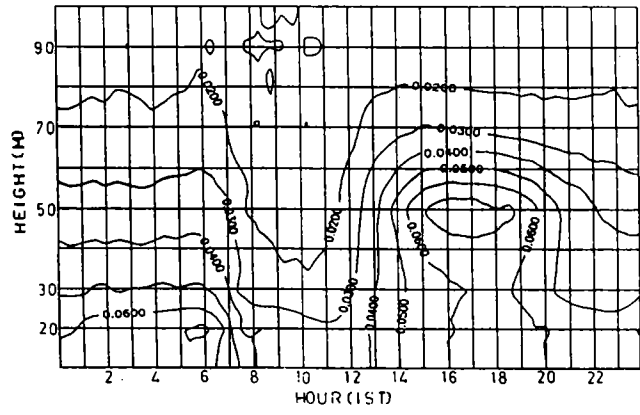
b February



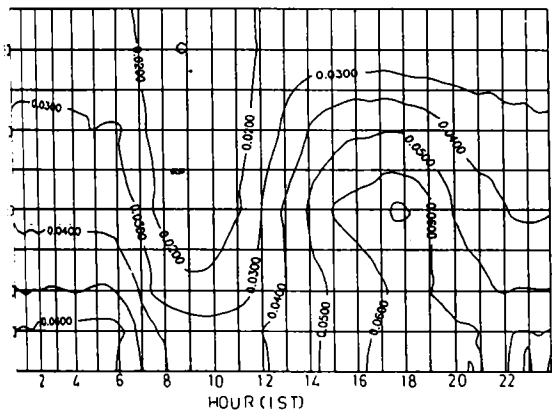
c March



d April



e May



f June

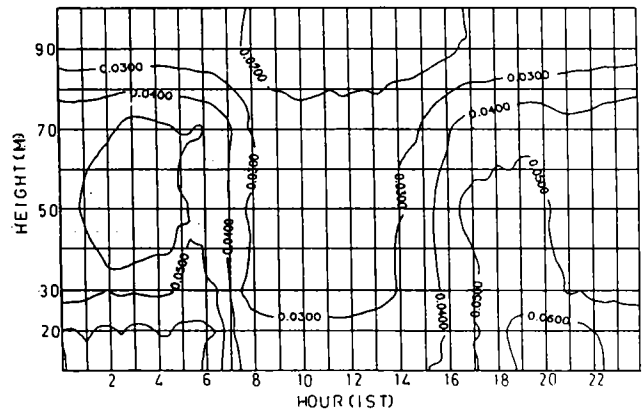
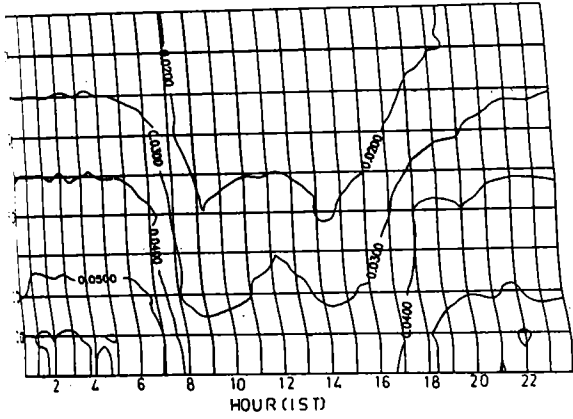
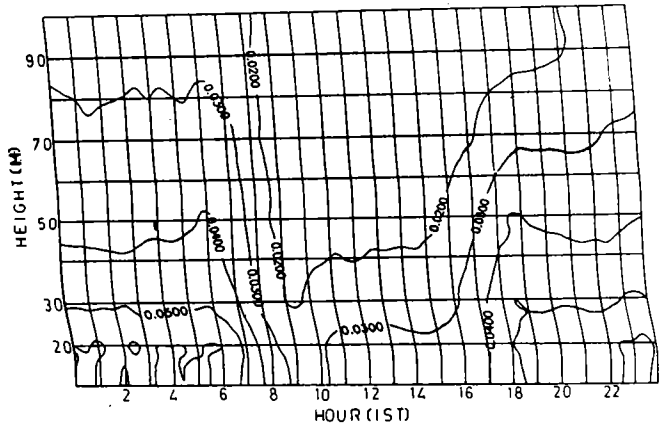


Figure 7.2 a-f Average scalar shear in different months

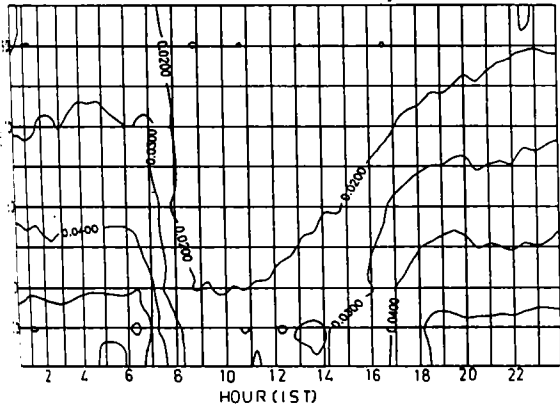
g July



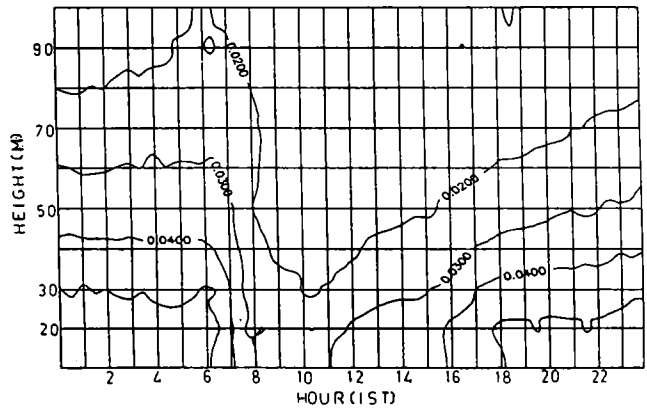
h August



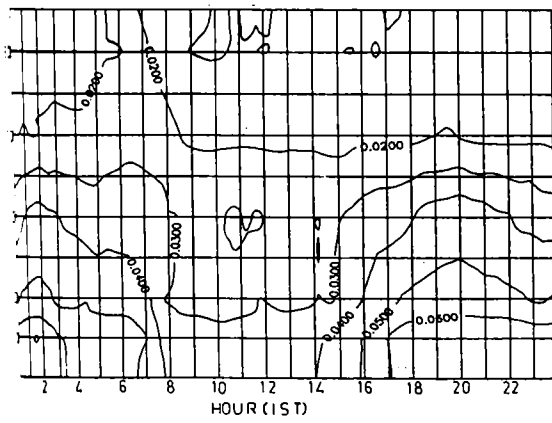
i September



j October



k November



l December

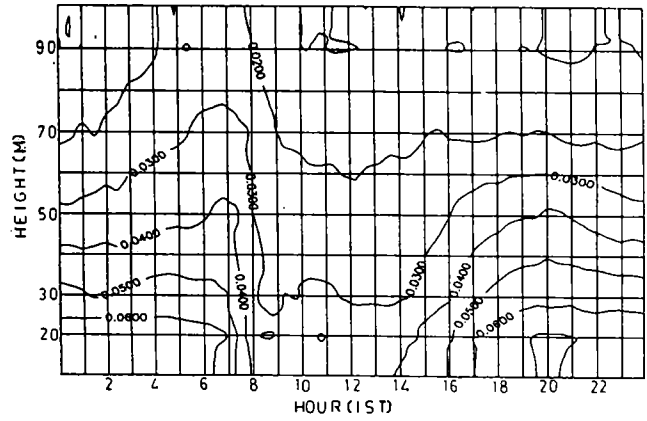


Figure 7.2 g-l Average scalar shear in different months

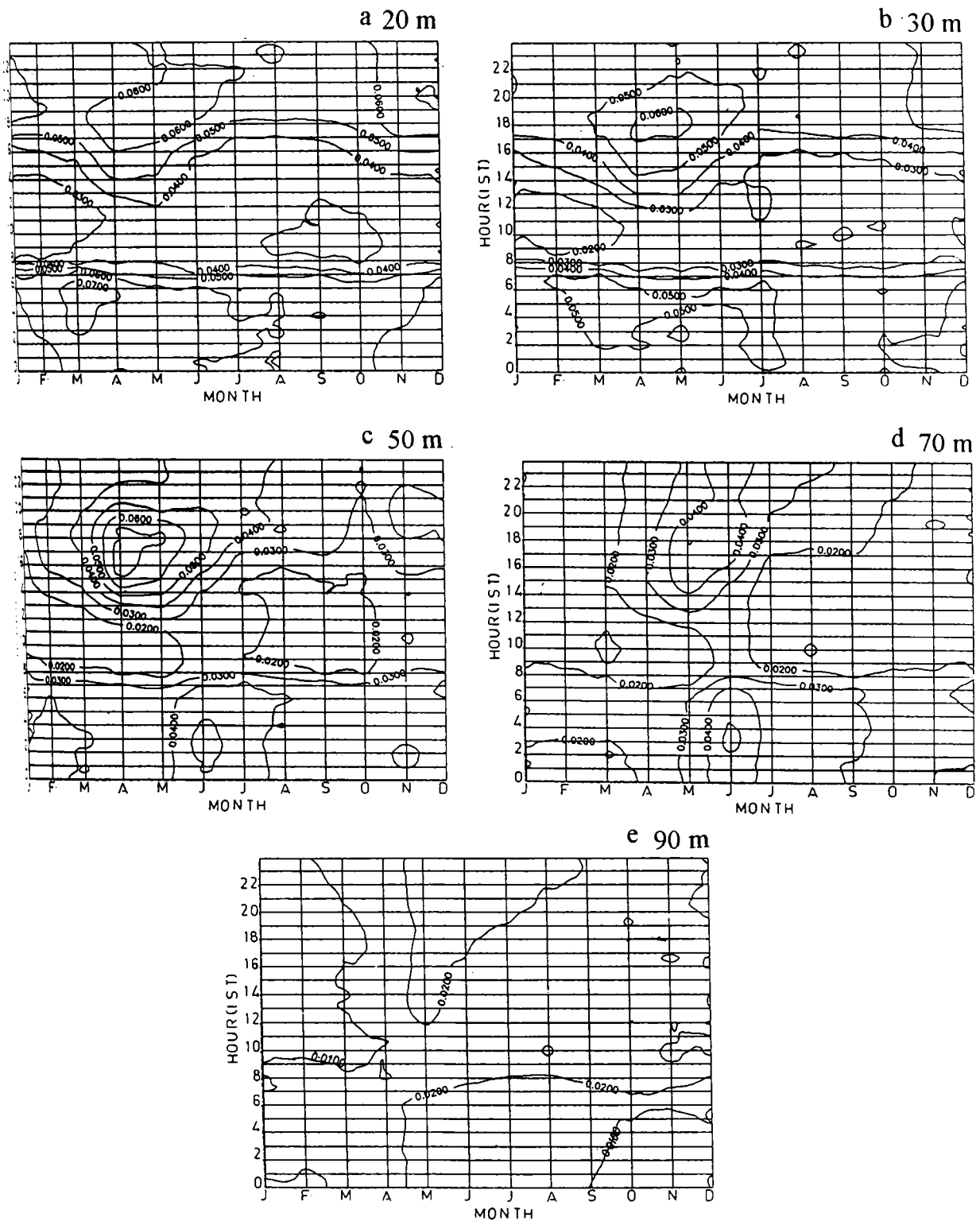


Figure 7.2.1 a-e Monthly variation of average scalar shear for specified shear levels viz., 20 m, 30 m, 50 m, 70 m and 90 m

0.01 s^{-1} in different levels from 20 to 90 m. High shears are observed in April and May around 1700 hr to 2000 hr IST. A COL region of constant shear values are most dominant from 50 m shear level upwards in June and July months.

7.5.3 Comparison between Average Total Shear and Average Scalar Shear

Figure 7.3(a)-(l) show comparison plots of average total shears and average scalar shears for each month. Average total shears always greater than the average scalar shears. A semi diurnal type of oscillation in total average shear is observed in southwest monsoon months, where two maxima and two minima are observed during the course of the day. The maxima are of almost same intensity, the second minima is relatively more intense than the first minima. The first maxima occurs around 0400 hr IST and the second maxima occurs around 1200 hr IST, i.e., they are separated by a period of 8 hours. Similarly first minima occurs around 0800 hrs IST and the second minima occurs around 1600 hr IST, i.e., they also separated by about 8 hours, like maxima.

The difference between total shears and scalar shears for any specific shear level is large in south west monsoon months, during around 1130 hr IST, which coincides with the second maxima in total shear diurnal curve. The difference is found to be the least in January.

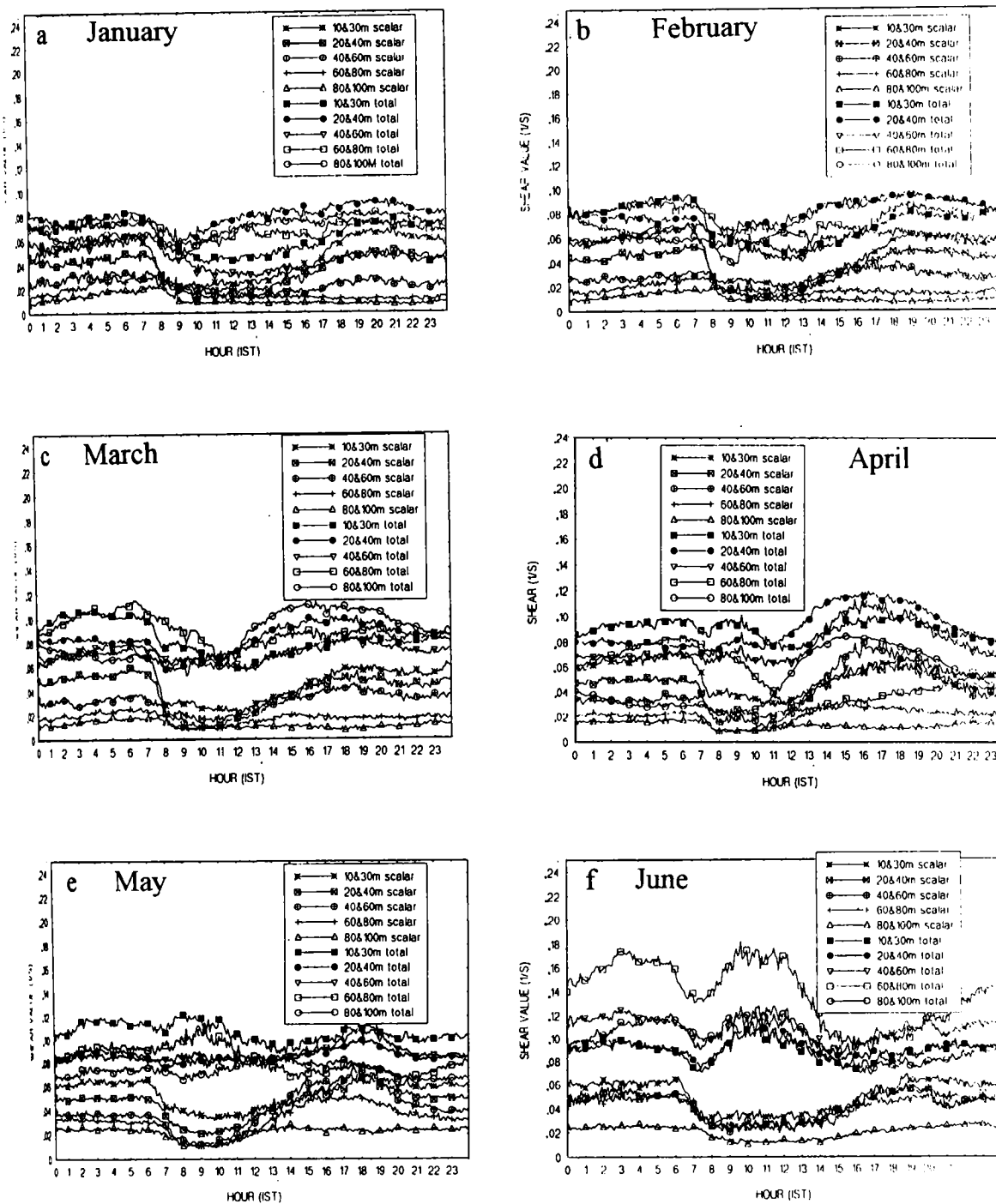


Figure 7.3 a- f Comparison of average total shear and average scalar shear

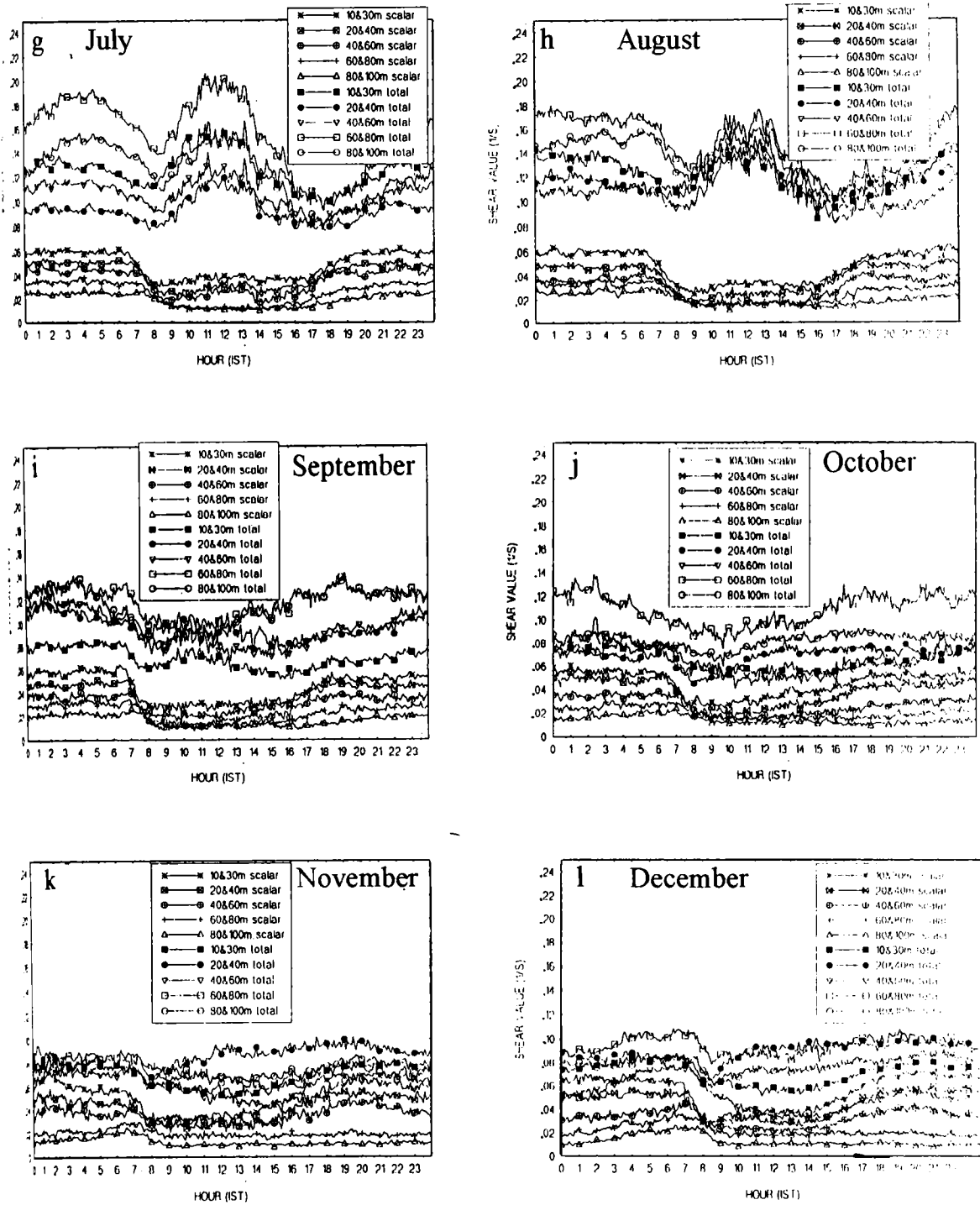


Figure 7.3g-l Comparison of average total shear and average scalar shear

Chapter 8

*Properties of Atmospheric Stability
in the 100 meter Tower Layer*

8.1 Introduction

The investigation of atmospheric stability fluctuations in the lowest part of the atmosphere is a very critical input in the diffusion modelling of pollutants in air pollution meteorology. In aerospace meteorology, leakage of hazardous rocket fuels in the range, explosions of rockets in the lowest atmospheric levels are of most concern. The present chapter describes in view of its applications in such areas of meteorology. Regulatory agencies on air pollution potential assessment consider different meteorological variables for their regulatory uses. Wind is the primary meteorological variable assessing the impacts of atmospheric transport, diffusion of gaseous pollutants and travel time of them.

The U.S Environmental Protection Agency (EPA), (1980) specifies that the atmospheric stability estimates can be based on horizontal wind direction fluctuations i.e., based on the standard deviation of wind directions (σ_θ). The U.S Nuclear Regulatory Commission (NRC), (1972) recommends an atmospheric stability classification scheme based on σ_θ variations. Diurnal variations of atmospheric stability in different months have been studied for the lowest 100 m layer of the atmosphere for the eastern coastal station Sriharikota. Diurnal variations of mean wind speed (\bar{U}) are also studied in connection with stability changes of the atmosphere. The σ_θ depending method for the estimation of atmospheric stability as suggested by NRC is used in the present analysis. The method is based on stability categorisation with respect to Pansquill categories in relation with σ_θ variations as provided in Table 8.1. Similar studies can be seen elsewhere (Slade, 1968; Turner, 1970; Pramila Goyal and Nivedika Karmakar, 1982; Irwin, 1983. Slade (1968) made a model for stability and σ_θ variations up to 150 m layer of atmosphere. Bowen et al., (1983) studied stability class determination by Richardson number (R_i) computation and they compared R_i with σ_θ . In their study they used approximately 15 minute averaged σ_θ from every 3.5 s wind informations. The mean wind speed profiles are drawn for Least Stable Time

Table 8.1
Stability classification and σ_θ variations

Stability Classification	Pansquill Categories	σ_θ Variations (deg.)	Generalisation in this study
Extremely Unstable	A	25.0	
Moderately Unstable	B	20.0	Unstable tendency
Slightly Unstable	C	15.0	
Neutral	D	10.0	Non occurrence
Slightly Stable	E	5.0	
Moderately Stable	F	2.5	Stable tendency
Extremely Stable	G	1.7	

(LST) and Highest Stable Time (HST) for the 100 m tower layer and the features are analysed in the present chapter along with the occurrence of their timings in each month.

8.2 Data

SET II (May 1993 to April 1996) data is used as input for the study. σ_0 computations are carried out with every five minute data points available for the seven tower levels in every half an hour. Average σ_θ for every half an hour is derived for each month and is used to arrive the monthly structure on the diurnal variations of atmospheric stability over the station. Length of the data record used for this study is quite sufficient as per regulations of EPA (1980) and NRC (1978), both recommend at least one year data for such studies. The mean wind speed profiles generated for LST and HST are the average quasi-steady state winds of that particular time and particular month.

8.3 Theoretical Considerations for the Derivation of Standard Deviation of Wind Directions (σ_θ)

As wind direction is a circular function with a discontinuity of scale at 360° , special treatment is required to arrive the values of σ_θ . For the generation of σ_θ , various investigators suggested different methodologies (Ackermann, 1983; Verrall et al., 1982; Yamartino., 1984). A study on the comparison of these three methods for calculating σ_θ has been presented by Turner (1986). The present study adopts the method devised by Ackermann (1983) shown as below.

For a specified time period t,

$$U = \Sigma u_i/N, \text{ means of zonal wind component (u).}$$

$V = \Sigma v_i/N$, means of meridional wind component (v), where N is the number of observations.

$$\sigma_u^2 = \Sigma u_i^2 - U^2/N-1, \text{ the variance of u.}$$

$\sigma_v^2 = \sum v_i^2 - V^2/N-1$, the variance of v .

$\sigma_{uv} = \sum u_i v_i - UV/N-1$, the covariance of u and v .

For a parameter z which is a function of x and y , ie., $z = f(x, y)$

$$\sigma_z = [(\partial z/\partial x)^2 \sigma_x^2 + (\partial z/\partial y)^2 \sigma_y^2 + 2 (\partial z/\partial x) (\partial z/\partial y) \sigma_{xy}]^{1/2} \quad (8.1)$$

and defining average values,

$$S = (U^2 + V^2)^{1/2}, \text{ the mean wind velocity} \quad (8.2)$$

$$D = \tan^{-1} (U/V), \text{ the mean wind direction} \quad (8.3)$$

which follows that

$$\begin{aligned} \partial S/\partial U &= 1/2 (U^2 + V^2)^{-1/2} (2U) \\ &= U/S \end{aligned} \quad (8.4)$$

$$\begin{aligned} \partial S/\partial V &= 1/2 (U^2 + V^2)^{-1/2} (2V) \\ &= V/S \end{aligned} \quad (8.5)$$

Substituting (8.4) and (8.5) in (8.1) and solving for σ_S gives

$$\sigma_S = [(\partial S/\partial U)^2 \sigma_u^2 + (\partial S/\partial V)^2 \sigma_v^2 + 2 (\partial S/\partial U) (\partial S/\partial V) \sigma_{uv}]^{1/2} \quad (8.6)$$

and leads to

$$\sigma_S = [U^2 \sigma_u^2 + V^2 \sigma_v^2 + 2 U V \sigma_{uv}]^{1/2} S^{-1/2} \quad (8.7)$$

Similarly

$$\partial D/\partial U = \partial/\partial U [\tan^{-1} (U/V)] = [1 + (U/V)^2]^{-1} V^{-1} \quad (8.8)$$

$$\partial D/\partial V = [1 + (U/V)^2]^{-1} (-U/V^2) \quad (8.9)$$

Substituting (8.8) and (8.9) in to (8.1) and solving for σ_θ gives

$$\sigma_\theta = [(\partial D/\partial U)^2 \sigma_u^2 + (\partial D/\partial V)^2 \sigma_v^2 + 2 (\partial D/\partial U) (\partial D/\partial V) \sigma_{uv}]^{1/2} \quad (8.10)$$

and final result gives

$$\sigma_{\theta} = [V^2 \sigma_u^2 + U^2 \sigma_v^2 + 2 U V \sigma_{uv}]^{1/2} S^{-2} \quad (8.11)$$

8.4 Results and Discussion

Figure 8.1(a)-(l) represent σ_{θ} variations along with diurnal variation of wind speed posed below the σ_{θ} variation plots in order to assess the wind speed variations in relation to atmospheric stability conditions.

8.4.1 Features on the Monthly Diurnal Stability Variations

In Figure 8.1(a)-(l) show diurnal characteristics of σ_{θ} and thereby the atmospheric stability for different months. σ_{θ} values for 10 m, 20 m, 40 m, 80 m and 100 m levels are shown in σ_{θ} variation figures. To know the wind speed profile characteristics, during LST and HST, mean wind speed (\bar{U}) profiles during these timings are included along with stability variation plots.

Generally, σ_{θ} variations are less in upper levels compared to lower levels, and they lie one over the other. From the graphs it is evident that $\sigma_{\theta} > 5.0^{\circ}$ can be treated as unstable regime tendency, $< 5.0^{\circ}$ stable regime tendency and a non occurrence of a neutral regime in this tropical coastal station.

During winter months the LST occurs around 0930 hr IST. Stable regime during this season occupies in evening hours. During March and April LST occurs 0900 hr and 1000 hr IST respectively. HST happens at 1730 hr IST. From 1300 hr to 2300 hr IST the atmosphere is stable. In the pre monsoon month (May), HST occupies around 1730 hr IST and is similar to that of April. The HSTs of April and May show, the highest stable atmospheres among all the months and characterise by the presence of high winds of the order of 5 ms^{-1} in the 100 m layer. During south west monsoon season, stable atmospheric dominancy happen early hours of the day around 0300 hr to 0400 hr IST. In September and October, stable atmospheric conditions are not a dominant feature. The north east monsoon month, November shows almost similar features of the forthcoming winter. In

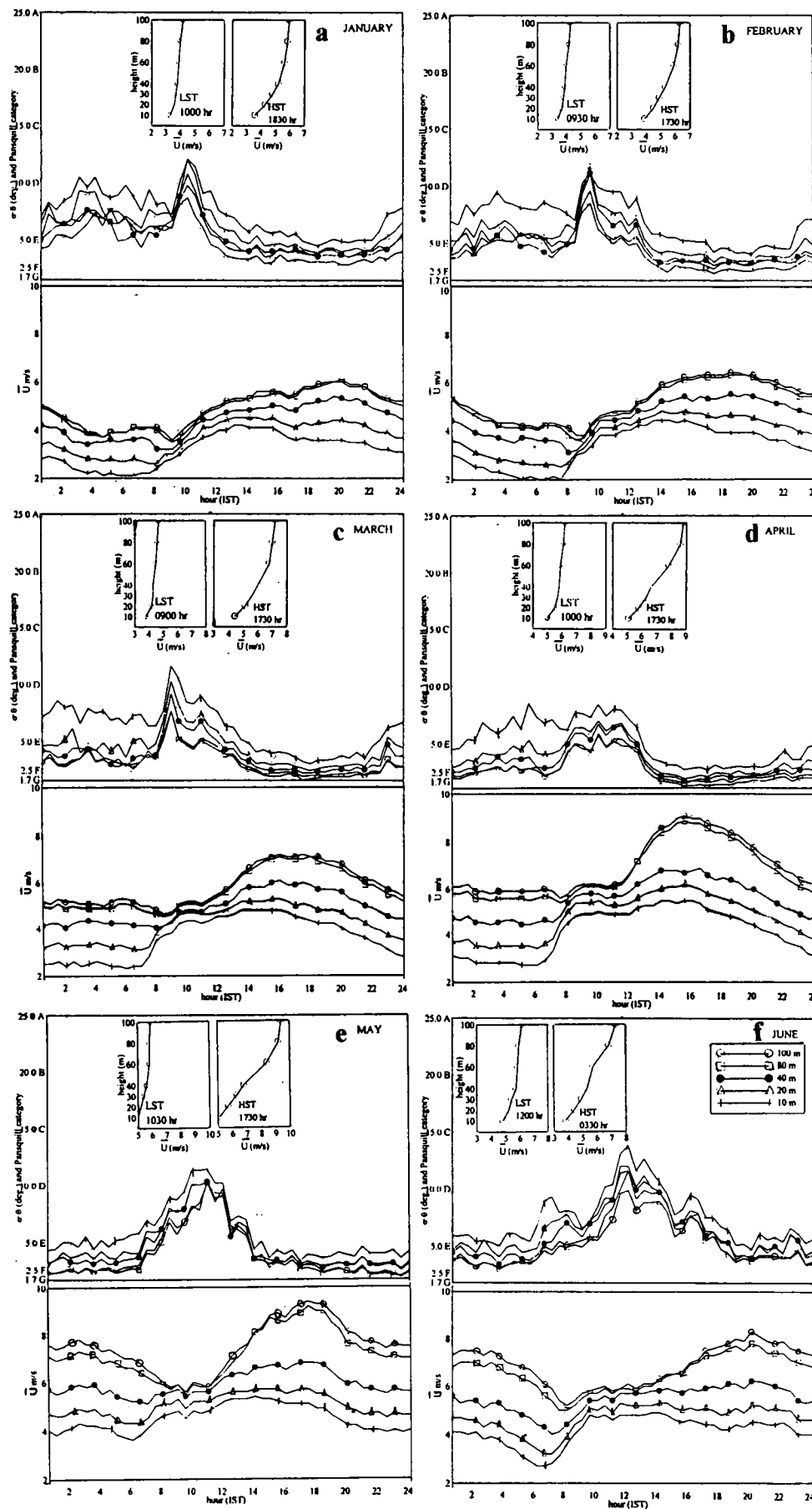


Figure 8.1a-f Diurnal variation of σ_θ and wind speed for different months

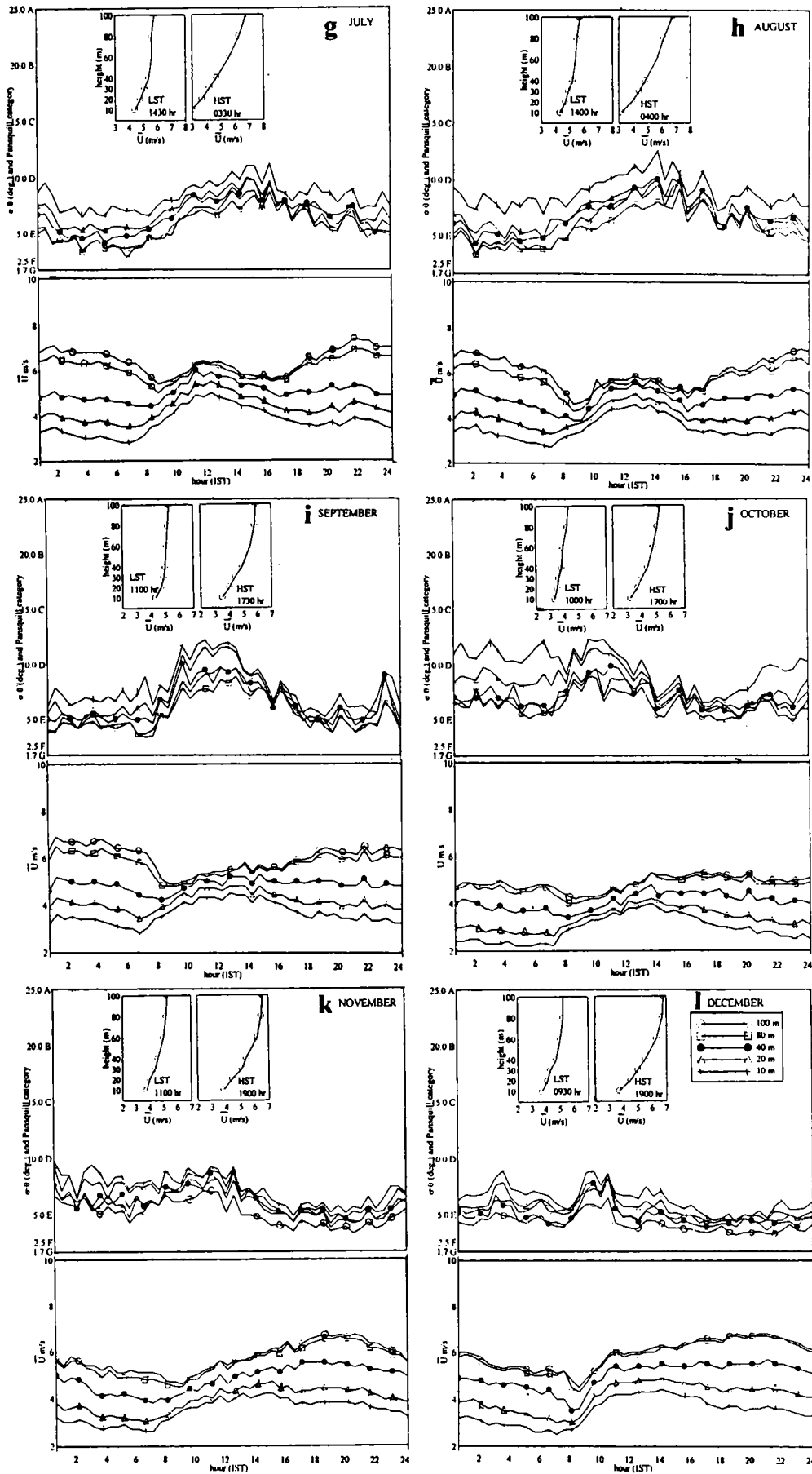


Figure 8.1g-1 Diurnal variation of σ_0 and wind speed for different months

December, the stable atmospheric conditions prevail between 1600 hr and 2100 hr IST.

The general behaviour of HST profiles in all months show increase of wind speeds with high wind shears. During the occurrence of LST, wind speed gradient with height (wind shear) are of minimum. This wind shear minimum contributes less wind variations of the order of 1 to 2 ms^{-1} from the top level to bottom level. An analysis of LST and HST on semi-logarithmic graph show slight concavity outwards or somewhat straight wind profile feature exists during LST above 40 m . This can be attributed with slight stable atmospheres in the upper levels compared to lower parts. This demarcation may be the effect of unstable regime profiles are more prone to surface roughness compared to stable profiles. The slopes are so steep in cases of LST. In the case of HST concavity of profile to outwards is existed throughout in semi-logarithmic plottings, show stabilised layer in the entire SBL.

In average diurnal variations of σ_θ greater than 15.0° (C class in Pansquill category) are not observed. But in the real atmospheric conditions like thunderstorm passages over the station, which is the extreme manifestation of atmospheric instability, σ_θ becomes more than 25° (belongs to A class in Pansquill category) in the entire SBL.

8.4.2 Diurnal Variations of Wind Speeds in relation to Stability Variations

Figure 8.1(a)-(l) also represent diurnal variations of wind speeds. Levels considered for stability variations are plotted in these graphs in order to study the characteristics of the diurnal wind speed variations. The wind merging property in diurnal wind variation curves due to high rates of momentum transfer towards the ground coincides with unstable conditions as per stability diurnal variation curves. In hours of stable atmospheric regime the wind speeds in lower and upper levels depart widely. In general, the departure of low and high level wind speeds are

minimum during unstable atmospheric conditions and they are in maximum during stable atmospheric situations.

8.4.3 Frequency Distributions of σ_0

Figure 8.2(a)-(l) show frequency distribution of σ_0 based on Pansquill category for each month for different levels. The general feature in the percentage occurrence of unstable atmospheres (ie., where σ_0 values are high) in the lower layers is predominant compared to upper layers, which prevails throughout the year. From these histograms it is understood that the station generally experiences major percentage occurrence of stable categories except in south west monsoon months, where the unstable percentage occurrences are also equally important. High incidence of the occurrence of thunderstorms are common during south west monsoon season over Sriharikota.

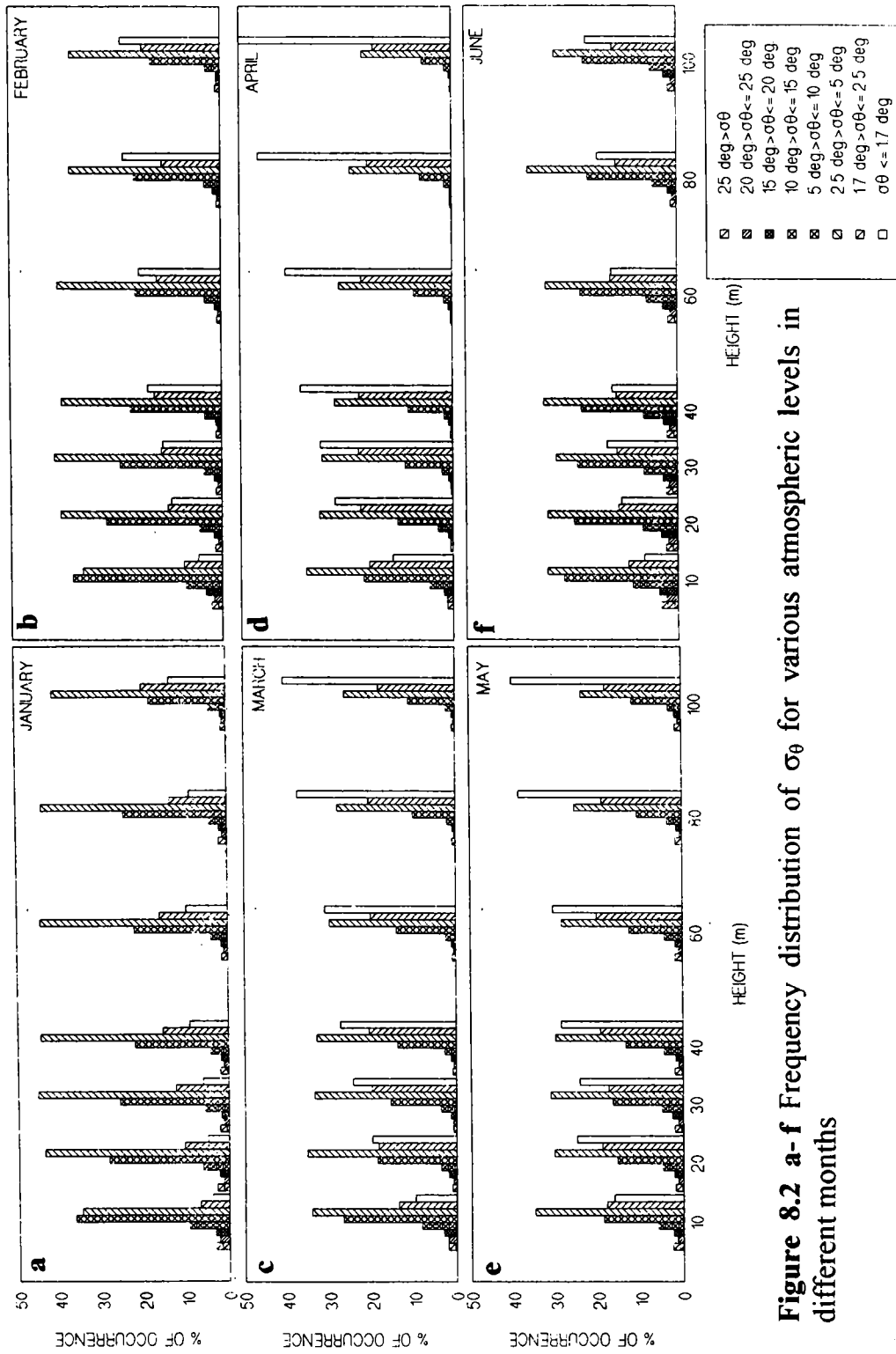


Figure 8.2 a-f Frequency distribution of σ_θ for various atmospheric levels in different months

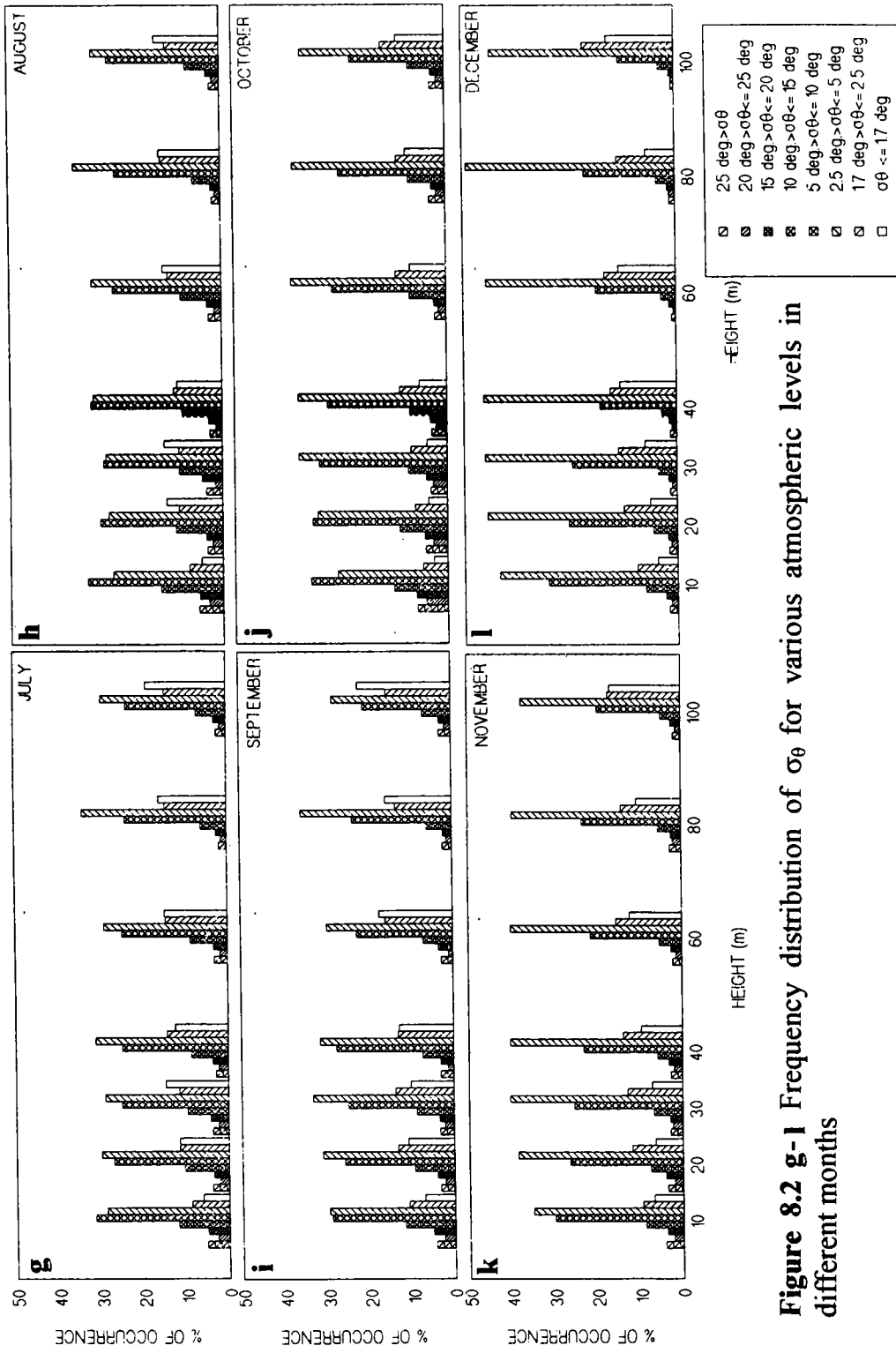


Figure 8.2 g-1 Frequency distribution of σ_θ for various atmospheric levels in different months

Chapter 9

Optimum Wind Probability Distribution

Models

and its Properties

9.1 Extreme Winds Distribution

9.1.1 Introduction

The statistical technique, Weibull distribution by Swedish physicist Weibull (1951) is one of the major areas in Extreme Value Theory (EVT) as explained by Smith (1990). One of the potential applications of this statistical technique in engineering fields is in wind energy studies. (Reed, 1975; Justus et al., 1976; Hennessey, 1977; Steward, 1978). The representation of extreme events distribution pays wide attention by Weibull distribution, because eventhough with the occurrence of new extreme value, the shape of the extreme value curve will remains the same through this tool. The advantage of Weibull distribution in comparison with similar distribution statistics can be seen elsewhere (Hennessey, 1977; Justus et al., 1978; Essenwanger, 1976) and properties of this distribution is elaborately explained by Bury (1975). Both meso- and synoptic-scale meteorological systems can contribute major modifications in the occurrence of extreme events. Monthly distribution of Weibull probability density function (*pdf*) curves or Weibull wind speed frequency curves are studied for peak wind speed events at levels 10 m, 20 m, 30 m, 40 m, 60 m, 80 m and 100 m over Sriharikota. The region lies in the east coast of peninsular India, and meso- and synoptic-scale systems like thunderstorms, sea breeze and low and high pressure systems brewing in the Bay of Bengal are very common. The present chapter is included in view of its applications in the design load analysis of structures, wind energy along the eastern coastline of the peninsula. Results of Weibull distribution so generated are compared with Gaussian (Normal) distribution and presented in this chapter.

9.1.2 The Weibull Model

In the present study, the two parameter (c,k) Weibull distribution is considered. The Weibull distribution of wind speed U is represented by the probability density function (wind speed frequency curve)

$$P_w(U) = (k/c) (U/c)^{k-1} \exp [-(U/c)^k] dU \quad (9.1.1)$$

where c is the scale factor (having units of speed) and k is the shape factor (dimensionless)

The equivalent cumulative probability function (wind speed duration curve) is

$$P(U \leq U_i) = \int_0^{U_i} P_w(U) dU = 1 - \exp [-(U_i/c)^k] \quad (9.1.2)$$

The shape factor k affect the basic "shape" of the model, which is an intrinsic distinguishing character of the model and is not related either to the origin or to the scale of measurements on abscissa. The values of c and k can be found out by using least-square fit to observed distribution. If the observed wind speeds are divided into n class intervals $0-U_1, U_1-U_2, \dots, U_{n-1}-U_n$ having frequencies of occurrence f_1, f_2, \dots, f_n and cumulative frequencies $P_1 = f_1, P_2 = f_1 + f_2, \dots, P_n = f_{n-1} + f_n$ then equation (9.1.1) transforms to the linear form $y = a + bx$ by the relation

$$x_i = \ln U_i \quad (9.1.3)$$

$$y_i = \ln [-\ln (1-P_i)] \quad (9.1.4)$$

Best-fit linear coefficient values a and b can be found either an unweighted or frequency of occurrence-weighted least-square process. The Weibull parameters c and k are related to the linear coefficients a and b as

$$c = \exp (-a/b) \quad (9.1.5)$$

$$k = b \quad (9.1.6)$$

9.1.3 Data and Methodology

Every five minute round the clock peak wind speed events measured by cup anemometers at levels 10 m, 20 m, 30 m, 40m, 60m, 80m and 100m from SET II data (May 1993 to April 1996) is taken as the input data. This voluminous data categorised into months from which means (\bar{U}) and standard deviation (σ) are computed for every five minute, starting from 0000 hr to 2355 hr IST, for all levels, in order to use in Gaussian distribution *pdf* computations as a part of comparison. The parameters (c,k) for levels are generated for every five minute pertain to a month. The *pdf* for every five minute peak wind sample at a particular level is computed by taking the corresponding c and k for that time. For a particular peak wind speed there can be different *pdf* values with respect to different times of occurrence. The largest *pdf* value observed for a particular peak wind speed is considered for constructing the monthly Weibull model. All such largest *pdfs* observed for different peak wind speeds are joined together and continuous curves are drawn at each level by applying spline interpolation, represents Weibull probability curve for that particular level. Cumulation of *pdfs* in percentage are derived for each level for different peak wind speed limits, such as $< 5 \text{ ms}^{-1}$, $> 5 \text{ ms}^{-1}$, $> 10 \text{ ms}^{-1}$, $> 12.5 \text{ ms}^{-1}$ and $> 15 \text{ ms}^{-1}$ as in Table 9.1.1. Same way Gaussian distribution cumulation of *pdfs* in percentage are also computed (Table 9.1.2) by using Gaussian *pdf*

$$P_g(U) = (1/\sigma\sqrt{2\pi}) \exp -(U - \bar{U})^2 / 2 \sigma^2 \quad (9.1.7)$$

9.1.4 Results and Discussion

9.1.4.1 Monthly Features on Weibull Curves

Figure 9.1.1 shows the monthly distribution of number of observations (N) of five minute peak wind events considered for the study at different levels and ranges from about 13500 to 25500 and is also listed in Tables 9.1.1 and 9.1.2. Monthly Weibull curves are shown in Figure 9.1.2(a)-(l). It is observed that there

can be different *pdfs* for the same peak event, and is attributed due to temporal variations in occurrences. Weibull curves for 40 m and 80 m are not included in Figure 9.1.2(a)-(l). All plots show unimodal positively skewed character of Weibull model. In all months except May, the *pdf* show maxima around 2.5 to 3.5 ms^{-1} between 20 m and 100 m. In the 10 m level the maximum *pdf* occurs for less than 2.5 ms^{-1} except in May where 3 ms^{-1} is observed. This is due to strong sea breeze incidence during May. The maximum *pdf* in all months along the Weibull curve slope rightwards as height increases which is depicted by dotted line in Figure 9.1.2(a). This sloping feature is associated with the *k* variation as suggested by Hennessey (1977). From the plots, a general feature can be easily seen as, for lower wind speeds of less than around 5 ms^{-1} having higher *pdfs* are encountered in lower levels compared to upper levels. For speeds greater than around 5 ms^{-1} to 6 ms^{-1} the chance of occurrence of an event is distributed uniformly in all the levels except in May and June, where it is around 10 ms^{-1} in May and 8 ms^{-1} in June. From these observations, the Weibull probability curves for the 100 m tower layer over Sriharikota show, the curves lay one over the other as 100 m lies in the bottom for wind speeds $< 5 \text{ ms}^{-1}$ to 6 ms^{-1} (10 ms^{-1} in May and 8 ms^{-1} in June). In October and November months the wind speed frequency curves show wide fluctuations eventhough they try to fit into the Weibull curve. This is due to low pressure synoptic systems persisting a week or more in the Bay of Bengal and change overs of weather to normal pattern.

9.1.4.2 Characteristics on the Cumulation of *pdfs*

From the above wind speed frequency curves, cumulation of *pdfs* in percentage are computed for events $< 5 \text{ ms}^{-1}$, $> 5 \text{ ms}^{-1}$, $> 10 \text{ ms}^{-1}$, $> 12.5 \text{ ms}^{-1}$ and $> 15 \text{ ms}^{-1}$. Table 9.1.1 gives cumulation of Weibull *pdf* in percentage for different months from 10 m to 100 m level. In all months, this percentage decreases from 10 m to 100 m for events $< 5 \text{ ms}^{-1}$, whereas the percentage increases from 10 m to 100 m for all other limits. Figure 9.1.3, 9.1.4, and 9.1.5 give vertical time

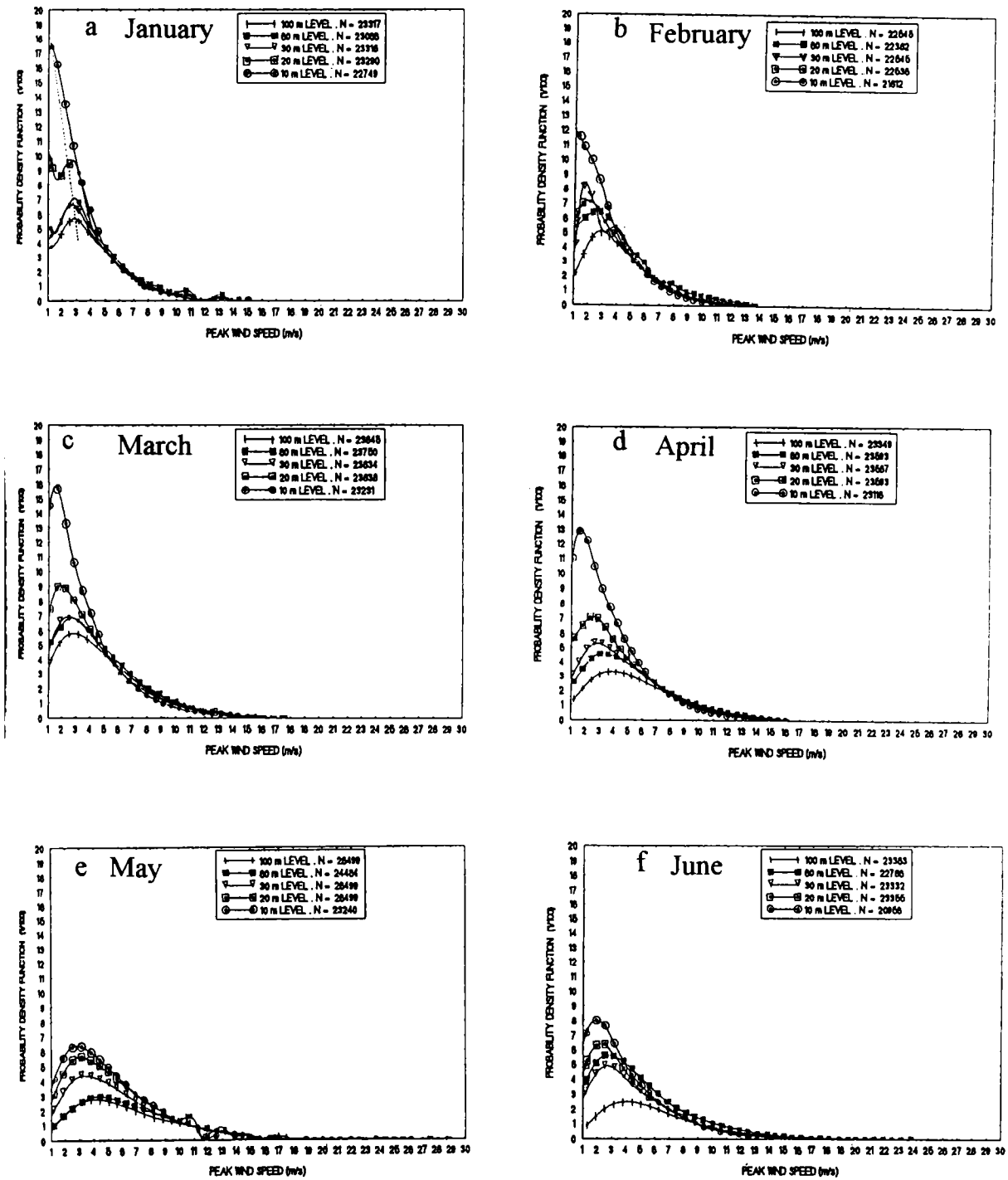


Figure 9.1.2 a-f Weibulldistribution curves for different months

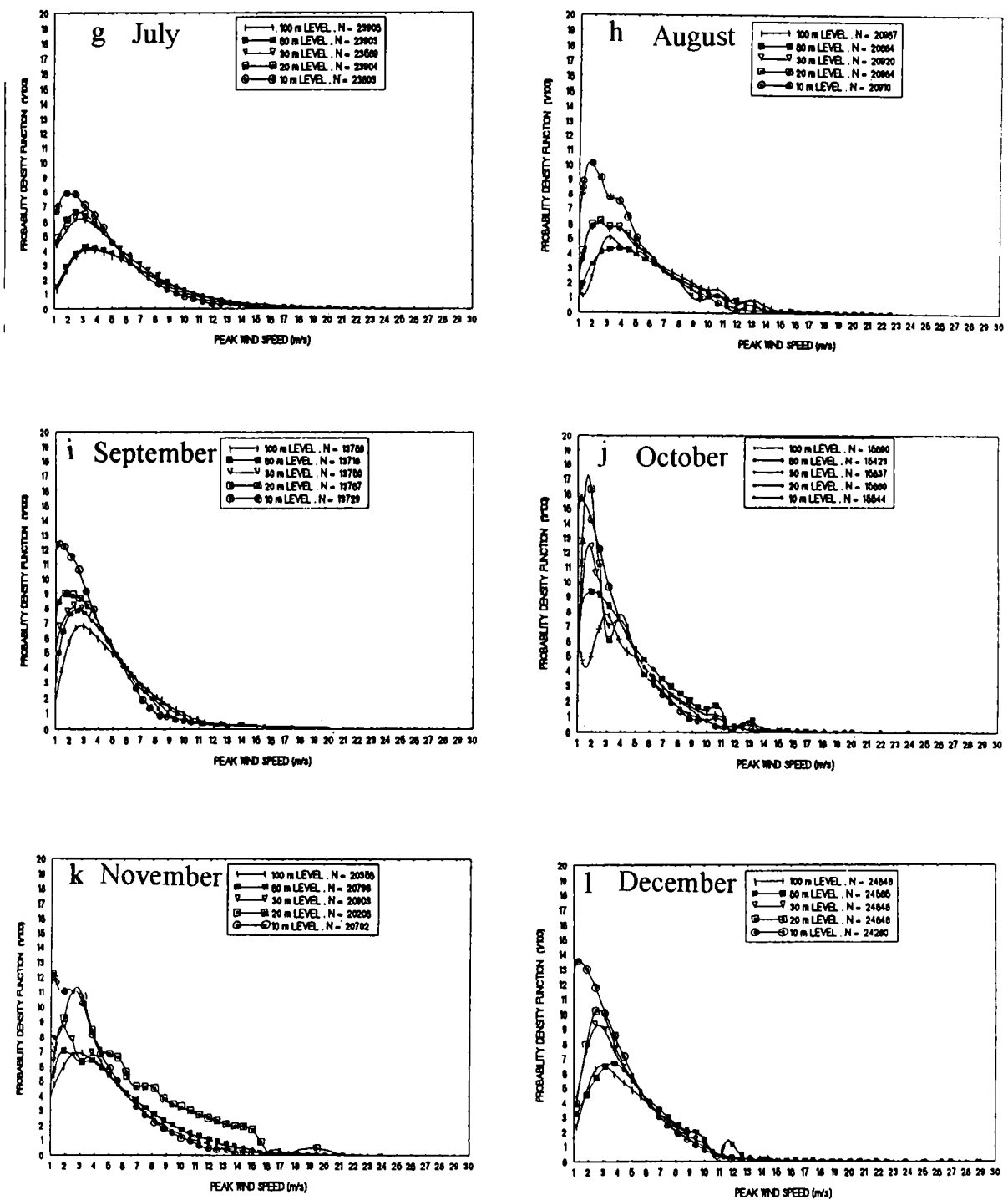


Figure 9.1.2 g-l Weibull distribution curves for different months

section graphs for the Weibull cumulation of *pdfs* in percent for different limits. Events $>12.5 \text{ ms}^{-1}$ and 15 ms^{-1} contour diagrams are avoided due to less percentages encountered. For less than 5 ms^{-1} , May month show least percent and September and October show highest. In the case of greater than 5 ms^{-1} , highest contour occupies from May to August due to meso-scale phenomena like thunderstorms, sea breeze and synoptic-scale low, high pressure systems. (high pressure systems are most persistent system during May in Bay of Bengal).

9.1.4.3 Comparison of Weibull and Gaussian Distribution

Table 9.1.2 tells the cumulation of Gaussian distribution *pdf* percentage similar to Weibull Table. Similarity exists in percentage for higher limits from 12.5 ms^{-1} limit. Eventhough Weibull shows some event occurrences for higher limits, the same thing is not depicted in the Gaussian distribution. This shows Weibull model capability to not to leak out information about an event. Also for any natural event, measures of central tendency like mean, median and mode should be well demarcated, and those are well demarcated through its positive skewness in Weibull model, whereas in the bell shaped Gaussian distribution these occur at the same point.

9.2 Wind Component Distribution

9.2.1 Introduction

Various problems dealing with vector quantities required the integral of elliptical Bivariate Normal Distribution (BND). The estimation of the frequency of winds from any given point, sector or area is possible by use of estimates of the statistical parameters of a wind distribution. This part of the chapter presents the representation of wind component modelling through BND as a theoretical model for wind vector distribution. The wind components, zonal and meridional can be separately modelled through Univariate Normal Distribution (UND) or Gaussian Distribution. But through Gaussian Distribution, the relation connecting zonal and

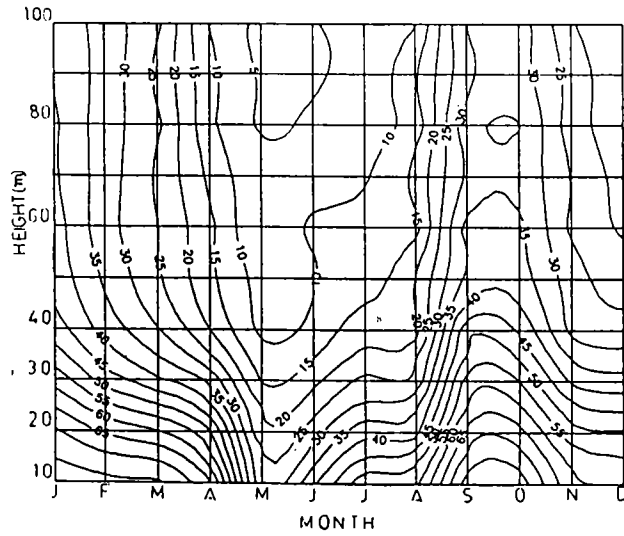


Figure 9.1.3 Weibull cumulation of probability density functions for $< 5 \text{ ms}^{-1}$

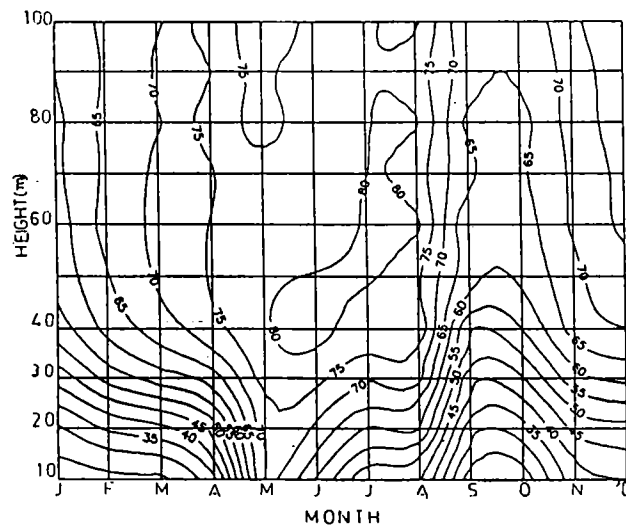


Figure 9.1.4 Weibull cumulation of probability density functions for $> 5 \text{ ms}^{-1}$

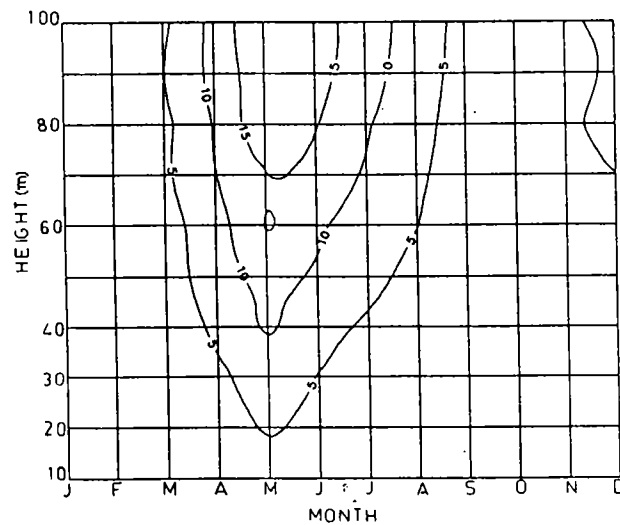


Figure 9.1.5 Weibull cumulation of probability density functions for $> 10 \text{ ms}^{-1}$

Table 9.1.1
Cumulation of Weibull distribution probability density function in percentage

Height (m)	N	< 5m/s	> 5m/s	> 10m/s	> 12.5m/s	> 15m/s
FOR JANUARY						
100.0	23317	39.62	59.87	0.49	0.02	0.00
80.0	23318	40.88	58.55	0.58	0.04	0.00
60.0	23088	42.28	57.29	0.43	0.01	0.00
40.0	22029	47.14	52.58	0.28	0.00	0.00
30.0	23318	57.95	41.87	0.18	0.00	0.00
20.0	23290	70.73	29.19	0.08	0.00	0.00
10.0	22749	78.08	21.90	0.01	0.00	0.00
FOR FEBRUARY						
100.0	22545	32.50	68.25	1.21	0.04	0.00
80.0	22546	32.14	68.43	1.39	0.05	0.00
60.0	22382	31.78	68.98	1.22	0.04	0.00
40.0	21451	37.79	61.60	0.60	0.02	0.00
30.0	22545	47.33	52.20	0.48	0.01	0.00
20.0	22538	63.91	35.91	0.18	0.00	0.00
10.0	21812	78.35	23.62	0.03	0.00	0.00
FOR MARCH						
100.0	23845	28.56	88.97	4.05	0.40	0.02
80.0	23847	28.43	89.27	3.89	0.39	0.02
60.0	23750	25.32	70.91	3.43	0.32	0.01
40.0	23079	30.30	87.58	1.97	0.14	0.00
30.0	23834	40.87	57.72	1.53	0.08	0.00
20.0	23838	60.39	38.72	0.86	0.03	0.00
10.0	23231	75.87	23.83	0.29	0.00	0.00
FOR APRIL						
100.0	23348	9.47	77.80	11.31	1.32	0.10
80.0	23593	11.17	77.27	10.29	1.19	0.09
60.0	17888	15.48	75.21	7.52	0.77	0.04
40.0	23488	19.88	73.49	6.09	0.53	0.01
30.0	23587	33.78	62.33	3.70	0.19	0.00
20.0	23593	50.85	46.78	2.30	0.09	0.00
10.0	23118	66.56	32.65	0.78	0.01	0.00
FOR MAY						
100.0	28499	3.79	72.20	19.47	4.08	0.48
80.0	28499	4.22	73.38	18.43	3.58	0.41
60.0	24464	4.66	78.68	15.73	2.78	0.12
40.0	28488	8.58	78.52	10.72	1.19	0.01
30.0	28498	14.03	77.47	7.89	0.60	0.00
20.0	28499	20.35	73.70	5.67	0.28	0.00
10.0	23240	24.49	72.28	3.18	0.08	0.00
FOR JUNE						
100.0	23383	4.73	75.99	17.38	1.85	0.07
80.0	23383	6.08	77.22	15.25	1.40	0.05
60.0	22788	11.81	78.97	10.88	0.71	0.02
40.0	22587	11.28	82.14	8.29	0.28	0.01
30.0	23332	18.90	78.18	4.70	0.21	0.01
20.0	23355	28.18	68.78	2.94	0.11	0.00
10.0	20958	39.58	59.01	1.37	0.05	0.00
FOR JULY						
100.0	23908	7.38	79.08	12.14	1.30	0.11
80.0	23233	8.88	79.84	10.43	1.15	0.10
60.0	23903	11.49	80.28	7.43	0.74	0.08
40.0	22038	18.91	78.31	4.38	0.38	0.03
30.0	23589	28.88	89.95	3.13	0.24	0.02
20.0	23904	38.74	59.07	2.03	0.15	0.01
10.0	23803	54.12	44.94	0.89	0.05	0.00
FOR AUGUST						
100.0	20987	9.21	81.65	8.30	0.80	0.05
80.0	20985	11.28	81.13	8.91	0.84	0.04
60.0	20884	12.49	81.94	5.14	0.41	0.02
40.0	20388	18.98	79.77	3.03	0.21	0.01
30.0	20920	25.88	72.25	1.95	0.13	0.01
20.0	20964	37.43	61.23	1.27	0.07	0.00
10.0	20910	53.18	48.28	0.53	0.03	0.00
FOR SEPTEMBER						
100.0	13788	30.77	85.47	3.42	0.32	0.02
80.0	13788	33.68	83.27	2.79	0.27	0.01
60.0	13718	37.72	59.93	2.18	0.17	0.01
40.0	13460	49.40	49.31	1.20	0.08	0.00
30.0	13750	58.35	40.83	0.94	0.08	0.00
20.0	13767	87.89	31.34	0.62	0.05	0.00
10.0	13729	78.52	21.18	0.30	0.02	0.00
FOR OCTOBER						
100.0	15690	32.70	85.84	1.50	0.14	0.02
80.0	15690	35.37	83.19	1.30	0.12	0.02
60.0	16423	38.38	82.58	0.98	0.09	0.01
40.0	14910	44.14	55.22	0.58	0.08	0.00
30.0	15837	54.94	44.87	0.35	0.03	0.00
20.0	15680	68.85	33.13	0.20	0.02	0.00
10.0	15544	77.98	21.93	0.10	0.01	0.00
FOR NOVEMBER						
100.0	20358	20.52	73.79	4.80	0.78	0.12
80.0	20381	22.34	72.10	4.87	0.78	0.13
60.0	20798	23.75	70.89	4.54	0.70	0.11
40.0	20303	28.25	67.40	3.85	0.41	0.09
30.0	20903	38.88	58.41	2.39	0.30	0.04
20.0	20208	51.79	48.87	1.22	0.11	0.01
10.0	20702	61.01	38.24	0.68	0.08	0.01
FOR DECEMBER						
100.0	24848	15.00	79.58	5.27	0.15	0.02
80.0	24848	18.79	77.48	5.52	0.18	0.03
60.0	24585	19.34	78.03	4.49	0.12	0.02
40.0	24011	27.10	70.10	2.71	0.07	0.02
30.0	24848	37.19	61.13	1.63	0.04	0.01
20.0	24848	50.93	48.30	0.73	0.03	0.00
10.0	24280	59.75	40.09	0.15	0.02	0.00

N: Total number of every 5 minute peak wind speed events at the level

Table 9.1.2
 Cumulation of Gaussian distribution probability density function in percentage

Height (m)	N	< 5m/s	> 5m/s	> 10m/s	> 12.5m/s	> 15m/s
FOR JANUARY						
100.0	23317	10.73	88.81	0.68	0.00	0.00
80.0	23318	12.09	87.05	0.86	0.00	0.00
60.0	23088	11.88	87.54	0.58	0.00	0.00
40.0	22029	15.04	84.88	0.31	0.00	0.00
30.0	23318	22.05	77.79	0.18	0.00	0.00
20.0	23290	27.32	72.62	0.08	0.00	0.00
10.0	22749	28.27	71.72	0.01	0.00	0.00
FOR FEBRUARY						
100.0	22545	7.18	90.73	2.07	0.01	0.00
80.0	22548	8.12	89.60	2.28	0.02	0.00
60.0	22382	7.90	90.08	2.02	0.02	0.00
40.0	21451	11.45	87.81	0.93	0.00	0.00
30.0	22545	19.80	79.83	0.58	0.00	0.00
20.0	22538	27.78	71.99	0.23	0.00	0.00
10.0	21812	28.28	71.70	0.04	0.00	0.00
FOR MARCH						
100.0	23845	5.85	88.27	7.58	0.29	0.01
80.0	23847	6.45	85.59	7.81	0.34	0.01
60.0	23750	8.24	88.72	8.74	0.30	0.00
40.0	23079	8.27	87.38	4.23	0.14	0.00
30.0	23834	14.27	82.50	3.17	0.08	0.00
20.0	23838	24.03	73.88	2.09	0.02	0.00
10.0	23231	28.79	72.33	0.87	0.00	0.00
FOR APRIL						
100.0	23349	0.79	75.42	21.51	2.18	0.10
80.0	23593	1.03	78.11	20.59	2.17	0.10
60.0	17888	1.97	79.18	17.22	1.81	0.04
40.0	23486	2.94	82.22	13.84	1.00	0.00
30.0	23587	6.05	81.45	12.08	0.43	0.00
20.0	23593	11.05	79.54	9.24	0.17	0.00
10.0	23118	15.23	80.11	4.85	0.02	0.00
FOR MAY						
100.0	28499	0.31	85.09	29.78	4.52	0.30
80.0	28499	0.38	87.90	27.53	3.93	0.28
60.0	24484	0.41	72.71	23.58	3.22	0.08
40.0	28488	0.97	81.22	18.48	1.34	0.00
30.0	28498	1.92	85.03	12.44	0.81	0.00
20.0	28499	3.24	87.02	9.50	0.24	0.00
10.0	23240	4.84	89.28	8.08	0.04	0.00
FOR JUNE						
100.0	23383	0.48	71.94	25.51	2.07	0.03
80.0	23383	0.88	74.83	23.02	1.48	0.01
60.0	22788	1.70	79.03	18.42	0.84	0.01
40.0	22587	1.91	88.00	9.91	0.18	0.00
30.0	23332	4.53	87.78	7.59	0.12	0.00
20.0	23355	7.83	88.90	5.20	0.08	0.00
10.0	20958	12.88	84.71	2.81	0.02	0.00
FOR JULY						
100.0	23908	1.11	78.87	17.98	1.20	0.04
80.0	23233	1.49	82.45	15.03	1.00	0.03
60.0	23903	2.37	88.80	10.39	0.83	0.02
40.0	22038	5.50	87.78	8.37	0.35	0.01
30.0	23589	9.39	85.05	5.34	0.22	0.00
20.0	23904	18.98	79.11	3.78	0.13	0.00
10.0	23803	27.19	70.78	1.99	0.04	0.00
FOR AUGUST						
100.0	20987	1.81	85.84	12.07	0.68	0.01
80.0	20985	2.45	87.18	9.85	0.52	0.01
60.0	20884	2.85	90.01	8.77	0.27	0.00
40.0	20388	4.97	90.88	4.03	0.12	0.00
30.0	20202	9.39	87.82	2.72	0.07	0.00
20.0	20964	15.89	82.35	1.93	0.03	0.00
10.0	20910	24.82	74.22	0.95	0.01	0.00
FOR SEPTEMBER						
100.0	13788	10.27	84.77	4.77	0.19	0.00
80.0	13788	12.00	84.31	3.58	0.13	0.00
60.0	13718	15.83	81.95	2.35	0.07	0.00
40.0	13480	27.43	71.44	1.10	0.03	0.00
30.0	13750	37.80	61.51	0.88	0.03	0.00
20.0	13787	48.52	50.88	0.59	0.02	0.00
10.0	13729	81.57	38.12	0.30	0.01	0.00
FOR OCTOBER						
100.0	15890	12.55	85.50	1.90	0.05	0.00
80.0	15890	14.12	84.20	1.85	0.04	0.00
60.0	15423	15.40	83.48	1.11	0.02	0.00
40.0	14910	21.28	78.14	0.58	0.01	0.00
30.0	15837	31.43	68.28	0.30	0.01	0.00
20.0	15880	40.48	59.39	0.15	0.00	0.00
10.0	15544	48.22	51.70	0.07	0.00	0.00
FOR NOVEMBER						
100.0	20358	7.02	83.80	8.37	0.77	0.04
80.0	20381	8.21	82.80	8.31	0.82	0.05
60.0	20798	8.99	81.82	8.39	0.78	0.04
40.0	20303	13.29	78.45	7.59	0.60	0.08
30.0	20903	17.75	77.79	4.23	0.23	0.01
20.0	20208	25.38	72.69	1.90	0.05	0.00
10.0	20702	29.70	89.35	0.94	0.02	0.00
FOR DECEMBER						
100.0	24848	2.91	87.15	9.85	0.09	0.00
80.0	24848	3.58	85.52	10.77	0.13	0.00
60.0	24585	4.52	88.95	8.48	0.07	0.00
40.0	24011	7.33	87.78	4.88	0.03	0.00
30.0	24848	11.89	85.29	2.82	0.01	0.00
20.0	24848	17.92	80.79	1.28	0.00	0.00
10.0	24280	21.05	78.78	0.19	0.00	0.00

meridional wind components are not in consideration, but there exists its relation through intra-level correlation coefficient. The prime objective is to develop a proper theoretical model for wind vector distribution through BND which are considered superior to Conventional Wind Rose (CWR) and UND. Properties of BND ellipses modelled in SBL over Sriharikota are also discussed.

9.2.2 UND and Its Limitations in Wind Vector Distribution

In meteorological coordinate system, wind vector (raw data) can be resolved into zonal (u) and meridional (v) components. The component distribution can be modelled by UND separately. The *pdf* of UND for zonal can be

$$P_g(u) = 1/\sqrt{2\pi} \sigma_u \exp [-(u-\bar{U})^2 / 2\sigma_u^2]; \quad -\infty \leq u \leq \infty \quad (9.2.1)$$

similarly for meridional $P_g(v)$

$$P_g(v) = 1/\sqrt{2\pi} \sigma_v \exp [-(v-\bar{V})^2 / 2\sigma_v^2]; \quad -\infty \leq v \leq \infty$$

where \bar{U} , \bar{V} , σ_u , σ_v are means and standard deviations of zonal and meridional components respectively. Numerical values of probability that u or v falls in the interval (u_1 and u_2 or v_1 and v_2);

$$P_g \{ u_1 = \bar{U} - t \sigma_u \leq u \leq u_2 = \bar{U} + t \sigma_u \} \text{ and}$$

$$P_g \{ v_1 = \bar{V} - t \sigma_v \leq v \leq v_2 = \bar{V} + t \sigma_v \} \quad (9.2.2)$$

where $t = 1.6449$ for 90% value probability and $t = 1.9602$ for 95% value probability based on theory of normal distribution. In this UND, the correlation between u and v , the intralevel correlation coefficient (ρ_{uv}) is not taken into account. This results in some improbable values of wind vectors for a given percentile.

9.2.3 Bivariate Normal Distribution Model

The philosophy behind the combined distribution holds good for u and v components which results in BND. When the two variables u and v are correlated, it is necessary but not sufficient condition for the marginal distribution $f(u)$ and $f(v)$ are to be normal and the joint distribution to be BND.

The probability density function for BND is

$$P_b(u,v) = 1 / (2\pi\sigma_u\sigma_v) \sqrt{1-\rho_{uv}^2} \exp \left[-1/2 (1 - \rho_{uv}^2) \right. \\ \left. \{ (u - \bar{U})^2/\sigma_u^2 - 2\rho_{uv} (u-\bar{U})(v-\bar{V}) / \sigma_u\sigma_v + (v - \bar{V})^2/\sigma_v^2 \} \right] \\ - \infty \leq u \leq \infty \\ - \infty \leq v \leq \infty \quad (9.2.3)$$

The probability distribution function can be derived by setting the terms of the exponent of equation (9.2.3) to a constant λ as

$$\{ (u - \bar{U})^2/\sigma_u^2 - 2\rho_{uv} (u-\bar{U})(v-\bar{V})/\sigma_u\sigma_v + (v - \bar{V})^2/\sigma_v^2 \} = \lambda^2 \quad (9.2.4)$$

The equation (9.2.4) is recognised as a family of ellipses depending on the value of λ^2 . The density function has constant values on these ellipses. So the ellipses generation out of equation (9.2.4) are referred to as ellipses of equal probability. The percentile ellipses can be generated based on λ value variations as

$$\lambda = \sqrt{2} \{ \sqrt{-\ln(1-P)} \} \quad (9.2.5)$$

where P is the probability. For 90% probability ellipse $\lambda = 2.146$ and 95% probability ellipse $\lambda = 2.447$.

9.2.4 Methodology for the Generation of BND Ellipses

In order to handle the equation (9.2.4) for the generation of BND ellipses the following steps are adopted. The equation (9.2.4) is rewritten as

$$AX^2 + BXY + CY^2 + DX + EY + F = 0 \quad (9.2.6)$$

where,

$$A = \sigma_v^2$$

$$B = -2 \rho_{uv} \sigma_u \sigma_v$$

$$C = \sigma_u^2$$

$$D = B\bar{V} + 2A\bar{U}$$

$$E = -(B\bar{U} + 2C\bar{V})$$

$$F = A\bar{U}^2 + C\bar{V}^2 + B\bar{U}\bar{V} - AC\lambda^2$$

For constructing the ellipse the range of variables ie., the smallest and largest values of X and Y for a given probability ellipse P is given by

$X_{L \rightarrow S} = \bar{U} \pm \sigma_u \lambda$ and $Y_{L \rightarrow S} = \bar{V} \pm \sigma_v \lambda$. So once the statistical parameters such as means, standard deviations and intra-level correlation coefficient (\bar{U} , \bar{V} , σ_u , σ_v , ρ_{uv}) are obtained for a given set of wind samples, the desired probability ellipses can be constructed in the following steps.

(1) Increment the values of X within the limit (ie., $X_{L \rightarrow S} = \bar{U} \pm \sigma_u \lambda$).

(2) Form a quadratic equation in Y from equation (9.2.6) as

$$CY^2 + (BX + E)Y + (AX^2 + DX + F) = 0 \text{ and can be in reduced form as } CY^2 + ZY + W = 0 \quad (9.2.7)$$

$$\text{where } Z = BX + E \text{ and } W = AX^2 + DX + F$$

(3) Put each increment values of X in this quadratic equation and find out the roots of Y as

$$Y = [-Z \pm \sqrt{Z^2 - 4CW}] / 2C \quad (9.2.8)$$

(4) The two roots obtained for Y represent two points in the ellipse. Locus of roots generated for different values of X from X_L to X_S together with X values will lead to the completed elliptical BND model for wind component distribution.

9.2.5 Features of 90% BND Ellipses in the SBL over Sriharikota

9.2.5.1 Data

SET II data is used as the input. The raw data, in speed and direction resolved into components. For each month from the all available data on zonal and meridional wind components the five statistical parameters (\bar{U} , \bar{V} , σ_u , σ_v , ρ_{uv}) are obtained for different levels in the SBL. The five parameters are used to construct an ellipse for a level pertain to a particular month. The ellipses are generated for 90% probability values by the methodology explained above.

9.2.5.2 Results on the Properties of Ellipses

Figure 9.2.1(a)-(l) show generated ellipses in the SBL level over Sriharikota for different months. 90% ellipses alone are drawn for levels 20, 40 and 100 m. Scattered points of 20 m level in the observed events of u and v components are incorporated in the BND ellipses to verify the validity of the elliptical distribution model constructed.

In all months, the distribution is elliptical, except in January where it is almost circular. But circular distribution is also a form of elliptical BND. In January the intra-level correlation coefficient (ρ_{uv}) is nearly 0.0.

Ellipse size increases with height and the orientation is based on the prevailing wind direction of the season. In all levels, the ellipse quadrant having more area possesses more number of occurrence of events. The scatter of observed points at 20 m level fall within the 20 m ellipse in an elongated fashion in conjunction with the orientation of the major axis of the ellipse.

One of the striking feature observed, is the joining of all level ellipses or coming closer to each other in a point as marked in Figure 9.2.1(g) with an arrow. The point may be treated as almost as a point of least probable occurrence of events. At this point, it is established that the feature on the occurrence of any events, if so happen will uniformly experience or distribute to all levels. That is if

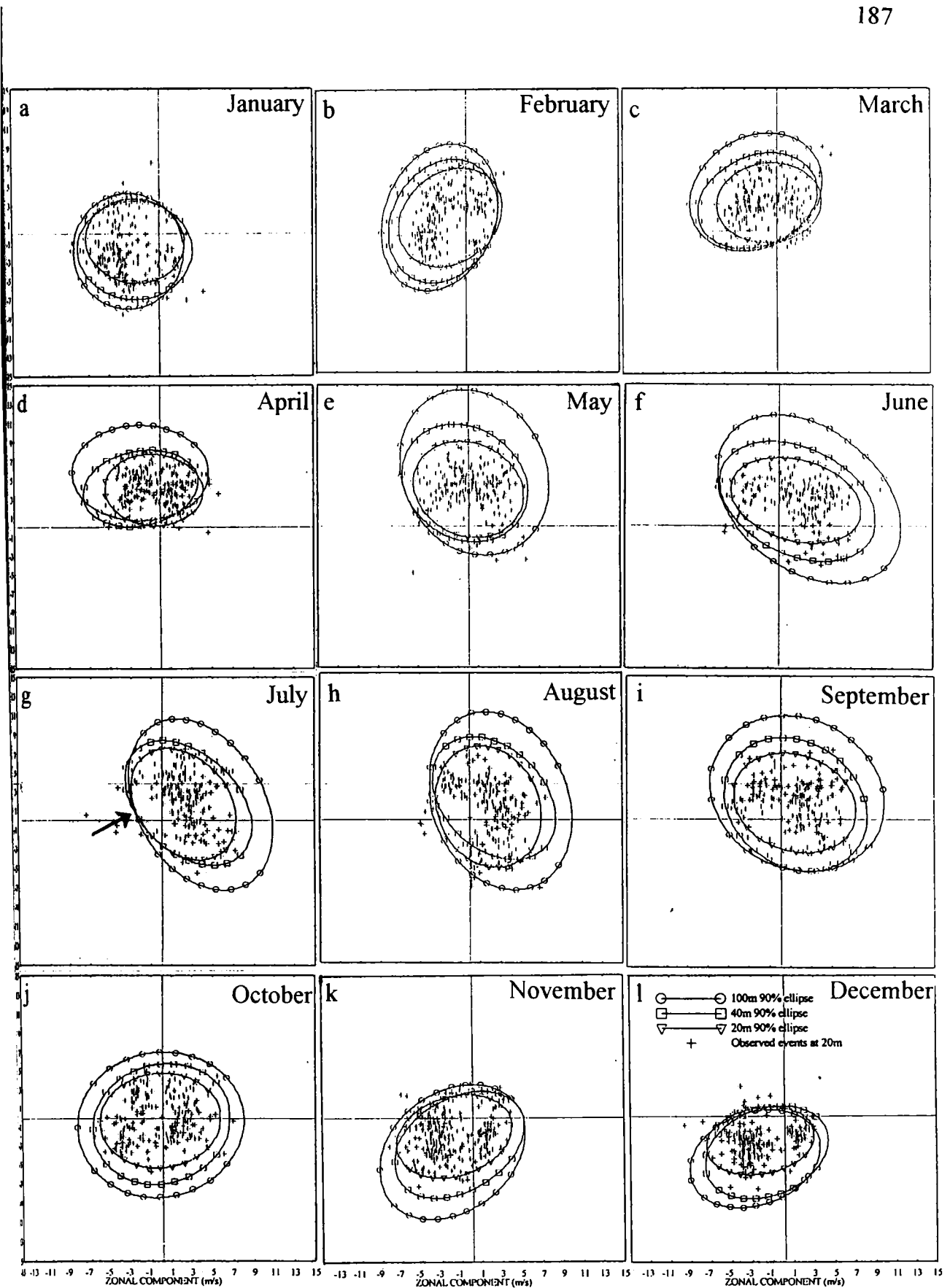


Figure 9.2.1 a-l Bivariate normal distribution ellipses for different months

any improbable wind feature is noticed in a level of SBL same thing will occur for all levels. The feature is not seen in October, which may be interpreted as the non occurrence of least probable events. In all respect, the analysis summarised the well organised bivariate normal elliptical distribution models in SBL for any levels and any month.

9.2.6 Comparison of BND and UND

A comparison between BND and UND has been carried out. June is considered as a representative month for the comparison study. Construction of 90% probability rectangle is formed for 20 m level for June month with values $\bar{U} + 1.644 \sigma_u = 6.5 \text{ ms}^{-1}$, $\bar{U} - 1.644 \sigma_u = -3.1 \text{ ms}^{-1}$, $\bar{V} + 1.644 \sigma_v = 6.4 \text{ ms}^{-1}$ and $\bar{V} - 1.644 \sigma_v = -0.7 \text{ ms}^{-1}$ as vertices of the rectangle in order to represent UND. This rectangle constructed is superimposed with the 90% BND ellipse constructed at 20 m level. The analysis is shown in Figure 9.2.2, in which improbable values are fallen outside the ellipse, but at the same time inside the rectangle (darkened area). Probable values are fallen inside the 90% ellipse itself, but outside the 90% rectangle (hatched area). So this analysis conclude that modelling with BND gives correct probable winds in wind components distribution, UND may lead to overestimation or underestimation of wind conditions. Transformation of coordinate to another (say, wind components in lateral and longitudinal to the station having importance in Boundary Layer Meteorology) is possible through BND model.

9.2.7 Advantages of BND over Conventional Wind Rose (CWR)

CWR has the usual breakdown of winds into direction and speed groups. BND gives an estimate of percentage of time that the vectors has a speed equal to or less than a selected value. BND gives an estimate of the percentage of time that the wind vectors come from a specific circular or elliptical area within certain

speed limits. It also gives a knowledge of the percentage of time that the wind vectors come from a specific quadrant or some portion.

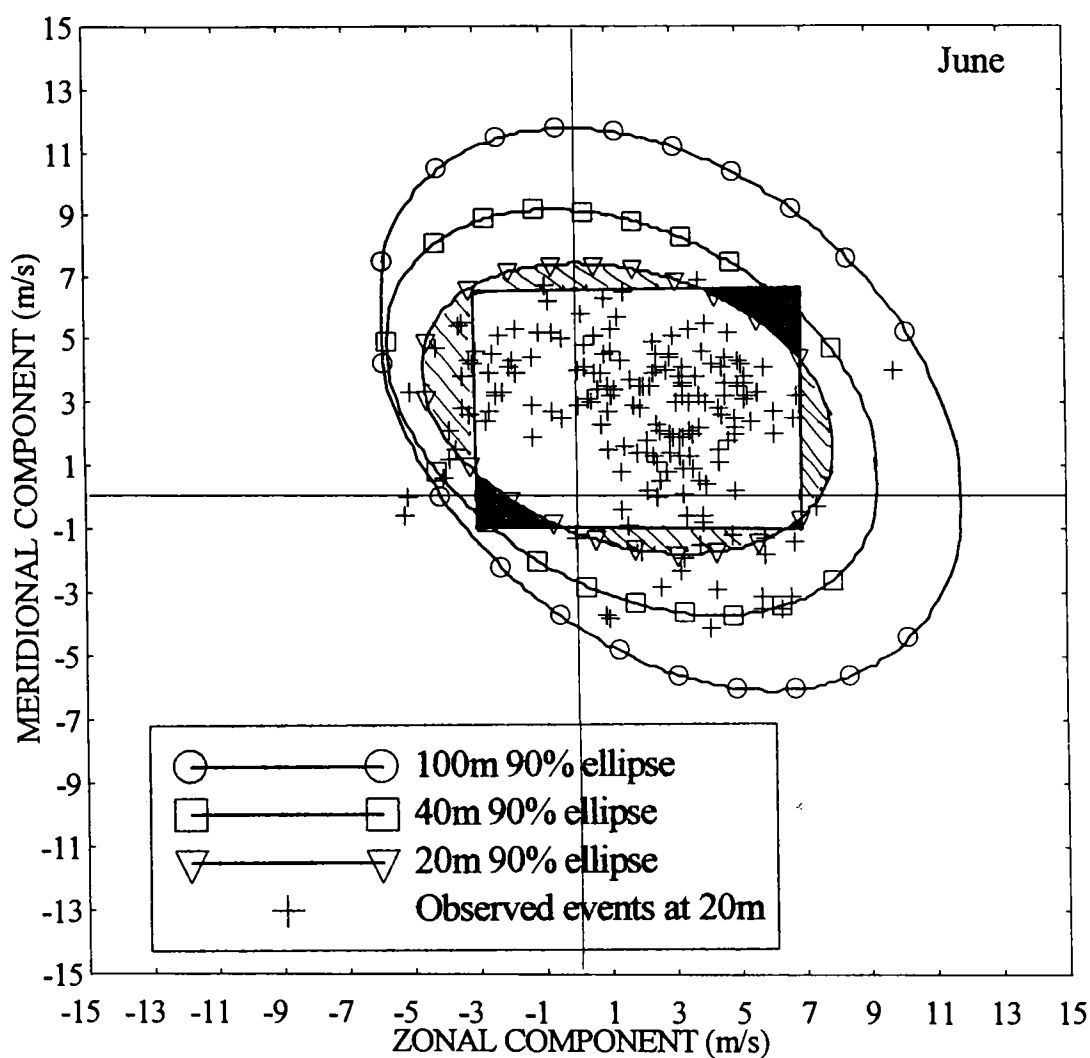


Figure 9.2.2 A comparison of 90 % BND ellipse and 90 % UND rectangle for 20 m level

Chapter 10
Summary and Conclusions

Studies on the vertical structure of horizontal wind variability in the Surface Boundary Layer (SBL) over Sriharikota, based on round the clock wind speed and direction measuring meteorological tower facility from seven levels in the 100 m layer since May 1993 have been carried out. The major conclusions drawn from investigations are summarised in this chapter.

A quantitative analysis on the SBL wind properties established the phenomenon of "wind merging" as wind speed start building up in the levels from surface to 40 m, and a decreasing trend in 60 to 100 m so as to form a region of minimum wind shear in the diurnal variation of mean wind speed. This phenomenon is linked with momentum exchange between levels and is observed throughout the year.

Eventhough momentum transfer to ground starts early, the establishment of its effect on lower layers takes almost one hour delay. The intense wind merging timing is observed around 1000 hr IST. Mean resultant wind direction variability between levels are found negligible. The mean wind direction has shown seasonal pattern and land-sea breeze change overs are vividly demarcated in the diurnal variation. The evolution of sea breeze front is observed in all levels at the same time and for full establishment of sea breeze in the entire SBL takes approximately one hour. The use of steadiness factor is found out as an excellent parameter to delineate onset of sea breeze for the station. An intense abrupt dip in diurnal variation in steadiness factor in the entire SBL is resulted during the onset of sea breeze.

The flow of mean peak wind speed is observed exactly the same as that of mean scalar wind speed in trend but with an increase in magnitude. Probability of mean wind speed in different wind directions are shown a general behaviour of percentage probability decrease in lowest speed class as height increases. At the same time the probability of very next higher class interval (with higher speeds) increases with height. Monthly wind climatology derived in various wind

variables are shown a prominent maximum in May and minimum in October for mean scalar wind speed. Westerlies to northerlies are seen as almost absent throughout the year in monthly climatology. The intra-level correlation coefficient between zonal and meridional component from May to September are in negative correlation, almost no relation in October and positive in other months.

Concavity in SBL wind profile upward associated with unstable SBL and downward linked with stable SBL are seen, and stable SBL on a bright sunshine day can prolong for 16 hours. The features of wind speed in association with thunderstorm wind are shown a difference of the order of 10 ms^{-1} between average and peak wind speeds within 5 minute. Wind direction fluctuations computed for different thunderstorm events have depicted high values and is more than 40° for a sandstorm event where maximum wind speed is more than 20 ms^{-1} . It is found that thunderstorm peak winds of $\geq 15 \text{ ms}^{-1}$ can lash more than 50 minute in duration. More than 70% of rain associated with peak winds of $\geq 15 \text{ ms}^{-1}$ are ended with rainfall intensity of less than 10 mmhr^{-1} . Thunderstorm rain associated with high winds are ceased quickly.

During cyclonic storm passage it is observed that there can be significant difference in mean wind speed from 10 m to 100 m level, but it is not so for peak wind speeds. Throughout the phase of cyclonic landfall, a slight veering in wind direction is noticed from lower levels to 100 m level. Number of occurrence of wind speed events during the progress of a cyclonic storm as it approaches towards the station with intensification from low pressure to cyclonic storm, is established the change of wind clustering classes from single to more than two model classes in a day, which may have high forecasting potential about landfall. Spectral characteristics of winds in association with low pressure system are observed in low frequencies as every hour there is an incidence of high and low amplitudes alternately in the entire SBL.

Exceedance probability of 5 ms^{-1} in the SBL over the station can happen at any time, and moderately strong winds of the order between 5 and 10 ms^{-1} are in existence during afternoon or evening. The coefficient of variation in wind speeds has reported high values in diurnal cycle during the occurrence of wind speed merging regime. Diurnal variations in intra-level correlation coefficient between zonal and meridional components have shown negative relation generally from June to September and positive relation in other months except in October, where the values are fallen between 0.3 to -0.3.

It is seen a high inverse relation among steadiness factor and standard deviation of wind directions, as high steadiness factor are associated with low standard deviation in wind directions and *vice versa*. Throughout the year standard deviation of wind directions are fallen between 15° to 45° . Mean scalar wind speeds are always found greater than mean resultant wind speed. The difference among them is so large during onset of sea breeze in diurnal variations. The diurnal variation in gust factor is shown high values during wind merging period which existed throughout the year. A property of gust factor decreases as height increases is noted in the analysis of gust factor variations.

The study on wind variability and elliptical approximation of wind hodographs investigated for this tropical coastal station established that Sriharikota is of meso-scale weather entity. Wind variability ratio increases from lower levels to upper levels. In south west monsoon months the station is of high ratio values and it gets affected with meso-scale weather features like thunderstorms. The variations in wind variability ratio in different months is clearly depicted its strong link to define meso-scale or synoptic-scale forcing domination for this station. Meso-scale forcing is characterised by diurnal wind variability and synoptic-scale forcing by interdiurnal wind variability. Clockwise elliptical rotation during the course of a day is clearly seen in mean wind hodographs for various months and the hodograph size increases from lower to

upper SBL. Generally more ellipticity in wind hodographs are noticed in association with high wind variability ratio.

On the structure of surface roughness parameter and power law exponent has explained a strong direct proportionality between them. From late night to morning hours the roughness values are maximum in the diurnal variations followed by a steep downward slope. Variations of surface roughness parameter with different wind directions are shown, lower values for onshore winds compared to that of offshore winds. Exponent in power law is less during a cyclone day compared to a normal day. This shows that the wind speed is inversely related to the exponent values. Frictional velocity is fallen between 0.4 to 0.6 ms^{-1} throughout the year.

Average total shears are observed greater values than scalar shears. The variations of total shears in various months have shown complex regimes. But quite systematic variations are seen in average scalar shears. Scalar shears are high in the lowest shear levels compared to upper levels. Throughout the year, scalar shear values are higher in the early hours of the day in lower levels and are systematically decreases towards the higher shear levels. A semi diurnal type of oscillation in average total shears are found in south west monsoon months. The separation between two maxima and between two minima are found in the order of 8 hours. The difference between scalar and total shears are more during south west monsoon and is least in winter months.

Properties of atmospheric stability by using wind as a sole parameter has given an excellent climatology on diurnal atmospheric stability over the station. Wind shears are lower during least stable conditions of the atmosphere and they are higher during high stable atmospheric conditions. The wind merging portion in the diurnal speed curves are in association with least stability of atmosphere. In hours of stable atmospheres the departure of low level and upper level SBL winds are at its maximum. Percentage occurrence of unstable atmosphere in the lower

layers are more compared to upper layers. Stable atmospheric conditions are generally observed in SBL except in south west monsoon, when stable and unstable atmospheres are almost equally in prevalence.

Extreme wind distribution characteristics through Weibull model, shows SBL peak winds are in positively skewed unimodal distribution. For lower wind speeds higher probability density functions are encountered in lower levels, whereas for higher wind speeds probability density functions are seen in almost equal distribution for various levels. Cumulation of probability density functions for Weibull model has shown a good comparison with the station wind climatology embedded with meso-synoptic scale weather flows. Comparison of Weibull and Gaussian distributions revealed the capability of Weibull distribution to not to leak out information about any extreme event. In Weibull all statistical central tendencies are in well separation unlike Gaussian distribution.

Bivariate normal distribution statistics derived for wind components distribution has provided a proper theoretical model for wind vectors distribution in SBL, Its capability assessed as superior to conventional wind rose and univariate normal distribution. Bivariate normal ellipses are formed for all SBL levels. Ellipse sizes are increased from lower levels to upper levels, and they oriented according to the seasonal wind direction climatology. Any least probable event occurrence in SBL winds are observed in equal distribution for all levels, depicted by bivariate normal distribution ellipses for different months. Comparison between bivariate normal distribution and univariate normal distribution showed as bivariate normal distribution gives probable winds whereas univariate normal distribution may lead to overestimation or underestimation of wind conditions. In bivariate normal distribution model, transformation of coordinates can be made possible. Bivariate normal distribution has shown its capacity to make informations regarding the percentage of time that the wind vectors come from a specific quadrant or some portion.

Various independent studies and investigations carried out and presented in different chapters in the thesis is having high direct application potential in engineering demands since wind is vitally important to all phases of commerce. The utilisation of wind modelling studied are briefed at different places in this thesis. Further studies can be aimed for the better understanding of wind flow modelling in the SBL by incorporating other meteorological parameters at different levels and locations in the Surface Boundary Layer.

- Ackermann, G. R.**, Means and standard deviations of horizontal wind components, *J. Clim. Appl. Meteor.*, **22**, 959-961, 1983.
- Adiga, B. B.**, Wind variation in a 120 m layer at Tarapur, *J. Inst. Eng. (India)*, **61**, 61-64, 1981.
- Alpert, P.**, Anti-clockwise rotation of the wind hodograph and its relation to thermal forcing. *Mesoscale Meteorology- Theories, Observations and Models*, D. Reidel Pub. Co., Dordrecht, The Netherlands, 1983.
- Alpert, P., and E. Eppel**, A proposed index for mesoscale activity, *J. Clim. Appl. Meteor.*, **24**, 472-480, 1985.
- Andre, J. C., G. De Moor, P. Lacarrere, G. Therry and R. du Vachat**, Modeling the 24-hour evolution of the mean and turbulent structure of the planetary boundary layer, *J. Atmos. Sci.*, **35**, 1861-1883, 1978.
- Arya, S. P.**, *Introduction to Micrometeorology*, Academic press, Inc, California, 1988.
- Auwera, L. V., F De Meyer and L. M. Malet**, The use of Weibull three-parameter model for estimating mean wind power densities, *J. Appl. Meteor.*, **19**, 819-825, 1980.
- Balling, R. C., Jr and R. S. Cerveny**, Long-term associations between wind speeds and the urban heat island of Phoenix, Arizona, *J. Clim. Appl. Meteor.*, **26**, 712-716, 1987.
- Bardsley, W. E.**, Note on the use of the inverse Gaussian distribution for wind energy applications, *J. Appl. Meteor.*, **19**, 1126-1130, 1984.
- Blackadar, A. K.**, A survey of wind characteristics below 1500 ft, *Meteor. Monogr.*, **4**, **22**, 3-11, 1960.
- Brent, B. M., J. M Dewarlt and A. I. Chen**, Stability-class determination-A comparison for one site, *6th Symp. Turbulence and Diffusion*, Boston M A, March 22-25, 1983.
- Brock, F. V., and D. J. Provine.**, A standard deviation computer, *J. Appl. Meteor.*, **1**, 81-90, 1962.
- Burry, K. V.**, *Statistical Models in Applied Science*, John Wiley & Sons, New York, USA, 1975.

- Busch, N. E.**, On the mechanics of atmospheric turbulence. *In workshop on micrometeorology* (D.A. Haugen, ed.), Amer. Meteor. Soc., Boston, 1-65, 1973.
- Busch, N. E., and L. Kristensen**, Cup anemometer overspeeding, *J. Appl. Meteor.*, **15**, 1328-1332, 1976.
- Carl, M. D., Tarbell, T. C., and Panofsky, H. A.**, Profiles of wind and temperature from towers over homogeneous terrain, *J. Atmos. Sci.*, **30**, 788-794, 1973.
- Champagne-Phillippe, M.**, Coastal wind in the transition from turbulence to mesoscale, *J. Geophys. Res.*, **94**, 8055-8074, 1989.
- Charnock, H.**, Wind stress on a water surface, *Q.J.R. Meteor. Soc.*, **81**, 639-640, 1955.
- Conradsen, K., L. B. Nielsen and L.P. Pram**, Review of Weibull statistics for estimation of wind speed distributions, *J. Clim. Appl. Meteor.*, **23**, 1173-1183, 1984.
- Cooley, J. M., and J. W. Tukey**, An algorithm for the machine calculation of Fourier series, *Math. Comput.*, **19**, 287-297, 1965.
- Crutcher, H. L.**, On the standard deviation wind rose, *J. Meteor.*, **14**, 28-33, 1957.
- Crutcher, H. L.**, Computations from elliptical wind distribution statistics, *J. Appl. Meteor.*, **1**, 522-530, 1962.
- Davenport, A. G.**, The relationship of wind structure to wind loading. *Proc. Conf. Wind Effects on Structures.*, Nat. Phys. Lab. Symp., vol I, HMSO, London, 53-102, 1965.
- Defand, F.**, Local winds, *Compendium of Meteor.*, Amer. Meteor. Soc., Boston, 662-667, 1950.
- De Marrais, G. A.**, Wind-speed profiles at Brookhaven National Laboratory, *J. Meteor.*, **16**, 181-190, 1959.

- Doran, J. C., and M. G. Verholek**, A note on vertical extrapolation formulas for Weibull velocity distribution parameters, *J. Appl. Meteor.*, **17**, 410-412, 1978.
- Draxler, R. R.**, Simulated and observed influence of the nocturnal urban heat island on the local wind field, *J. Clim. Appl. Meteor.*, **25**, 1125-1133, 1986.
- Dyer, A. M.**, A review of flux-profile relationship, *Bound. Layer Meteor.*, **7**, 363-372, 1974.
- EPA.**, Ambient monitoring guidelines for prevention of significant deterioration (PSD), *EPA-450/4-80-012*, U S Environmental Protection Agency, EPA, Research triangle park, N.C, 1987.
- EPA.**, On-site meteorological data work group, On-site meteorological program guidance for regulatory modeling applications *EPA-450/4-87-013*, Office of air quality planning and standards, U S Environmental Protection Agency, EPA, Research triangle park, NC, 1987.
- ESDU.**, Characteristics of wind speed in the lower layers of the atmosphere near the ground: strong winds (neutral atmosphere), *ESDU data item. 72026, Amend. A,B*, October 1974.
- Essenwager, O. M.**, *Applied Statistics in Atmospheric Science, Part A, Frequencies and Curve Fitting*, Elsevier, U S A, 1976.
- Estoque, M. A.**, A theoretical investigation of the sea breeze, *Q.J.R. Meteor. Soc.*, **87**, 136-146, 1961.
- Fielder, F., and Panofsky, H. A.**, Atmospheric scales and spectral gaps, *Bull. Am. Meteor. Soc.*, **51**, 1114-1119, 1970.
- Fisher, E. L.**, An observational study of the sea breeze, *J. Meteor.*, **17**, 645-660, 1960.
- Frenzei, W. C.**, Diurnal wind variations in central California, *J. Appl. Meteor.*, **1**, 405-412, 1962.
- Frost, R.**, The velocity profile in the lowest 400 feet, *Meteor. Mag.*, **76**, 14-17, 1947.
- Fujita, T.**, Results of detailed synoptic studies of squall lines, *Tellus*, **7**, 405-436, 1955.

- Fujita, T., and H. R. Byers**, Spearhead echo and downburst in the crash of an airliner, *Mon. Wea. Rev.*, **105**, 129-146, 1977.
- Garratt, J. R.**, Review of drag coefficients over oceans and continents, *Mon Wea. Rev.*, **105**, 915-929, 1977.
- Garrett, A. J., and F. G. Smith**, Average diurnal behaviour of surface winds during summer at sites in complex terrain, *J. Clim. Appl. Meteor.*, **24**, 174-183, 1985.
- Gedzelman, S. D.**, *The Science and Wonders of the Atmosphere*, Wiley, New York, 1980.
- Geissler., E.D (ed.)**, *Wind Effects on Launch Vehicles*, Technivision services, England, 1970.
- Gill, G. G., L. E. Ollsson, J. Sela and M. Suda**, Accuracy of wind measurements on towers or stalks, *Bull. Amer. Meteor. Soc.*, **48**, 665-674, 1967.
- Hahn, C. J.**, A study of the diurnal behaviour of boundary layer winds at the Boulder atmospheric observatory, *Bound. Layer Meteor.*, **21**, 231-245, 1981.
- Harris, E. K., and R. A. Mc Cornick**, A simple procedure for estimating the standard deviation of wind fluctuations, *J. Appl. Meteor.*, **2**, 804-805, 1963.
- Haurwitz, B.**, Comments on the sea-breeze, *J. Meteor.*, **4**, 1-8, 1947.
- Heald, R. C., and L. Mahrt.**, The dependence of boundary layer shear on diurnal variation of stability, *J. Appl. Meteor.*, **26**, 859-867, 1981.
- Hennessey, J. P.**, Some aspects of wind power statistics, *J. Appl. Meteor.*, **16**, 119-129, 1977.
- Hewson, E. W., J.E. Wade and Baker, R. W.**, A Handbook on the use of Trees as an Indicator of Wind Power and Potential, U S Dept. of energy Rep. *RLO-2227-79/3*, 1979.
- Hicks, B. B.**, Some evaluations of drag and bulk transfer coefficients over water bodies of different sizes, *Bound. Layer Meteor.*, **3**, 201-213, 1972.

- Hicks, B. B., P. Hyson and C. J. Moore**, a study of eddy fluxes over a forest, *J. Appl. Meteor.*, **14**, 58-66, 1975.
- Hindu Daily**, India, Flying through 'confused air', March 20, 1997.
- Hsu, S. A.**, Boundary-Layer trade wind profile and stress on a tropical coast, *Bound. Layer Meteor.*, **2**, 284-289, 1972.
- Hsu, S. A.**, Dynamics of the sea breeze in the atmospheric boundary layer: A case study of the free convection regime, *Mon. Wea. Rev.*, **101**, 187-194, 1973.
- Hsu, S. A.**, Determination of the power law wind profile exponent on a tropical coast, *J. Appl. Meteor.*, **21**, 1187-1190, 1982.
- Hsu, S. A.**, *Coastal Meteorology*, Academic press, Inc., California, 1988.
- Huschke, R. E.**, *Glossary of Meteorology*, Amer. Meteor. Soc., Boston, 1959.
- Hyson, P.**, Cup anemometer response to fluctuating wind speeds, *J. Appl. Meteor.*, **11**, 843-848, 1972.
- Hwang, H.J.**, Power density spectrum of surface wind speed on Palmyra Island, *Mon. Wea. Rev.*, **98**, 70-74, 1970.
- Irwin, J. S.**, Estimating plume dispersion-A comparison of several sigma schemes, *J. Clim. Appl. Meteor.*, **22**, 92-114, 1983.
- Ishida, H.**, Seasonal variation of spectra of wind speed and air temperature in the mesoscale frequency range, *Bound. Layer Meteor.*, **52**, 335-348, 1990.
- Joffre, S. M.**, Power laws and the empirical representation of velocity and directional shear, *J. Clim. Appl. Meteor.*, **23**, 1196-1203, 1984.
- Jones, J. I. P., and F. Pansquill.**, An experimental system for directly recording statistics of the intensity of atmospheric turbulence, *J. Meteor. Soc.*, **85**, 225-236, 1959.
- Justus, C. G., and W. R. Hargraves., A. Mikhail and D. Graber**, Methods for estimating wind speed frequency distributions, *J. Appl. Meteor.*, **17**, 350-353, 1978.

- Justus, C. G., W. R. Hargraves and Ali Yalein**, Nationwide assessment of potential output from wind power generators, *J. Appl. Meteor.*, **15**, 673-678, 1976.
- Justus, C. G., and A. Mikhail**, Height variation of wind speed and wind distribution statistics, *Geophys. Res. Lett.*, **3**, 261-264, 1976.
- Justus, C. G.**, Wind energy, *In Handbook of Applied Meteorology* (D.D. Houghton, ed.), John Wiley & Sons, New York, 1985.
- Kaganov, E. L., and A. M. Yaglom**, Errors in wind speed measurement by rotating anemometers, *Bound. Layer Meteor.*, **10**, 15-34, 1976.
- Kaimal, J. C., Wyngaard, J. C., Izumi, Y., and Cote, O.R.**, Spectral characteristics of surface layer turbulence, *Q. J. R. Meteor.*, **98**, 563-589, 1972.
- Kaimal, J. C., Wyngaard, J. C., Haugen, D. A., Cote, O. R., Izumi, Y., Caughey, S. J., and Readings, C. J.**, Turbulence structure in the convective boundary layer, *J. Atmos. Sci.*, **33**, 2152-2169, 1976.
- Kondo, J., and H. Yamazawa**, Aerodynamic roughness over an inhomogeneous ground surface, *Bound. Layer Meteor.*, **35**, 331-348, 1986.
- Lawson, T. V.**, *Wind Effects on Building, vol 2, Statistics and Meteorology*, Applied science publishers, England, 1980.
- Lettau, H. H., and B. Davidson.**, *Exploring the Atmospheres First Mile*, Pergamon Press, New York, 1957.
- Loomis, F. E.**, *A Sea-breeze Bibliography*, Conn. Acad. Trans., **II**, 209-269, 1871.
- Lumley, J. L.**, The spectrum of nearly inertial turbulence in a stably stratified fluid, *J. Atmos. Sci.*, **21**, 99-102, 1964.
- Lumley, J. L., and H. A Panofsky**, *The Structure of Atmospheric Turbulence*, Interscience, London, 1964.
- Luo, J. Y., and Zhu, R. Z.**, The analysis of wind spectrum characteristics in surface layer in Badaling area of Beijing, *9ICWE*, New Delhi, India, 36-46, 1995.

- Lyons, W. A.**, Turbulent diffusion and pollutant transport in shoreline environments, Lectures on Air Pollution and Environmental Impact Analysis, D.A Haugen (ed.), *Amer. Meteor. Soc.*, 136-208, 1975.
- Markee, E. H.**, On the relationships of range to standard deviation of wind fluctuations, *Mon. Wea. Rev.*, **91**, 83-87, 1963.
- Matveev, L. T.**, *Fundamentals of General Meteorology, Physics of the Atmosphere*, Israel prog. for scientific translations, Jerusalem, 1967.
- Mc Been, G. A.**, The Planetary Boundary Layer, *WMO Tech. Note 165*, World Meteorological Organisation, Geneva, 1979.
- Menon, P. A., and C. K Rajan.**, *Climate of Kerala*, Classic publishing house, Cochin, 1989.
- Monin, A. S., and A. M Yaglom**, Statistical Fluid Mechanics, Mechanics of Turbulence, vol I, 3rd printing, MIT press, London, 1971.
- Mori, Y.**, Spectrum of long-period fluctuations of surface wind at Marcus Island, *Mon. We. Rev.*, **108**, 1456-1461, 1980.
- Moses, H. H., and H. G. Daubeck**, Errors in wind measurements associated with tower mounted anemometers, *Bull. Amer. Meteorol. Soc.*, **42**, 190-194, 1961.
- Namboodiri, K. V. S., P. S. Prakash Rao and G. V Rama**, Thunderstorm/lightning features over Sriharikota, *ISRO Tech. Rep. No. ISRO-SHAR-TR-038-94*, 1994.
- Nappo, C. J.**, Mesoscale flow over complex terrain during the Eastern Tennessee Trajectory Experiment (ETTEX), *J. Appl. Meteor.*, **16**, 1186-1196, 1977.
- NRC (U.S Nuclear Regulatory Commission).**, *Onsite Meteorological Programs Regulatory Guide 1.23*, Washington, D.C, 1972.
- NRC (U.S Nuclear Regulatory Commission).**, *Standard Format and Content of Safety Analysis Reports for Nuclear Power Plants*, LWR ed., Regulatory Guide 1.70 Revision.3 Washington, D.C, 1978.
- Narayanan, V., and T. L. Devassy**, Vertical wind shear in the lowest layers of the atmosphere over Thumba, India, *Ind. J. Meteor. and Geophys.*, **23**, 97-100, 1972.

- Narayanan Nair, K., Sen Gupta, K., P. K Kunhikrishnan, Radhika Ramachandran, S. Muraleedharan Nair, K. C. Suma Bai and T. Sunil.**, Interaction of mesoscale processes to atmospheric boundary layer for a tropical sea-shore station, In global change studies, Indian Space Research Organisation, *Scientific Rep. No. ISRO-GBP-SR-42-94*, 107-123, 1994.
- Narayanan Nair, K.**, On low level jet at coastal station Thumba, *Ind. J. Radio. and Space Phys.*, **28**, 55-59, 1999.
- Neumann, J.**, On the rotation rate of the direction of sea and land breezes, *J. Atmos. Sci.*, **34**, 1913-1917, 1977.
- Oke, T. R.**, *Boundary Layer Climates*, Methuen & Co. Ltd., London, 1978.
- Oort, A. H., and A. Taylor**, On the kinetic energy spectrum near the ground, *Mon. Wea. Rev.*, **97**, 623-636, 1969.
- Panchal, N. S., and Chandrasekharan, E.**, Terrain roughness and atmospheric stability at a typical coastal site, *Bound. Layer Meteor.*, **27**, 89-96, 1983.
- Panofsky, H. A., and G. W. Brier**, *Some Applications Statistics to Meteorology*, College of Mineral Industries, The Pennsylvania State University, 1965.
- Panofsky, H. A., and Peterson, E. L.**, Wind profiles and change of surface roughness at Riso, *Q. J. R. Meteor. Soc.*, **98**, 845-854, 1972.
- Panofsky, H. A.**, Tower Micrometeorology, In *Workshop on Micrometeorology* (D.A Haugen, ed.), 151-174, Amer. Meteor. Soc., Boston, 1973.
- Panofsky, H. A.**, Matching in the convective planetary boundary layer, *J. Atmos. Sci.*, **35**, 272-276, 1978.
- Panofsky, H. A., and J.A. Dutton**, *Atmospheric Turbulence*, Wiley, New York, 1984.
- Pansquill, F.**, The estimation of the dispersion of windborne materials, *Meteorol. Mag.*, **90**, 33-49, 1961.
- Pansquill, F.**, *Atmospheric Diffusion*, 2nd ed. Halsted Press, New York, 1974.

- Pearce, R. P.**, The calculation of a sea-breeze circulation in terms of the differential heating across the coast line, *Q. J. R. Meteor. Soc.*, **81**, 351-381, 1955.
- Pearson, R. A.**, On the assymetry of the land breeze/sea breeze circulation, *Q. J. R. Meteor.*, **101**, 529, 1975.
- Peltier, L. J., J.C. Wyngaard, S. Khanna, and J.C. Brasseur**, Spectra in the unstable surface layer, *J. Atmos. Sci.*, **53**, 49-61, 1996.
- Paulson, C. A.**, The mathematical representation of wind speed and temperature profiles in the unstable atmospheric surface layer, *J. Appl. Meteor.*, **9**, 857-861, 1970.
- Pearson, R. A., G. Carcnoni and G. Brusasca**, The sea breeze with mean flow, *Q. J. R. Meteor. Soc.*, **109**, 809-830, 1983.
- Pierson, W. J.**, The measurement of the synoptic scale wind over the ocean, *J. Geophys. Res.*, **88**, 1683-1708, 1983.
- Poppendiek, H. F.**, *Amer. Meteor. Soc. Meteor. Monograph*, **I**, 4, 1951.
- Powell, M. D.**, Wind measurement and archival under the automated surface observing system: User concerns and opportunity for improvement, *Bull. Amer. Meteor. Soc.*, **74**, 615-623, 1993.
- Prakash, W. J. J., Radhika Ramachandran, K. Narayanan Nair, K. Sen Gupta and P. K. Kunhikrishnan**, On the structure of sea breeze fronts observed near the coast line of Thumba, India, *Bound. Layer Meteor.*, **59**, 111-124, 1992.
- Prakash, W. J. J., Radhika Ramachandran, Narayanan Nair, K., Sen Gupta, K., and Kunhikrishnan, P. K.**, On the spectral behaviour of atmospheric boundary layer parameters at Thumba, India, *Q. J. R. Meteor. Soc.*, **119**, 187-197, 1992.
- Pramila Goyal and Nivedita Karmakar**, Study of sheared wind roses and stability frequency fo Mathura, *Proc. Symp. Enviro. Phys. Atmo. Bound. Layer*, Indian Istitute of Tropical Meteorology, India, 1982.

- Ramachandran, R., J. Winston Jeeva Prakash, K. Sen Gupta, K. Narayanan Nair and P. K. Kunhikrishnan**, Variability of surface roughness and turbulent intensities at a coastal site in India, *Bound. Layer Meteor.*, **1**, 1-16, 1994.
- Ramage, C. S.**, *Monsoon Meteorology*, Acad. Press, New York, 1971.
- Rama, G. V.**, SHAR News, ISRO- *The house magazine of SHAR Centre*, **52**, 4-5, 1998.
- Reed, W. J.**, Wind power climatology, *Weatherwise*, **27**, 236-242, 1975.
- Reed, W. J.**, Cape Canaveral sea breezes, *J. Appl. Meteorol.*, **18**, 231-235, 1979.
- Reil, H.**, *Introduction to the Atmosphere*, Mc Graw Hill, Inc, USA, 1972.
- Rijkoort, P. J.**, Dependence of observed low level wind shear on averaging period and lapse rate, *WMO Tech. Note No. 93*, 185-194, 1969.
- Sachdev, R. N., and K. K. Rajan**, An electronic computing wind vane for turbulent studies, *J. Appl. Meteor.*, **10**, 1331-1338, 1971.
- Scott, J. R.**, A regression method for estimating time changes of elliptically distributed winds, *Q. J. R. Meteor. Soc.*, **82**, 337-341, 1956.
- Sedefian, L.**, On the vertical extrapolation of mean wind power density, *J. Appl. Meteor.*, **19**, 488-493, 1980.
- Sen Gupta, K., P. K. Kunhikrishnan, Radhika Ramachandran, J. Winston Jeeva Prakash and K. Narayanan Nair**, On the characteristic of coastal atmospheric boundary layer, In global change studies, Indian Space Research Organisation Scientific Report No. *ISRO-GBP-SR-42-94, 92-106*, 1994.
- Sivaramakrishnan, T. R., and P. S. Prakash Rao**, Sea breeze features over Sriharikota, India, *The Meteor. Mag.*, **118**, 64-67, 1989.
- Slade, D. H.**, *Meteorology and Atomic Energy*, U.S Atomic Energy Commission, Div. Of Tech. Inf. Oak. Ridge, Tennessee, USA, 1968.
- Smagorinsky, J.**, Global atmospheric modeling and numerical simulation of climates, In HESS, W.N (ed.), *Weather and Climate Modification*, Wiley, New York, 1974.

- Smedman-Hogstrom, A., and Hogstrom, U.**, Spectral gap in surface layer measurements, *J. Atmos. Sci.*, **32**, 340-350, 1975.
- Smedmann-Hogstrom, A. S., and U. Hogstrom**, A practical method for determining wind frequency distributions for the lowest 200 m from routine meteorological data, *J. Appl. Meteor.*, **17**, 942-954, 1978.
- Smith, M. F.**, A short note on a sea breeze crossing East Anglia, *Meteor. Mag.*, **103**, 115, 1947.
- Smith, O., S. Adelfang and G. Batts**, Wind models for NSTS ascent trajectory biasing for wind load alleviation, *28th Aerospace Sciences Meeting*, 1990, Reno, Nevada, 1990.
- Smith Richard**, Extreme value theory, *In Handbook of Applicable Mathematics*, Supplement, Wiley, New York, 1990.
- Sparks, W. R., and B. Keddie**, A note on the optimum averaging time of wind information for conventional aircraft landing, *Meteor. Mag.*, **100**, 129-134, 1971.
- Staley, D. O.**, The low level sea breeze of north west Washington, *J. Meteor.*, **14**, 458-470, 1957.
- Staley, D. O.**, The surface sea breeze: Applicability of Haurwitz-type theory, *J. Appl. Meteor.*, **28**, 137-145, 1989.
- Stauffer, D. R., N. L. Seaman, and F. S. Binkowski**, Use of four dimensional data assimilation in a limited area mesoscale model, Part II: Effects of data assimilation within the planetary boundary layer, *Mon. Wea. Rev.*, **119**, 734-754, 1991.
- Stewart, D. A., and Essenwager, O. M.**, Frequency distribution of wind speed near the surface, *J. Appl. Meteor.*, **17**, 1633-1642, 1978.
- Stull, B. R.**, *An Introduction to Boundary Layer Meteorology*, Kluwer academic publishers, Dordrecht, The Netherlands, 1994.
- Surridge, A. D.**, On the measurement of atmospheric winds, *Bound. Layer Meteor.*, **24**, 421-428, 1982.
- Sutton, O. G.**, *Micrometeorology*, Mc Graw Hill book co., Inc, New York, 1953.

- Takle, E. S., and J. M. Brown**, Note on the use of Weibull statistics to characteristics wind speed data, *J. Appl. Meteor.*, **17**, 556-559, 1978.
- Taylor, G.I.**, The spectrum of turbulence, *Proc. R. Soc.*, **A164**, 476-490, 1938
- Tennekes, H.**, The atmospheric boundary layer, *Physics today*, **27**, 52-63, 1974.
- Tennekes, H.**, Similarity relations, scaling laws and spectral dynamics, In *Atmospheric Turbulence and Pollution Modeling* (Nieuwstadt, F.T.M., and Van Dop, H, eds.), D.Reidel Pub. Co., Dordrecht, Holland, 37-68, 1982.
- Thompson, R. S.**, Note on the aerodynamic roughness length for complex terrain, *J. Appl. Meteor.*, **17**, 1402-1403, 1978.
- Thuillier, R. H., and V. O. Lappe**, Wind and temperature profile characteristics from observations on a 1400 ft tower, *J. Appl. Meteor.*, **3**, 299-306, 1964.
- Touma, J. S.**, Dependence of the wind profile power law on stability for various locations, *J. Air Pollut. Control Assoc.*, **27**, 863-866, 1977.
- Turner, D. B.**, *Workbook of Atmospheric Dispersion Estimates*, U.S Dept. of health sciences, NAPCA Cin Annati, Ohio, USA, 1970.
- Turner, D. B.**, Comparison of three methods for calculating the standard deviation of the wind direction, *J. Clim. Appl. Meteor.*, **25**, 703-707, 1986.
- Van der Hoven.**, Power spectrum of horizontal wind speed in the frequency range from 0.0007 to 900 cycles per hour, *J. Meteor.*, **14**, 160-164, 1957.
- Verrall, K. A., and R. L. Williams**, A method for estimating the standard deviation of wind directions, *J. App. Meteor.*, **21**, 1922-1925, 1982.
- Weibull, W.**, A statistical distribution function of wide applicability, *Trans. A.S. M.E.*, **73.**, 1951.
- Weinstock, J.**, A theory of gaps in the turbulent spectra of stably stratified shear flows, *J. Atmos. Sci.*, **37**, 1542-1549, 1981.
- Wills, G. E., and J. W. Deardorff**, On the use of Tailors translation hypothesis diffusion in the mixed layer, *Q. J. R. Meteor. Soc.*, **102**, 817-822, 1976.
- WMO**, World Meteorological Organisation., Vertical shear in the lowest layers of the atmosphere, *WMO Tech. Note No. 93*, 1969.

- WMO**, World Meteorological Organisation., Technical regulations, II,
Meteorological service for international air navigation, *WMO-No. 49*, 1988.
- Wyngaard, J. C.**, On surface-layer turbulence, In *Workshop on
Micrometeorology*, (D.A. Hougen, ed.), 101-149, Amer. Meteor. Soc.,
Boston, 1973.
- Wyngaard, J. C.**, Cup, propeller-vane and sonic anemometers in turbulence
research, *Ann. Rev. Fluid Mech.*, **13**, 399-423, 1974.
- Yaglom, A. M.**, Comments on wind and temperature flux-profile relationships,
Bound. Layer Meteor., **11**, 89-102, 1977.
- Yamartino, R. J.**, A comparison of several single-pass estimators of the standard
deviation of wind direction, *J. Clim. Appl. Meteor.*, **23**, 1362-1366, 1984.
- Zhang, S. F.**, A statistical analysis of the power law and the logarithmic law using
wind data from a 164 m tower, *Bound. Layer Meteor.* **20**, 117-123, 1981.
- Zhong, S., and S.E. Takle.**, An observational study of sea-and land breeze
circulation in an area of complex coastal heating, *J. Appl. Meteor.*, **33**,
1426-1438, 1992.

